General Disclaimer

One or more of the Following Statements may affect this Document

- This document has been reproduced from the best copy furnished by the organizational source. It is being released in the interest of making available as much information as possible.

- This document may contain data, which exceeds the sheet parameters. It was furnished in this condition by the organizational source and is the best copy available.

- This document may contain tone-on-tone or color graphs, charts and/or pictures, which have been reproduced in black and white.

- This document is paginated as submitted by the original source.

- Portions of this document are not fully legible due to the historical nature of some of the material. However, it is the best reproduction available from the original submission.

2

7.6 - 1 0.4 1.8

IN SITU SPECTRORADIOMETRIC CALIBRATION OF EREP IMAGERY AND ESTUARINE

AND COASTAL OCEANOGRAPHY OF BLOCK ISLAND SOUND AND ADJACENT NEW YORK

COASTAL WATERS

Edward F. Yost
Science Engineering Research Group
C.W. Post Center-Long Island University
Greenvale, New York 11548

Abstract

A two-part Interpretation Techniques Development Study of Skylab multispectral imagery was conducted.

The first part of the study resulted in photographic procedures for making multispectral positive images which greatly enhance the color differences in land detail using an additive color viewer. An additive color analysis of the geologic features near Willcox, Arizona, using enhanced black-and-white multispectral positives allowed compilation of a significant number of unmapped geologic units which do not appear on geologic maps of the area. Factors of correspondence were developed which, at wavelengths from 400 to 1100 nm, related Skylab S-191 spectrometer data to in situ ground spectral measurements. The numerical value of these factors of correspondence depends on the atmospheric optical depth.

The second part of the study demonstrated the feasibility of utilizing Skylab remote sensor data to monitor and manage the coastal environment by relating physical, chemical, and biological ship sampled data to S-190A, S-190B, and S-192 image characteristics. Photographic reprocessing techniques were developed which greatly enhanced subtle low brightness water detail. Using these photographic contrast-stretch techniques, two water masses having an extinction coefficient difference of only 0.07 measured simultaneously with the acquisition of S-190A data were readily differentiated. By digitizing S-190A multispectral imagery in registration, the non-homogeneous vertical stratification of Block Island Sound waters with differences in suspended solids of one milligram per liter were detected. Significant differences between conventional tidal current charts and the actual patterns of water flow in Long Island Sound were established. The existence of two large counter-clockwise gyres heretofore undetected, were verified using S-190B color imagery. Digital analysis of S-190A multispectral negatives and subsequent single and multiple image classification of Block Island Sound waters demonstrated that complex sub-surface mixing patterns could be detected from S-190A image brightness characteristics. The average extinction coefficient for white light was measured by ship in Block Island Sound to be 0.335, with a value of 0.400 for the blue band and 0.554 for the red band extinction coefficients. Under these optical water characteristics, surface, sub-surface water non-homogeneities can be charted and estimates of suspended particles over 5 microns in size can be made.

i

Table of Contents

Section I

Introduction

This report presents the results of a two-part Interpretation Techniques Development Study to:

-- Part A: Quantitatively relate photographic characteristics of Skylab multispectral photography and spectrometer data to measurements of the reflectance of ground objects.

-- Part B: Determine the feasibility of utilizing Skylab remote sensor data to monitor and manage the coastal environment.

Part A

A quantitative analysis of the characteristics of S-190A multi-spectral photography was performed at the outset to establish optimum procedure for printing black-and-white multispectral photographic positives of semi-arid desert-like terrain. A procedure was developed which, when used to print positive transparencies from NASA release Skylab multi-spectral negatives, produced excellent composite color images when projected on an additive color viewer screen. An extensive qualitative interpretation analysis was performed using an additive color viewer and the reprocessed positive images. The purpose was to examine spectral reflectance image characteristics of a large and relatively homogeneous ground object exemplified by the Willcox Playa.

The principal area of interest in this study, the Willcox Playa, is a large, dry lake located in southeastern Arizona. The central part of the playa has a hard and compact crust. The outer areas of the playa

contain soft, dry, and porous surfaces which become flooded during the infrequent rains.

Reflectance spectra were taken in situ on the playa prior to the launch of Skylab and during 1973. These latter measurements were made at twelve sample stations in the playa and correlated with soil moisture measurements simultaneously taken.

In order to quantitatively examine image density characteristics, digital image processing procedures were developed using TV digitization of the images in registration, storage in a PDP-11 computer disc, image processing, statistical analysis, and display programs.

Using this digital image processing system, a spectral analysis of the reflectance characteristics of the Willcox Playa were performed. Near simultaneous underflight multispectral imagery was also analyzed. The relative effect of the atmosphere in each of the four spectral bands was measured. The statistics of the relative screen brightness range in each of the four S-190A multispectral images were established for desert areas and a procedure was developed to correct for atmospheric effects in each of the four bands.

Part B

An interdisciplinary project to demonstrate the feasibility of utilizing satellite imagery for oceanographic studies was conducted. The project was undertaken jointly by Long Island University and the New York

Ocean Science Laboratory as a continuing effort related to an on-going

program to study Block Island Sound and adjacent New York coastal waters.

A base line study of the characteristics of Block Island Sound and New

York Bight was made in order to construct a background of data within

which to place the specific data collected at the sampling stations during

the pass of Skylab.

The fundamental problem in oceanography is sampling and, in

particular, synoptic sampling analogous to the sampling programs in

meteorology. It is, however, economically impossible to operate ships

on an adequate scale to cover the needs of not only the oceans but, more

importantly, the coastal zones and estuaries. Currently, the placing of

buoys equipped with adequate transducers to provide the required informa-

tion is also problematical from both an engineering and economic stand-

point. Satellite imagery, however, provides the synoptic overview of an

area that forms the basis for further monitoring.

The program to acquire oceanographic "baseline data" in BlockIsland

Sound and New York Bight areas was conducted by the New York Ocean Science

Laboratory. Twenty-four cruises were made to collect water samples at

different stations for temperature, salinity, nutrients, oxygen, pigments,

organics, phytoplankton, and particle size determinations.

Photographic reprocessing techniques were developed which, when

applied to any of the Skylab S-190A multispectral photography supplied to

investigators, will yield greatly improved detectability of subtle water

and land phenomena. These techniques have been related to the calibration

gray scale supplied with the imagery in order to provide quantified data

on the photographic transformations applied. Application of these

techniques to the S-190A multispectral photography taken of Block Island

-3-

Sound and New York Bight formed the basis for subsequent additive color
and digital image analysis.

S-190A multispectral photography and S-192 scanner data were used
in this analysis. Additive color analyses were performed to extract
information regarding the location, source, and dispersion of the Shagwong
Reef plume. In addition, digital image analysis was undertaken to quan-
titatively examine image density characteristics of the S-190A multi-
spectral photography of northern Block Island Sound and Long Island Sound.

Block Island Sound

Block Island Sound is a partly enclosed body of water between Rhode
Island and Long Island, New York, separating the waters of Long Island
Sound (and also the Peconic Bay system) from the coastal waters of the
Atlantic Ocean. Figure 1 shows the chart of Block Island Sound and station
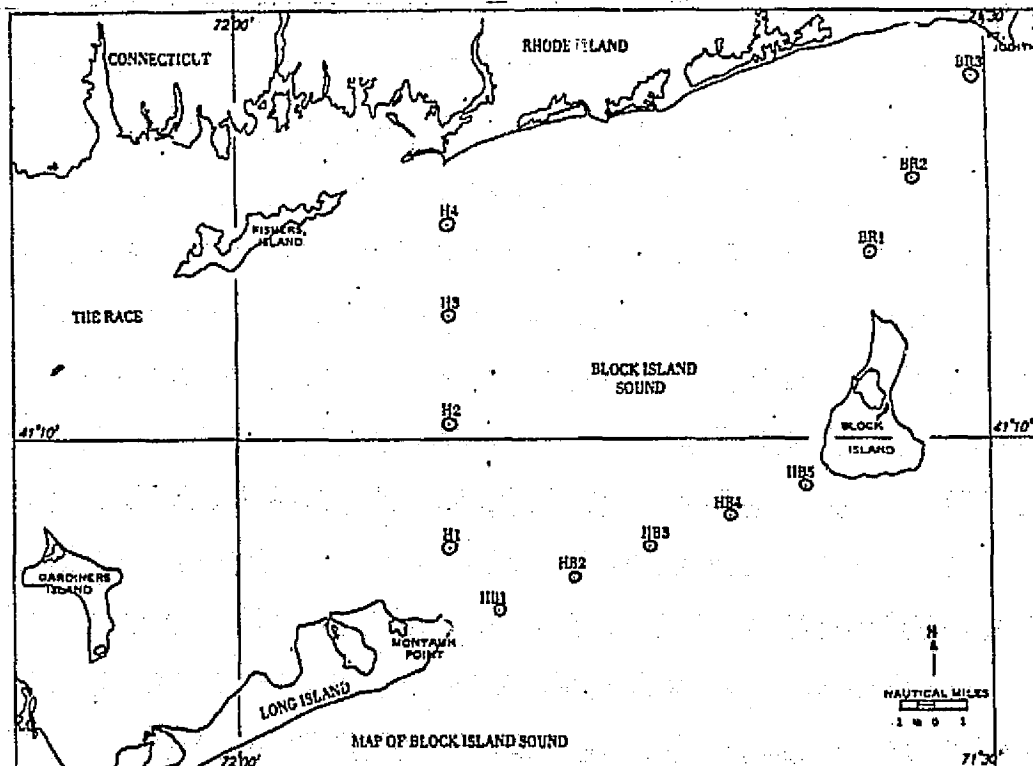
Figure 1. Chart of Block Island Sound showing transects and station locations.

locations where the water samples were collected on twenty cruises between 24 August 1972 and 19 June 1973 during the baseline data compilation program. Block Island Sound has a surface area of approximately 1350 square kilometers and is bounded on the north by Rhode Island by Long Island, New York, to the south. The mean depth in Block Island Sound is approximately 40 meters and has a total volume in excess of 54×10^3 cubic meters (1.9 million gallons).

The deepest depression in the sound is close to 100 meters. The head of Block Canyon intrudes into Block Island Sound between Montuak Point on Long Island and Block Island, having a maximum depth in this area of approximately 70 meters. An excellent review of the oceanography of Block Island Sound was presented by Williams (1967). A typical set of four positive S-190A images over Block Island Sound acquired on 19 Sept. 1973 is shown in Figure 2 on the following page.

New York Bight

New York Bight covers approximately 48×10^3 square kilometers with an average depth of about 60 meters. Long Island bounds the area to the north and the New Jersey coast to the west. The entrance to New York Harbor is at the apex of the northern and western boundaries and is the major outfall for the area. The outer boundary is approximately defined by the 100 fathom curve.

Figure 3 shows a chart of the New York Bight and the locations of stations at which the water samples were collected during the baseline data compilation of four cruises between 21 September 1972 and 1 June 1973. A variety of municipal and industrial wastes are disposed of by barge dumping
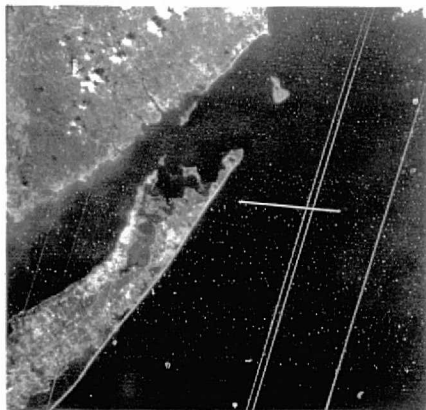
Filter AA - 500-600 nm
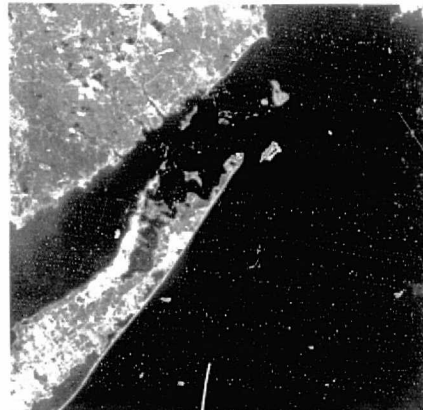
Filter BB - 600-700 nm
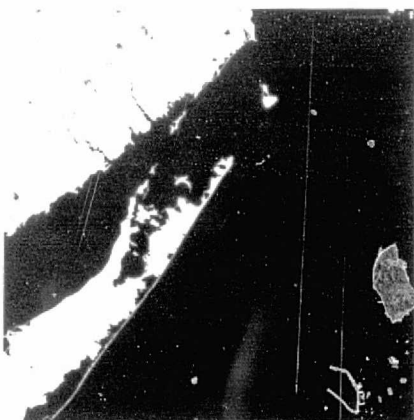
Filter CC - 700-800 nm
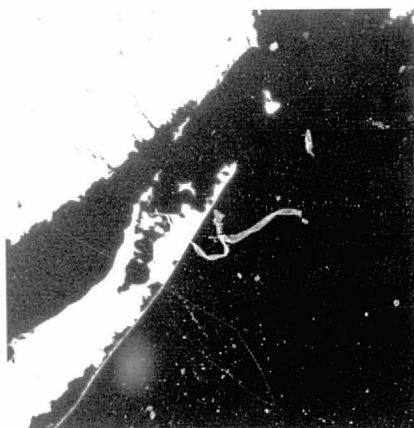
Filter DD - 800-900 nm

Figure 2. Four Skylab-3 S-190A multispectral photographic images of Block Island Sound obtained on 19 September 1973.
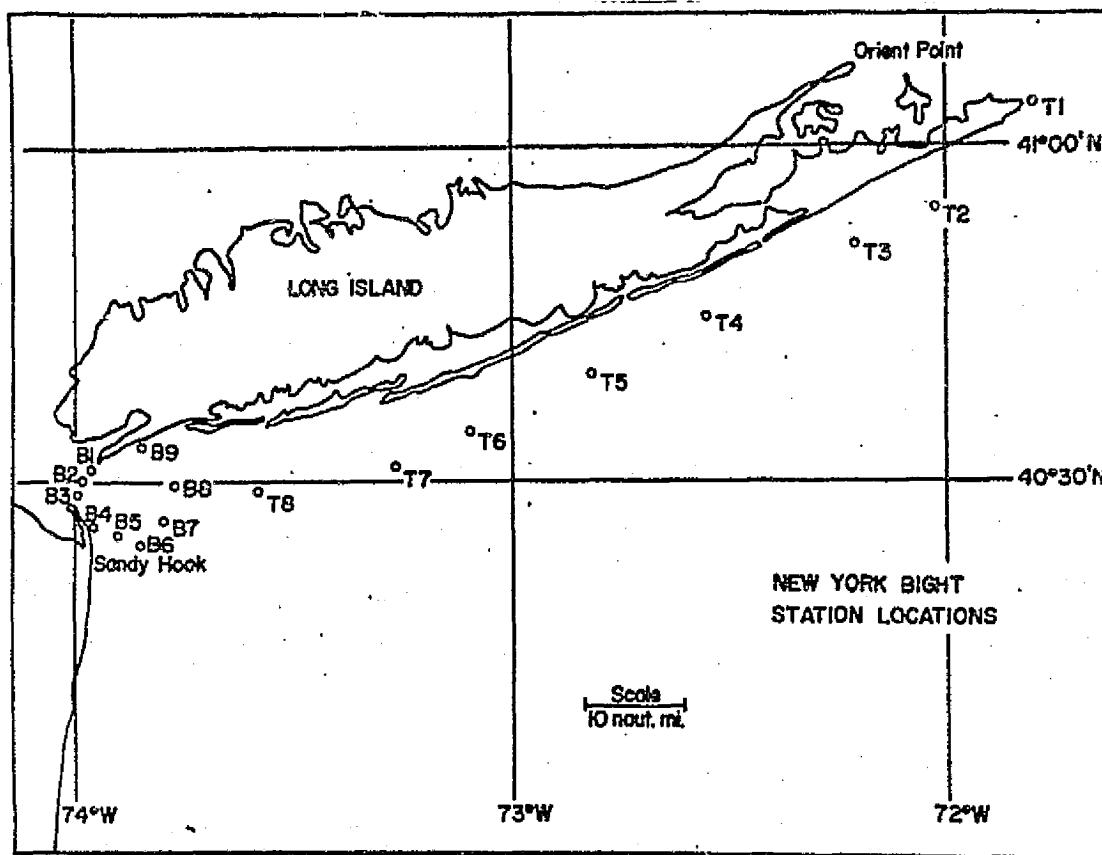
Figure 3. Chart of New York Bight showing station locations.

in the waters of the Bight, including sewage sludge and acid wastes. The flow and fate of these inputs into the area is not yet completely known.

The total volume of New York Bight is approximately 29×10^9 cubic meters. The general topography is broad and almost flat with the exception of Hudson Canyon, which runs generally northwest-southeast and cleaves the shelf from the 1000 fathom curve to the entrance to New York Harbor at the apex of the Bight. A general review of the oceanography of the New York Bight can be found in a publication by Hollman (1971). Figure 4 shows a set of positive photographs in the four bands imaged by Skylab-3 over New York Bight on 12 September 1973.
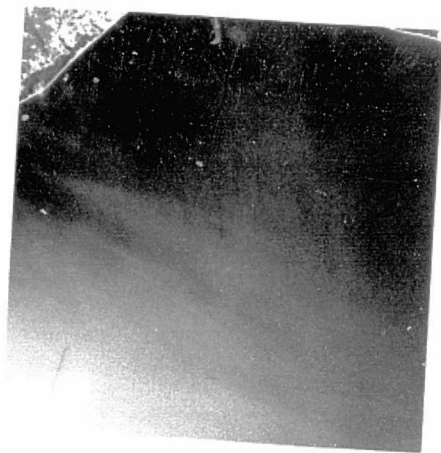
Filter AA - 500-600 nm
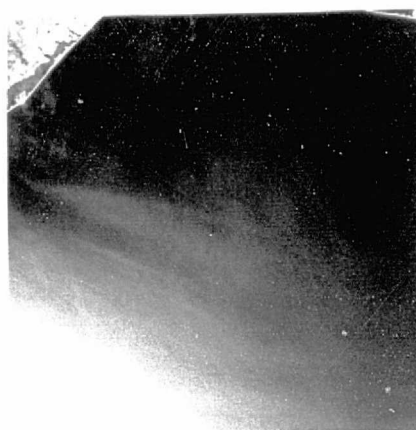
Filter BB - 600-700 nm
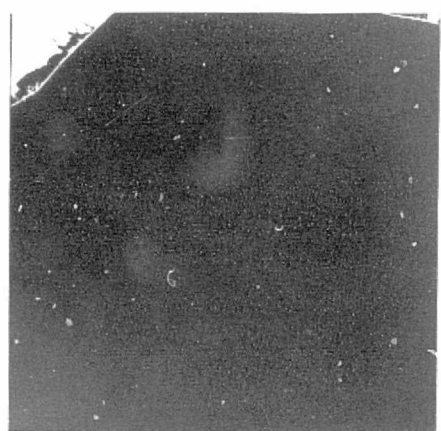
Filter CC - 700-800 nm

Filter DD - 800-900 nm

Figure 4. Four Skylab-3 S-190A multispectral photographic images of New York Bight obtained on 12 September 1973.

The Water Sampling Baseline Data Compilation Program

Two transects were followed in the New York Bight. The first transect runs parallel to the shore of Long Island from Montauk Point to Rockaway Inlet and comprises eight stations, as shown in Figure 3. These stations are sampled once on the day spent in transect from Montauk to Rockaway and are repeated two days later on the return transect. The second transect is a large arc sweeping through the apex of the New York Bight and comprises nine stations, so that all of the various dump-site positions (as provided by the U.S. Army Corps of Engineers, personal communications) are included in the transect (Table 1). Continuous surface profiles of temperature and pigments were obtained whenever the vessel was underway between the stations.

Three transects of Block Island Sound were selected, as shown in Figure 1, where large color differences in water masses were expected on the basis of previous sampling programs. The exact locations of the stations that each transect comprises are tabulated in Table 2. Each transect was occupied by continually sailing back and forth during a tidal cycle and sampling at up to six depths at each station. The water was collected in five-liter Niskin bottles for chemical and biological analysis.

This general sampling program was later modified slightly to allow for continuous flow fluorometer profiling throughout Block Island Sound on the day prior to the satellite overpass. Surface samples were also drawn for chemical and biological analysis. With this modified program, one in-depth sampling of the "H" transect was conducted during the day of surface profiling and the other two transects sampled in-depth on the following day.

Transect	Station	Latitude	Longitude
TR	TR 1 (E/W)	41°04.6'N	71°49.0'W
	" 2 "	40°54.5'N	72°01.5'W
	" 3 "	40°49.0'N	72°18.5'W
	" 4 "	40°44.0'N	72°33.6'W
	" 5 "	40°39.2'N	72°48.5'W
	" 6 "	40°34.4'N	73°04.0'W
	" 7 "	40°31.0'N	73°13.5'W
	" 8 "	40°29.5'N	73°34.5'W
New York Bight	NYB 1	40°32.4'N	73°56.6'W
	" 2	40°30.5'N	73°58.0'W
	" 3	40°29.2'N	73°59.6'W
	" 4	40°25.1'N	73°56.0'W
	" 5	40°24.4'N	73°51.3'W
	" 6	40°23.0'N	73°48.2'W
	" 7	40°25.5'N	73°45.0'W
	" 8	40°30.0'N	73°44.0'W
	" 9	40°33.8'N	73°48.6'N

Table 1. Station locations in New York Bight.

Transect	Station	Latitude (North)	Longitude (West)	Mean Depth (meters)
"H"	H1	41°06.8'	71°51.5'	12.2
	H2	41°10.4'	"	41.1
	H3	41°13.8'	"	51.8
	H4	41°16.5'	"	38.1
"HB"	HB1	41°04.8'	71°49.4'	13.4
	HB2	41°05.8'	71°46.3'	12.5
	HB3	41°06.7'	71°43.3'	34.7
	HB4	41°07.5'	71°40.2'	18.3
	HB5	41°08.4'	71°37.3'	13.1
"BR"	BR1	41°15.7'	71°34.8'	36.6
	BR2	41°18.0'	71°33.0'	36.6
	BR3	41°20.8'	71°30.5'	9.1

Table 2. Station locations in Block Island Sound.

Parameters Sampled

The parameters sampled for include temperature, salinity, nutrients, oxygen, pigments, organics, phytoplankton, light attenuation, particle size determinations, and fluorometer readings.

Temperatures were measured with bathythermographs and thermometers. Light attenuation values were obtained with an irradiance meter consisting of a photo-cell and various glass filters. Fluorometer readings were obtained with a Turner fluorometer using a continuous flow door. These three parameters were measured in situ.

Water samples for chemical and biological analysis were collected in five-liter Niskin bottles.

Salinities were obtained using a laboratory conductivity cell (Beckman Model RS-7), oxygen, chlorophylls, and nutrients, using the methods as described in Strickland and Parsons (1968).

Particle size determinations were performed with a Coulter Counter, Model B.

Techniques and Equipment Used in Image Analysis

Additive Color Analysis of Skylab Imagery

S-190A photographic data products were analyzed using additive color viewing analysis techniques. The procedures used, with appropriate instrumentation and significant theories, are described in the subsequent paragraphs.

Spectral Data Model 70 viewer, shown in Figure 5, was an essential instrument for use in the interpretation and analysis of Skylab S-190A multispectral photography. The device produces a single color presentation for the spatially calibrated photos by projecting the image of one
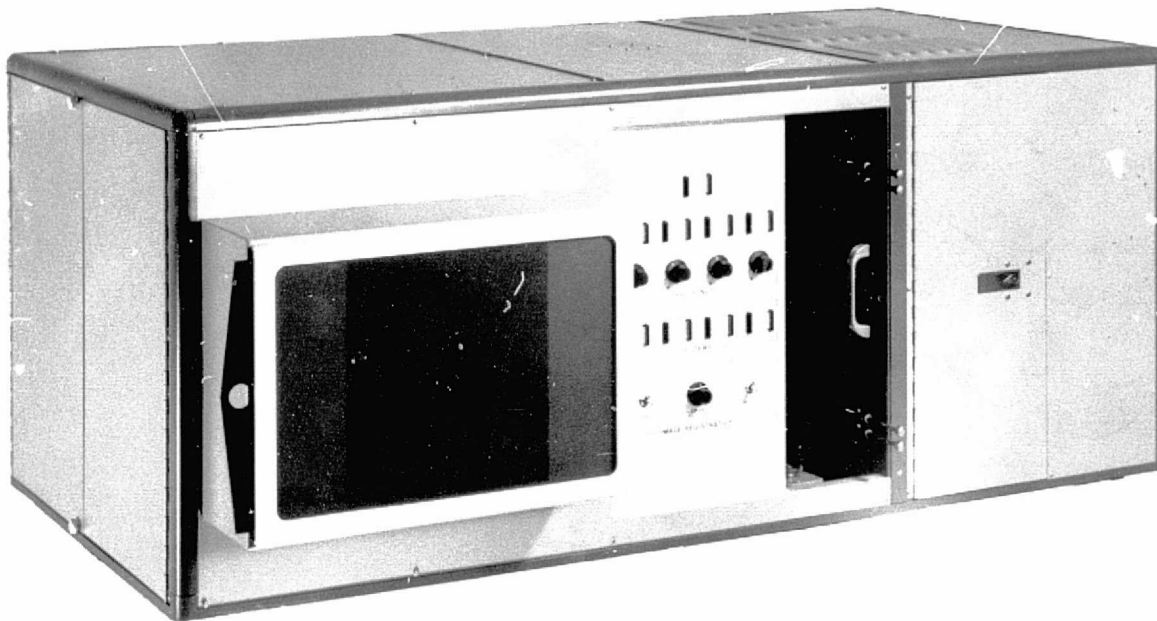
Figure 5. Spectral DAta Model 70 viewer used for additive color analysis of S-190A multispectral photography.

photo on top of the other using different color light sources. This technique of analysis permits a scientist to select a set of bands and to interpret within results from a single color presentation. In addition, a multispectral viewer provides the scientist with the capability of altering the color of the presentation in order to enhance the particular relationships he may be seeking. Fundamentally, the multispectral technique allows one to create a color presentation specifically for the purpose of his discipline and interests.

In order to quantitatively evaluate multispectral color images, color must be colorimetrically defined as that conscious sensation which is exhibited when light of a specific spectral energy distribution enters the eye. It has been experimentally shown that differences in this energy

distribution cause variations in the observed response of the eye and may be described in terms of three distinct psychophysical variables. The first is hue which is basically that quality of color which leads to the definition of an object as being red, green, yellow, etc. Saturation, the second quality of color, is described as the amount of white in a given hue. It may be also considered as the concentration of the color. For instance, it is the difference between red and pink. As the amount of saturation in a color decreases, it approaches pure white. Brightness, which is the third variable of color, is described as the amount of visible energy contained in a certain hue which is saturated to a specific value.

Digital Image Processing Equipment and Techniques

A digital analysis of the S-190A photographic imagery was performed. The purpose was to make a statistical analysis of Skylab photographic data in order to determine the spectral and temporal variations of the image characteristics, as well as to devise procedures for classification of terrain and water features.

The equipment used for this purpose was a Spatial Data "System 800". This device, shown in Figure 6, is described in some detail in Appendix G .

This system for digitizing and analyzing multispectral photographs operates as follows:

-- Four multispectral black-and-white transparencies are placed on a light box. These photographs are digitized in registration one at a time by a TV camera. The transmitted brightness (e.g., the density) of each multispectral photograph is digitized into 8-bit binary numbers (256 density levels) in a 512 x 576 point matrix.
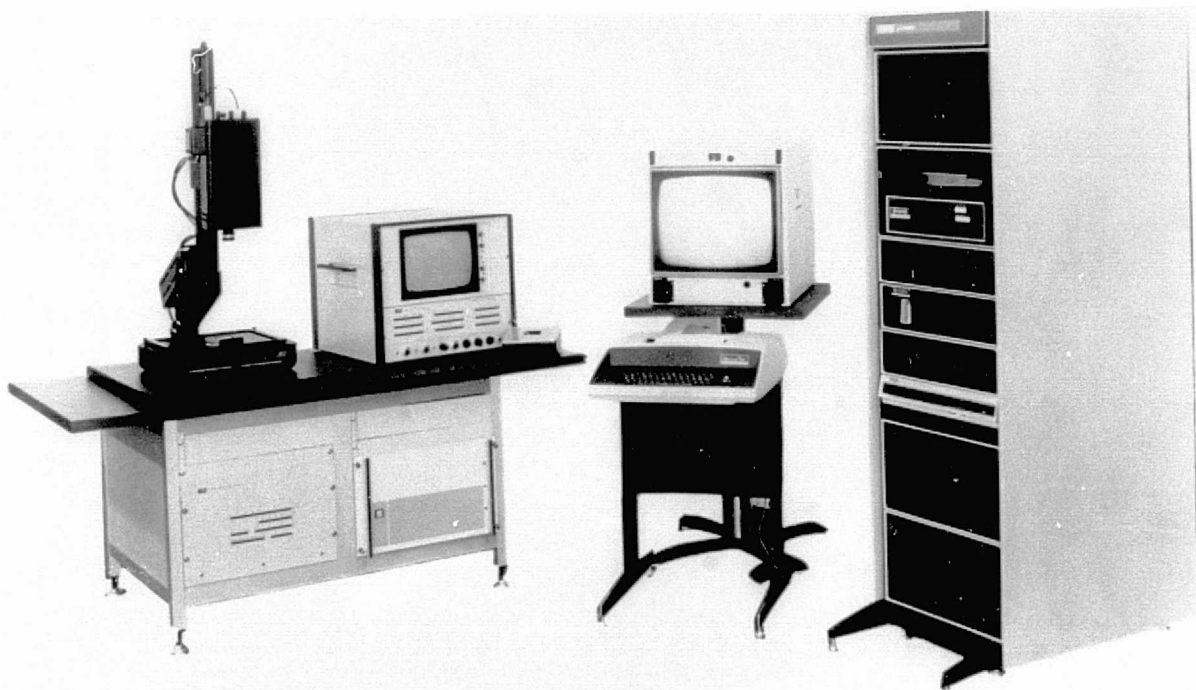
Figure 6. The "System 800" digital processing equipment for S-190A multispectral photographs.

-- The 512 x 576 x 8-bit digitized image from each multispectral
   photograph is stored on the disc of a PDP-11/E-04 computer.

-- A series of programs are used to process the images. For
   instance, addition, subtraction, multiplication, and division
   of any combination of the four multispectral photographs is
   accomplished by the computer and a serie_ of programs. A
   description of these programs is included in subsequent
   paragraphs.

-- A digital disc is used to store the processed image and to
   display it on a color TV monitor. The display is in eight

colors. A Decwriter also produces hard copy of statistical results and of operating program sequence.

A description of the "System 800" programs is as follows:

-- MARKER: Reads, saves, and generates joystick-indicated fiducial marks for multiple-picture registration.

-- DIGIT: Digitizes a video picture into a named computer disc picture file.

-- HISTOR: Generates a line histogram on a black-and-white monitor displaying the gray scale distribution of a given multispectral picture and accepts joystick inputs to partition the gray scale for DISPLAY.

-- DISPLAY: Copies a picture from computer disc to the data disc using slice values from HISTOR or a uniform default partition.

-- AREA: Outputs eight numbers corresponding to the percentages of the full picture of each color on the color TV display.

-- ADDER: Sets [picture 2] = [(picture 1)+(picture 2)]/2, where pictures 1 and 2 are named computer disc picture files.

-- NEGATE: Produces the compliment of a given picture.

-- CONTEX: Performs a contrast expansion of a given picture within variable limits.

-- SHIFT: Replaces a picture by itself shifted any number of pixels up, down, left, or right.

-- GRID: Generates a variable spaced white-on-black grid on the color TV display.

DIAGON: Performs various exercising, diagnostic, and display functions under keyboard control.

Eight-bit digitization was selected in order to divide the density range of the photographs into 256 levels. The scanner used for digitization used a special vidicon-type television camera tube and special circuits to accurately sense the light emitted by the image to be digitized. A light image of the object is produced on the photo-sensitive face of the camera tube by an optical system containing an ordinary camera lens. Brightness at any point on the image is a function of an X and Y coordinate position on the tube face. Image brightness is then defined as a third dimension, Z.

The brightness, or Z-value, is converted into an electrical voltage (video signal) by repeatedly scanning the image with an exploring spot formed by the electron beam of the camera tube. This spot generates an electrical video signal which indicates the brightness at its instantaneous position. The video signal is transmitted through a video amplifier to the TV display, where it controls the brightness of a reproducing spot formed by the CRT electron beam. The reproducing spot moves over the viewing screen in a path similar to, and synchronous with, the exploring spot. The reproducing spot reconstructs the brightness distribution in the image area, both in magnitude (Z) and position (X-Y) and thus generates a television picture of the object.

The scanner path covering the image area consists of a series of straight parallel lines. The spot moves from left to right across each line at a constant speed and then returns to traverse the next line. The spot returns back to the top upon completion of the bottom line. During the horizontal and vertical retrace periods, the exploring and

reproducing spots are disabled, or blanked so that the image itself is
scanned only during the forward, left to right motion of the spots.

In order to reduce flicker in the reproduced picture, the scanning
lines are interlaced. That is, instead of moving across the horizontal
lines in the sequence 0, 1, 2, 3, 4, ..., the spot first covers the
even-numbered lines (0, 2, 4, ..., 478) and then the odd-numbered lines
(1, 3, 5, ..., 479). The scanning beam completes two interlacing scanning
patterns (fields) to cover the entire image or frame. Each field takes
1/60 second to complete; the entire image is scanned 30 times a second.
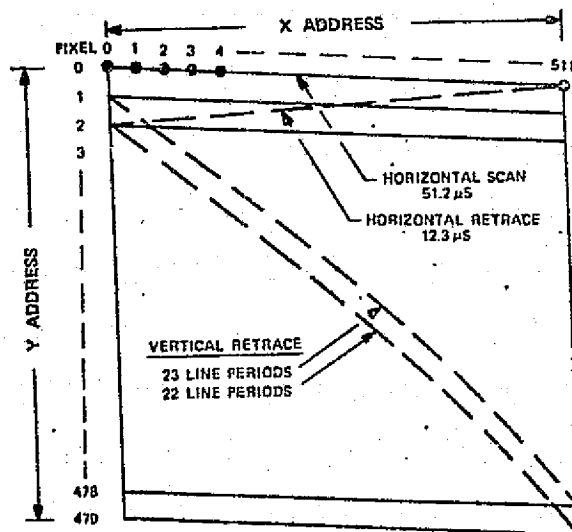
Television Scan Pattern

A sync generator provides the signals for synchronizing the exploring
spot on the scanner and the reproducing spot on the display. Digital count-
ing circuits divide each line into 512 parts while counting the lines
through each frame. The instantaneous digital values represent X and Y
positions of the scanning spot. The X-Y addresses select 245, 760 points
or pixels in the picture; X-values range from 0 to 511, Y-values range
from 0 to 479. The instantaneous voltage from the video amplifier represents

the brightness of the image at each X-Y position. This brightness value
is sampled and digitized under computer control.

The X-Y registers store the desired pixel position. The registers
are loaded from the computer and their contents are continuously compared
with the spot position indicated by the digital counters. When the scan-
ning spot reaches the stored X-Y address, i.e., the desired position, the
address comparator issues a compare pulse to the sample control. Commands
from the computer to sample and digitize a pixel are received by the
sample control through the controller.

The video signal is processed and standardized prior to digitiza-
tion by the signal conditioner which performs these functions. First, it
corrects the signal to compensate for "shading", i.e., changes in the
sensitivity of the camera tube across the image plane. Second, it ampli-
fies the signal, linearly or logarithmically, as selected by a front panel
mode switch, to provide a standardized relation between image brightness
and the digitized Z-value. Third, the signal conditioner adjusts the
sensitivity and offset of the video signal so the digitized Z-values cover
the desired image brightness range. These adjustments can be made manually,
via the front panel, or automatically by digital control data from the
computer. The control data are stored in the set-up, the zero, and the
range registers which together control the signal conditioner circuits
through special digital-analog converters. The standard video is sampled
and digitized into an 8-bit binary Z-value. The Z-value is stored in the
Z-register where it can be accessed by the computer through the controller.
These features insure the accurate digitization of the Skylab photographic
images for subsequent computer analysis.

Section 2

In Situ Spectral Reflectance Measurements

and

Analysis of S-191 Spectrometer Data

Spectral reflectance measurements were made in situ at Willcox
Playa, Arizona. The equipment, techniques used, and significant data
obtained are described herein, including the soil moisture data obtained
at the playa. During the SL-2 Skylab mission, in situ measurements of
solar radiation (450-1100 nm) were made at Willcox Playa, Arizona, in
order to provide comparative calibration measurements for the S191
spectrometer. Specifically, a conversion was developed whereby the
percent reflectance of ground objects (for a known atmosphere) could
be established.

In situ ground spectral measurements consisted of incident solar
radiation and optical depth, diffuse solar radiation and directional
reflectance normal to the surface of the playa.

Solar Radiation Calibration Measurements and Analyses

ISCO (Instrument Specialties Company) spectroradiometer was
used to measure direct, diffuse, and total solar radiation for a certain
number of measurements of target reflectance from 400 to 1300 nm (nano-
meters). This instrument uses a wedge-interference filter system with a
15 nm bandwidth over the 400-to 750 nm region and a 30 nm bandwidth over
the 750 to 1300 nm region. The sensing element is a stable photodiode.
A light chopper system permits automatic zero and dark current adjustments
160 times a second. The instrument uses a fiber optics probe with a
diffuser mounted on the end, as the light gathering element. The diffuser

is made of Teflon and has a cosine response.

The total and diffuse solar radiation was measured by placing the
diffuser face-up and level with respect to the ground. Diffuse solar
radiation measurements were obtained by shading the diffuser from the
direct solar beam.

The target's directional reflectance (perpendicular to the surface
of the playa) was obtained by measuring the radiance from a calibrated
"white" reflectance standard and then measuring the radiance from the
surface.

Direct incident solar radiation was measured using the ISCO spectro-
radiometer to derive atmospheric optical depth. A collimator was attached
over the diffuser collector to measure the direct incident solar beam.

The ISCO spectroradiometer was laboratory calibrated using a ribbon
filament tungsten type standard (traceable to NBS) lamp. This results in
an absolute accuracy of ±4 percent on the 400 to 750 nm region, and a ±7
percent absolute accuracy in the 750 to 1300 nm region. Although the instru-
ment was calibrated in terms of wavelength at the factory, continuous
checks are made by periodically placing a calibration filter in the light
path. The data recorded using that instrument is repeatable to between
one to three percent, depending upon wavelength and gain setting.

Measurements and Analyses of the Spectral Reflectance Data

A definite haze layer existed over the playa area during the early
morning on 3 June 1973, followed by a build-up of small, scattered cumulus
clouds that caused intermittent shadowing of the playa.

Total Solar Radiation

. The absolute quantity of total solar radiation, near the time of overflight was measured and is shown in Figure 7. In order to assure that the total measurement was indeed representative of conditions, two separate measurements were made.

Atmospheric Optical Depth

Ground observations indicated a significant haze layer existing over Willcox Playa area during early morning, along with a build-up of cumulus clouds. The optical depth would therefore be unstable as the day progressed. The atmospheric optical depth, near the time of overpass, can be derived by

$$\tau = \frac{\ln M_0 - \ln M}{\sec \Theta_0}$$

where M_0 is calculated from previous data. The results are shown in Figure 8.

Target Directional Reflectance

The directional reflectance of the playa at station #2 (see page 39) was derived in the manner discussed above. Intermittent cloud shadows caused the directional reflectance measurements to be subject to some variability. The directional reflectance data is shown in Figure 9.

Spectral Reflectance Measurements of Willcox Playa Prior to Skylab-2

Willcox Playa, located in the southeastern part of Arizona, is a large dry lake which was clearly resolved on ERTS-1 imagery and on Skylab-2 multispectral photography. It is bounded on the southeast and northeast by cultivated fields and coarser alluvial slopes to the west. The playa
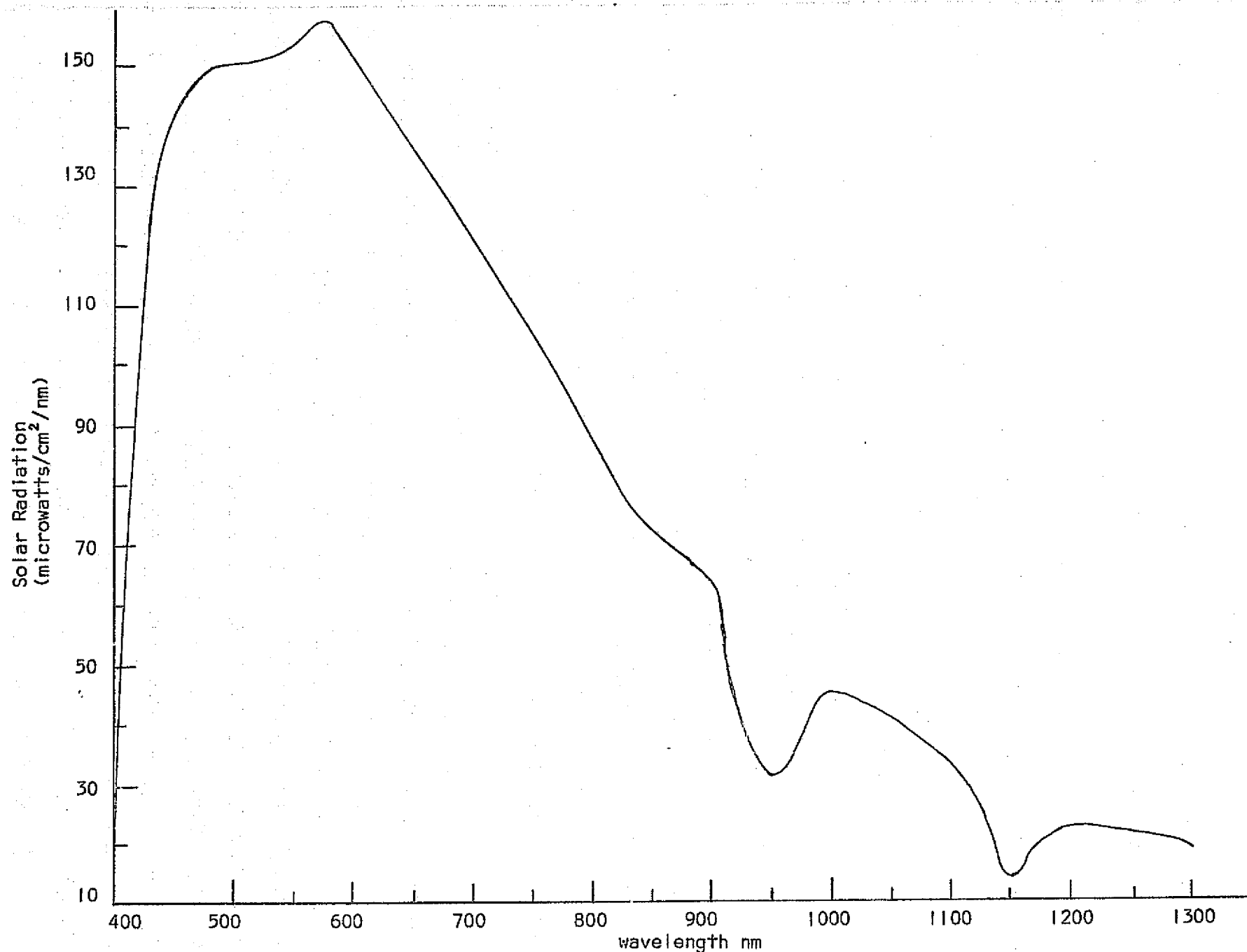
Figure 7 . Total solar radiation over Willcox Playa on 3 June 1973.

Figure 8. Atmospheric optical depths -
Willcox Playa, Arizona - at the time of
Skylab-2 overpass 1227MST.
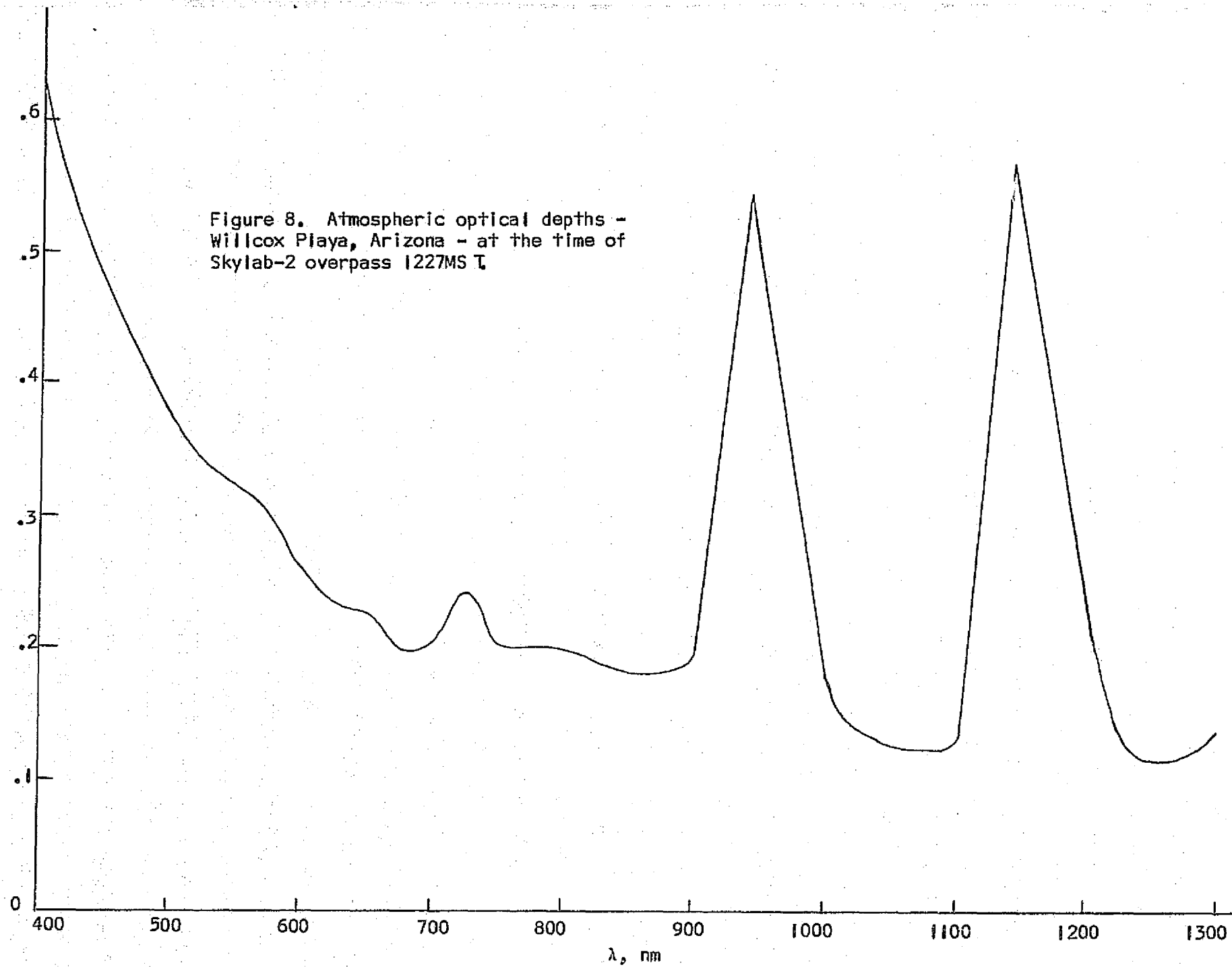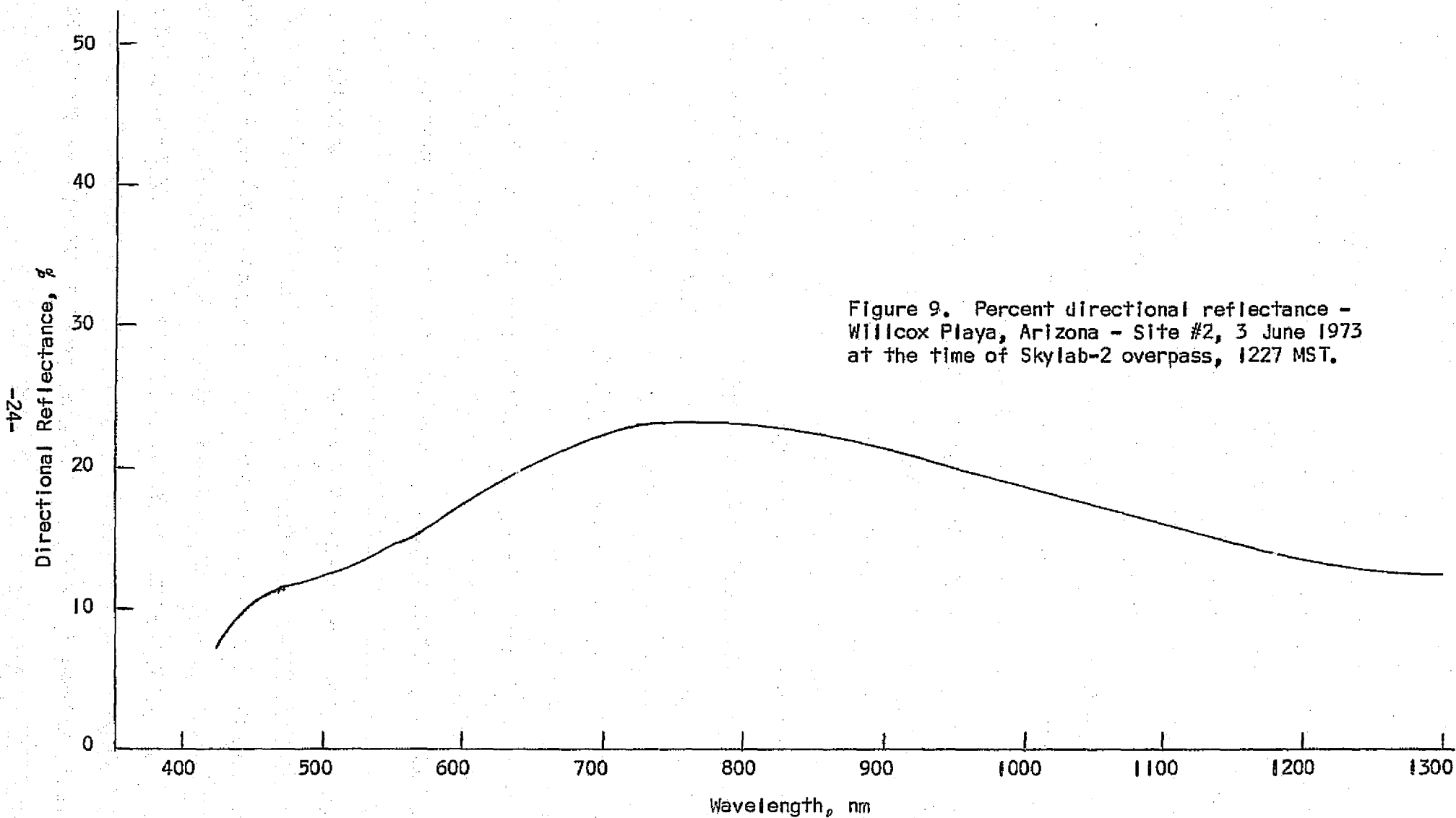
Figure 9. Percent directional reflectance – Willcox Playa, Arizona – Site #2, 3 June 1973 at the time of Skylab-2 overpass, 1227 MST.

surface is flat and periodic flooding serves as a levelling agent. Variations in sediment size and composition, as well as the availability of surface and ground water, produce a variety of landforms. The central region of the playa is hard, compact crust which has no micro-relief, except that created by mud shrinkage. The dry surface consists of mud polygons which are a light gray buff color. Soft, dry, and porous surfaces are often salt-stained and lead to the sticky-wet areas found where the water table is near the surface. The soft puffy soils are usually a light brown color depending on the salt and moisture content. The playa is dynamic and it changes in response to the surrounding terrain. The surface drainage on and adjacent to the dry lake changes as a function of the rainfall and a technique is necessary to monitor the dynamics of the area. Spectral reflectance measurements of the dry playa surface indicate a surprising degree of uniformity.

Prior to the launch of Skylab, measurements were made of the incident solar irradiance spectra at the Willcox Playa, Arizona. Simultaneous spectroradiometric radiance measurements were obtained of the playa and large plowed and grass fields adjacent thereto. These data were computer processed to provide relative percent directional reflectance data of homogeneous terrain objects large enough to be well resolved on the space imagery.

The quantitative spectral analysis of soils, vegetation, and rocks requires that simultaneous and accurate measurements of incident and reflected radiation be made. Since the spectral energy relfected by an object varies with that which is incident upon it, the spectroradiometric measurement must be made at the same instant of time. The arrangement of the instrumentation used to obtain simultaneous measurements of incident

and reflected radiation is shown in Figure 10. Two instruments were required to obtain reflected radiance measurements due to photo-multiplier sensitivity limitations.

A spectroradiometer, using a wedge interference filter system enabling the spectrum from 380-1250 nm to be continuously scanned, was used to measure the spectral distribution of incident solar irradiance. The instrument was equipped with a diffusing screen so that its directional response was proportional to Lambert's cosine law. This technique of measuring incident irradiance was used since solar energy falls upon the earth's surface and is reflected into an entire hemisphere, regardless of its original direction of propagation. True cosine response also eliminates the need for precise aiming to the instrument.

Whereas a radiometer measures in units of energy rate intensity such as microwatts per centimeter square, a spectroradiometer measures in units of energy rate intensity per bandwidth, such as microwatts per centimeter square per nanometer. This latter system of units is most meaningful for measurements of radiation since a graph of the spectral distribution of radiant intensity versus wavelength can be obtained. The area under such a curve can be made numerically and dimensionally equal to energy available in the spectral bands of the S-190A multi-spectral photographic camera and S-191 infrared spectrometer. The spectroradiometer used was capable of measuring from 0.01 to 1000 microwatts per centimeter square per nanometer. These values correspond roughly to illumination levels of 0.03 to 30,000 foot candles.

The calibration of the spectroradiometer was verified before and after the experiment. A spectral standard lamp, serially numbered and
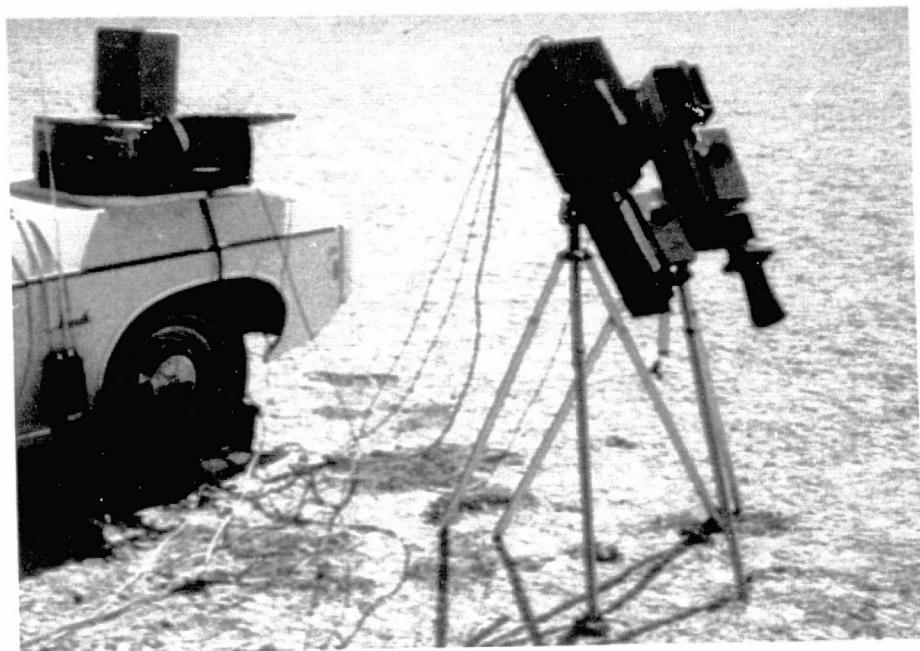
Figure 10. Arrangement of instruments for measuring the spectral distribution of incident and reflected solar radiation in the 380-1250 nm region of the spectrum.

calibrated against the National Bureau of Standards reference, was used. The lamp was of the ribbon filament tungsten type and had a nominal accuracy of plus or minus five percent relative to the NBS standard.

The half bandwidth of the spectroradiometer used to measure the incident illumination is approximately 15 nanometers in the 380-750 nm range and 30 nanometers in the 750-1250 nm range. Stray light response to unwanted wavelengths of 15 nm bandwidth and far from the wavelength of interest is usually in the order of 0.01 percent.

The periodic calibration of the spectroradiometer used for measuring incident sunlight allowed an accuracy of plus or minus seven percent

in the long wavelengths and plus or minus ten percent in the short wave-
lengths of the spectrum. Most of this error, of course, comes from
uncertainty in the secondary standard used. The relative accuracy of
all points with respect to each other throughout the wavelength range
measured is approximately plus or minus three percent.

The reflectance radiometer system allowed measurements of the average
power of the solar radiation reflected by soils and vegetation in the
Willcox Playa area. By means of a grating monochromator, these readings
can be made at selected wavelengths over a bandwidth determined by the
grating and slits. This instrument basically consists of an optical
system which limits the entrance of energy to a twelve degree field,
a monochromator grating to spectrally isolate the visible energy to a
five nanometer halfband pass, and the infrared energy to a ten nanometer
halfband, as well as detector heads to sense the magnitude of the inci-
dent energy.

The reflectance spectroradiometer is designed so that light re-
flected from an object passes through a diffuser system and is directed
by the collective lens into the monochromator housing via the entrance
slit. Calibration accuracy is obtained when the light incident on the
diffuser is imaged on the entrance slit, completely filling the slit
area with light. A collective lens in the beam input optics in front
of the monochromator entrance slit, collects the incident light which
is properly matched with the diffuser to create a uniform illuminating
bundle inside the monochromator housing. This bundle of light is then
incident on a plane diffraction grating where it is angularly disper-

sed according to wavelength. Each wavelength present in the source
bundle reflects off the diffraction grating at a different angle. The
grating can be rotated to direct any selected wavelength bundle onto
the center of a concave mirror. The mirror collects the light and,
with the help of a quartz corrector lens, forms an image of the entrance
slit on the exit slit.

The visible range grating is a 1350 groove per millimeter grating
covering from 350-800 nanometers in the first order and is blazed at
500 nanometers. The reciprocal linear dispersion is 6.4 nanometers per
millimeter. The combination of grating and slits determines the dis-
persion of the system. The effective widths of the visible grating was
20 nanometers as determined by the entrance and exit slit widths are
2.68 and 1.5 millimeters respectively. These particular grating widths
were selected in order to obtain sufficient photomultiplier response
when measuring targets of low reflected brightness.

The visible spectroradiometer utilized a photo diode detector to
produce a signal proportional to the intensity of the light which strikes
it. However, in order to obtain sufficient sensitivity in the infrared,
a cooled photomultiplier detector must be used to produce an output
signal which is of sufficient amplitude to allow significant results
to be obtained.

Readout was accomplished using a self-ranging picoammeter. This
device has the advantage of displaying digitally the detector current
output of the spectroradiometers. Thus calibration and dark current
values can be readily obtained and monitored. In addition, no scale
switching is required and readings can be obtained rapidly.

In order to obtain accurate data, the spectroradiometers were calibrated before and after the experiment. The calibration of the instrument can shift due to such factors as the collection of dust on the optical surfaces or a variety of other random factors. The electronic circuitry of the instrument is very stable and maintains uniform response but, nevertheless, the accuracy of the instrument was verified.

Data Analysis Techniques:

If a sufficient number of sets of independent measurements of incident and reflected radiation (at 27 points in the spectrum from 350-1100 nm) are made and the readings averaged at each wavelength, it is possible to make the Central Limit Theorem apply to the distribution of average reflectance values. Thus,

$$z_{ij} = [\frac{x_{ij1}}{y_{ij1}} \quad \frac{x_{ij2}}{y_{ij2}} \quad \frac{x_{ij3}}{y_{ij3}}] \frac{100}{n}$$

where: x_{ijk} = the k th measurement of reflected radiation at wavelength i, object j.

y_{ijk} = the k th measurement of incident solar radiation at wavelength i, object j.

z_{ij} = the average percent directional reflectance at wavelength i, object j.

n = number of readings.

By the Central Limit Theorem, the distribution of z_{ij} will be approximately normal regardless of the distribution of the individual values of x_{ijk} and y_{ijk}. This, of course, assumes that measurement errors are independent and randomly distributed.

A flow diagram of this computer program is shown in Figure II.

Note: Computed for (I) each wavelength, and (2) each object.
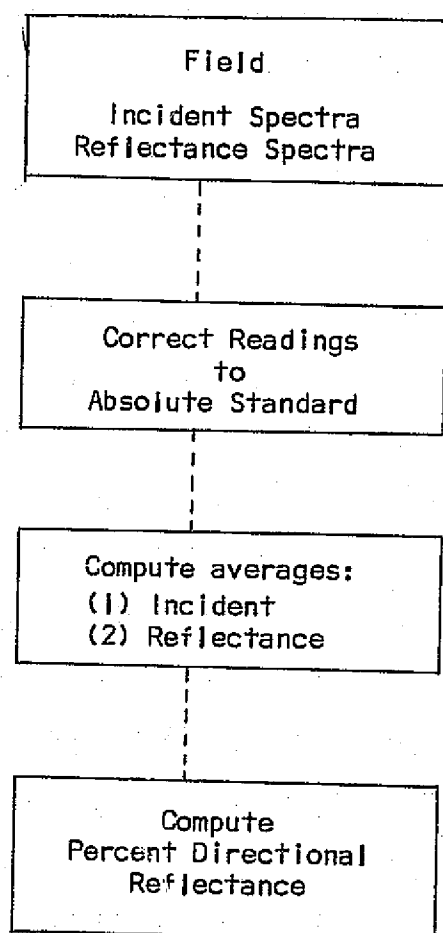
Figure II.   Flow diagram of percent directional reflectance readings.

Computer Output:

. The computer output format of the computations performed on the incidence and reflectance spectra is shown in Figure I2.   Associated with each wavelength (first column) is the instrument reading (second column) and corrected value of incident sunlight (third column) in

microwatts per square centimeter. The reflectance measurements and

associated corrected readings (which are determined by the standard

lamp calibration) are shown in the fourth and fifth columns.

```
DATE:3/6/73
TIME:1140-1210 MST
WEATHER + LOCATION:CLR. WILL ART
TARGET:GRASS
```

WAVE LENGTH (NM)	SUN READING (UW)	ACT. SUN SPECTRA (UW)	REFLECT READING (W*E-10)	ACT. REF SPECTRA (UW*E-2)	PERCENT DIR. REF (E-1)
380	15.5	72.912	1.033	6.225	.853768
400	66	105.336	3.58	11.929	1.13247
425	127	131.699	6.27	19.1724	1.45977
450	179	151.255	10.41	27.7316	1.78719
475	205	160.105	12.38	30.4089	1.89894
500	204	153	13.3	30.7696	2.01123
525	195	139.815	21.7	47.2382	3.37919
550	168	133.92	23.1	57.1494	4.25743
575	160	132	16.89	47.5724	3.60397
600	178	124.778	12.2	48.4064	3.85825
625	169	117.793	7.88	33.6515	2.85694
650	167	111.222	4.43	27.715	2.49186
675	176	113.344	2.89	22.3045	1.96756
700	145	97.73	1.577	55.5071	3.55595
725	147	88.641	1.643	77.3462	8.72579
750	125	81.73	.917	115.791	14.1641
750	* 93	88.9735	5145.46	119.451	13.4341
750	61	96.197	12286.	123.171	12.8941
800	53	79.223	12650.	121.945	15.3919
850	53	71.333	12673.	111.876	15.6925
900	44	58.872	9490.	81.7030	13.9791
950	32	41.824	4550.	47.6385	11.3932
1000	36.5	45.8075	3250.	55.879	12.1937
1050	34.5	39.675	1153.	54.2915	13.6841
1100	38	29.91	218.	42.51	14.2126
1150	16.5	15.9825	23.8	24.9959	15.6922
1200	19	15.435	10.7	34.4487	22.2469

* = AVERAGE OF TWO INSTRUMENT READINGS

Figure 12. Computer output format of incident and reflectance spectra.

The percent directional reflectance value shown in the sixth column

is the ratio of the value in the fifth column divided by that in the third

column. The last column is the value of a standard illuminant times the

percent reflectance. Thus, the actual power reflected by an object can be

computed by knowing the incident radiation and the data in the sixth column

of this output.

Figure 13 shows the associated computer plot of percent directional reflectance as a function of wavelength. This is an example of the percent directional reflectance of grass obtained in situ. The chlorophyll reflection band at 550 nm and chlorophyll absorption band at 675 nm are clearly evident as is the mesophyll reflection above 725 nm.

Incident Solar Radiation:

The intensity and spectral distribution of solar radiation falling upon the earth's surface varies with solar angle and atmospheric conditions. Measurement of the absolute amount of solar energy which strikes the terrain is important since all ground objects reflect different amounts of radiation in each spectral band which is in direct proportion to that which is incident.

Theoretical analysis of solar illumination based upon air mass calculations and Raleigh scattering are of little practical value in predicting the spectral distribution of solar energy which actually reaches the ground. This is primarily due to the existence of unknown amounts of Mie scattering and absorption in the atmosphere due to particles which are large compared to the wavelength of the radiation.

Figure 14 demonstrates this condition. Spectroradiometric readings of solar energy (both sunlight and diffuse skylight) using a lambertian detector were measured during a four day interval at Willcox, Arizona. Spectral intensity in microwatts per centimeter squared per nanometer from 380-1200 nanometers is shown for four of these measurements between 1104 and 1515 MST on March 6, 1973.
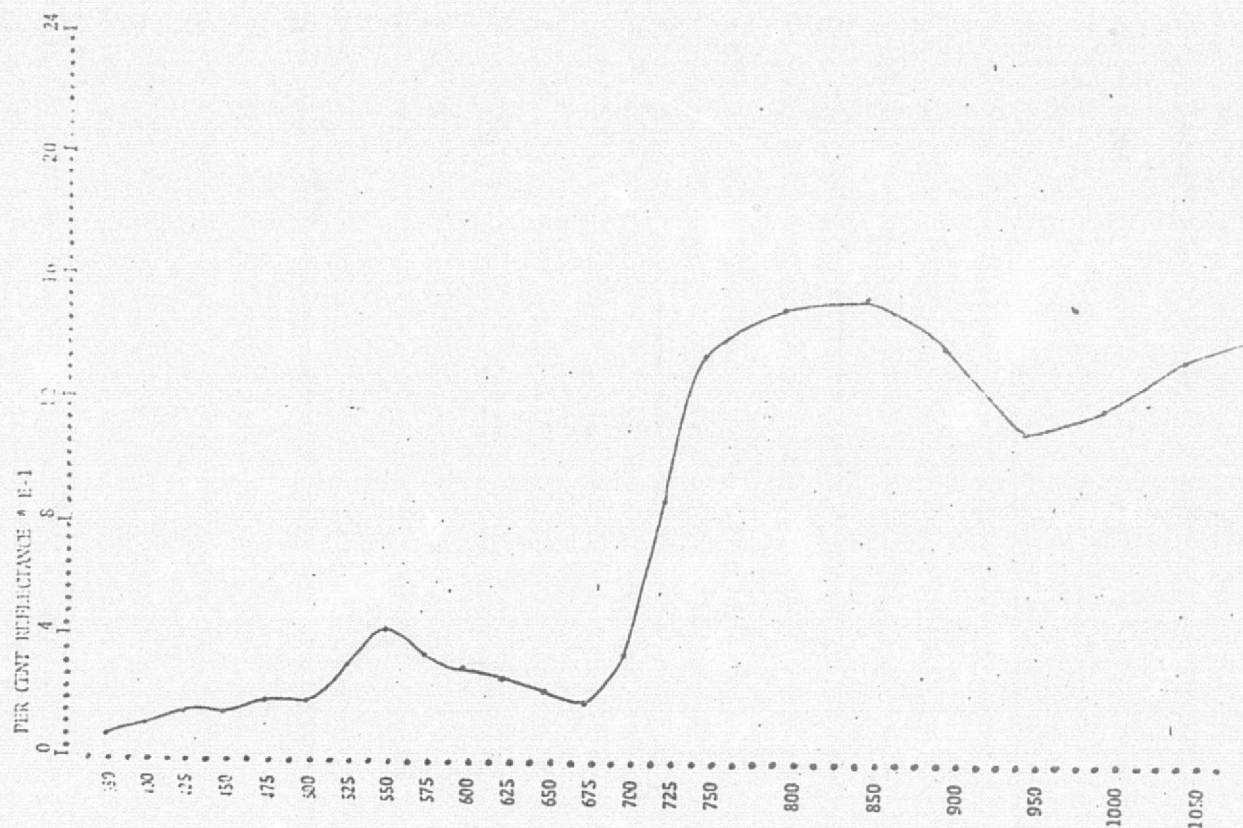
Figure 13. Computer plot of percent directional reflectance as a function of wavelength.
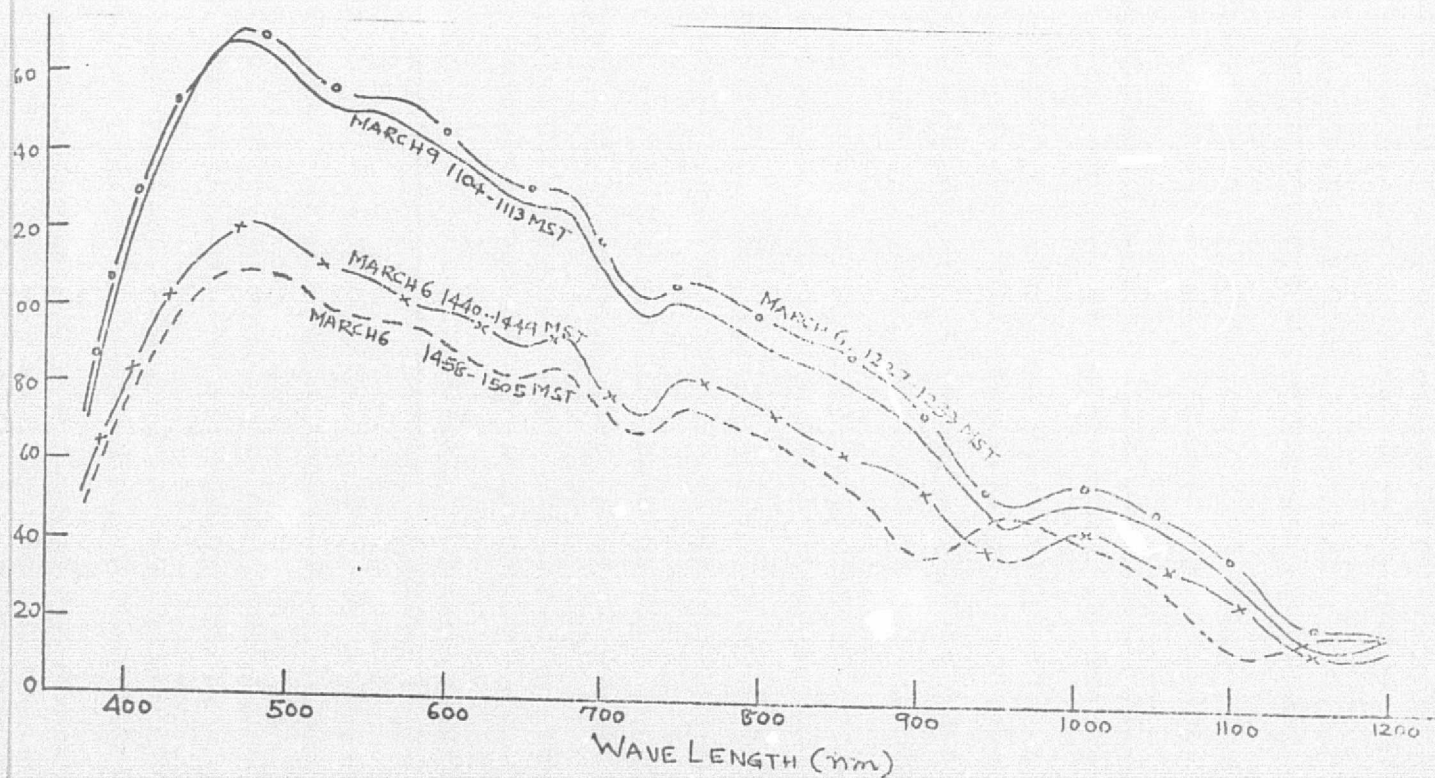
Figure 14. Spectral distribution of solar radiation incident at the Willcox Playa test site at different times during the day.
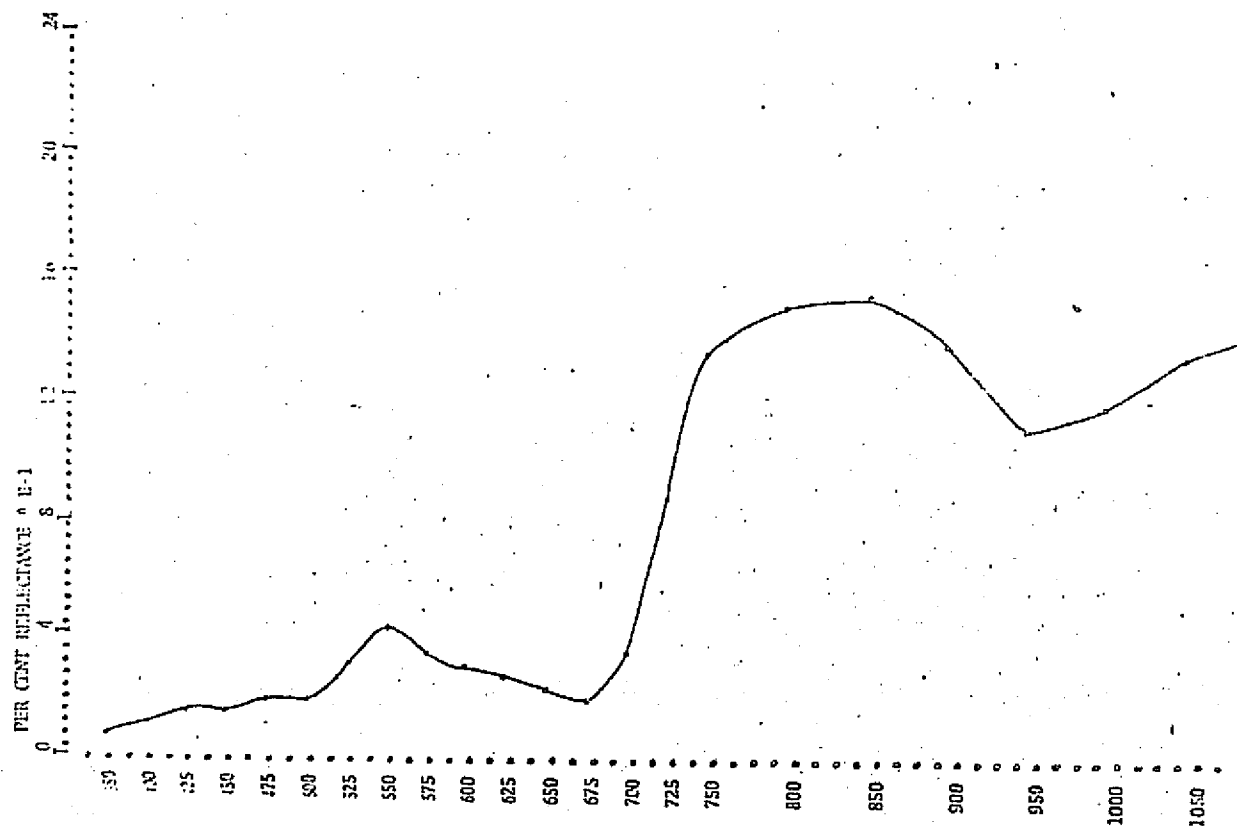
Figure 13. Computer plot of percent directional reflectance as a function of wavelength.
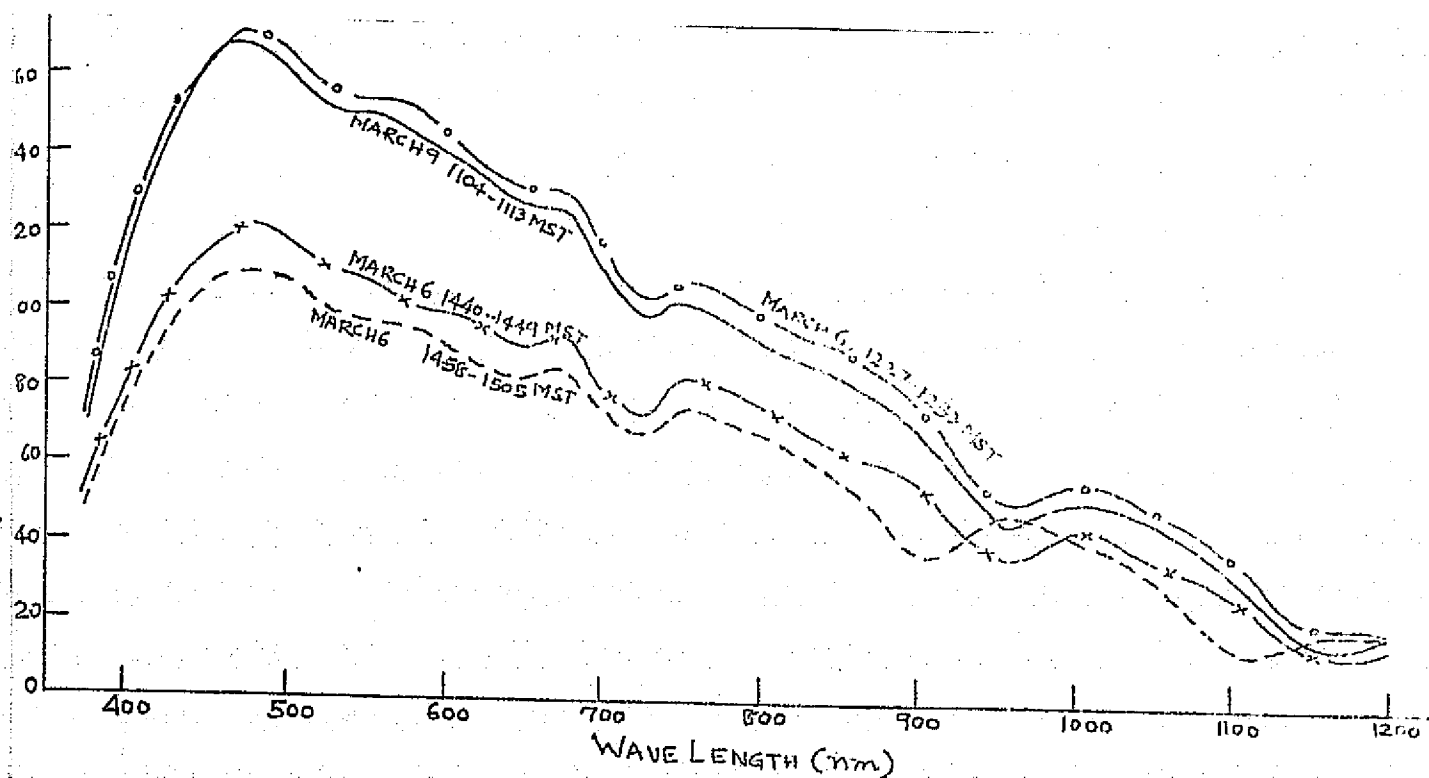
Figure 14. Spectral distribution of solar radiation incident at the Willcox Playa test site at different times during the day.
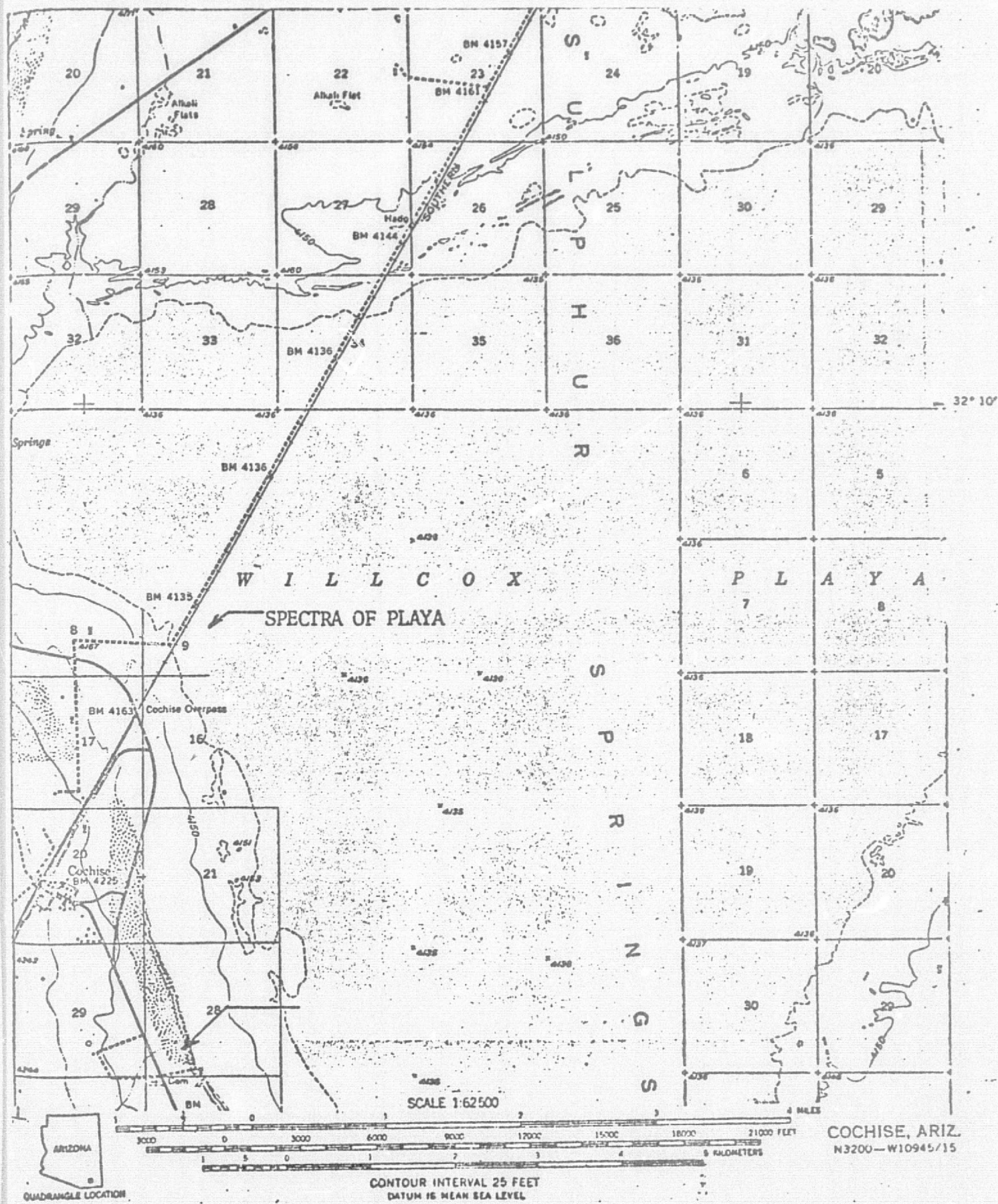
Figure 15. Location at which incident and reflectance spectra were measured.
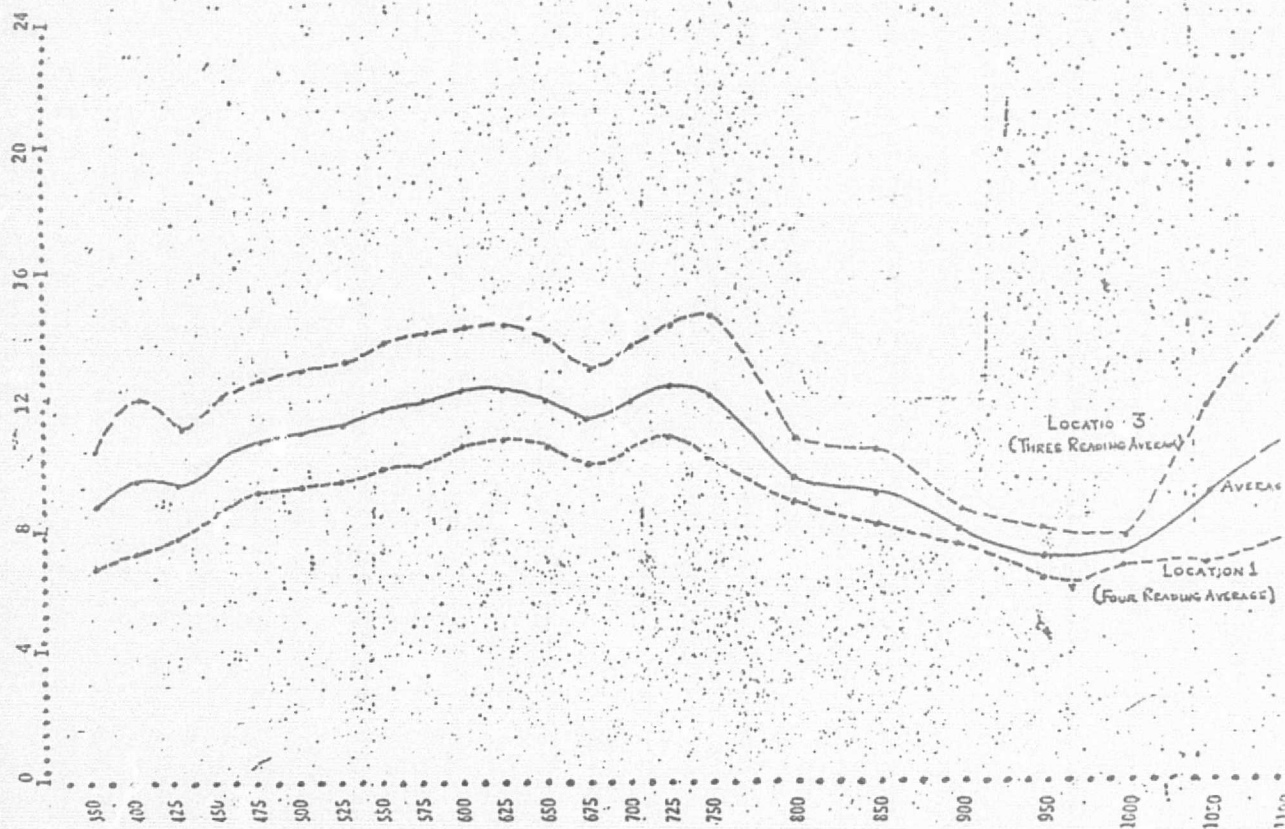
Figure 16. Percent directional reflectance of two locations on the Willcox Playa, Arizona.

The first feature clearly evident from this data is the large variation in intensity with wavelength as a function of time (solar angle). The characteristic absorption band below 380 nanometers at 725 and 950 nanometers is also clearly evident.

The percent directional reflectance of the Willcox Playa, Arizona, was obtained for two adjacent areas at the location shown in Figure 15. Simultaneous spectroradiometric measurements of incident global solar radiation were made along with measurements of the radiation reflected by the playa.

The reflectance spectroradiometers were oriented so as to prevent

any specular reflection from the playa surface from entering the input optics of the instrument. The partly cloudy atmospheric conditions that existed required that extreme care and patience be used in making these measurements.

The incident and reflected spectroradiometric data were corrected and the percent directional reflectance calculated using the computer program discussed previously.

The percent directional reflectance data presented in Figure 16 indicate considerable uniformity in the reflectivity of the playa surface. Although there appears to be slight brightness differences between the two areas, the shape of the reflectance curves is quite similar.

Additional Reflectance Spectra of Willcox Playa

The reflectance spectra of twelve locations in the Willcox Playa was obtained in the Fall of 1973. The precise locations recorded on two separate occasions are shown in Figure 18. The appearance of the Playa from the roadway is shown in Figure 19; Figure 17 is a photograph of the Playa also looking eastward.

The incident solar radiation falling on the Playa measured in micro watts per square centimeter per nanometer at 1022 PDT on 4 September 1973 is shown in Figure 23.

Figure 17. Willcox Playa, looking east.

The percent directional reflectance of the twelve locations on the Playa is shown in Figures 24 and 25. Considerable small local differences were found to exist about site I due to soil moisture variations and hence three sets of reflectance spectra were taken at this location. These variations in the apparent condition of the Playa are shown in the photographs in Figures 20 through 22.

Table 3, lists the percent soil moisture at each location. The soil samples were taken at the same time as was the reflectance spectra.
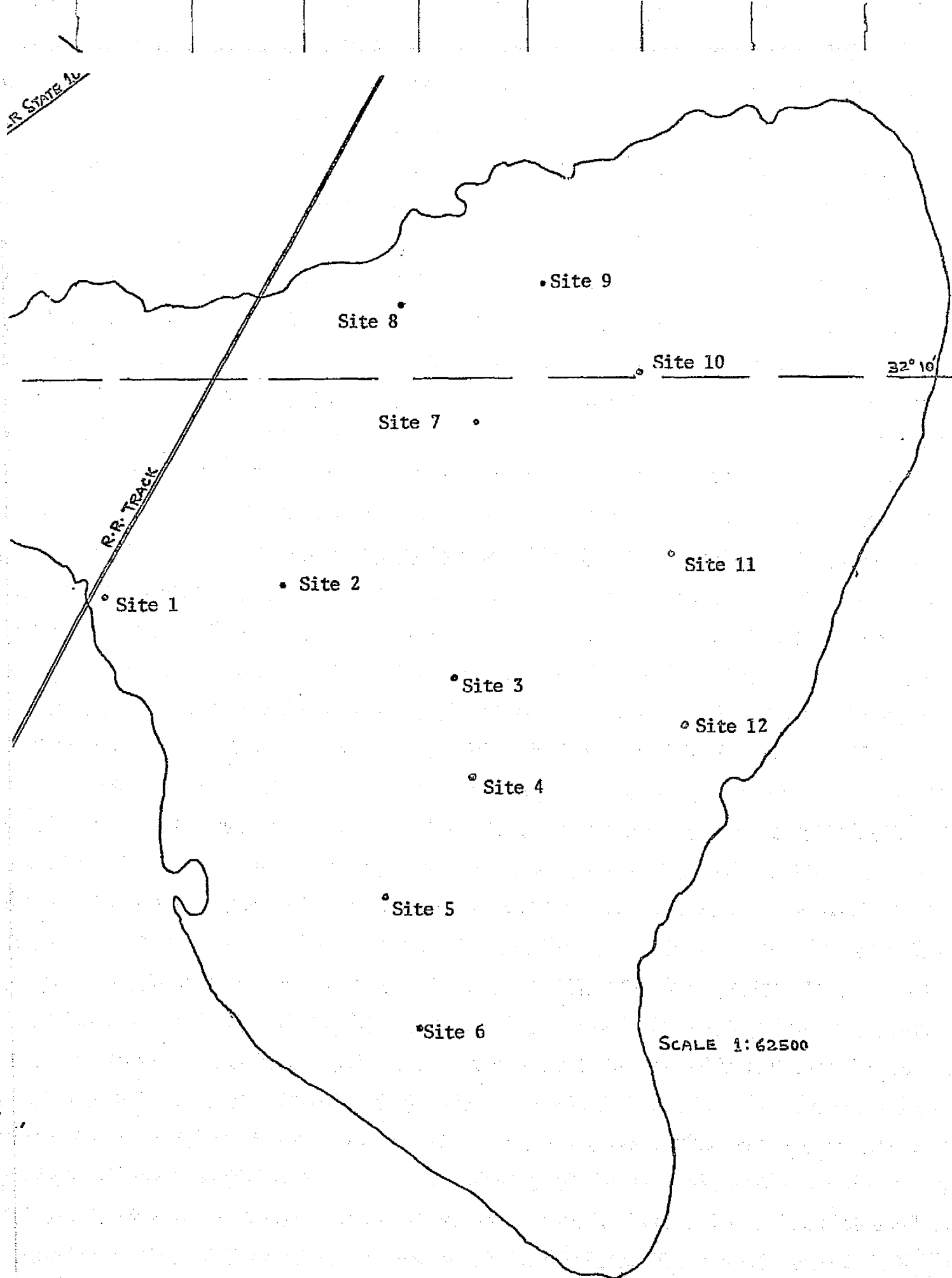
Figure 18. Locations in Willcox Playa, Arizona, where Spectra was taken during Fall 1973.

Figure 19. Willcox Playa, viewed from road looking east.

Site	Weight of Sample (grams)	Percent Soil Moisture
1A	8.7710	5.851
1B	9.5476	5.486
1C	10.6016	67.672
2	8.6695	4.191
3	8.2077	3.708
4	7.0687	3.851
5	7.7994	4.417
6	8.9289	4.288
7	8.1270	3.559
8	11.4335	3.428
9	8.8666	3.068
10	9.9244	4.590
11	8.7659	3.392
12	9.0585	3.663

Table 3. Soil Moisture at different locations in Willcox Playa, Arizona.
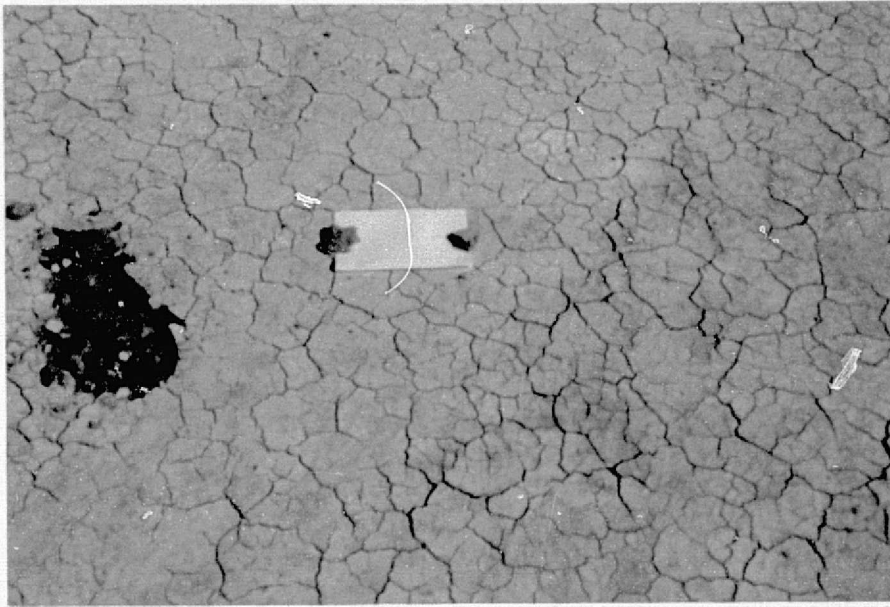
Figure 20. Willcox Playa location IA, soil moisture 5.9 percent.
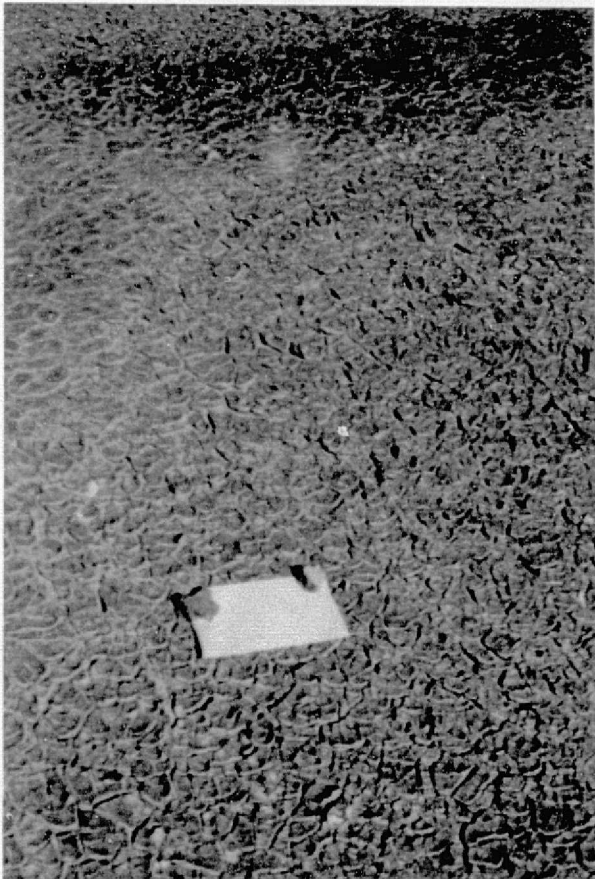
Figure 21. Willcox Playa location IB, soil moisture 5.5 percent

Figure 22. Willcox Playa location IC, soil moisture 67.7 percent
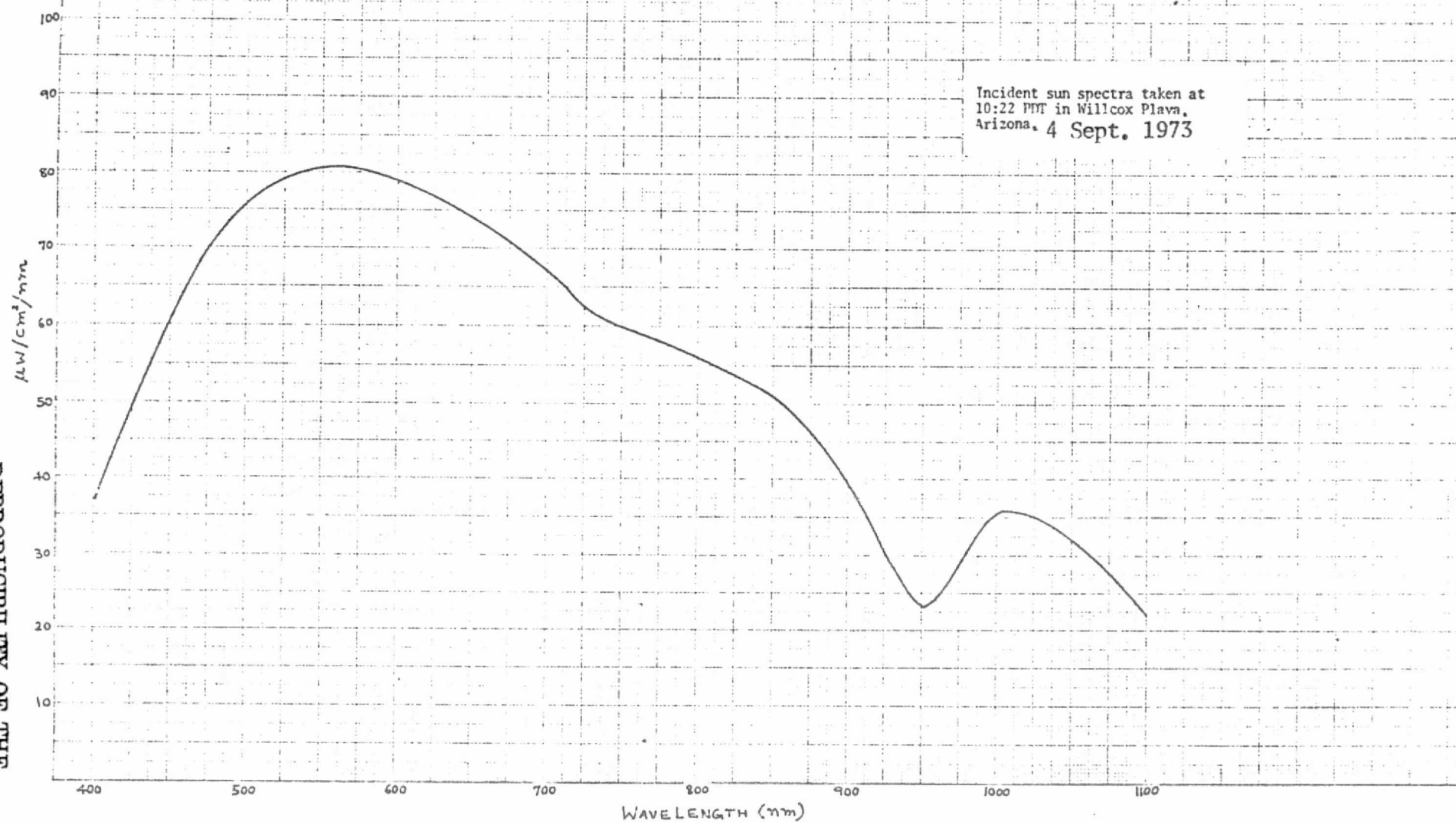
Figure 23.   Incident Sun Spectra taken in Willcox Playa on 4 September 1973.
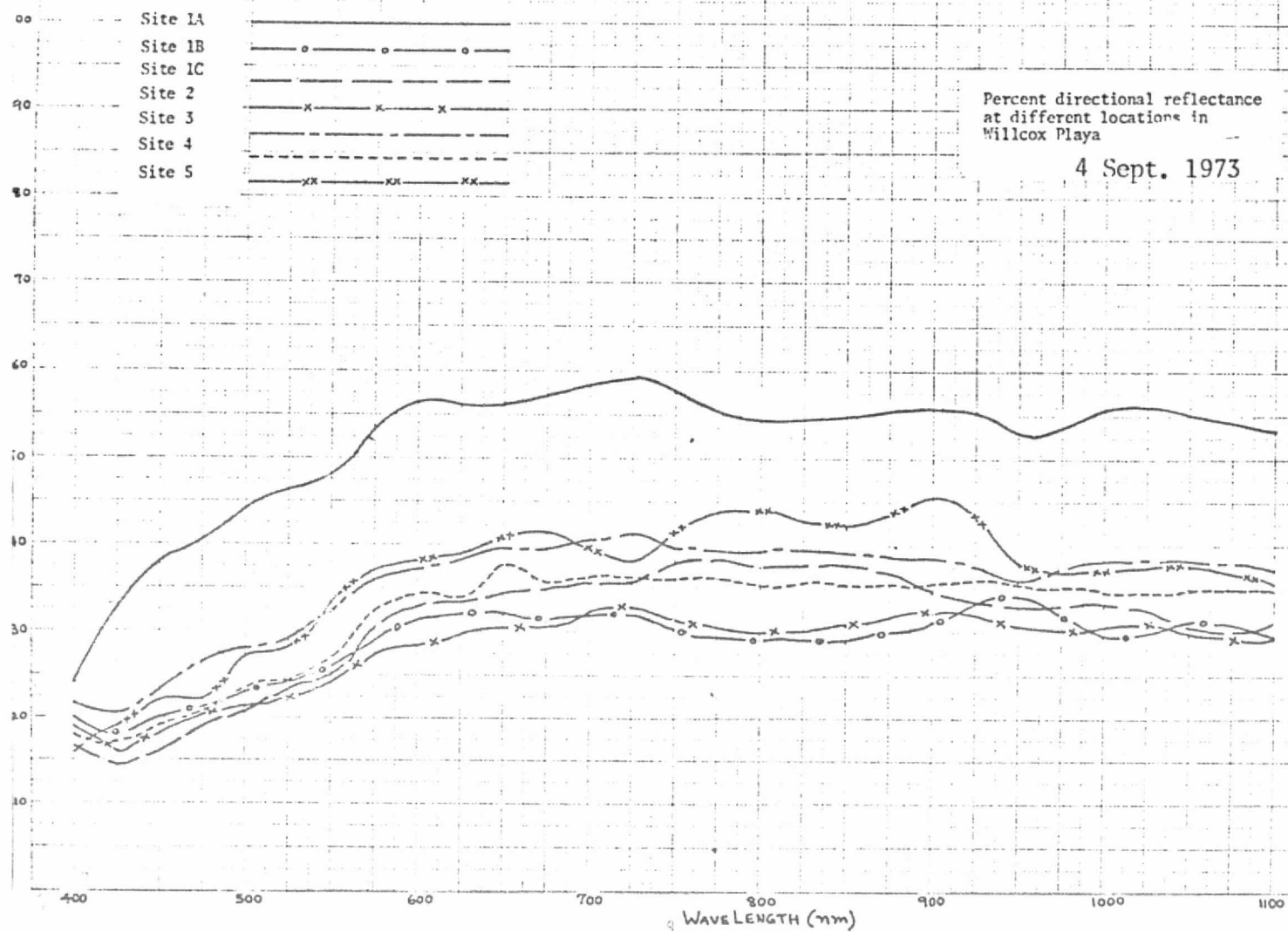
Figure 24. Percent directional reflectance at different locations in Willcox Playa on 4 Sept. 1973.
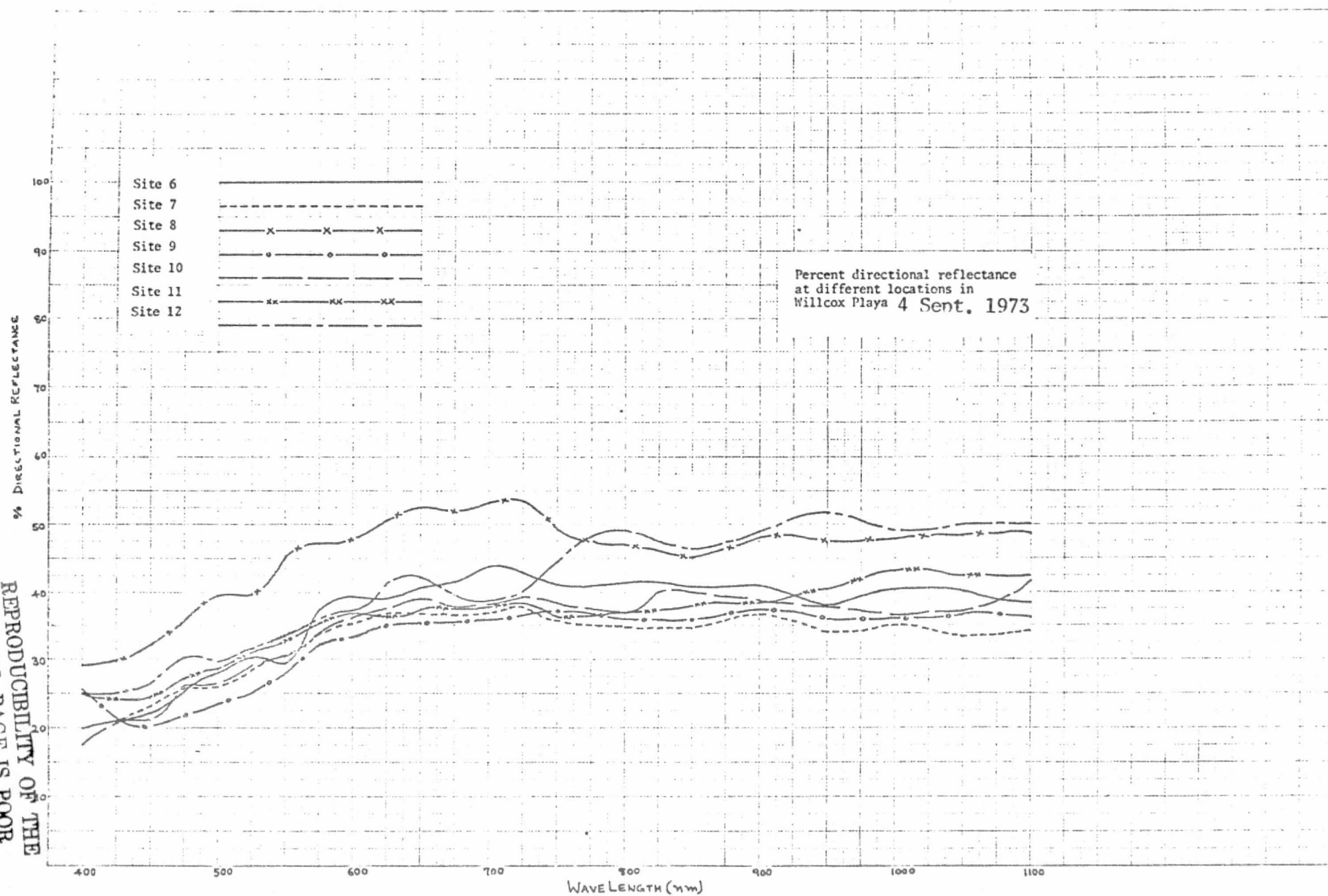
Figure 25. Percent directional reflectance at different locations in Willcox Playa on 4 Sent. 1973.

-44-

The percent soil moisture data obtained were plotted against the percent reflectance at 650 nm and 950 nm shown below.
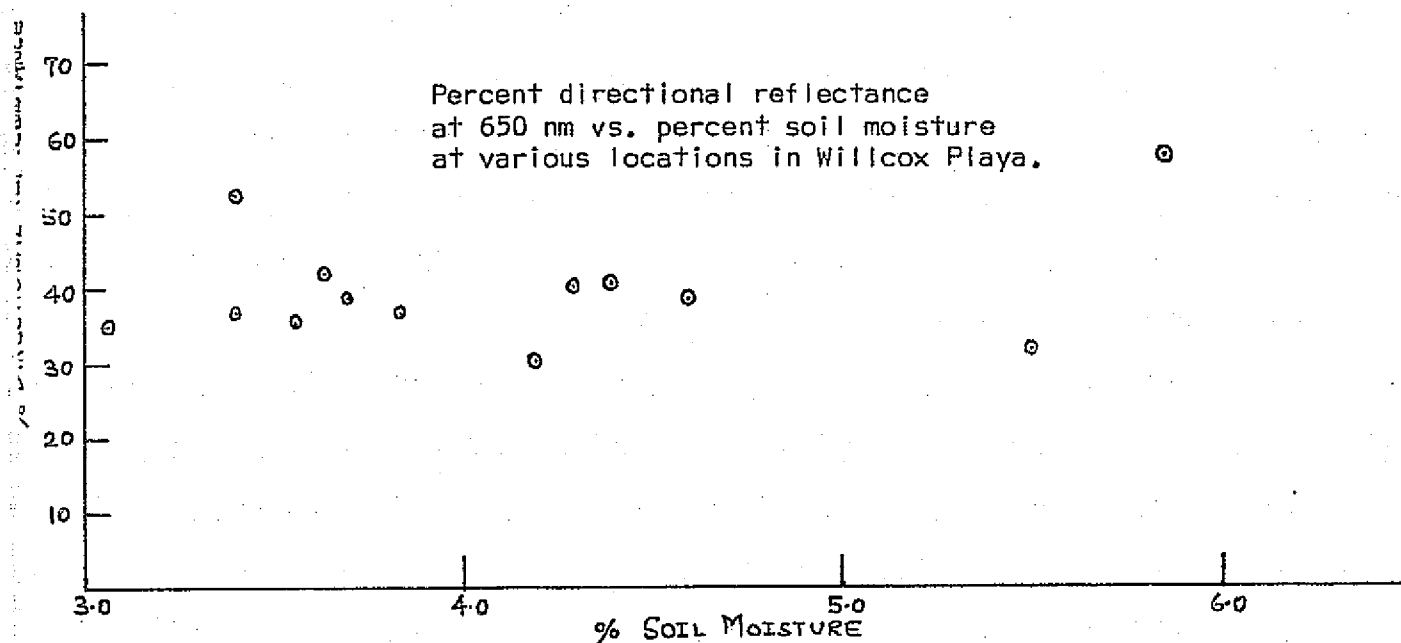
Figure 26. Percent reflectance at 650 nm vs. percent soil moisture.
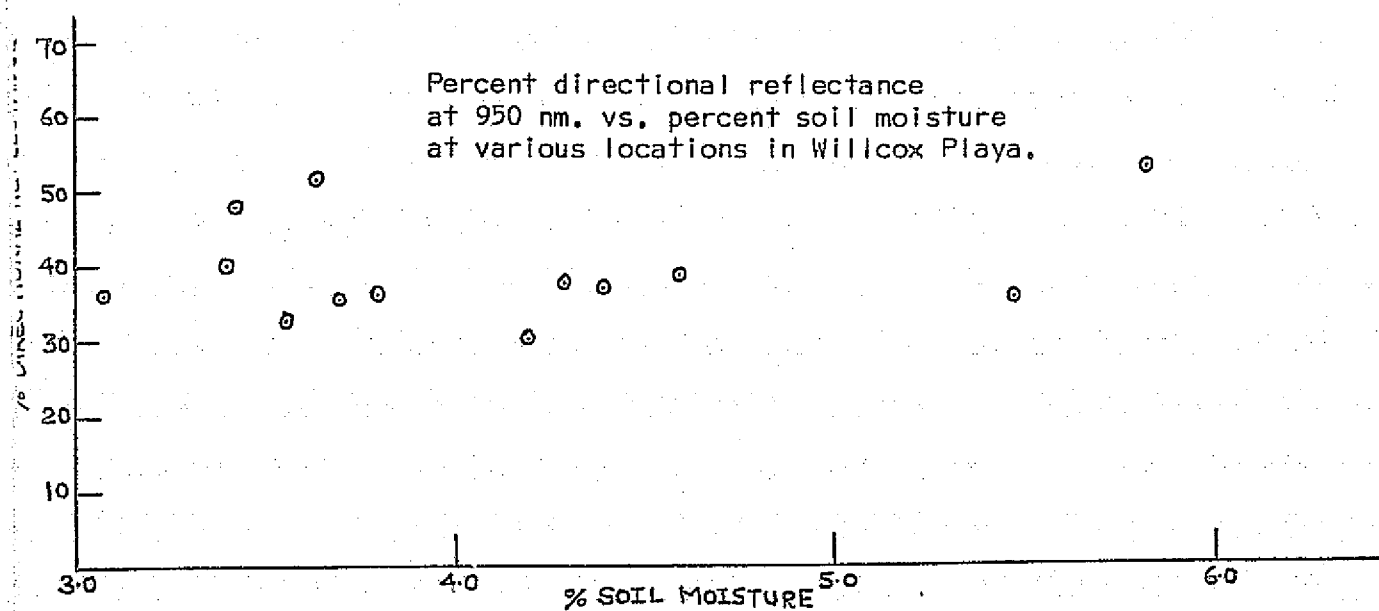
Figure 27. Percent reflectance at 950 nm vs. percent soil moisture.

Incident sun spectra taken
in Willcox Playa, Arizona,
on 16 November 1973.
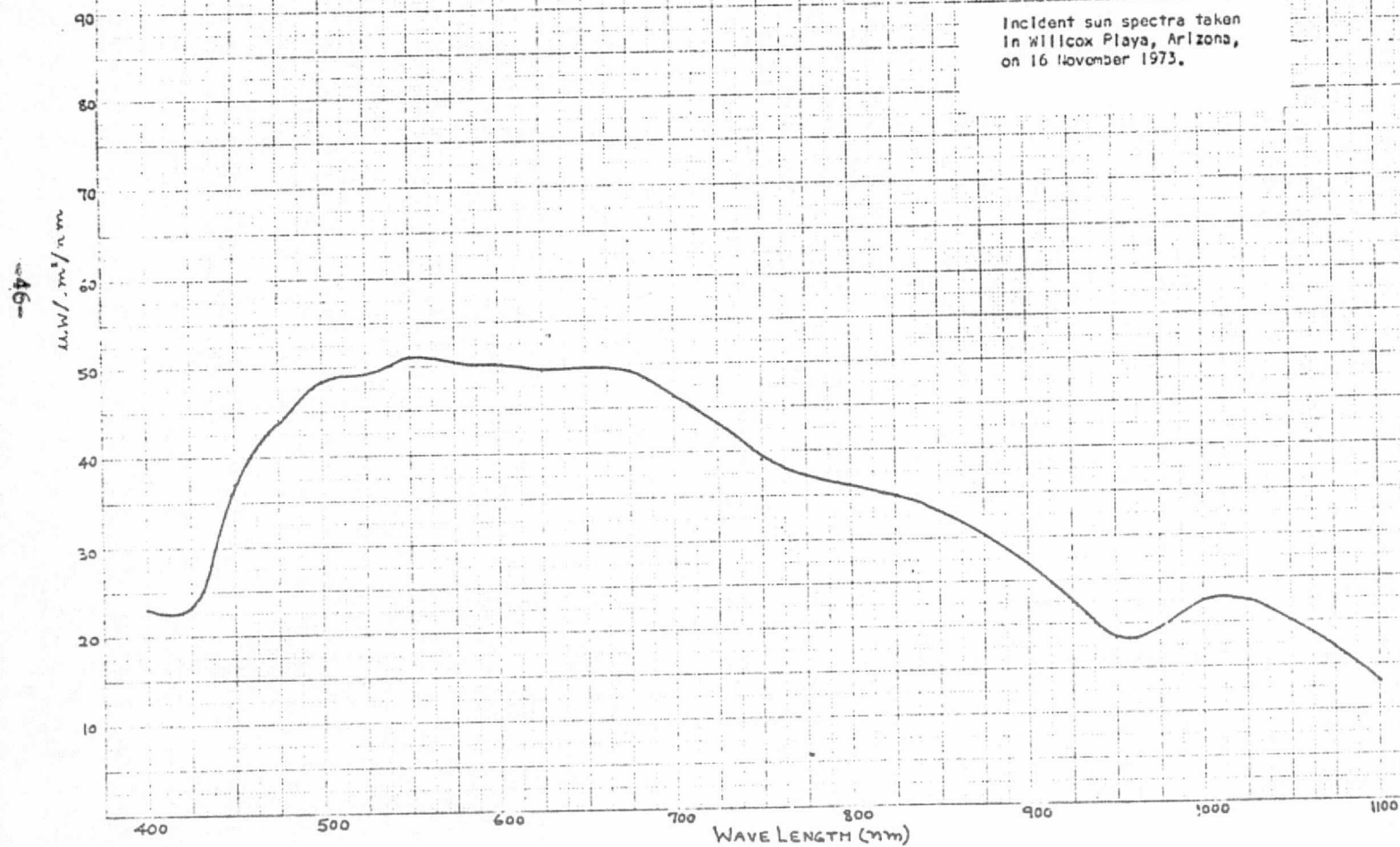
Figure 28. Incident Sun Spectra taken in Willcox Playa on 16 November 1973.
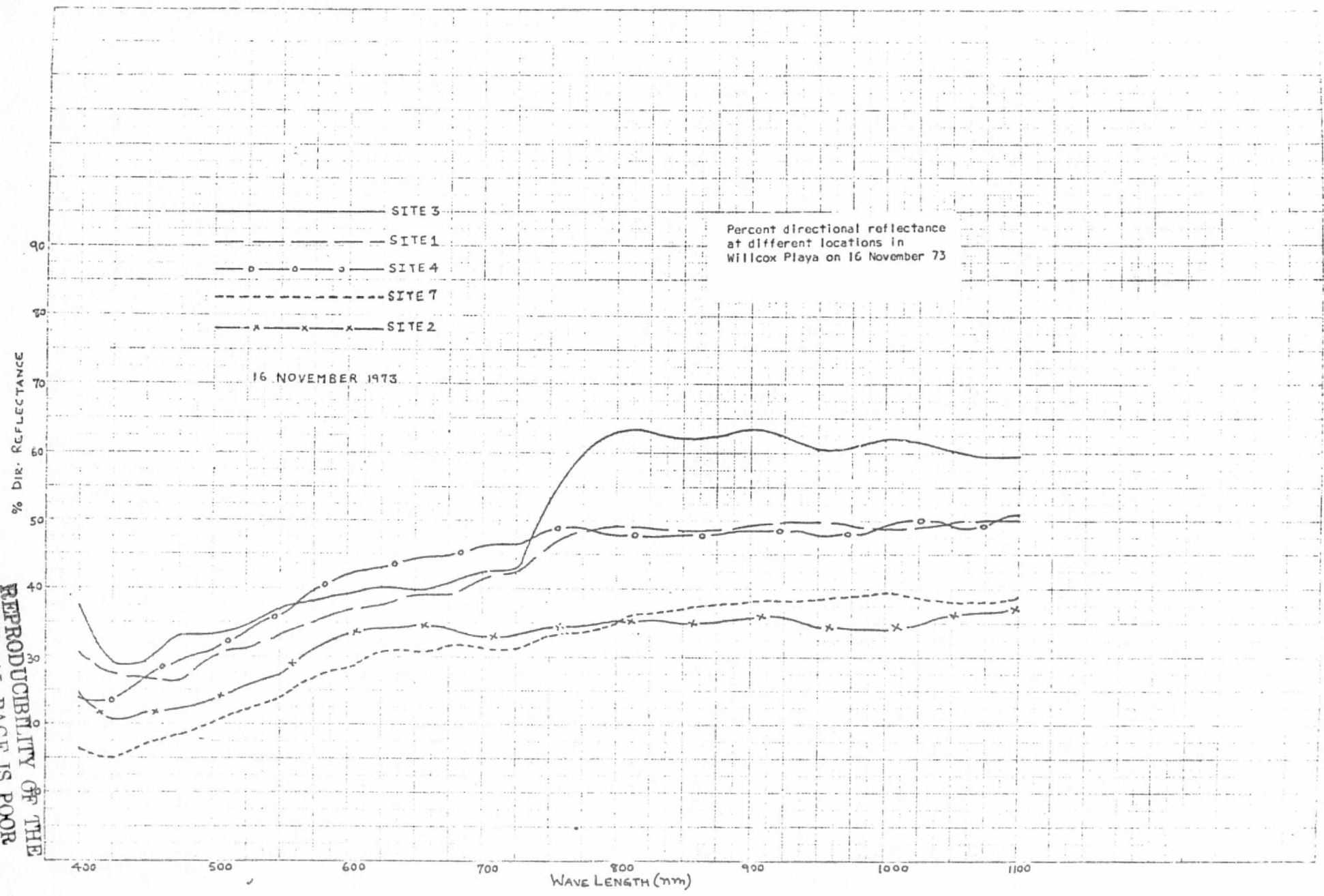
Figure 29. Percent directional reflectance at different locations in Willcox Playa on 16 November 1973.
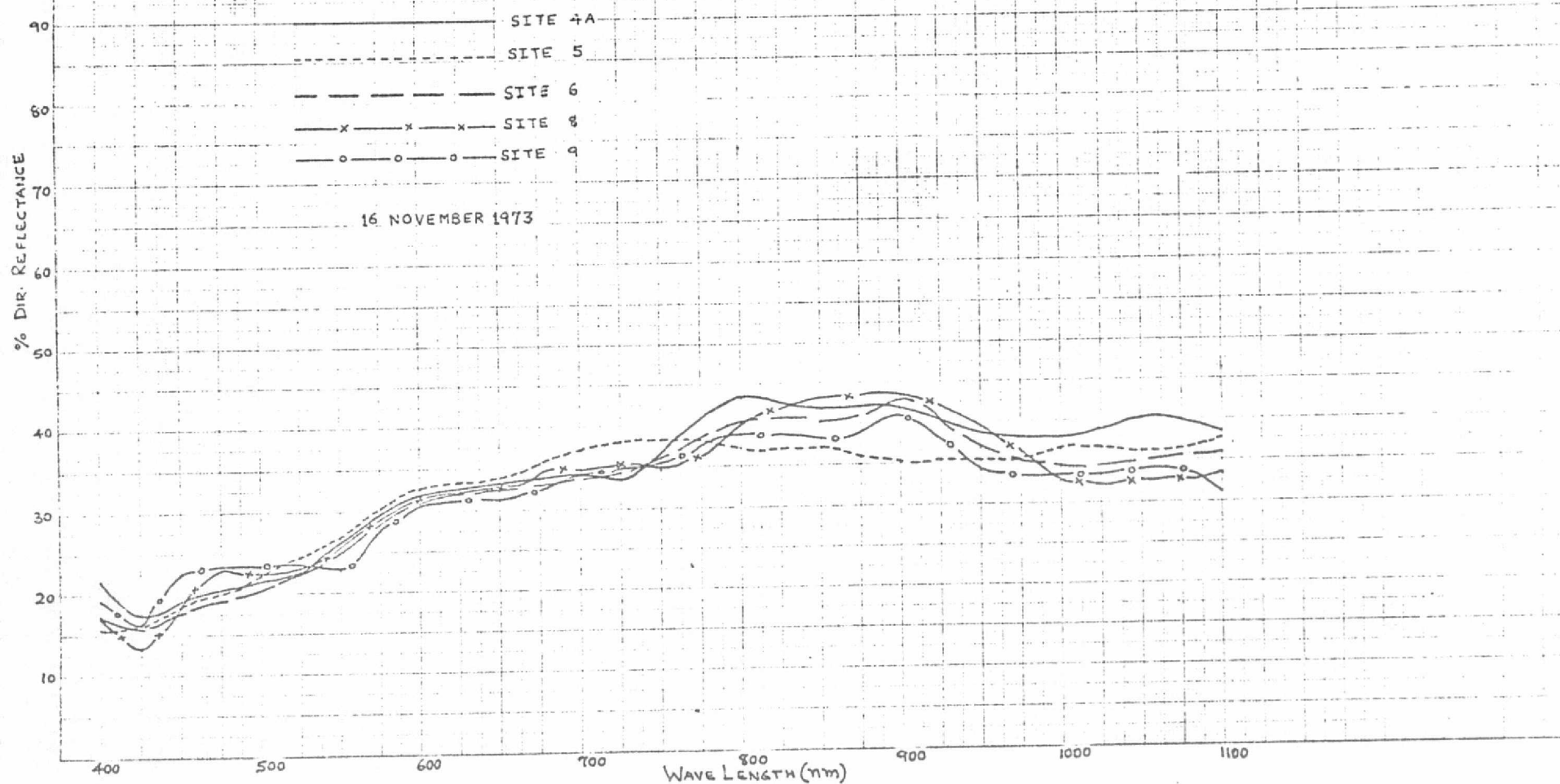
Figure 30 . Percent directional reflectance at different locations in Willcox Playa on 16 November 1973.

As can be seen from the two graphs in Figures 26 and 27, soil moisture and percent reflectance at these two wavelengths are uncorrolated on the Willcox Playa.

Figure 28 is a graph of the incident solar irradiance at the Willcox Playa measured in micro watts per square centimeter per nanometer. The data was taken on 16 November 1973, at 1020 PDT. Nine of the twelve locations shown in Figure 18 were recorded and the percent directional reflectance measured. These data are shown in Figures 29 and 30.

S-191 Spectrometer Data

The desired reflectance information is difficult to obtain directly from the S191 radiance measurements because these measurements are a function of unknown solar and atmospheric parameters caused by the atmospheric column between the sensor and the target. The radiance measured by the S191 infrared spectrometer from a given target, depends not only upon the absorption and scattering by the atmosphere between the target and the sensor. This atmospheric column attenuates the radiance reflected from the target to the sensor and adds to the radiance by backscatter of sunlight from the atmosphere.

Spectral radiance measurements in watts/$(cm^2$-Ster-μ) were obtained by Skylab S191 sensor over Willcox Playa on 3 June 1973. This experiment was performed during EREP Pass 3, Ground Track 6 (Rev. 290/291) and the time of pass over the site was 19:26:27 GMT.

The Skylab S191 visible/infrared spectrometer covers the visible, near-infrared, and thermal infrared regions of primary interest to earth resources. The data is recorded by the following six high-speed channels:

1. Thermal detector output for source radiance greater than reference radiance, designated A1.

2. Thermal detector output source radiance less than reference radiance, designated A6.

3. Si detector output at high gain, designated A3.

4. Si detector output at medium gain, designated A5.

5. Si detector output at low gain plus PbS detector output, designated A2.

6. Voltage proportional to filter wheel position, designated A4.

The voltage output of each detector is proportional to the difference between the radiance into the spectrometer aperture and radiance from the appropriate reference source - the temperature controlled black body in the thermal channel and the black chopper blade in the short wavelength channel.

In this report, only the radiance data recorded between 400 and 1100 nm was examined. The data is recorded by the short wavelength channels A3 and A5 for this part of the spectrum. Channel A3 contains the most accurate values until it saturates, then A5 should contain values accurately until A3 desaturates.

Short wavelength radiance data from channels A3 and A5 at five different points in Willcox Playa is presented in Table 4. These five different sets of data were closest to the exact time of Skylab overpass. A graph of the average of these five sets of S-191 data appear in Figure 31.

Start Time Stop Time	19:26:24.59 19:26:25.54	19:26:25.54 19:26:26.49	19:26:26.49 19:26:27.44	19:26:27.44 19:26:28.39	19:26:28.39 19:26:29.34
Wave Length (nm)	Aperture Rad. 10^{-2} Watts cm^2-nm-Ster.	Aperture Rad. 10^{-2} Watts cm^2-nm-Ster.	Aperture Rad. 10^{-2} Watts cm^2-nm-Ster.	Aperture Rad. 10^{-2} Watts cm^2-nm-Ster.	Aperture Rad. 10^{-2} Watts cm^2-nm-Ster.
400	.361	.393	.379	.375	.377
440	.951	1.021	1.017	1.018	.998
480	1.478	1.495	1.513	1.488	1.500
520	1.456	1.465	1.460	1.441	1.452
560	-	-	-	-	-
600	-	-	-	-	--
640	-	--	-	-	-
680	-	-	-	-	-
720	1.551	1.551	1.541	1.540	1.543
760	1.453	1.449	1.441	1.442	1.438
800	1.477	1.457	1.448	1.449	1.433
840	1.289	1.281	1.277	1.278	1.272
880	1.117	1.098	1.104	1.105	1.099
920	.704	.687	.686	.708	.687
960	.462	.464	.458	.462	.460
1000	-	-	-	-	-

Skylab Mission: 2

EREP Pass: 3

Flight Date: 3 June 1973

Ground Track: 6

Site: Willcox Playa

Time of Overpass: 154:19:26:27 GMT

Table 4. Five sets of radiance data (S191) over Willcox Playa taken on 3 June 1973.
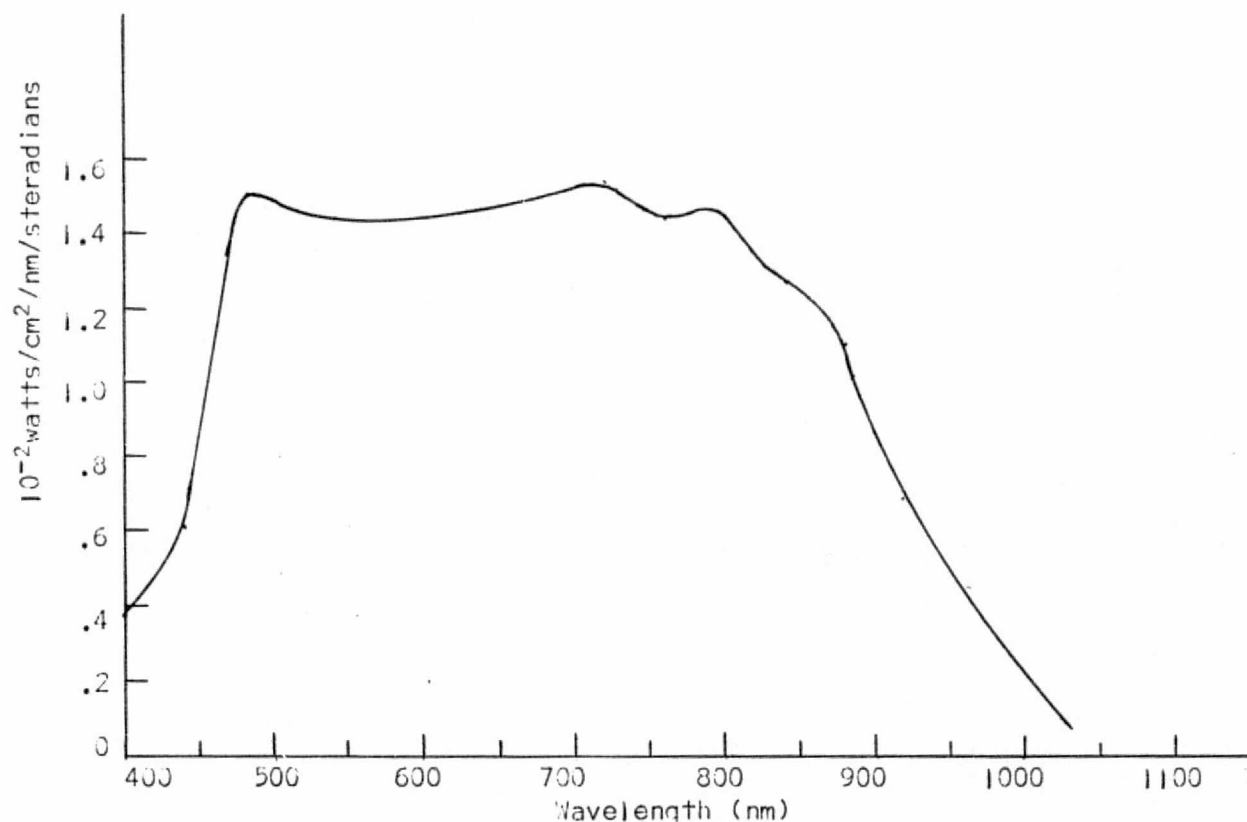
Figure 31. S-191 spectrometer aperture radiance (10^{-2}watts/cm^2/nm/
steradian) taken of Willcox Playa on 3 June 1973.

A "factor of correspondence" to be applied to each of the S-191

aperture radiance values shown in Table 4 (and in Figure 31 above) which

would equate these data to the radiance of the playa simultaneously

measured on the ground was computed. These data are listed in Table 5

and have been graphed in Figure 32.

It must, of course, be clearly understood that these "factors of

correspondence" apply only to the atmospheric optical conditions which

existed at the time the data was taken. These conditions are quantitatively

described by the optical depth depicted in Figure 8.

Wavelength (nm)	Solar Radiation ($\mu w/cm^2/nm$)	% Dir. Reflectance	Reflected Radiation ($\mu w/cm^2/nm$)	Aperture Radiance	Factors of Correspondence
400	30	6	1.8	.379	4.75
450	142	10	14.2	1.12	12.68
500	150	12	18.0	1.50	12.00
550	153	14	21.4	1.52	14.08
600	150	17	25.5	1.53	16.67
650	134	20	26.8	1.54	17.40
700	120	22	26.4	1.53	17.25
750	103	24	24.7	1.48	16.69
800	86	24	20.6	1.45	14.20
850	72	22	15.8	1.25	12.64
900	62	21	13.0	.85	15.29
950	32	20	6.4	.55	11.63
1000	46	18	8.3	.43	19.30
1050	41	17	7.0		
1100	34	13	4.4		

Table 5. Calculation of factors of correspondence between S-191 aperture radiance and radiance of the Willcox Playa, 3 June 1973.
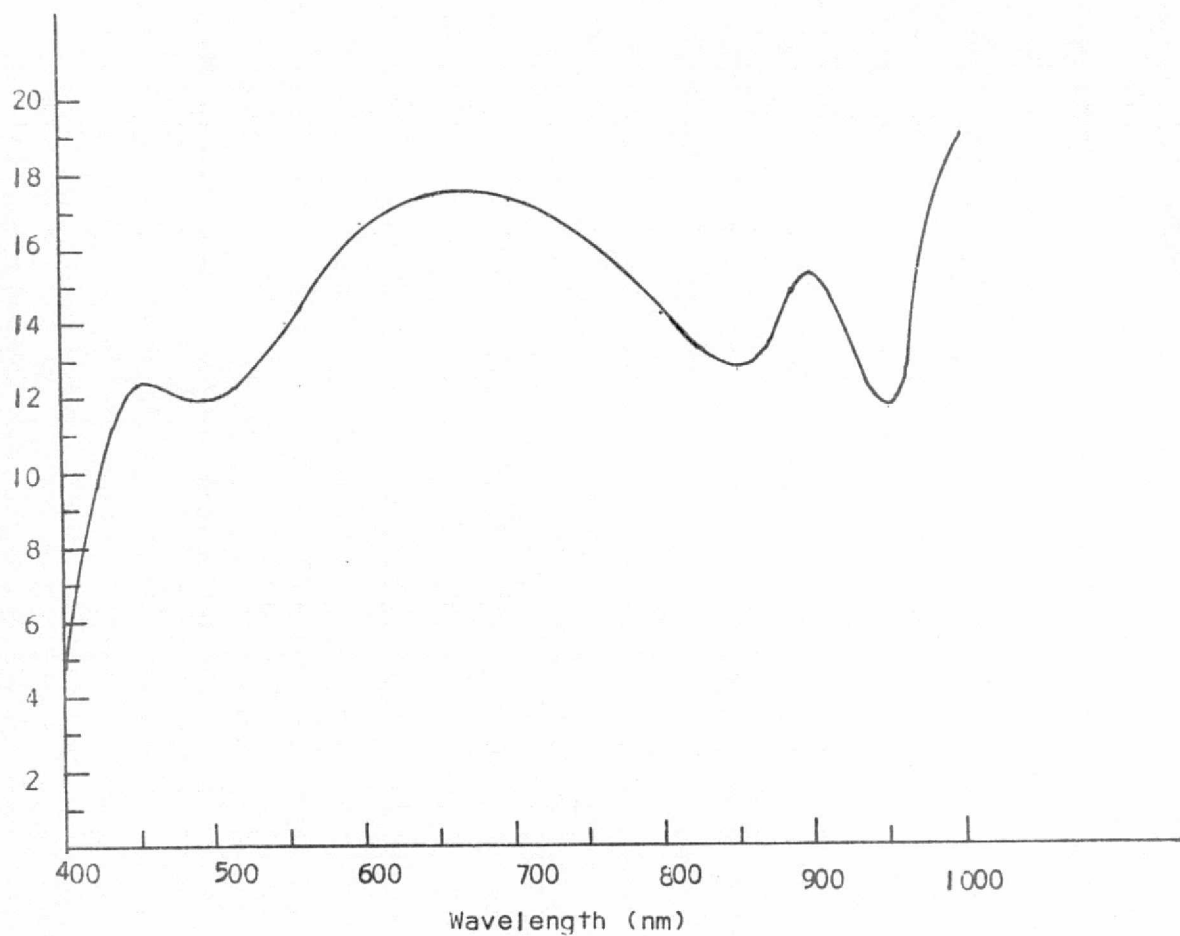
Figure 32. "Factors of correspondence" between S-191 aperture radiance and the radiance of the Willcox Playa simultaneously measured on the ground on 3 June 1973.

Section 3

Digital Image Processing of S-190A Multispectral Photography

of the Willcox Playa, Arizona

A digital analysis of Skylab S-190A photographic data products was performed using the computerized "System 800". This system digitizes multispectral photographic transparencies into the disc of a PDP-11 computer; processes the data using a series of image analysis programs; displays the resultant data on a color TV monitor and prints out the associated hard copy on a Decwriter. A description of the "System 800" is contained in Section 1 and in Appendix G.

Analysis of Skylab-2 S-190A black-and-white multispectral imagery acquired on 3 June 1973 and aircraft underflight multispectral imagery of Willcox Playa, Arizona, were made.

Willcox Playa Spectral Image Analysis

Four Skylab-2 S-190A black-and-white negatives (Frame No. 181), acquired on 3 June 1973, were analyzed using the "System 800". These images were taken in the following bands:

Frame No.	Band Pass
06-183	500 to 600 nm
05-183	600 to 700 nm
01-183	700 to 800 nm
02-183	800 to 900 nm

These four black-and-white images were linearly digitized in registration using MARKER and DIGITIZE programs. In order that direct

comparison could be made, identical ranges were used for digitizing each
of the four images into 256 levels. The digitized gray levels in each
photograph were then partitioned into eight (8) color-coded partitions
and the percent of the total 294,912 pixels falling onto each partition
was computed using HISTOGRAM and AREA programs. The resulting digital
brightness distribution is shown in Table 6 below.

Digitized Grey Levels	Color Code	S-190 A Bands			
		500 to 600 nm	600 to 700 nm	700 to 800 nm	800 to 900 nm
0-32	Black	2.30	21.46	1.58	0.98
33-64	Red	2.40	32.20	1.66	0.42
65-96	Green	9.10	29.78	7.66	1.48
97-128	Yellow	12.02	9.64	30.14	4.72
129-160	Blue	26.44	3.02	39.54	18.28
161-192	Magenta	26.28	1.34	16.98	28.14
193-224	Cyan	15.20	0.78	1.74	29.50
225-255	White	6.20	1.66	0.62	16.40
	Totals	99.94	99.88	99.92	99.92

Table 6. Digital brightness percent area classification of Skylab
S-190A black-and-white multispectral images (Frame No. 181) of Willcox
Playa and vicinity acquired on 3 June 1973.

A histogram has been graphed of the digitized brightness levels in
each of the four spectral bands and is plotted in Figure 33. Table 7 shows
the expected value and standard deviation of the distribution of brightness
in each of the four multispectral images.

Positive reproductions of the four black-and-white multispectral
negatives which were digitized in the linear mode are shown in Figure 34 .

-56-
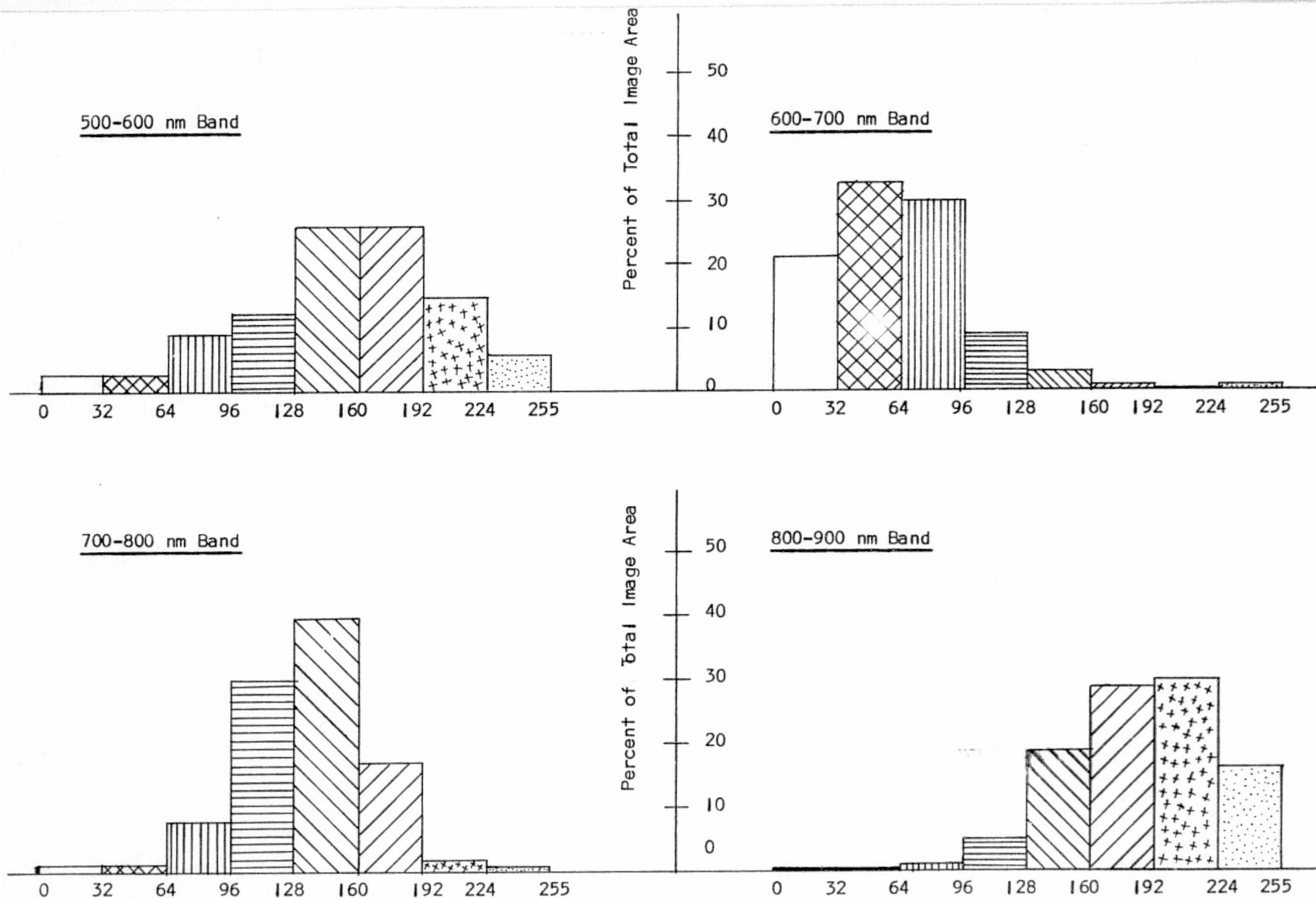
Figure 33. Histogram of digital brightness percent area classification of Skylab S-190A black-and-white multispectral images (Frame No. 181) of Willcox Playa and vicinity acquired on 3 June 1973.

500-600 nm Band
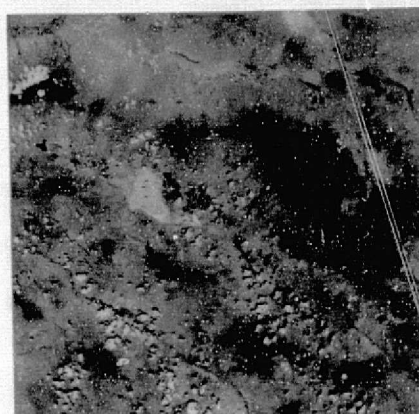
600-700 nm Band
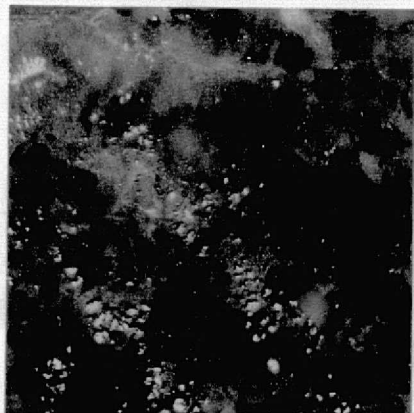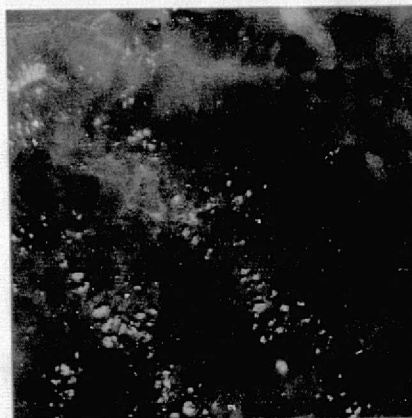
700-800 nm Band

800-900 nm Band

Figure 34. Skylab-2 S-190 multispectral photography of Willcox Playa, Arizona, taken on 3 June 1973 (Frame No. 181).

	500 to 600 nm	600 to 700 nm	700 to 800 nm	800 to 900 nm
Sample Average, $\overline{x}$	153.1	65.8	132.9	183.4
Sample Standard Deviation, s	50.0	43.7	35.1	42.3

Table 7 . Statistics of the brightness distribution of Skylab   190A (Frame No. 181) of Willcox Playa and vicinity acquired on 4 .... 1973.

The corresponding gray level partitions in each band are shown in Figure 35. From this latter figure one can see that the density range within the playa is greatest in the 500-600 nm band where it encompasses the range from 128 to 224 and is least in the 600-700 nm band (192-255). Also shown in Figure 35 is the average of the sum of the 500-600 nm band and the 800-900 nm band which resulted in a density range, exclusive of clouds and shadows, of from 96 to 192. The average of these two bands provided the greatest range of brightness within the playa.

In order to perform a more detailed analysis of the image of the playa itself, removing to the maximum extent possible terrain outside the boundary of this dry lake, frame no. 181 was magnified and digitized in the log mode. Table 8 lists, by S-190 band, the log brightness distribution in all four bands. The resulting System 800 digital grouping of the log brightness of the playa in all four bands, as well as an average of the 500-600 nm band and the 800-900 nm band, is shown in Figure 36.

Atmospheric Effects in Desert Areas

The relative effect of the atmosphere in each of the four spectral bands was analyzed using the S-190 multispectral imagery of Willcox Playa
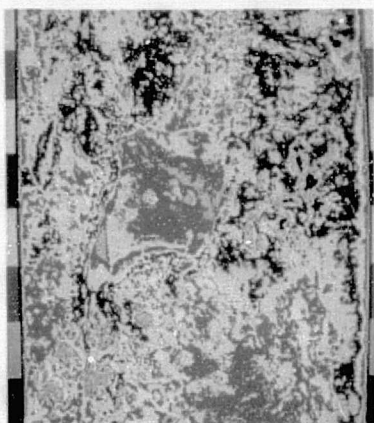
500-600 nm Band
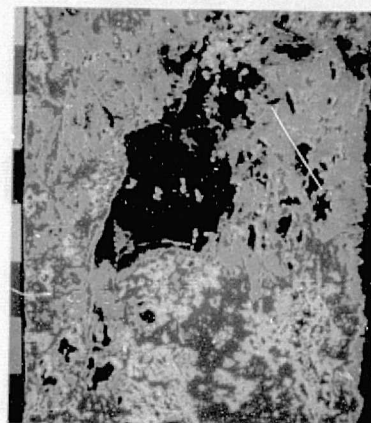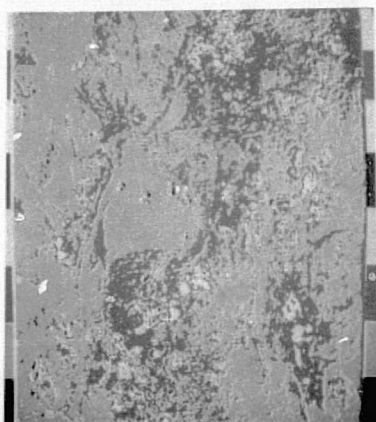
600-700 nm Band

700-800 nm Band

800-900 nm Band

Average of the sum of
the 500-600 nm band and
the 800-900 nm band.

Figure 35. System 800 digital gray level partitions of Skylab-2 S-190
Frame No. 181 of Willcox Playa.
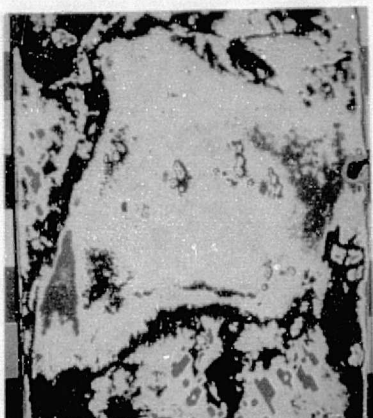
500-600 nm Band
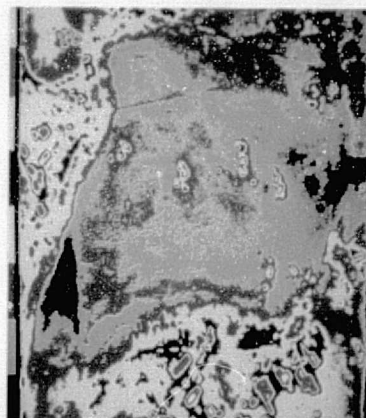
600-700 nm Band

700-800 nm Band
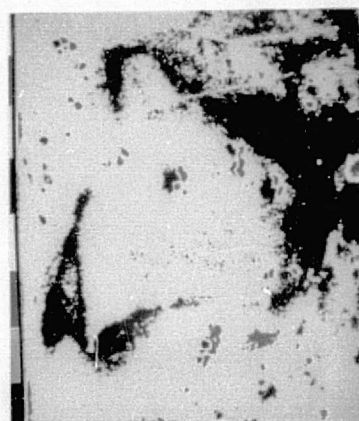
800-900 nm Band

Average of 500-600 nm
band and 800-900 nm band.

Figure 36. System 800 log digital brightness groups of an enlarged portion
of Skylab-2 S-190 Frame 181 of Willcox Playa.

Digitized Grey Levels	Color Code	S-190 A Bands			
		500 to 600 nm	600 to 700 nm	700 to 800 nm	800 to 900 nm
0-32	Black	1.32	5.00	1.16	1.04
33-64	Red	0.46	29.90	0.10	0.12
65-96	Green	5.46	31.84	1.06	0.30
97-128	Yellow	40.78	23.80	16.68	1.88
129-160	Blue	33.58	6.08	76.38	37.34
161-192	Magenta	16.18	1.76	4.48	58.28
193-224	Cyan	2.08	1.38	0.04	0.96
225-255	White	0.02	0.14	0	0
	Totals	99.88	99.90	99.90	99.92

Table 8. Digital Brightness percent area classification of image of Willcox Playa contained in S-190A Skylab Multispectral Imagery Frame No. 181. (3 June 1973).

acquired on 3 June 1973. The multispectral negatives of Frame No. 181 were log digitized as described in the preceding paragraphs. The digitization range of all four of the negative S-190 photographic images of the playa was adjusted to give the same range for all four images in order to maintain a constant relative relationship of the eight digitization levels between the four spectral bands.

Ten digital brightness measurements of clouds, cloud shadows, and the playa immediately adjacent to cloud shadows were made using HISTR program. The sketch in Figure 37 shows the relationship as it appeared from the ground and as it was recorded in the image. The mean ($\bar{x}$) and standard deviation (s) are tabulated in Table 9.

Spectral Bands	Cloud		Shadow		Playa	
	$\bar{x}$	s	$\bar{x}$	s	$\bar{x}$	s
500 to 600 nm	94.4	6.6	187.6	6.9	120.5	7.5
600 to 700 nm	60.6	11.8	169.1	9.3	69.0	9.4
700 to 800 nm	120.4	6.8	175.9	4.9	137.7	4.2
800 to 900 nm	144.6	4.3	198.1	9.8	166.7	4.8

Table 9 . Statistics of atmospheric effects by cloud shadow measurements in Skylab S-190 multispectral negatives taken on 3 June 1973. (Frame No. 181).
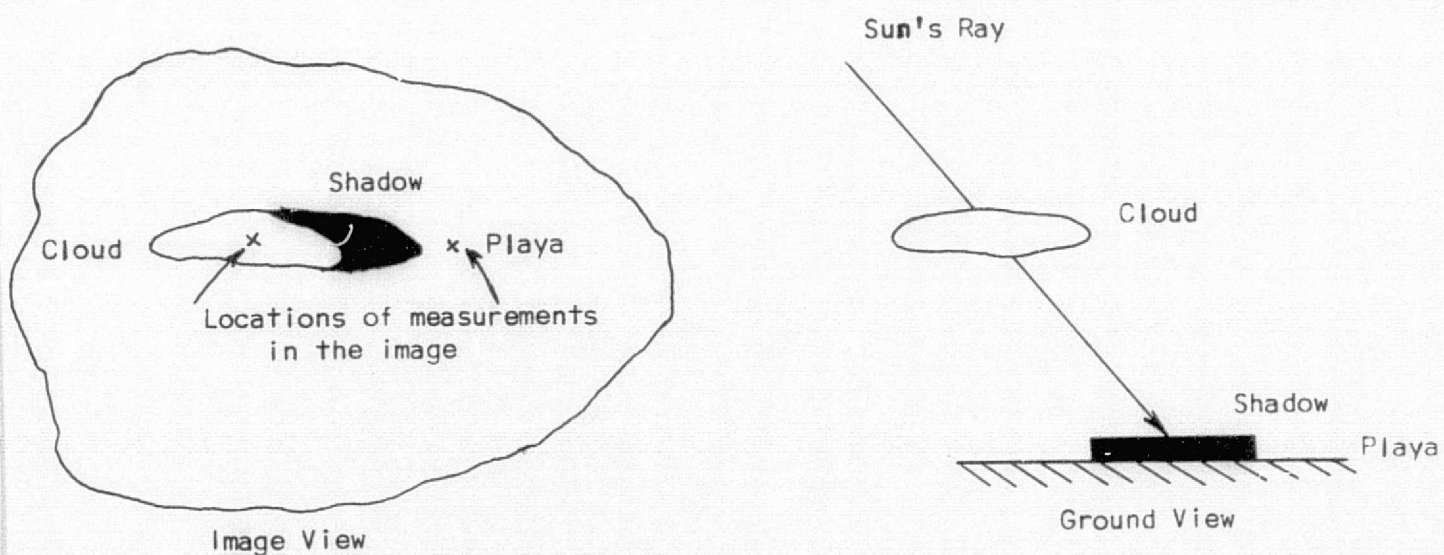
Figure 37.. Cloud shadow image formation in S-190A negatives.

The complete printout of all measurements, the statistics of which are shown on the preceding page, is contained in Appendix D. The statistics in this table were computed from a sample of 10 (e.g., n = 10) random measurements of each of the three areas in each of the S-190 black-and-white negatives as follows:

$$\text{Sample Mean} \equiv \overline{x} = \frac{\sum\limits_{i=1}^{10} x_i}{10}$$

$$\text{Sample Standard Deviation} \equiv s = \left[\frac{\sum\limits_{i=1}^{10} (x - \overline{x})^2}{9} \right]^{1/2} = \left[\frac{\sum\limits_{i=1}^{10} x_i^2 - 10\overline{x}^2}{9} \right]^{1/2}$$

An analysis of the density of the images of clouds, shadows, and playa appearing in all four bands was performed and related to the film exposure data appearing in SL/2 sensitometric data package. The step wedges supplied for cross calibration of densitometers with the standard unit at J.S.C. could not be used due to excessive variation in the density for a given step. For instance, step no. 11 in wedge 10008 had a density range of 1.26 to 1.51 depending upon the location on the step which was measured.

The digital brightness data of Frame No. 181 negatives appearing in Table 6 were then transformed into relative exposure. These relative exposures are plotted with respect to the 800-900 nm band digital brightness in Figure 38.

Comparison of S-190A and Underflight Imagery

The four S-190A black-and-white multispectral negatives of Frame No. 181 were enlarged using the System 800 input TV optics so that the north end of Willcox Playa was the only portion of the image which was

-64-
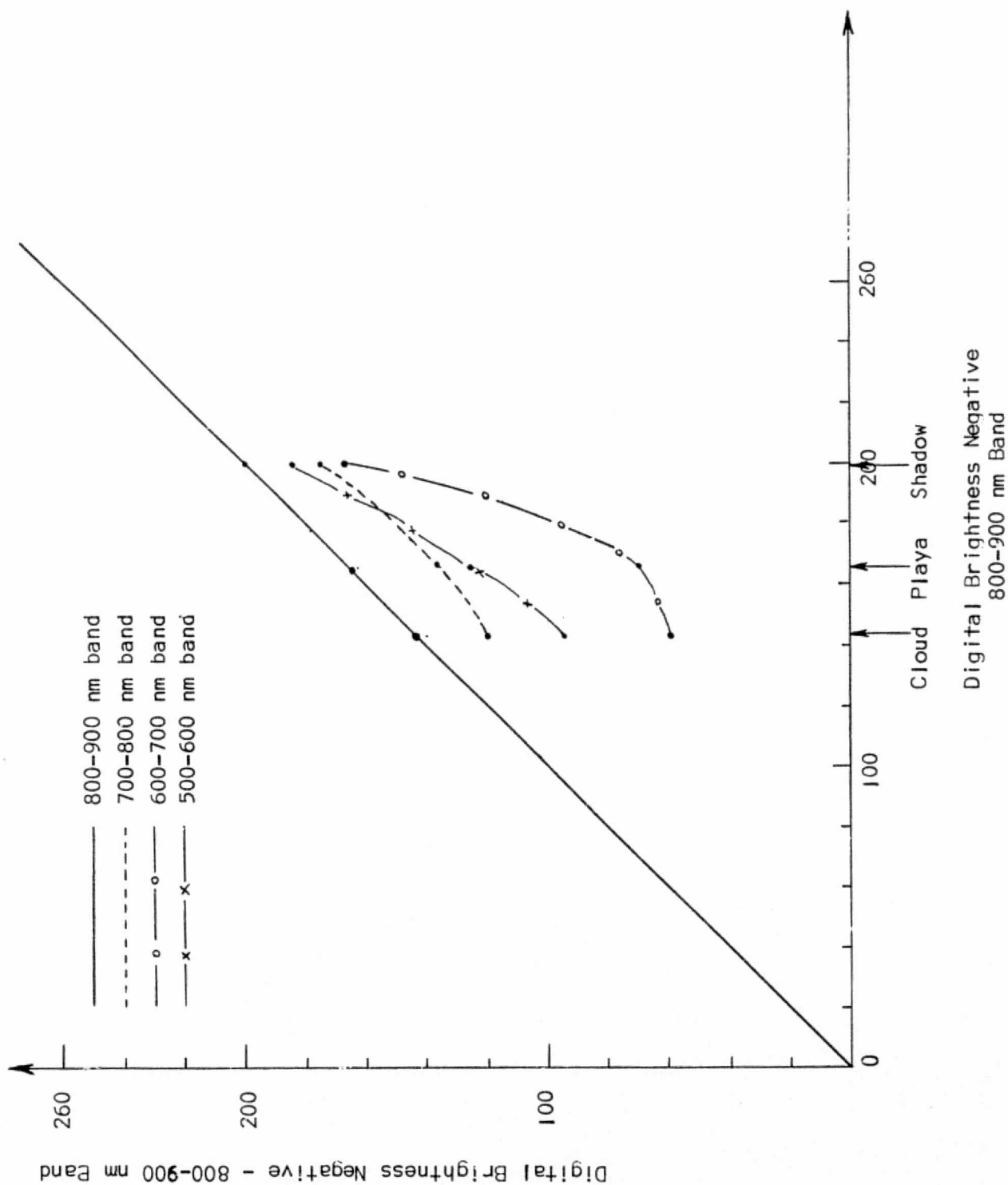
Figure 38. Digital brightness of S-190A bands compared to 800-900 nm band for clouds, terrain in sun, and terrain in shadow.

digitized. Each of the four bands was log digitized without varying the minimum or maximum video signal level. DIGIT, AREA, and HIS OR programs were run and the percent of the total area in each of eight digital levels was calculated as shown in Table 10.

Five digital image brightness measurements of the image of the north part of the playa, adjacent to the railroad tracks, were made in each of the four bands. The statistics associated with these measurements are shown in Table 11.

Underflight AMPS imagery, acquired on 5 June 1973 at an altitude of 18,000 feet, covering the north end of Willcox Playa was log digitized and analyzed using the System 800. Digitization of the input was performed on all bands using the same minimum and maximum values of the video signal. These minimum and maximum video signal values were, however, different from those used in digitizing the Skylab imagery because of differences in the density between the multispectral imagery acquired by the spacecraft and the aircraft. Figure 39 shows the four black-and-white aircraft multi-spectral images used in this analysis.

The results of the System 800 digital brightness classification are presented in Table 12. It is assumed that the numbers in this table represent the variability within one measurement of the playa made using the Skylab S-190A imagery. The average and standard deviations of these values are presented in Table 13.
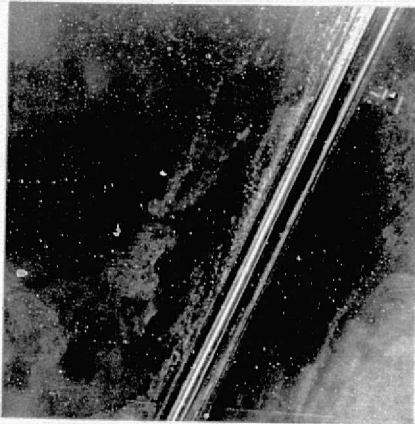
500-600 nm Band
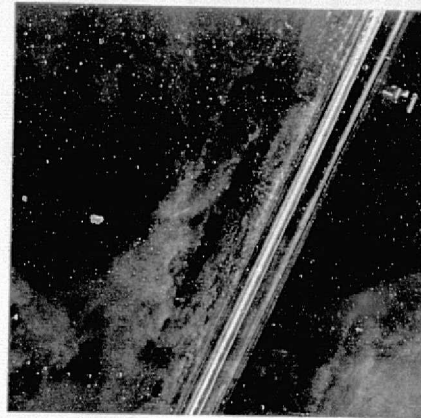
600-700 nm Band
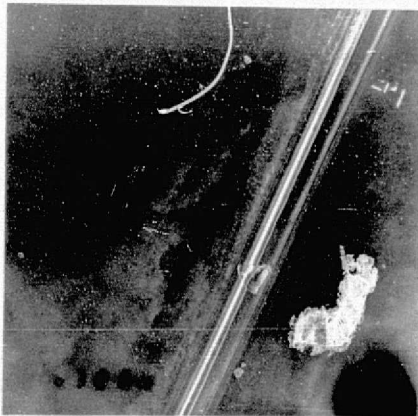
700-800 nm Band
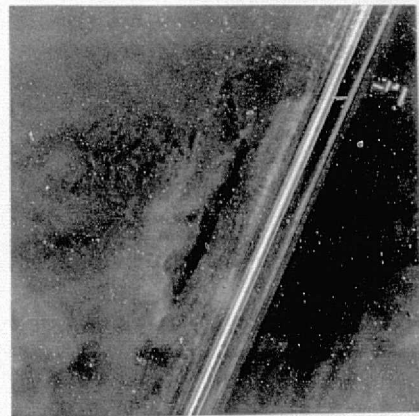
800-900 nm Band

Figure 39. Aircraft underflight AMPS multispectral imagery of the north end of Willcox Playa acquired on 5 June 1973 which was analyzed using the System 800.

Digitized Gray Levels	S-190A Bands			
	500-600 nm	600-700 nm	700-800 nm	800-900 nm
0-32	3.86	52.50	2.02	1.24
33-64	9.76	25.60	1.80	.64
65-96	37.84	18.46	27.08	2.94
97-128	34.52	2.36	66.52	40 .
129-160	13.24	.66	2.46	53.70
161-192	.70	.34	.04	.70
193-224	0	0	0	0
225-255	0	0	0	0
Totals	99.92	99.92	99.92	99.94

Table 10. Digital brightness percent area classification of S-190A black-and-white multispectral images of the north end of Willcox Playa acquired on 3 June 1973 (Frame No. 181).

Statistics	S-190A Bands			
	500-600 nm	600-700 nm	700-800 nm	800-900 nm
Sample Average: ($\bar{x}$)	82	22.2	100.8	132.6
Sample Standard Deviation (s)	2.55	5.59	4.32	4.50

Table 11. Statistics of five digital brightness measurements of the north end of Willcox Playa - Image 181, 3 June 1973.

Digitized Gray Level	AMPS Bands			
	500-600 nm	600-700 nm	700-800 nm	800-900 nm
0-32	1.26	1.34	1.12	1.28
33-64	.48	.78	.02	.58
65-96	2.36	4.44	.40	2.52
97-128	28.60	58.80	2.00	7.,12
129-160	65.46	34.32	46.02	17.42
161-192	1.76	.26	50.32	0
193-224	0	0	0	0
225-255	0	0	0	0
Totals	99.92	99.94	99.88	99.92

Table 12. AMPS aircraft underflight image precent digital brightness classification of the oorth end of Willcox Playa made from imagery acquired 5 June 1973 (Frame No. 61-073).

Statistic	AMPS Bands			
	500-600 nm	600-700 nm	700-800 nm	800-900 nm
Sample Average ($\bar{x}$)	131.7	119.8	157.6	115.1
Sample Standard Deviation (s)	22.9	22.6	24.1	18.6

Table 13. Statistics of the brightness distribution of aircraft AMPS underflight multispectral photography percent digital brightness classification.

Section 4

Photometric and Additive Color Analysis

of S-190A Multispectral Photography of the Willcox Playa

Including Geologic Interpretation

A photometric analysis was performed of the S-190A black-and-white multispectral photography taken on 3 June 1973 over the Willcox test site. The purpose was to establish the best procedures for printing multi-spectral positives of semi-arid desert-like terrain (such as exists around Willcox, Arizona) for analysis using additive color techniques.

Release negatives of the 500-600 nm, 600-700 nm, 700-800 nm, and 800-900 nm bands were conventionally processed to achieve a one-to-one manping of negative into positive density. The graph of negative gray scale versus positive gray scale is shown in Figure 40 which shows the accuracy with which the calibration step wedge was processed.
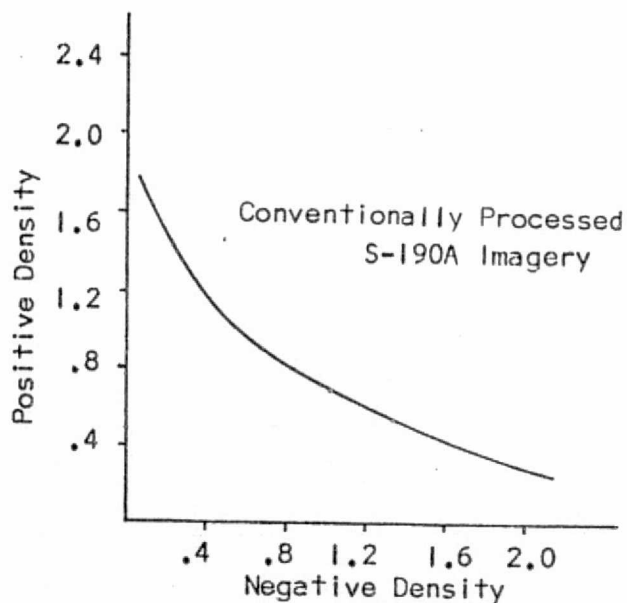
Figure 40. Negative-positive density relationships of "conventionally processed" S-190A black-and-white multispectral photographs.

Image matched prints of the conventionally processed positive transparencies are shown in Figure 34 in the preceding section.

In order to create color composites which contained the maximum possible information, it was necessary to reprocess "conventionally processed" imagery. Contrast-stretched positive transparencies were produced by adjusting the density and contact printing of the S-190 release 70mm negatives. A Spectral Data Model 40 contact printer was used for this purpose. The illumination at the film plane of this printer is uniform over a 70mm field, within limits of measurement. The degree of "contrast-stretch" and the density level of the area of interest were controlled by adjusting the following parameters.

-- Film Type

-- Exposure

-- Chemistry

-- Degree of Development

These parameters were varied to produce film positives in which image detail within the land areas was maximized. The density levels of land areas were required to be compatible with each other and low enough to produce a composite image on an additive co-or viewer screen. This composite had to have sufficient brightness to allow discrimination between small color differences.

"Image-matched" reproductions of these transparencies are shown shown in Figure 42 on page 74. These "image-matched" reproductions are visual impressions of the appearance of the transparencies when viewed on a commercial light table. Due to the inherent difference of film and paper media, a sensitometric match between the two is not possible.

Reprocessed S-190A Imagery:
————————— 500-600 nm
- - - - - - - - 600-700 nm
—x————x—— 700-800 nm
—o————o—— 800-900 nm
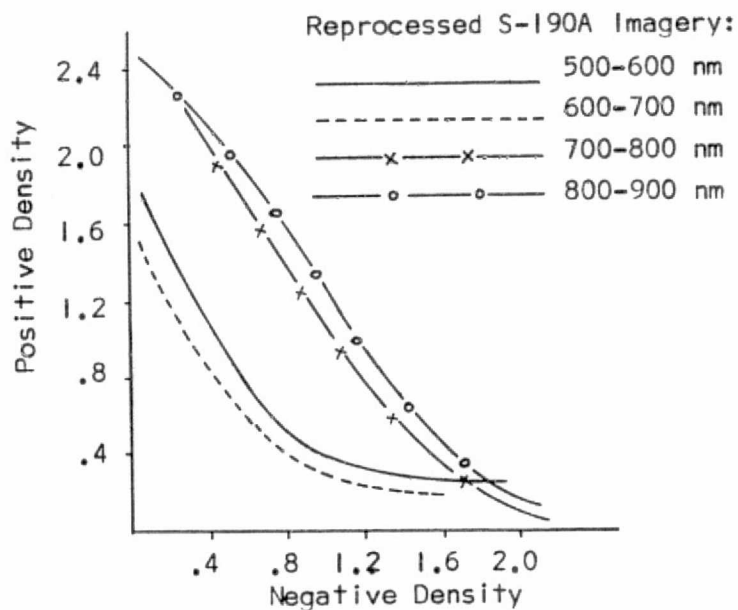
Figure 41. Negative-positive density relationships of S-190A black-and-white multispectral photographs which have been "contrast-stretched" to emphasize land detail.

However, these reproductions are useful in visualizing the quantitative data shown in Figure 41, which data is a graphical representation of the negative-positive density relationships of these images.

In the graphs shown in Figure 41, the density of each step of the gray wedge in the positive transparency for each band has been plotted on the y axis as a function of the density of the same step in the S-190A release negative on the x axis. Since this gray scale is subject to the same copying and processing as the image to which it is attached, it may be used for densitometric analysis of the imagery.

The measured steps of the gray scale on each image record the
brightness range of the land areas. A comparison of these data in the
four bands shows that it is necessary to increase the scope of the
negative-positive density relationship curve with increasing wavelength.
Because of this low brightness range in Band 4, a single contrast-
stretched positive could be made which would be acceptable. With
increasing wavelength, it becomes necessary to make different positives
from the same negative.

. The two factors which have the greatest effect upon the additive
color composite image are the density levels (maximum and minimum) and
density range of the areas of interest. The data concerning these
factors has been compiled in. Table 14.

Additive color composites, using both conventionally processed
and "contrast-stretched" positive transparencies, were made using a
Spectral Data Model 70 additive color viewer. An example of one such
color image made from "contrast-stretched" transparencies in which the
500-600 nm band is imaged as blue, the 600-700 nm as green, and the
800-900 nm band as red is shown in Figure 43.

Evaluation of Contrast-Stretched Imagery

An evaluation of terrain features which could be interpreted using
contrast stretched imagery was performed which had as its focus geologic
land features.

A study was performed, employing visual analysis only, to investigate
the application of Skylab additive color images to geology and related
disciplines.

-73-
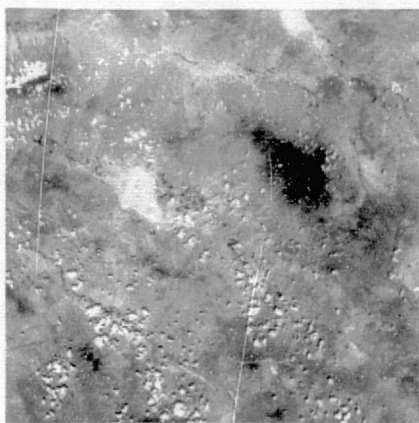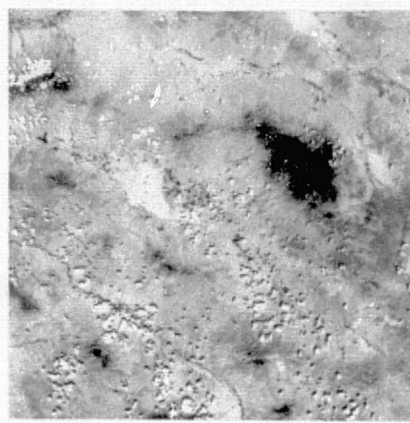
500 - 600 nm Band

600 - 700 nm Band
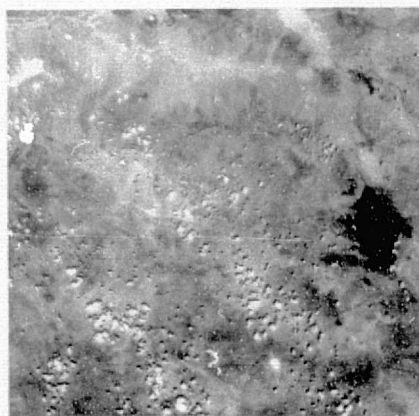
700 - 800 nm Band

800 - 900 nm Band

Figure 42. Image-matched prints of S-190A multispectral transparencies which have been "contrast-stretched" to emphasize land detail.

Transparency No.	Density Min. Max.	Density Range
500-600 nm:		
Negative	.97 - 1.69	.72
Conventional Positive	.75 - 1.32	.57
Land-stretched Positive	.21 - 1.60	1.39
600-700 nm:		
Negative	.97 - 1.69	.72
Conventional Positive	.75 - 1.32	.57
Land-stretched Positive	.13 - .81	.68
700-800 nm:		
Negative	1.55 - 1.98	.43
Conventional Positive	.43 - .85	.42
Land-stretched Positive	.24 - .64	.40
800-900 nm:		
Negative	1.55 - 1.98	.43
Conventional Positive	.43 - .85	.42
Land-stretched Positive	.26 - .71	.45

Table 14. Densitometric factors affecting composite image color of land areas.

The images used were made from contrast-stretched positives, the photometric characteristics of which are shown in Figure 41. The two basic types of geologic information for which the image was examined were: (1) the detection of structural lineations, and (2) the discrimination of lithologic units.

Geologic, vegetation, and soil maps were visually compared with the S-190A image for any possible correlations. Basaltic rock units which were recorded on the state geologic map of Arizona showed up

clearly on S-190A additive color images. The intricate geology in the mountain ranges was not readily detectable. The most recent fluvial deposits which were not recorded on the state geologic map were imaged and easily seen on this Skylab imagery.

Lithological discrimination was to be solely based upon color differences on the image and not upon other parameters such as texture, topographic expression, and drainage patterns which commonly are used in aerial photographic interpretation.

This geologic information can be put into two separate categories: first, information which has already been recorded on existing sources, i.e., geologic maps, and second, information which has not been recorded either because this information was undetected or it came into existence subsequent to the published sources.

Procedure:

To see how much of the previously recorded information could be detected on the image, visual comparison was made between the image and various published maps. If there appeared to be a significant amount of information common to both data, the information contained on the published map was drawn on a clear vinyl overlay which was then placed over the ERTS image for a more detailed visual analysis. The additional information which was on the image, but not on the geological maps, was drawn on separate overlays. The information on these overlays was then compared to non-geological data, such as soil and vegetation maps.

The main source of geological information used in this study was the 1969 state geological map of Arizona published by the ARizona Bureau of Mines and the U.S. Geological Survey. It would have been most desirable to have compared the images with more detailed geologic maps having a

larger scale. Unfortunately, virtually no U.S. Geologic quadrangle maps
exist for this area. There were a few U.S.G.S. miscellaneous geological
investigation maps in this area, but these were poor in quality and con-
tained only geologically monotonous areas. The one exception was a U.S.
G.S. M.G.I. map of the southern portion of the Mule Mountains. Corre-
lations between this map and ERTS images are discussed in detail. One
coincidental advantage in using the state geologic map was that visual
comparison with the S-190A color composite was facilitated because both
were made to the same scale of 1:500,000.

Non-geological sources included a small scale, very generalized
vegetation map of the state of Arizona published by the University of
Arizona; several soil maps which were included in the soil survey of the
Sulphur Spring Valley area, 1954; and the general soil map of Cochise
County, Arizona, published by the Soil Conservation Service in 1971.

Since there seemed to be some correlation between the additive
color image and the state geologic map, all the lithologic and structural
information contained on the map was transferred to an overlay which was
then placed over the image - this is shown in Figure 44. The most
noticeable of these correlations was the delineation of the two major
basaltic occurrences in the area. These volcanic rock units can be
clearly distinguished as having a darker visual signature than the
surrounding areas. Even the small outlines of these units can be easily
seen.

It was found that a large percent of the intricate geology in
the mountain ranges cannot be detected from the image. The most obvious
reason for this is that most areas in the ranges are heavily obscured

by vegetation. However, on close examination, some lithologic contacts in the ranges were detectable. For example, the major contact between the granite and the schist (Tkg and PCsc, respectively, on the geologic overlay) in the Little Dragoon Mountains could be observed on the image. No faults could be detected in the ranges.

Among the additional information contained on the image, but not on the geologic state map of Arizona, were the various color subdivisions of the basins (Figure 45). These different colors could not be checked for the possible correlation with different alluvial types because the alluvial deposits on the state geologic map were so greatly generalized that any such correlation was impossible to make. The vegetation and soil maps were also examined for possible correlations. The vegetation map was too generalized and the soil maps were too large-scaled and detailed for the resolution of the image to be of any use. No correlations were made with these materials. It is still not known what the different colors in the basins, which appear in the S-190A additive color composite, represent.

Other features imaged, but not appearing on the state geologic map, are the most recent fluvial deposits or alluvium. These recent deposits have a white visual signature on the additive color image. In this ERTS frame they can be seen along the San Simon River, San Pedro River, and around the Willcox Playa, in Arizona.

These locations of the most recent fluvial deposits can be easily explained. During pluvial periods (times when the area's climate was more humid than today), stream water was high and deposits were laid down along the major drainage lines. Also, during these wet times, the Willcox Playa was a fresh-water lake with several streams flowing into it. As

these streams entered the standing lake water, they lost some velocity
and had to deposit their load. Thus, fluvial deposits became concentrated
around the perimeter of Willcox Playa. During interfluvial periods, such
as the present, the lake water dries up and evaporates. Gypsum, rock salt,
etc. are precipitated and deposited in the center of the playa.
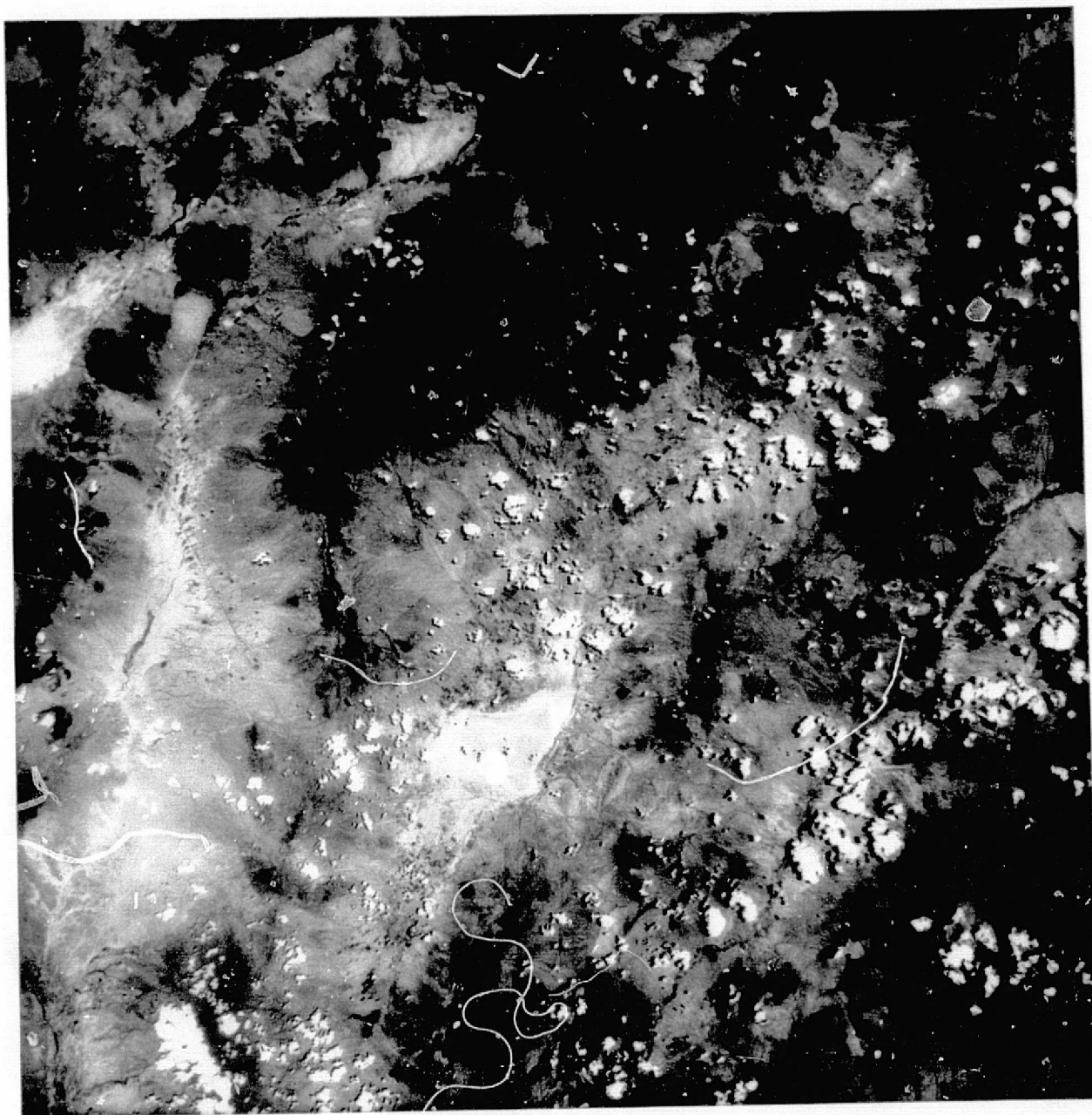
Figure 43. Additive color composite of contrast-stretched S-190A black-and-white multispectral images taken of Willcox Playa, Arizona, on 3 June 1973. The 500-600 nm band is imaged as blue, the 600-700 nm band as green, and the 800-900 nm band as red.
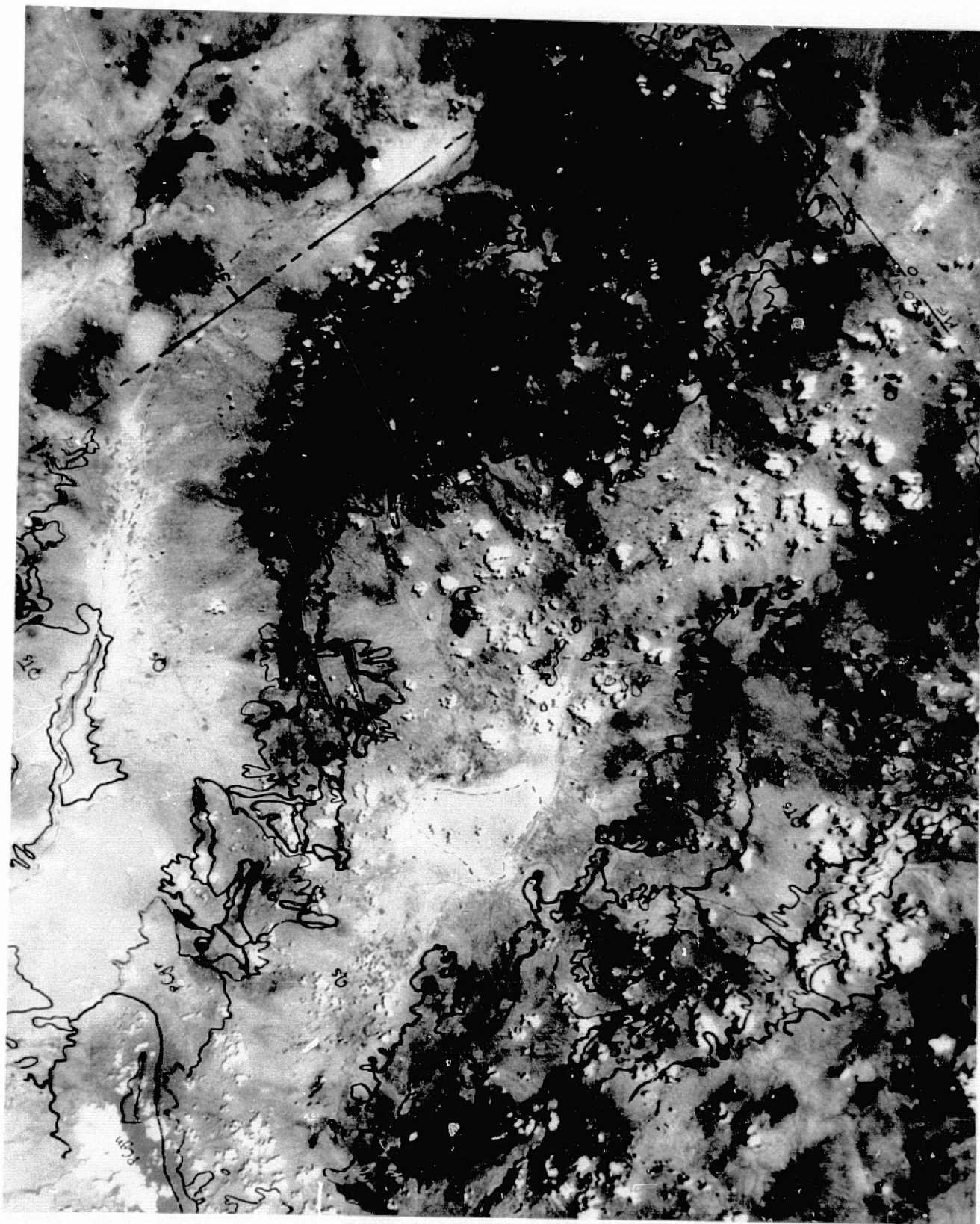
Figure 44. Overlay of known geology superimposed on Skylab-2 S-190A additive color image of 3 June 1973.
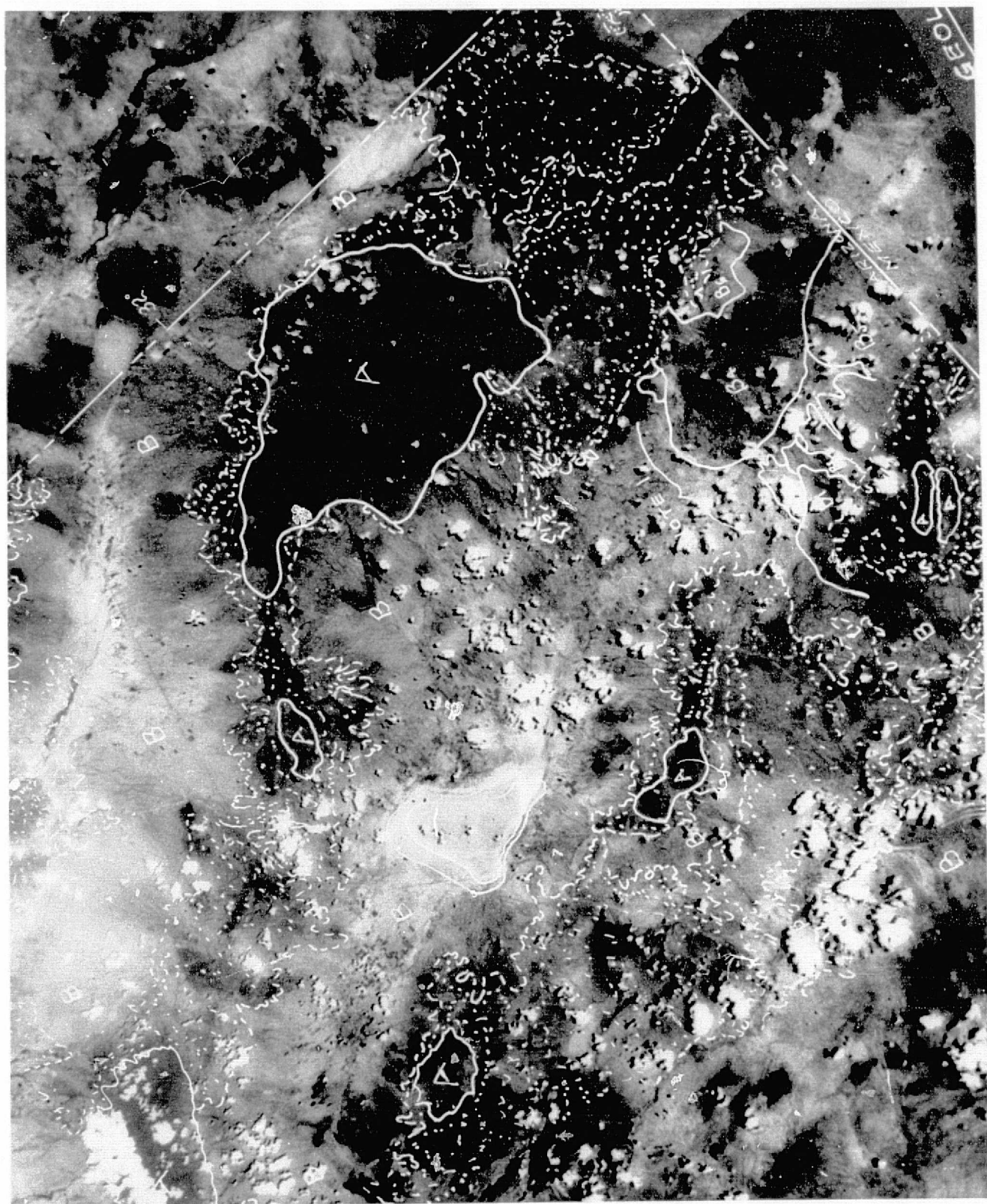
Figure 45. Overlay of additional geologic information contained in Skylab-2 S-190A image, but not appearing on state geologic maps.

Section 5

Physical, Chemical, and Biological Sampling

of New York Coastal Waters

The collection of "baseline" oceanographic data of Block Island Sound and New York Bight are described herein. These data provided the baseline picture of the characteristics of these waters within which the data collected at the instant of Skylab-3 pass could be placed in perspective.

Baseline Data Collection of Oceanographic Data in Block Island Sound and New York Bight

In 1972-73, twenty-four cruises were conducted in Block Island Sound and New York Bight areas to collect and analyze water samples at different stations in order to construct baseline data over a period of time which would give sufficient indications of the gross pattern of oceanographic activity. Three transects with twelve stations were covered in Block Island Sound and nine stations in New York Bight. Some of the analysis was done on board the research vessel KYMA immediately after collecting the water samples. The data was acquired for: (1) physical oceanography, (2) chemical oceanography, and (3) biological oceanography.

Techniques Used in Determining Physical Oceanographic Parameters

To collect baseline physical oceanographic data, temperature, salinity, and calculated density values were obtained at multi-depths for most stations sampled in Block Island Sound. Only surface salinity samples were taken on the New York Bight cruises.

When stations were sampled more than once per cruise, averages of temperature, salinity, and density (σ_t) were calculated at standard depths of 0, 10, 20, 30, 35, and 40 meters. Flood and ebb averages of these parameters were also calculated over each cruise. Horizontal profiles (contours of t°C, S°/oo, and σ_t in depth versus distance) were made for each crossing of a transect.

The downwelling irradiance of the visible spectrum was measured at each station in Block Island Sound using an upward-facing irradiance meter (submarine photometer), comprising a photocell and cosine collector equipped with glass filters.

The extinction coefficient, $\overline{k}$, for these light values is defined by the equation:

$$I(z) = I(z=0)\exp - \overline{k}z$$

where $I(z=0)$ is the total visible light energy in a particular wavelength band that is incident upon the naviface, $I(z)$ is the remaining light energy at the depth $z(m)$, and $\overline{k}$ is the total "extinction" coefficient for the particular wavelength band in units of m^{-1}.

On most cruises, irradiance measurements were taken as near to noon as possible at each station. Linear regression analyses were performed and correlation coefficients calculated for data sets using total particle counts and average extinction coefficients for each of the Block Island Sound and New York Bight stations.

-84-

Regression analysis and correlations were also calculated between monthly fresh water discharge into Long Island Sound and the monthly surface and bottom salinity values at the Block Island Sound stations. Dilution factors, D, defined by:

$$D = (\Delta S/\overline{S}) \times 100\%$$

where ΔS is the annual range and $\overline{S}$ the mean salinity at a station, were also calculated.

Chemical Oceanographic Techniques

At each station, the locations of which have been previously described, samples were collected from selected depths with 5-liter Niskin bottles. Once on board, samples for the measurements of salinity, oxygen, and phytoplankton analyses were removed. The remainder of the sample was then filtered through Whatman GF/C filters in an all-glass filtration system. The filter pads were then placed in individual vials and frozen for later analysis of chlorophyll and particulate phosphorus. Samples of the filtrate were removed for the measurement of reactive and total soluble phosphorus, nitrite, and nitrate nitrogen, and silica.

Salinity was determined with a conductivity system (Beckman RS7-B) and oxygen was determined by the method described by Carpenter (1966). Reactive, total soluble and particulate phosphorus, silica, and chlorophyll were determined according to the methods described by Strickland and Parsons (1968). Nitrite and nitrate nitrogen were determined by the method described by Wood et al (1967).

On 12 May 1973, through the cooperation of the local power squadrons and other private yachts, a synoptic sampling of the surface waters was conducted. Salinity and suspended solids samples were collected at 0900

1200, and 1500 hours. The method described by Strickland and Parsons (1968) was used for these analyses.

Biological Sampling Techniques

Samples for the analysis of phytoplankton and suspended particles were collected from the surface at each station in 5-liter Niskin bottles, concurrently with the chemical samples. One liter of water was removed from the bottle, immediately concentrated in a continuous plankton centrifuge to less than 10 ml, and brought to a final volume of 10 ml with filtered (0.45μ) seawater and neutral buffered formalin (a final concentration of 3 percent). This concentrated sample was returned to the laboratory for microscopic analysis of the phytoplankton population.

An additional 50 ml aliquot was withdrawn from the Niskin bottle and placed in a 50 ml glass vial. This sample was refrigerated until return to the laboratory, when it was immediately analyzed for suspended particles with a Coulter Counter, Model B.

Aliquots of the concentrated sample were placed in a nanoplankton counting chamber (Palmer and Maloney, 1954) and various types of microscopic counts, depending on cell size and number, were performed under 100X and 400X magnification. At least 10 field counts (a wide field being delineated by the microscopic field and a narrow field by a whipple disc placed in one eyepiece) were performed under each magnification, and three survey counts (a scan of the entire counting chamber) were performed under 100X magnification. The average counts were multiplied by the appropriate factors to yield results as cells per liter.

Immediately upon return to the laboratory, the refrigerated 50 ml sample was analyzed for suspended particles with a Coulter Counter, Model B. Two aperture tubes (30μ and 100μ) were employed so that particles between $0.16μ^3$ and $635μ^3$ (equivalent diameter of 0.68μ to 10.67μ) could be counted. Particles between 1 and 10μ equivalent diameter were counted at 1 micron intervals. Particles above 10.67μ equivalent diameter were also counted for the most of the samples.

Oceanographic Baseline Data Results

The oceanographic results obtained from the analysis of data collected under the sampling program for Block Island Sound and New York Bight are described below. A detailed narrative of these results, along with the summary and methods of data reduction, is included in the appendices of this report: Appendix A – Physical Oceanography, Appendix E – Chemical Oceanography, and Appendix F – Phytoplankton and Suspended Particles. Also contained in these appendices are the graphs, tables, and oceanographic charts describing the specific characteristics of Block Island Sound and New York Bight water masses.

Physical Oceanography

The annual temperature regime within Block Island Sound and New York Bight is largely governed by solar radiation and correlates with the mean month temperatures in the atmosphere, lagged one month. For these waters, the maximum temperatures occur in August, the minimum in February. Vertical temperature gradients are largely governed by vertical mixing and diffusion between a surface layer composed of largely harbor and sound water and a bottom layer of coastal water.

The annual salinity regime is mainly regulated by the stream discharge entering Long Island Sound and New York Harbor. The two major sources of this stream discharge are the Connecticut River for the Sound and the Hudson River for the harbor. There is also approximately a one-month lag between maximum stream discharge and the corresponding salinity minimums.

Linear correlations at a one-month lag and dilution fᵣ ᵢ..s, D, were calculated for Block Island Sound. The highest correlations occur at the center stations of the H and HB transects and the weakest correlation occurs at Station BR3 (55%). Weak correlations at depth (30m) imply a two-layered system, with a surface layer that is composed of less saline Long Island Sound waters and a bottom layer of saline coastal waters. Vertical mixing and diffusion is relatively weak in Block Island Sound, as indicated by these high correlations and dilution factors.

The average extinction coefficient for Block Island Sound in the visible spectral band was 0.335, as compared to a mean value for the New York Bight of 0.663, almost a factor of 2 greater. The mean value for the blue band is 0.400 in Block Island Sound and 1.048 in the New York Bight; for the red band, the value is 0.554 and 0.876 in the Sound and Bight respectively. The disparity in these two wavelength bands dramatizes the shift of the peak of maximum transmissivity from shorter to higher wavelengths with increasing turbidity.

The average extinction coefficients for each transect in Block Island Sound were correlated with total particle counts as determined with a Coulter Counter and for particle counts greater than 5μ in equivalent diameter. Highest correlations occur with particles greater than 5μ,

but less than 10μ in size. Similar results were obtained for the New York Bight stations. These results reflect nonselective attenuation, particularly absorption, since the lower limit of the total particle count is approximately 0.7μ in equivalent size so that selective or Raleigh scattering is not included in these calculations. The correlations would be significantly improved if the resolving power of the Coulter Counter could be increased; however, this is an engineering design problem that hopefully will be resolved in the future.

Chemical Oceanography

In Block Island Sound, the nutrients (phosphates, nitrates, and silicates) showed the seasonal variations typical of temperate waters. Indications are that the supply of nitrogen to these waters is limited and that, under the appropriate conditions, the nutrients are utilized by the phytoplankton rather quickly. Although relatively large seasonal changes in concentration were noted, the correlations between these parameters and chlorophyll a were not considered significant.

In early October 1972 what appeared to be the remnants of an algae bloom were found at those stations occupied along the H transect. Little evidence of such conditions was found for the other transects. Chlorophyll a concentrations generally remained low (0.5-1.0 mg/m³) through the remainder of the fall and winter. A spring flowering of relatively short duration was present in March. Peak chlorophyll a concentrations of 9.4 mg/m³ were present at Station H1. The amount of chlorophyll a present in the surface waters of this transect gradually decreased from the high value noted at Station 7 to 2.1 mg/m³ at Station 4. No evidence of a spring outburst of similar magnitude was found in the waters of the other transects.

The reasons for this may be that the frequency of sampling was such that the bloom was missed along the other transects, or the data reduction techniques affected the graphical presentation. In respect to the latter, the range of chlorophyll a at BRl was 1.69-3.39; at BR2 a range of 2.01-2.60 mg/m^3, and at BR3 a range of 0.85 to 3.04 mg/m^3. Along the HB transect, inclement weather prevented sampling from 14 February until 25 Apr., and, undoubtedly, the spring bloom was missed.

This study was designed to provide a background data base upon which the conditions which existed at the moment in time at which the Skylab EREP data was collected could be fitted in some meaningful fashion. The sampling program was designed to collect data on the effect of both tidal and non-tidal forces upon a given parameter and, consequently, to yield information pertinent to the above. Skylab-3 12 September 1973 data was collected at approximately 1200 hours and at that time higher concentrations of both particulate phosphorus and the pigmented population were present at Station HI than at the remaining stations. This station also showed the greatest range of concentration for both of these parameters. Since this range of variation is typical of the variability to be expected for most parameters, it is particularly important that additional information be gathered relevant to the variability of all parameters in both short- and long-term space and time.

With respect to the former, an experiment was conducted on 12 May 1973, with the help of the local power squadrons and private yachts, to collect synoptic samples for the measurement of suspended material, salinity, and temperature in the surface waters of Block Island Sound and adjacent waters. In this preliminary experiment, logistics prevented the collection

of samples for chlorophyll. The location of each of the sampling vessels is shown in Appendix A. The sampling times were 0900, 1200, and 1500 hours. It should also be noted that, although care was exercised in the storage of the samples, certain of those collected early in the day remained in the plastic containers for more than ten hours prior to filtration.

The synoptic distribution of temperature, salinity, and ·· ponded solvents is shown in Appendix A. For each of the three parameters observed large ranges in values and concentrations were noted. The effect of the tidal forces upon the distribution of these parameters was apparent.

In New York Bight, the concentration of nutrients and chlorophyll was generally higher along the New York Harbor transect than along the TR transect. This was especially apparent in the nitrate concentrations. Evidences for seasonal trends were particularly evident in the nitrate and silicate data.

No significant correlation between the nutrients, particulate phosphate, and chlorophyll a was found for the TR transect at any time. Along the NYB transect, however, strong correlations were found between the concentration of chlorophyll a and soluble organic phosphorus. It was also noted that the correlation was strongest in May. For example, the overall correlation of soluble organic phosphorus with chlorophyll a for the NYB transect was 0.88. In December and January, the correlations were not significant (r=0.01 and 0.12 respectively), while in May the correlation was 0.95.

Phytoplankton and Suspended Particles

The high correlation between phytoplankton and suspended particles

>10.7µ equivalent diameter in Block Island Sound (0.858) indicates that the phytoplankton may contribute largely to the suspended material in this region. In contrast, the lower correlation between these parameters in the New York Bight (0.586) indicates that other factors are adding to the suspended load in this area. Suspended materials are being brought into the area by the Hudson River outflow, as evidenced by the high total particle counts and lowered salinity values (see Appendix A) at station NYB3.

The phytoplankton population was highest at the New York Bight and Block Island Sound stations, with the TR stations having the lowest number of cells. There are indications that the organic enrichment caused by the disposal of sewage sludge in the New York Bight may play a role in maintaining the relatively high phytoplankton population in this region.

In Block Island Sound, the stations around Montauk Point generally exhibited the largest phytoplankton populations, these populations probably originating in the waters of the Peconic Bay-Gardiners Bay system.

Block Island Sound can be divided into three regions: (1) northern Block Island Sound, influenced by the coastal waters of Connecticut, Rhode Island, and the Cape Cod region; (2) southern Block Island Sound, influenced by the waters of the Peconic Bay-Gardiners Bay system; and (3) central Block Island Sound, influenced by the waters of Long Island to the west and the Atlantic Ocean to the east.

In the experiment, conducted on 12 May 1973, the largest population occurred in the Peconic Bay-Gardiners Bay region, with a smaller population found in northern Long Island and Block Island Sound waters. These populations were separated by the sparsely populated waters apparently originating in central and southern Long Island Sound, passing through central Block

Island Sound, and meeting the waters of the Atlantic Ocean between Montauk

Point and Block Island. This type of circulation of the surface waters

was shown previously by Nuzzi (1973) and Austin (1973).

Section 6

Ground Truth at Shagwong Reef

Satellite imagery provides a synoptic overview of features in complex estuaries and coastal environments which, in many cases, would be missed by usual ship sampling techniques. River plumes and effluents which are clearly apparent on satellite imagery are nearly invisible to the observer at sea level. Perhaps even more important are those locations where waters appear to have color characteristics that are different from their surroundings. These "discolored" water masses may have no relationship to harbor effluents or river plumes, but are distinct water types that have unique origins.

Extensive ship sampling programs correlated with ERTS-1 imagery in the area of Montauk Point, Long Island, New York indicated that a very distinct and fairly persistent plume of water was associated with Shagwong Reef located three nautical miles northwest of Montauk Point. Since this plume appears in ERTS satellite imagery taken during both flood and ebb stages of the tide, it is hypothesy that it is <u>not</u> an advected phenomena since it does not appear to be transported to the area by currents or tides. This plume is hypothesized to be generated in the area of the Shagwong Reef itself.

It is believed that the Shagwong Reef plume is caused by seasonal biological phenomena composed principally of organic material. It is also hypothesized that the action of tidal currents which bring organic detritus to the surface by scouring action is <u>not</u> the cause of this plume since there is no significant seasonal difference in tidal flow in this area. Yet,

there are periods in late winter and in September when the plume does
not appear in ERTS satellite images.

Two sampling stations were positioned in the area of Shagwong Reef
in Block Island Sound approximately three nautical miles northwest of
Montauk Point, Long Island. The location of these stations was selected
based upon the appearance of a plume of water in this area on ERTS-1
images. The stations were positioned so that Station One (SI, 41°06.2'N,
71°55.3'W) would be outside of the plume area and Station Two (S2, 41°06.2'
N, 71°54.9'W) within the plume. S2 was the upstream station during the
ebb tide cycle.

Two extensive sampling programs were conducted on 9 August 1973
and another on 12 September 1973. No data was recorded by Skylab on
9 August because of total overcast conditions (100 percent cloud cover
at the test site). Data was acquired by Skylab on 12 September 1973 and
was used in the analysis.

Detailed physical, chemical, and biological sampling was conducted
at both sampling stations throughout the day. Water samples were collected
hourly for analysis of salinity, suspended solids, total particle phyto-
plankton, reactive phosphorous, total dissolved phosphorous, particulate
phosphorous, pigments, and suspended solids. Temperature was measured in
situ at several depths at each station.

The Skylab 3 overpass occurred at approximately 1310 EDT on 12
September 1973, at which time a maximum ebb current condition existed
at Shagwong Reef. At this time, the current was 43.8 cm/sec. in a
direction 069° true. The optical characteristics of the water were
measured in the suspected location of the plume (S2) fifteen minutes
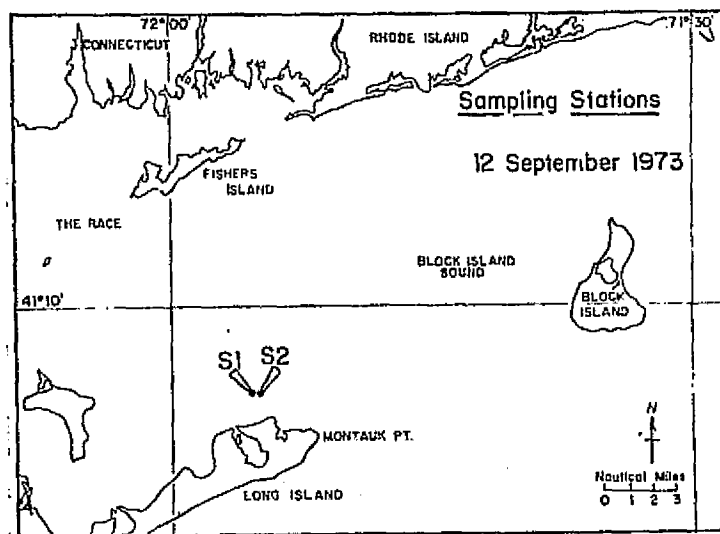
Figure 46 . Chart showing the location of Shagwong Reef.
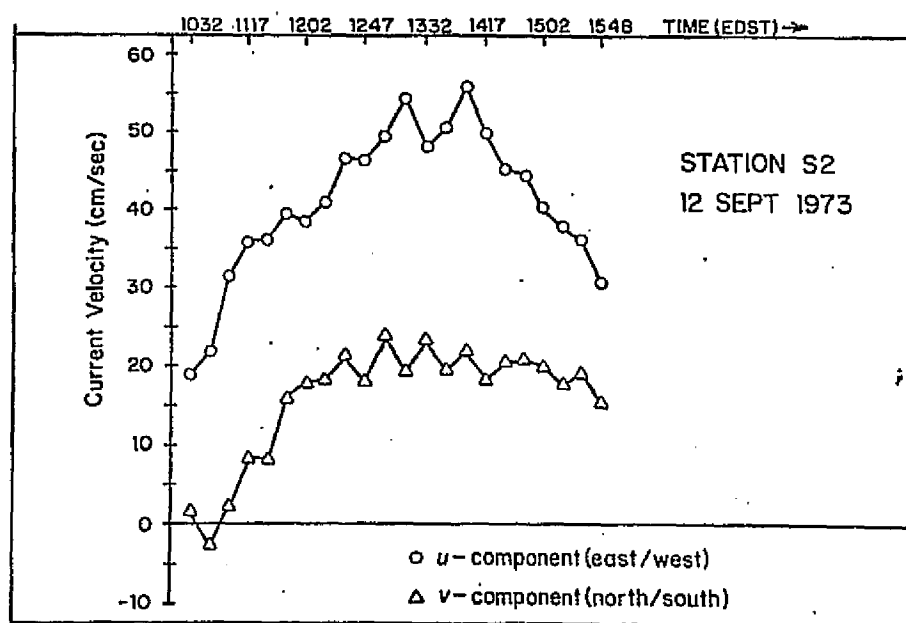
Figure 47. Current meter data.

before the Skylab pass. The average extinction coefficient ($\overline{k}$) at 1255 EDT was found to be -0.26 per meter. At SI, which was located so as to be outside the plume, the average extinction coefficient was measured to be -0.33 per meter. This measurement at SI was made at 1215 EDT, fifty-five minutes prior to the Skylab pass.

The "extinction coefficient" is a measure of the attenuation of incident sunlight (downwelling irradiance) as a function of depth within the water column and is defined by the equation:

$$I(z) = I(z=o) \exp(-kz)$$

where:

$I(z=o)$ = total irradiance at the surface

$I(z)$ = remaining irradiance at the depth z (in meters)

A summary of the optical characteristics of the water at the Shagwong Reef within an hour of the Skylab pass on 12 September 1973 are summarized below in terms of that depth to which a prescribed percentage of solar irradiance incident upon the water's surface penetrated.

	Station SI (outside plume) 1215 EDT	Station S2 (within plume) 1255 EDT
100%	Surface	Surface
75%	-0.6 m	-1.3 m
50%	-2.0 m	-2.6 m
25%	-4.6 m	-5.0 m
10%	-8.3 m	Below Bottom
1%	Below Bottom	Below Bottom
$\overline{k}$	-0.33 per meter	-0.26 per meter

Table 15. Optical characteristics of the Shagwong Reef plume at the approximate time of Skylab 3 pass on 12 September 1973.

The details of the methods used to collect and analyze all physical, chemical, and biological water samples taken are described in Appendices A, E, and F. A summary of the results of the analyses appears in Tables 17 through 19 at the end of this section. A summary of the salient features which existed at 1310 EDT, the time of the overpass, is presented below:

Parameter Measured		Station S1 (Outside Plume)	Station S2 (Within Plume)
Temperature (°C)	Surface	20.1	19.8
	-5 m	19.9	--
	-7 m	--	19.8
	-10 m	19.8	--
Salinity (0/00)	Surface	29.79	29.83
	-5 m	29.81	--
	-7 m	--	29.86
	-10 m	29.85	--
Density (σ_+)	Surface	20.81	20.90
	-5 m	20.85	--
	-7 m	--	20.93
	-10 m	20.91	--
Suspended Solids (mg/l)	Surface	2.19	2.79
	-5 m	1.77	--
	-7 m	--	2.68
	-10 m	3.67	--
Chlorophyll α (µg/l)	Surface	2.67	2.55
	-5 m	2.94	--
	-7 m	--	2.28
	-10 m	2.45	--
Total Particles ($\times 10^6$/l)	Surface	185	206
	-4 m	190	--
	-8 m	207	203
Total Cell Count ($\times 10^3$/l)	Surface	10.5	15.2
	-4 m	14.3	--
	-8 m	6.7	4.8

Table 16. Principle water characteristics within and outside of Shagwong Reef at the time of Skylab 3 pass, 1310 EDT on 12 September 1973.

A graphical synopsis of the optical characteristics, suspended solids, and total particles at Shagwong Reef, as a function of depth at or near the time of Skylab 3 overpass, is shown in Figure 48.

		Station S1					Station S2		
Time	Depth(m)	T°C	S°/oo	σ_t	Time	Depth(m)	T°C	S°/oo	σ_t
1100	0	20.0	29.80	20.83	1106	0	19.8	29.83	20.90
	5	19.8	29.84	20.90		7	19.9	30.08	21.07
	10	19.5	30.01*	21.05					
1202	0	20.1	29.79	20.80	1207	0	19.8	29.83	20.90
	5	19.8	29.80	20.85		7	19.8	29.87	20.94
	10	19.6	29.87*	20.95					
1300	0	20.1	29.79	20.80	1255	0	19.8	29.83	20.90
	5	19.9	29.80	20.85		7	19.8	29.86	20.93
	10	19.8	29.84*	20.90					
1400	0	20.0	29.82	20.85	1400	0	19.8	29.85	20.94
	5	19.8	29.86	20.89		7	19.8	29.88	20.94
	10	19.7	29.92*	20.99					
1500	0	20.2	29.83	20.80	1445	0	19.8	29.87	20.92
	5	20.0	29.86	20.85		7	19.8	29.88	20.94
	10	19.8	29.94*	20.99					
1600	0	20.2	29.81	20.79	1555	0	19.8	29.85	20.92
	5	20.0	29.84	20.82		7	19.8	29.88	20.94
	10	19.9	29.87*	20.90					

*Extrapolated

Table 17. Temperatures, salinities, and σ_t for the September 12, 1973 experiment.
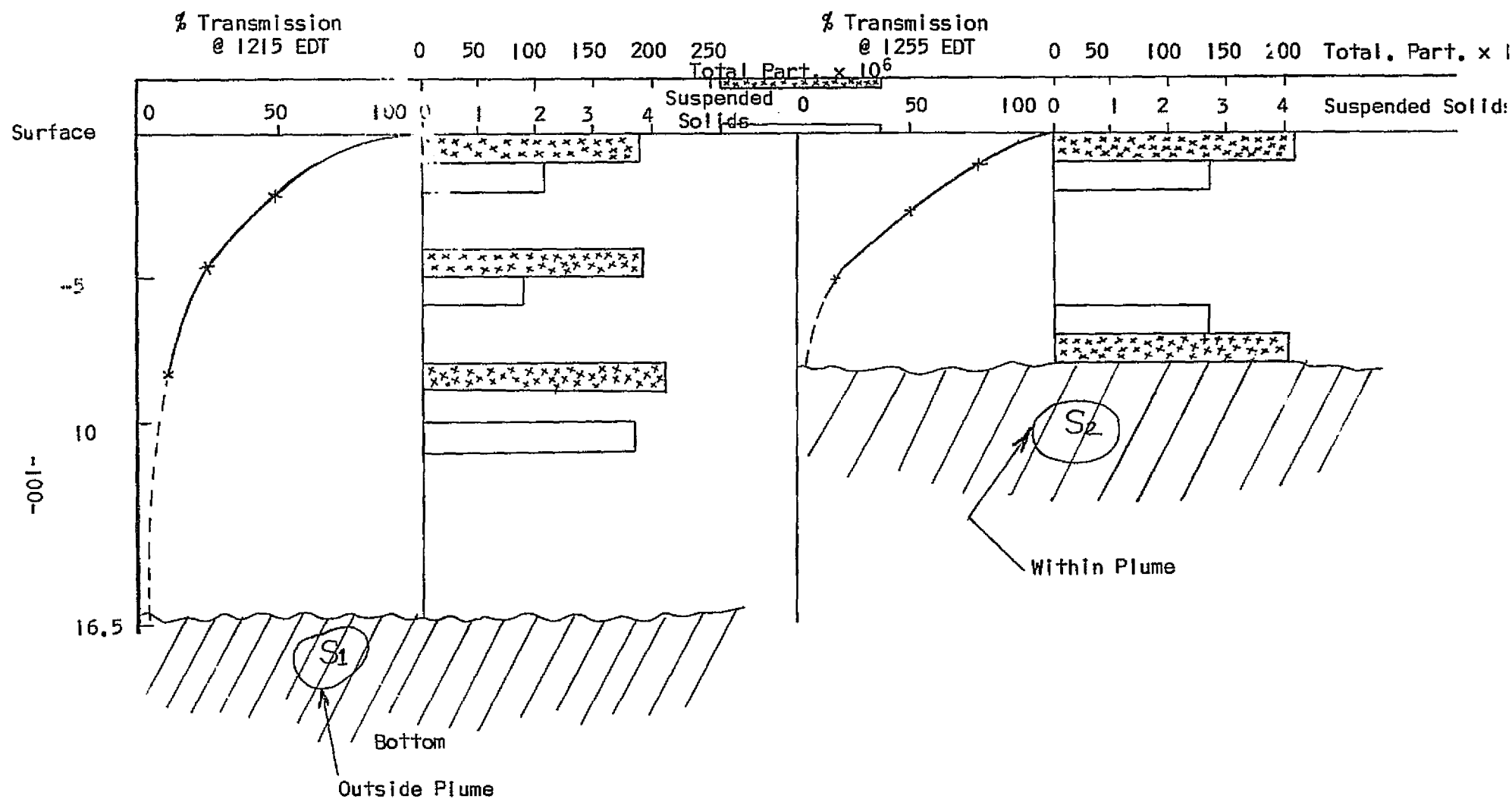
Figure 48. Transmission of solar irradiance, total particles, and suspended solids at Shagwong Reef as a function of depth at or near the time of Skylab 3 overpass on 12 Sept. 1973.

Station S-1

Time	Depth (m)	Suspended Solids (mg/l)	R-PO$_4$ (μg-at/l)	T-PO$_4$ (μg-at/l)	P-PO$_4$ (μg-at/l)	Chl a (μg/l)
1100	0	3.20	1.04	1.26	1.06	1.69
	5	2.34	1.04	1.43	1.27	1.99
	10	2.21	1.08	1.59	0.89	1.58
1202	0	2.54	1.01	1.21	1.15	2.35
	5	2.58	0.99	1.37	1.64	0.75
	10	1.27	1.03	1.37	1.30	0.95
1300	0	1.85	1.02	1.76	1.78	2.65
	5	1.58	1.03	2.31	1.78	2.97
	10	3.78	1.00	1.32	1.63	2.46
1400	0	3.91	1.06	1.32	1.45	2.74
	5	2.70	1.04	1.43	1.54	2.79
	10	2.93	1.07	1.48	1.40	2.41
1500	0	2.08	0.98	1.32	1.13	0.66
	5	7.74	0.96	1.32	1.44	2.60
	10	2.25	9.99	2.47	1.30	2.50
1600	0	3.85	0.94	1.43	1.02	2.15
	5	2.13	0.94	1.26	1.40	2.36
	10	1.64	1.00	1.98	1.42	2.25

Station S-2

Time	Depth (m)	Suspended Solids (mg/l)	R-PO$_4$ (μg-at/l)	T-PO$_4$ (μg-at/l)	P-PO$_4$ (μg-at/l)	Chl a (μg/l)
1106	0	6.06	1.09	1.81	0.87	3.21
	7	1.86	1.24	1.87	0.86	1.54
1207	0	13.64	1.04	1.54	1.51	1.05
	7	1.92	1.05	1.43	1.27	1.76
1255	0	3.12	1.06	1.37	1.45	2.52
	7	2.77	1.09	1.37	1.45	2.43
1400	0	1.70	1.01	1.26	1.65	2.63
	7	2.37	1.02	1.32	1.56	1.58
1445	0	4.65	0.97	1.15	1.18	1.50
	7	6.43	1.06	1.70	1.34	2.40
1555	0	1.56	0.94	1.59	1.50	2.35
	7	1.29	0.97	1.26	1.43	2.34

Table 18. Variations in suspended solids, phosphorous, and chlorophyll a, 12 September 1973.

Time (EDST)	S1 - Surface Total Particles per liter x 10^6	S1 - Surface Particles >10.67μ per liter x 10^3	S1 - Surface Cells per liter x 10^3	S1 - (3.5-4m) Total Particles per liter x 10^6	S1 - (3.5-4m) Particles >10.67μ per liter x 10^3	S1 - (3.5-4m) Cells per liter x 10^3	S1 - (7-8m) Total Particles per liter x 10^6	S1 - (7-8m) Particles >10.67μ per liter x 10^3	S1 - (7-8m) Cells per liter x 10^3	S2 - Surface Total Particles per liter x 10^6	S2 - Surface Particles >10.67μ per liter x 10^3	S2 - Surface Cells per liter x 10^3	S2 - (8m) Total Particles per liter x 10^6	S2 - (8m) Particles >10.67μ per liter x 10^3
1100	215	238	14.2	249	193	7.6	218	189	7.6	140	208	8.6	176	236
1200			6.7			3.8			14.3			8.6		
1300	185	202	10.5	190	247	14.3	207	148	6.7	206	275	5.7	203	263
1400			5.7			8.6			9.5			9.5		
1500	158	175	12.4	194	149	12.4	299	148	20.9	204	183	4.8	201	181
1600			4.8			13.3			9.5			4.8		
Average of all sampling periods	186	205	9.1	211	196	10.0	241	162	11.4	183	222	7.0	193	227

Table 19. Distribution of particles and phytoplankton, 12 September 1973.

Section 7

Photo-Optical Analysis

of S-190A and S-190B Photography for Water Detail

This section describes photographic reprocessing of Skylab-3
S-190A black-and-white multispectral imagery. Also presented are the
results of photo interpretation analyses of both reprocessed and released
multispectral images, as well as interpretation of both S-190A color and
S-190B color transparencies.

Photographic Reprocessing of S-190A Multispectral Images

The general procedure used in the reprocessing of each multi-
spectral image is illustrated by the set of characteristic curves, as
shown in Figures 49 and 50. The slope of the conventionally processed
multispectral images was a faithful relationship between negatives and
positives is required were well matched. The minimum density of the
500-600 nm negative was excessive however. These curves were generated
plotting the gray scale density on the x axis with the positive gray
scale density plotted on the y axis. Unfortunately, all the water areas
in the negative have low negative densities causing high minimum densi-
ties and relatively small density differences in water detail for a
large change in density in the negative image.

The conventionally processed positive imagery was placed into
the Spectral Data Model 70 viewer and the spectral records were projected
as follows:
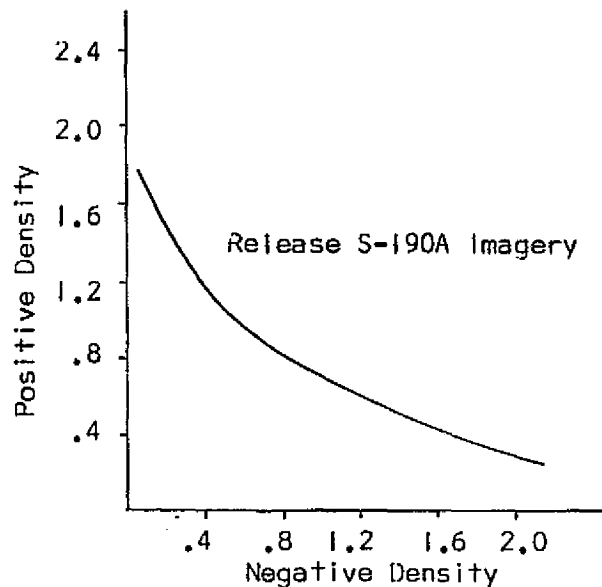
Figure 49. Typical curve of negative density vs. positive density of conventionally processed transparencies.

500-600 - Blue	700-800 - Red
600-700 - Green	800-900 - Red

Only one of the infrared records was projected at a time with the two visible bands. Of all the records, the 500-600 nm band had the most detail in both land and water.

The release negatives were used to generate a second set of positives which would enhance detail in the water mass. Both the exposure and processing were altered to "stretch" the low brightness regions as shown in Figure 50. Notice that those low-density regions on the negative in Figure   have now been "stretched" to increase the density image. The minimum density has also been reduced in all bands. Contrast increased by using E. 2420 duplicating film and processing in D-19. The scene brightness range for both water and land is small so that a single reproduction of the green record was used for the enhancement of
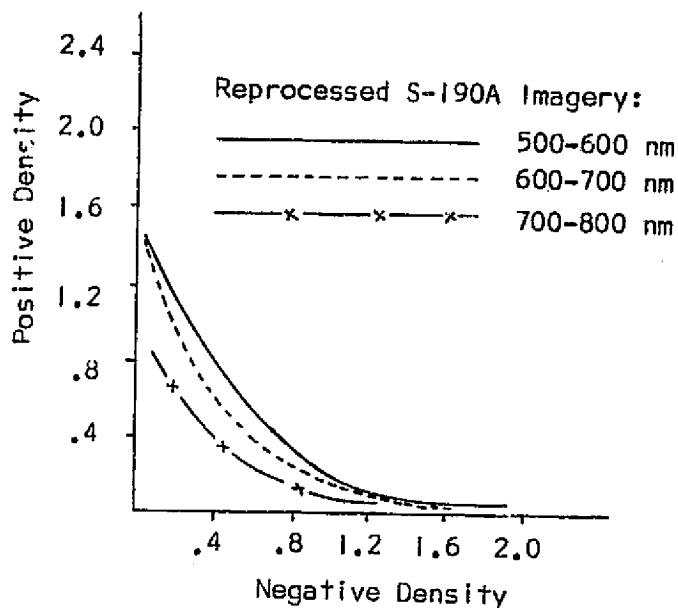
Figure 50. Curve of negative density vs. density of "stretched" positives which were reprocessed to enhance water detail.

both water and land areas. The most meaningful comparison of the effects of reprocessing was made by additive color photo interpretation of differences in the water. The densitometric factors affecting the density of water images are shown in Table 20 on the following page.

Shagwong Reef

Skylab-3 passed over the Shagwong Reef test site , located three nautical miles northwest of Montauk Point, Long Island, at 1311 EDT on 12 September 1973. At that time it was approximately three hours after slack ebb began at the race. From the tidal current chart shown in Figure 51, one would have estimated an ebb current of about 1 knot at Shagwong Reef which is not significantly different from the 43.8 cm/ sec. current velocity measured at 1311 EDT.

Transparency No.	Density Min. Max.	Density Range
500-600 nm:		
Negative	.96 - 1.39	.43
Conventional Positive	.97 - 1.32	.35
Water "Stretch" Positive	.33 - 1.92	.59
600-700 nm:		
Negative	.51 - 1.39	.88
Conventional Positive	.97 - 1.76	.79
Water "Stretch" Positive	.14 - 1.19	1.05
700-800 nm:		
Negative	.16 - .51	.35
Conventional Positive	1.76 - 2.36	.60
Water "Stretch" Positive	.45 - .91	.46
800-900 nm:		
Negative	.16 - .51	.35
Conventional Positive	1.76 - 2.36	.60

Table 20. Densitometric factors affecting composite image color of water areas.

Reproductions of reprocessed S-190A multispectral photography, taken in the 500-600 nm and 600-700 nm bands, are shown in Figure 52. Water areas of significantly different density in these two images, as well as in the S-190A color image, have been compiled on the three charts reproduced in Figure 53. Using these figures, the following conclusions can be drawn:
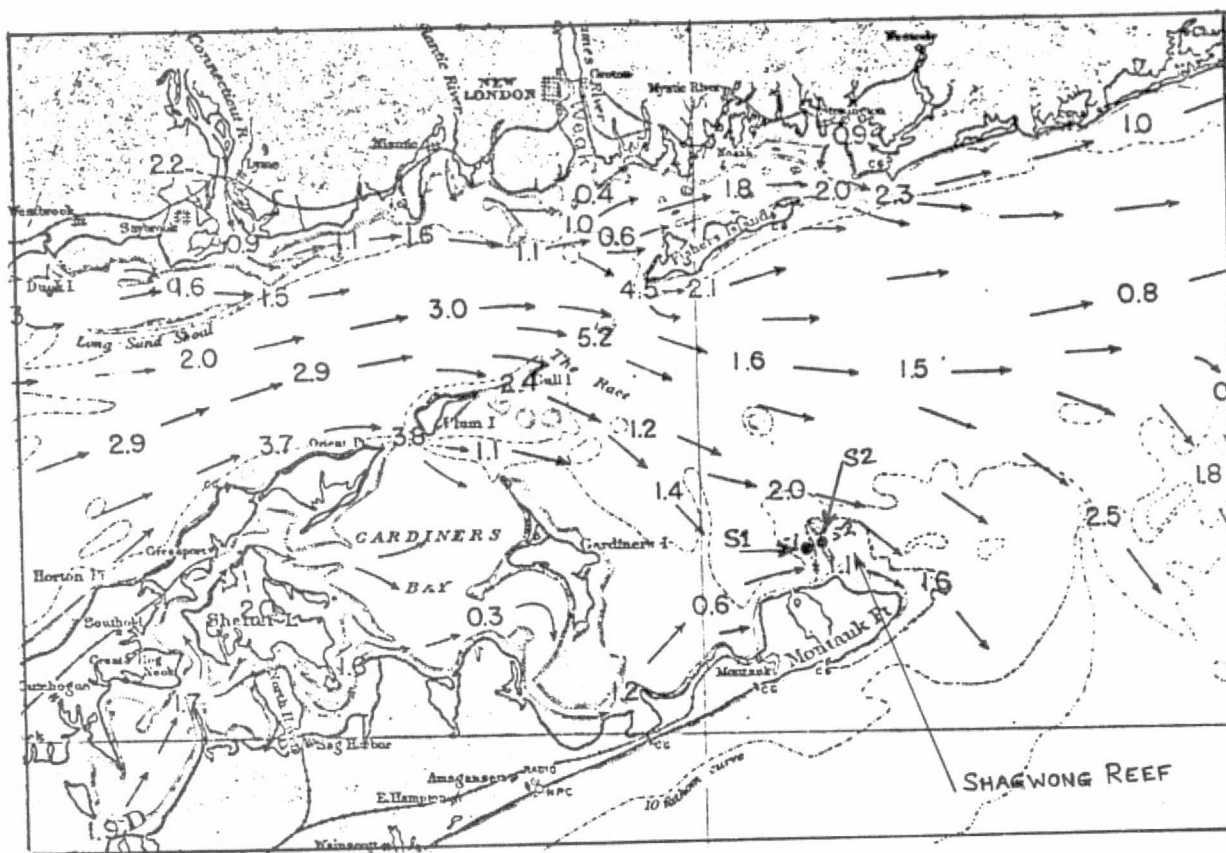
Figure 51. Tidal current at Shagwong Reef at 1311 EDT, 12 September 1973, approximately three hours after slack ebb begins at the race (velocities in knots).

-- S-190A multispectral photography, when reprocessed to

maximize water detail, exhibits sufficient density

difference in both the 500-600 nm and 600-700 nm bands

to readily allow differentiation between two water

masses which have an optical characteristic difference

of 0.07 per meter extinction coefficient (i.e., 0.26

vs. 0.33 per meter); differences in suspended solids

of 0.6 mg/l (2.19 vs. 2.79 mg/l); and differences in
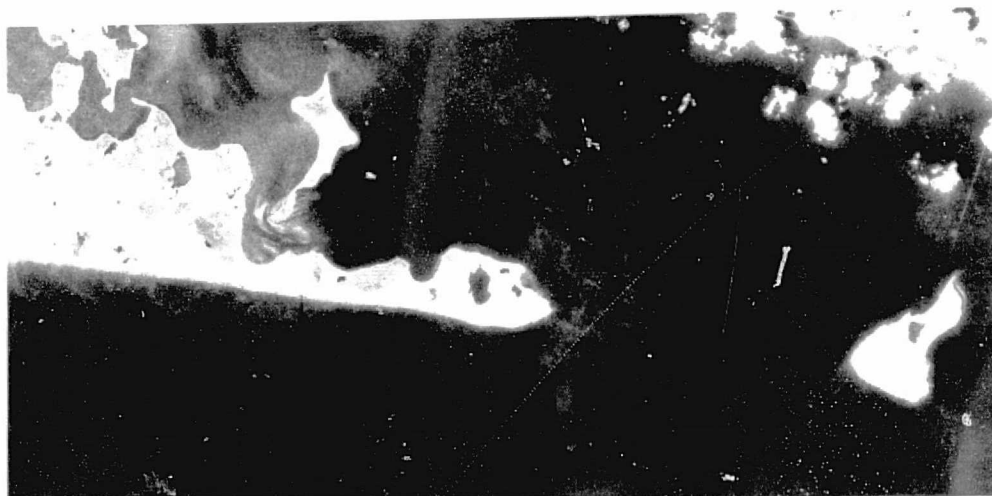
500 - 600 nm Band

600 - 700 nm Band

Figure 52. S-190A multispectral imagery of the Shagwong Reef area in
Block Island Sound - Skylab-3, 12 September 1973, 1311 EDT.

total particles of 21×10^6 per liter (185 vs. 206 $\times 10^6/1$).

-- The 600-700 nm band enhanced multispectral photo produced a distinct density boundary between two water masses which is hypothesized to be significantly due to a difference in total cell count of 4700 per liter (10,500 vs. 15,200 per liter), as well as a total particle count difference of 21 million particles per liter).

-- A sharp image density boundary on the 600-700 nm multispectral image, accompanied by a more diffuse boundary in the 500-600 nm band, indicates non-homogeneous vertical stratification of suspended solids and total particles in water having practically identical temperatures, salinities, and densities. Suspended solid differences of one milligram per liter (2.68 vs. 3.67 mg/1), at depths between seven and ten meters, were distinguished between waters that were for all other purposes practically homogeneous.

-- Water masses having the above optical characteristics and suspended solids could not be differentiated on S-190A color infrared imagery and were just at the threshold of perceptibility in color S-190A imagery.
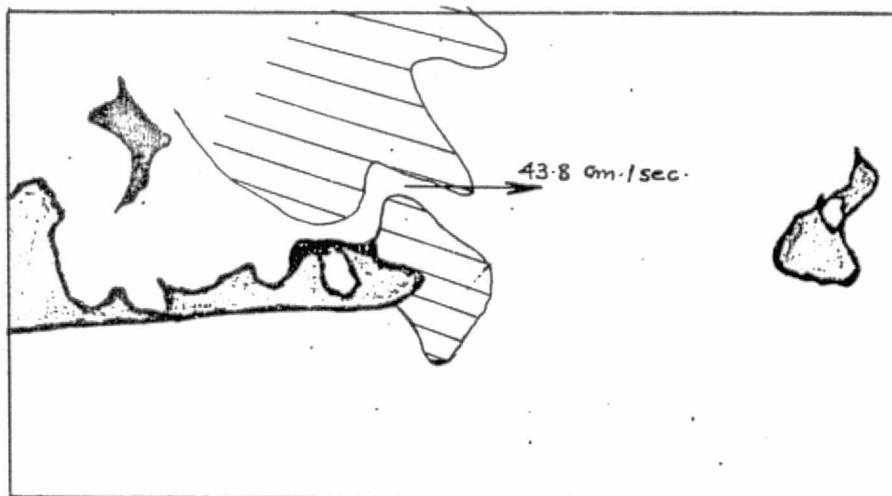
500 - 600 nm Band
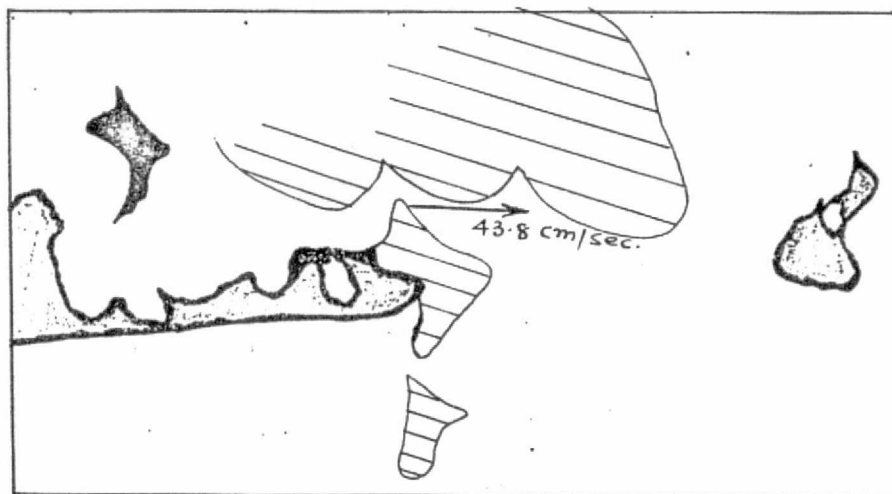
600 - 700 nm Band
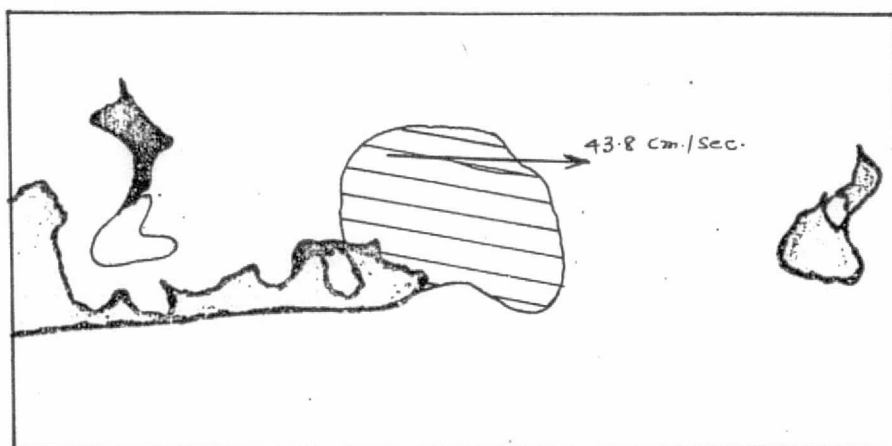
Color

Figure 53. Comparative interpretation of image brightness of the Shagwong Reef, Block Island Sound, in S-190A imagery taken on 12 September 1973 at 1311 EDT.

Long Island Sound

The movement of water in Long Island Sound is controlled by the semi-diurnal tide upon which there is imposed a non-tidal circulation pattern driven by a combination of effects from fresh water inflow, salinity, temperature, and density gradients and bottom topography. Along with the tidal flow, this net flow is continually being modified at the surface by the prevailing wind conditions. During the summer months, the winds are generally from the south and southwest.

There is evidence that in the eastern end of the Sound there exists a large counter-clockwise gyre that is supported by the estuarine circulation pattern. An examination of S-190B imagery acquired on 19 September 1973 at 1629 EDT comfirmed this. Figure 54 shows a chart of water turbidity which indicates two large counter-clockwise water movements. The bottom waters incoming from Block Island Sound upwell and mix with the surface waters along the Connecticut shore which then, in turn, move southward and become part of the net westward flow of surface waters through the race and plum gut. Figure 55 shows the tidal current charts of the Sound at this time. No gyres are indicated. Although this circulation pattern may predominate in the eastern two-thirds of the Sound, there is a possibility that the large gyre is broken up into a series of gyres due to the effects of the tidal flows and lateral differences. Such a secondary gyre has been plotted in Figure 54, east of New Haven along the Connecticut shore. A large counter-clockwise gyre has been found in the eastern end of the Sound with a weaker clockwise gyre in the central portion and evidence of another counter-clockwise gyre further west. This gyre scheme is influenced, to a large degree, by fresh water discharge and weather patterns. Indication
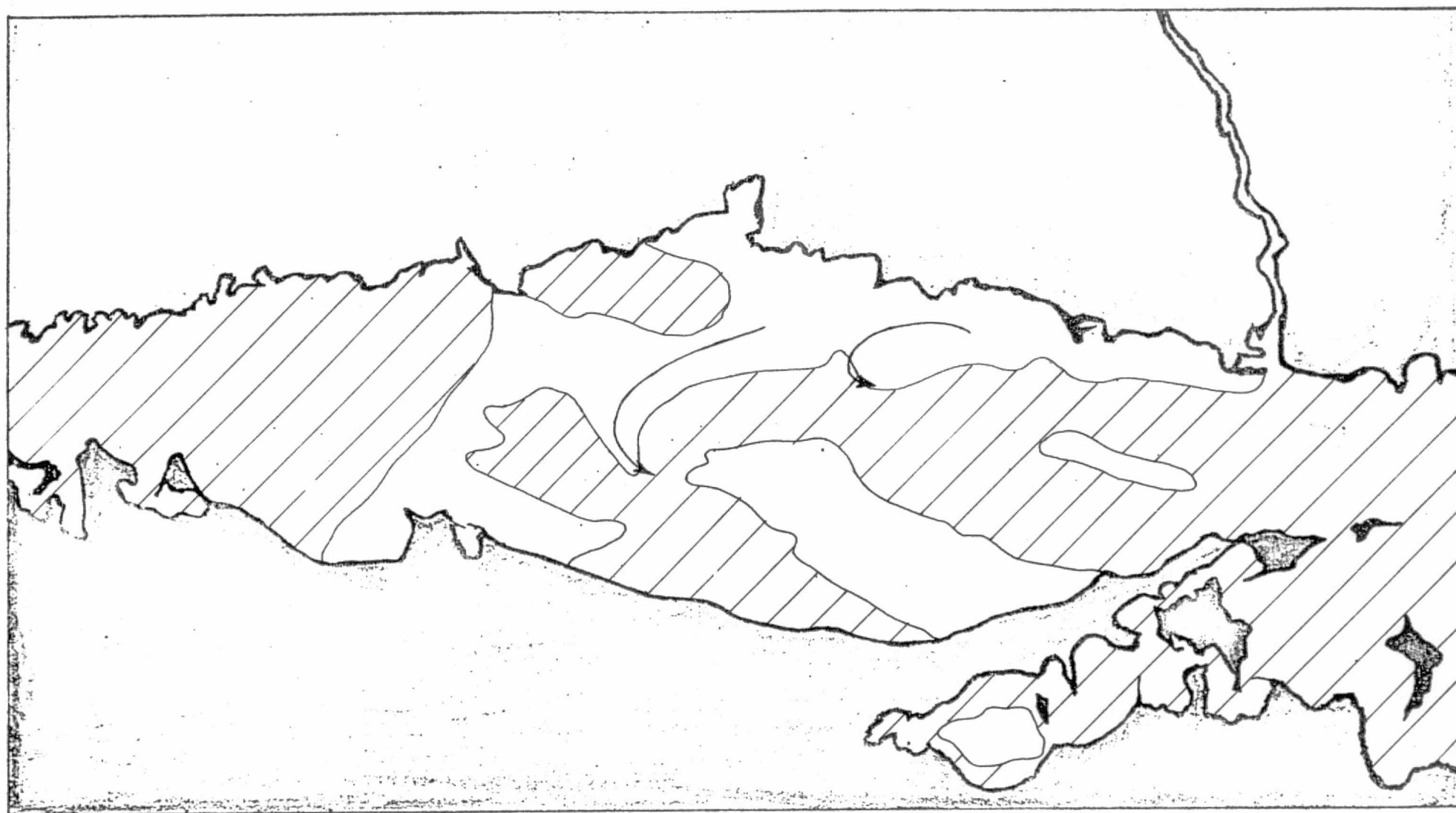
Figure 54. Interpreted location of suspended materials in Long Island Sound in S-190B color transparency taken by Skylab-3 on 19 September 1973 at 1629 EDT.
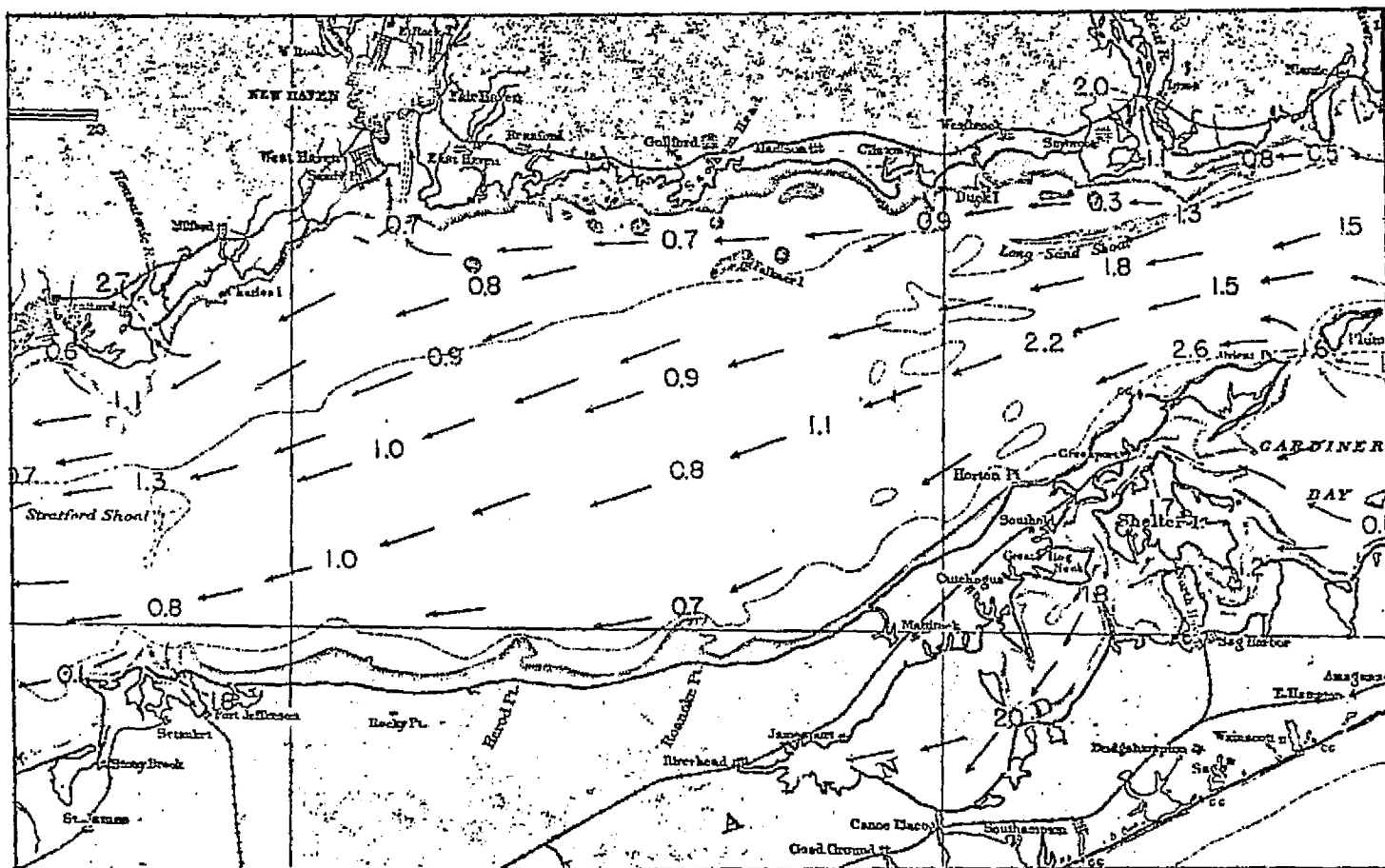
Figure 55. Approximate tidal current in Long Island Sound at 1629 EDT on 19 September 1973 (velocities are in knots).

of a south clockwise gyre, north of Eaton's Neck, can be seen in Figure

56   which is a color composite from an additive color viewer screen made

using S-190A release positives of 500-600, 600-700, and 700-800 nm bands.

An area of upwelling is also indicated along the northern shore of Long

Island between Mattituck Inlet and Orient Point in both the S-190A multi-

spectral imagery and in the S-190B color transparencies.   This upwelling
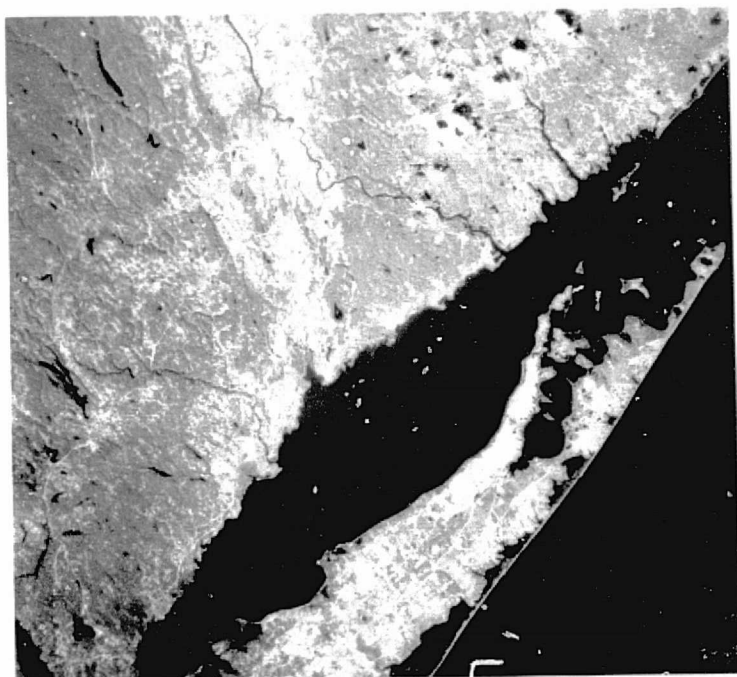
Figure 56. Additive color composite of Long Island Sound made using S-190A multispectral black-and-white positives. Image y was acquired on 19 Sept. 1973 at 1629 ED T. 500-600 nm band is imaged as blue, 600-700 nm band as green, and the   band as red.

is not due as much to the general circulation patterns as it is to the

strong prevailing winds when they occur offshore.

Block Island Sound

Skylab-3 S-190A and B photography of Block Island Sound, acquired at 1629 ED Ton 19 September 1973, was visually interpreted without any photographic enhancement prior to the computer analysis described in the following section. Figure 57 shows the approximate tidal current condition at that time which was four and one half hours after slack flood began at the race. At this time it can be seen that the current is beginning to ebb at Montauk Point, while the race is still flooding.
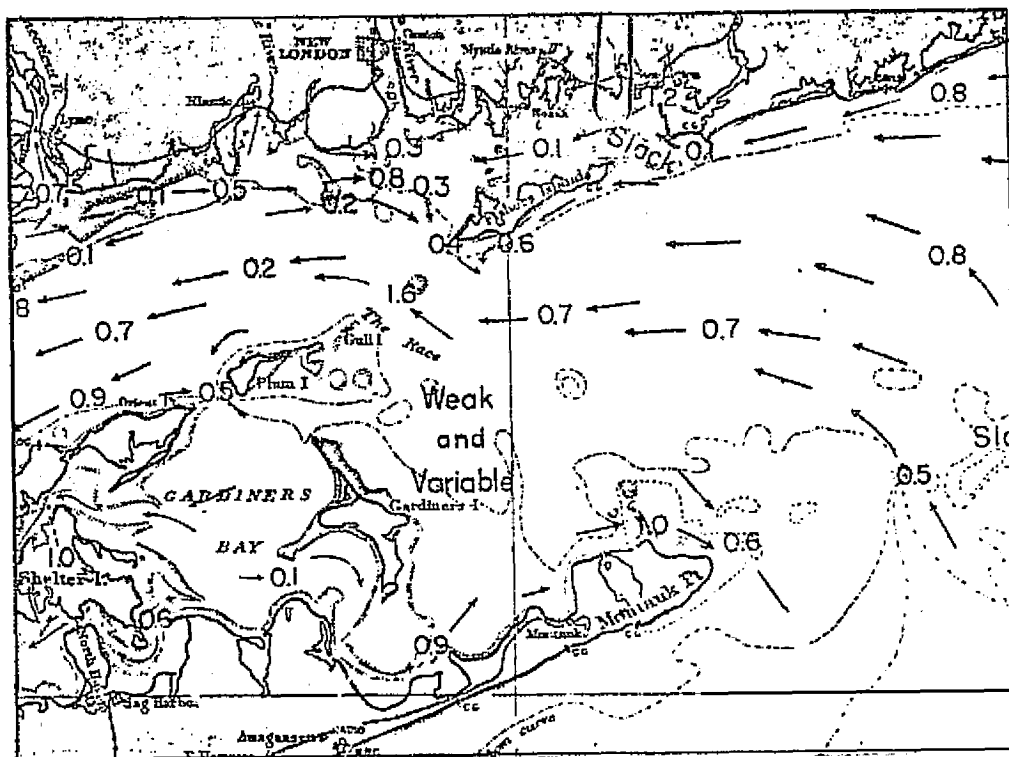
Figure 57. Approximate tidal current in the western portion of Block Island Sound at 1629 ED Ton 19 September 1973, five hours after slack flood begins at the race (velocities are in knots).

Figure 58 is a compilation of water density differences that could be discerned by visual photo interpretation of S-190B color imagery. Water discoloration was plotted east of Gardners Island (where the current was weak and variable), in Gardners Bay between Gardners Island and Orient Point, and on the northern portion of Montauk Point and western side of Block Island.

Figure 58. Interpreted location of suspended materials in S-190B color transparency acquired at Block Island Sound by Skylab-3 on 19 September 1973 at 1629 EDT.

Unenhanced positive S-190A multispectral black-and-white transparencies were analyzed in an additive color viewer. The 500-600 nm band was imaged as blue, the 600-700 nm band as green, and the 700-800 nm band as red. The resultant color composite photographed from the viewer screen is shown in Figure 59.
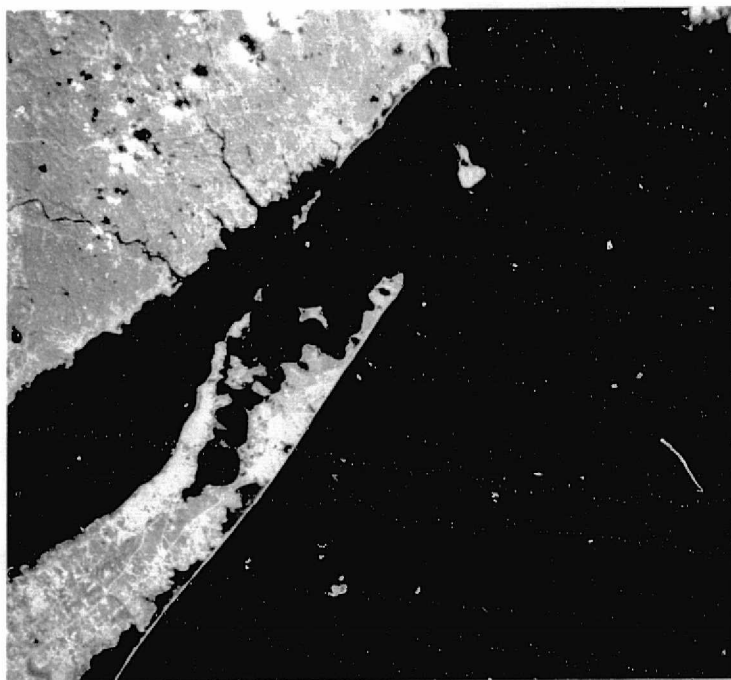
Figure 59. Additive color composite of Block Island Sound (island at right) made using S-190A black-and-white multispectral positives. Imagery was acquired on 19 September 1973 at 1629 EDT. 500-600 nm band is imaged as

The discolored water mass in Gardners Bay is readily seen in this

figure. Photo interpretation of the image on the viewer screen resulted

in identification of similar areas of water discoloration as was indicated in the S-190B color imagery.

New York Bight

A comparative analysis of black-and-white S-190A multispectral photography and the color-color infrared S-190 imagery of New York Bight, acquired by Skylab-3 at 1312 EDT on 12 September 1973, was performed. Unenhanced multispectral positive transparencies were analyzed using an additive color viewer and compared to the color and color infrared transparencies examined on a light table.

Figure 60 is a reproduction of a color composite created on the additive color viewer screen. It was found that this two-color rendition in which the 500-600 nm band is imaged as green and the 600-700 nm band as red produced the best color discrimination of the dump areas (extreme left center of the figure). The outline of a second dump can also be detected in this image. The suspended solids in the waters here exceed 20 milligrams per liter.

Figure 60. Additive color composite of S-190A black-and-white photo-
graph of New Yor Bight taken on 12 September 1973 at 1312 EDT. Acid
dump is at left and Long Island coast at upper left. 500-600 nm posi-
tive is imaged as greenand the 600-700 nm positive is imaged as red.

Digital Image Processing of S-190A Photography

of New York Coastal Waters

Skylab-3 S-190A multispectral photographs were processed using

the computerized "System 800." This system digitizes in registration

over one quarter of a million picture elements (pixels) into 256 bright-

ness levels for each multispectral photo.

Skylab-3 S-190A black-and-white multispectral photographs acquired

on 19 September 1973 covering Long Island Sound and Block Island Sound

were analyzed initially. Subsequently, southern New England coastal

waters south of Cape Cod , Massachusetts were processed using the

"System 800."

Block Island Sound

One set of Skylab-3 S-190A black-and-white negatives (Frame No.

239), acquired on 19 September 1973, was digitized in registration. Since

the purpose of this analysis was to investigate water detail, only the

multispectral photographs taken in the 500-600 and 600-700 nm bands were

used. The System 800 digital image output is shown in Figure 61.

Frame No. 239 of Block Island Sound was initially log digitized

using the MARKER, DIGIT, HISTOGRAM, AREA and DISPLAY programs. The results,

as displayed on the system color TV monitor, were compared with a similar

linear digitization of the same water features. In performing the compari-

son, the input video of each band was adjusted separately for each
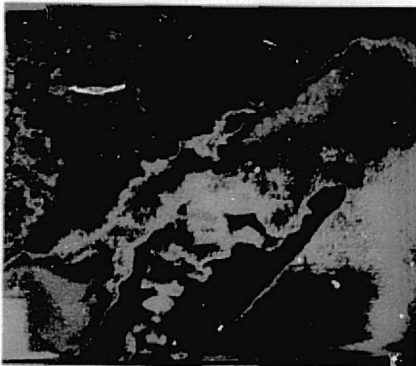
500-600 nm Band
Multispectral Photograph

600-700 nm Band
Multispectral Photograph
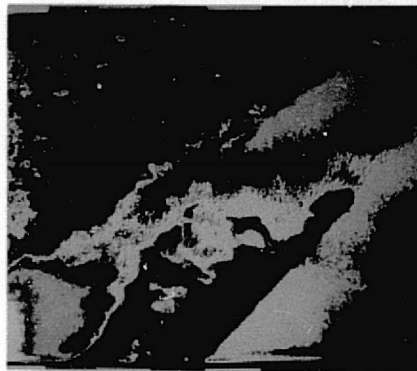
Average of the 500-600 nm band
plus 600-700 nm band photos shown above.

Figure 61. Color coded output of the "System 800" showing digitally processed S-190A imagery of Block Island Sound taken by Skylab-3 on 19 September 1973 (Frame No. 239).

multispectral photograph to bring out the maximum water detail for each.

A visual comparison of the resultant image detail showed considerably greater water image contrast existed when linearly digitized than when the image was digitized on the log mode. Consequently, only the _linear_ digitization of the photographic multispectral imagery was performed. The resultant digital brightness distribution is shown in Table 21 below.

Digitized Gray Levels	Color Code	S-190A Bands	
		500-600 nm	600-700 nm
0-32	Black	44.28	20.72
33-64	Red	11.44	11.18
65-96	Green	13.14	12.32
97-128	Yellow	11.70	22.82
129-160	Blue	11.68	20.50
161-192	Magenta	5.68	6.42
193-224	Cyan	1.32	3.12
225-255	White	0.68	2.82
	Totals ...	99.92	99.90

Table 21. Digital brightness percent area classification of Skylab-3 S-190A black-and-white multispectral images (Frame No. 239) of Block Island Sound acquired on 19 September 1973.

A histogram has been plotted of the digitized brightness levels in each of these two bands in Figure 62. Table 22 shows the Expected Value and Standard Deviation of the distribution of brightness in both multispectral images.
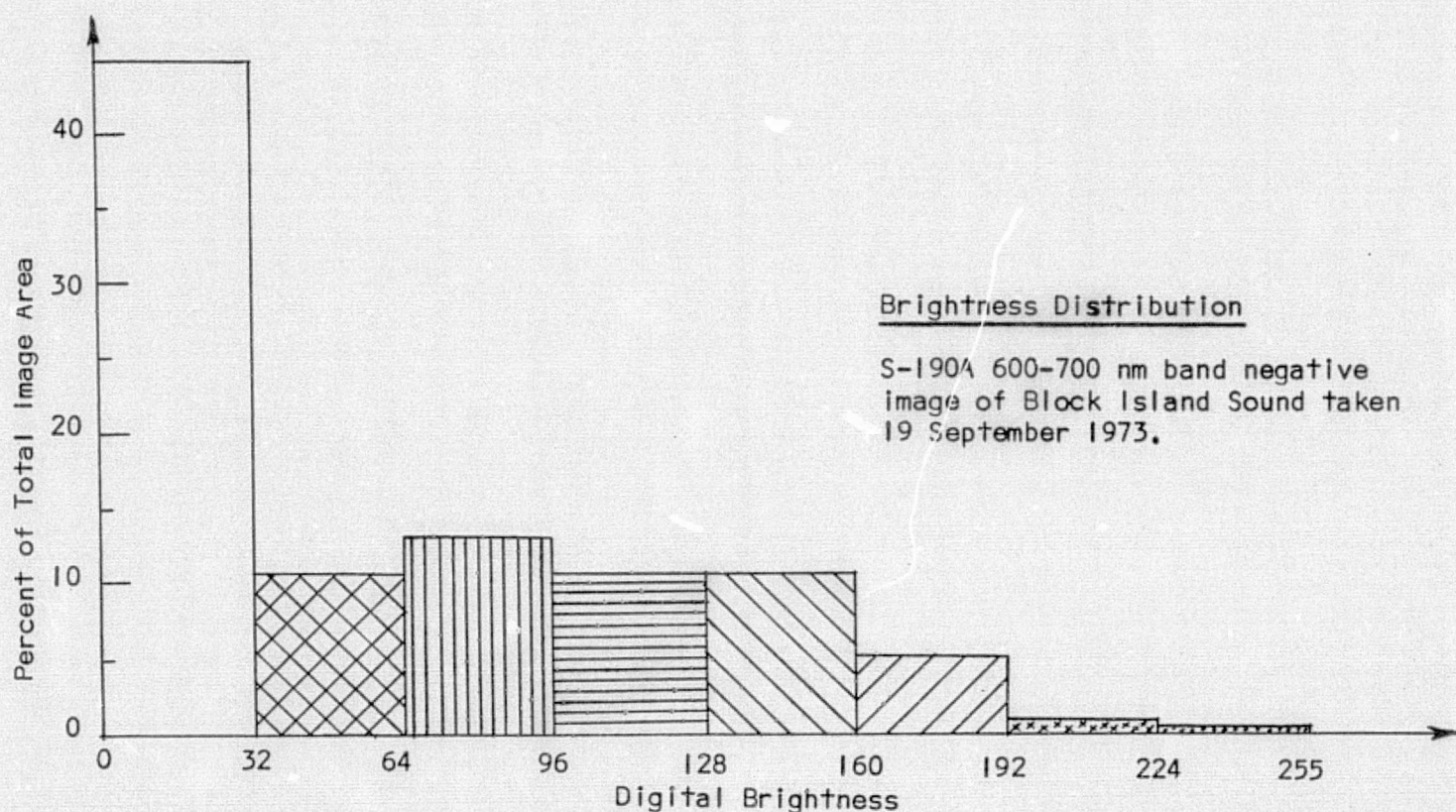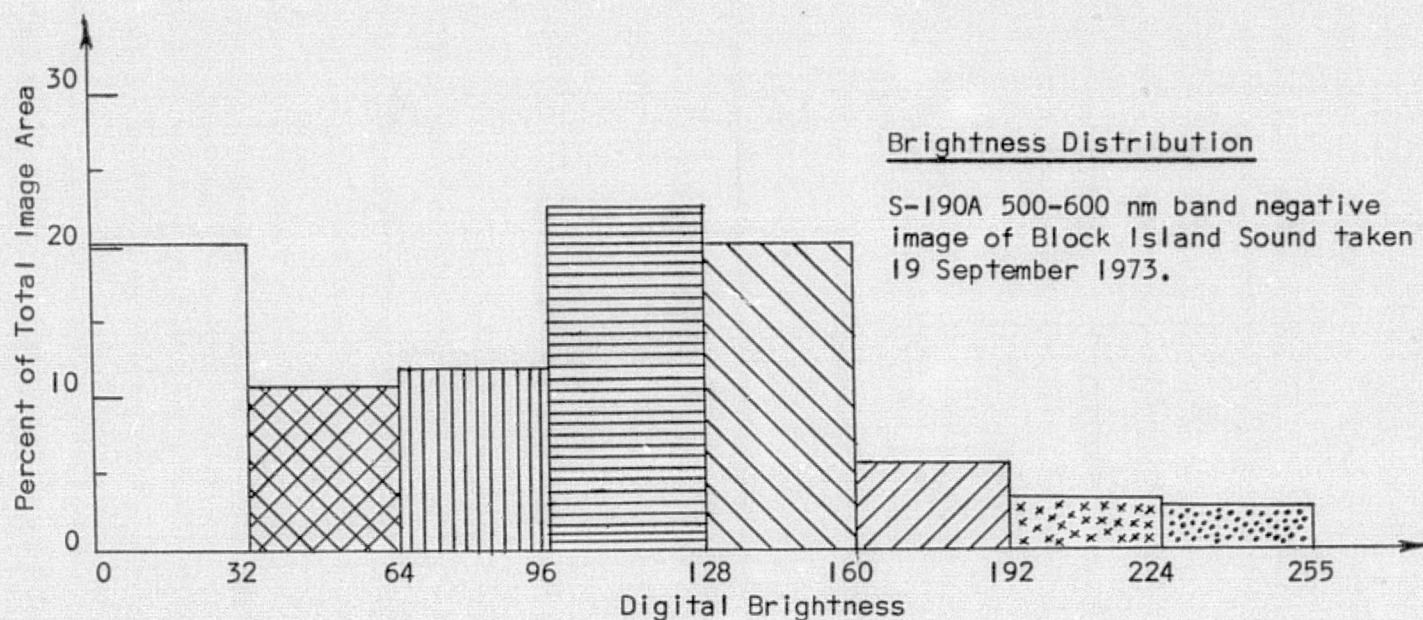
Figure 62. Histogram of digital brightness percent area classification of Skylab-3 S-190A multispectral photography of Block Island Sound acquired on 19 September 1973.

Bands (nm)	Mean $\bar{x}$	Standard Deviation s
500-600	67.84	56.9
600-700	98.24	59.7

Table 22. Statistics of the distribution of digitized brightness of 19 September 1973 Skylab-3 multispectral photography of Block Island Sound.

The digital brightness contours in both the 500-600 nm and 600-700 nm S-190A multispectral images, as well as the average of both of these bands, have been compiled into the following three charts of Block Island Sound.

Figure 63 shows the digital density in the 600-700 nm band which, represents total particles (and suspended solids) in the upper water layer. Superimposed on this chart are the average measured extinction coefficients in the red band acquired at eleven sampling stations. Figure 64 shows the similar computation for the 500-600 nm band, including "green band" extinction coefficients at the same eleven sampling stations. The average digital brightness for both these bands, along with the extinction co-efficient for the entire visible spectrum, is shown in Figure 65.

A simultaneous comparison of these three thematic charts allows an interpretative analysis of the dynamics of Block Island Sound to be at EDT on 19 September 1973.
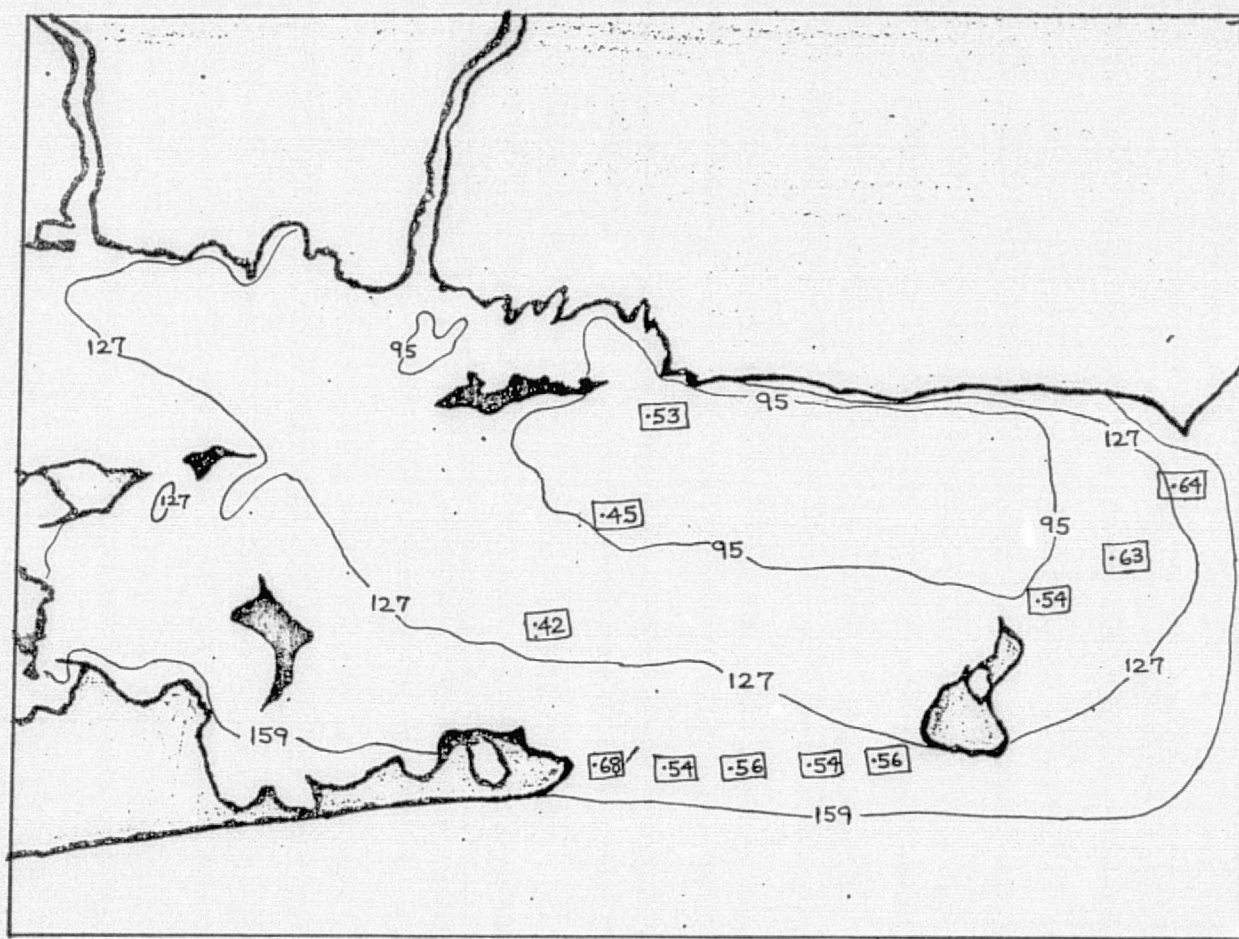
Figure 63.   600-700 nm S-190A multispectral photograph relative digital image brightness contours of Block Island Sound with average extinction coefficients in the red band shown for eleven sampling stations (Frame No. 239).
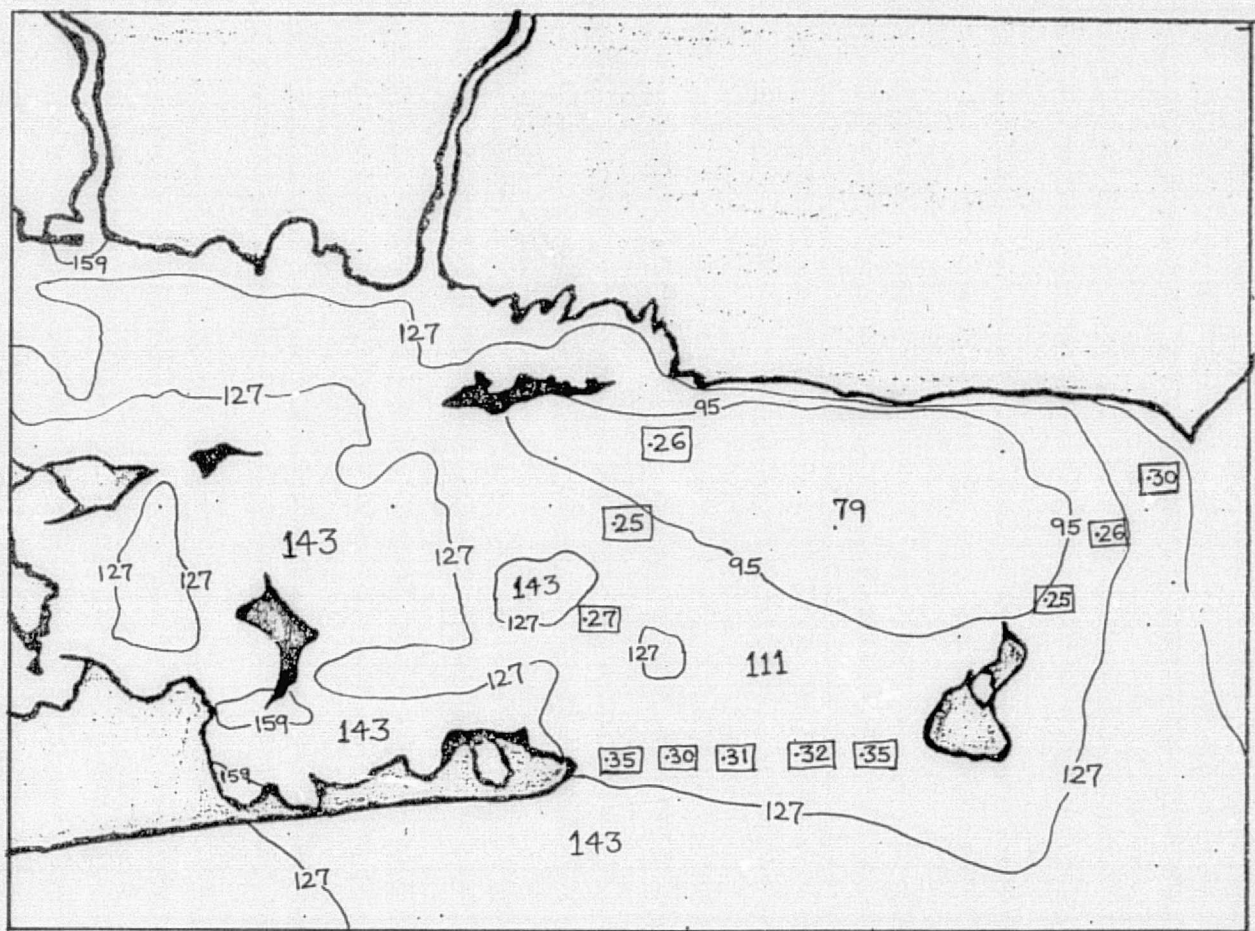
Figure 64. S-190A 500-600 nm multispectral photo relative digital image brightness contour of Block Island Sound. Green band average extinction coefficients are shown within squares for eleven sampling stations (Frame No. 239).
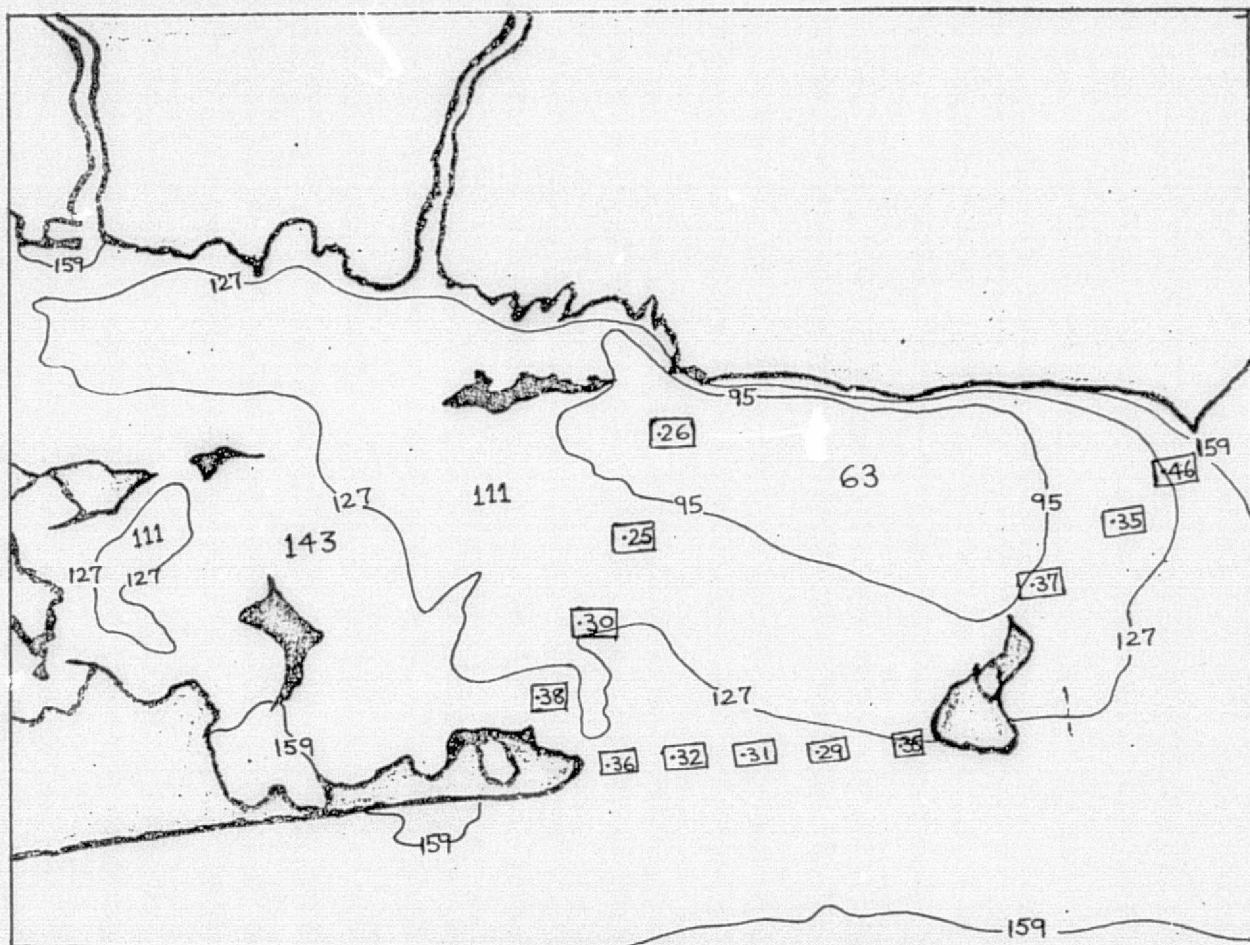
Figure 65. 500-600 nm and 600-700 nm average digital brightness in
S-190A multispectral photography of Block Island Sound. Average
extinction coefficients are superimposed for twelve sampling stations
(Frame No. 239).

From Table 11-12 in Appendix A, one can see that a correlation exists between extinction coefficient and total particles with a linear correlation coefficient of approximately 0.75 (for particles above 5 microns in size) for all sampling stations in Block Island Sound.

From Table 11-5 in Appendix A, it is seen that the average spectral extinction coefficients are greatest in the red band, being approximately twice as great as in the green band.

This forms the rationale for establishing a vertical model of the mixing, using Figures 63 through 65 can be performed.

-- Water from the Peconic Bay system continues out along the south shore of Long Island into the ocean between Montauk Point and Block Island. Although on the surface this appears to be a uniform flow (Figure 63), we see that a complex sub-surface mixing pattern (Figure 65) exists. This water is more turbid than other water in Block Island Sound, having an average visible extinction coefficient of about .38.

-- A water flow which is relatively homogeneous with depth can be seen to flow in a northwest-southeast direction from the Connecticut River estuary to Block Island. This water lies underneath the water mass emanating from Peconic Bay and, consequently, is more dense.

-- Little, if any, sub-surface flow of Long Island water is occurring between Block Island and Point Judith. The practically identical contours between these two points show no vertical mixing taking place.

-- A circular water mass which is homogeneous with depth

exists off the shore which is bound on the west by

Fisher's Island, on the north by the Rhode 'sland

coast, on the south by the Long Island Sound water

mass, and on the east by the Rhode Island Sound water

mass.

Long Island Sound

A second set of S-190A black-and-white negatives (Frame No. 240),

acquired on 19 September 1973 by Skylab-3 covering Long Island Sound,

was also linearly digitized in registration to bring out the maximum water

detail. The resultant digital brightness distribution of the processed

imagery using MARKER, DIGIT, HISTOGRAM, AREA, AND DISPLAY programs is

shown in Table 23 on the following page.

A histogram of the digitized brightness levels in each of these two

multispectral photographs of Long Island Sound is plotted in Figure 66 .

The Expected Value and Standard Deviation of the distribution of brightness

in these multispectral photographs is presented in Table 24 , also on the

following page.

An analysis of the System 800 color-coded digital outputs was made

(photo copies of the color. TV output are presented in Figure 67). Figure 68

is a relative digital image brightness chart of the 500-600 nm band and

Figure 69 is a similar chart of the 600-700 nm band. A comparative analysis

of these two figures, in conjunction with the average sum and differences of

the image brightness of Long Island waters, shows the following:

Digitized Grey Levels	Color Code	S-190A Bands	
		500-600nm	600-700nm
0-32	Black	26.76	51.16
33-64	Red	15.52	9.00
65-96	Green	18.04	12.48
97-128	Yellow	19.10	9.22
129-160	Blue	11.40	8.10
161-192	Magenta	3.92	5.92
193-224	Cyan	2.92	3.28
225-255	White	2.24	0.70
	Totals	99.90	99.86

Table 23. Digital brightness percent area classification of Skylab-3 S-190A black-and-white multispectral images (Frame No. 240) of Long Island Sound acquired on 19 September 1973.

Bands (nm)	Mean ($\bar{x}$)	Standard Deviation
500-600	82.40	57.6
600-700	63.36	61.1

Table 24. Statistics of the distribution of digitized brightness of 19 September 1973 Skylab multispectral photography of Long Island Sound.

-- The most turbid water in the sound at this time
(4 1/2 hours after slack flood on 19 Sept. 1973)
exists in New Haven harbor. There is no apparent
change in turbidity, with spectral brightness.
The visible extinction coefficient is estimated
to be about .65, indicating a large quantity of
suspended solids.

-- A large counter-clockwise sub-surface gyre exists
midway between New Haven harbor and Herod Point,
Long Island. This gyre is evident in the 500-600
nm band in Figures 67 and 68, but is absent in the
600-700 nm band in Figure 67.

-- Little vertical mixing appears to take place west
of Stratford shoal (midway between Bridgeport and
Port Jefferson). The water west of New Haven is
clearer, similar to that east of the Connecticut
River estuary.

-- Turbid water entering the sound from the Connecticut
River is overriding Long Island Sound water and being
carried out into the middle of the Sound.

-- A significantly turbid water mass occurs at Mattituck
Inlet, the source of which is an apparent upwelling.
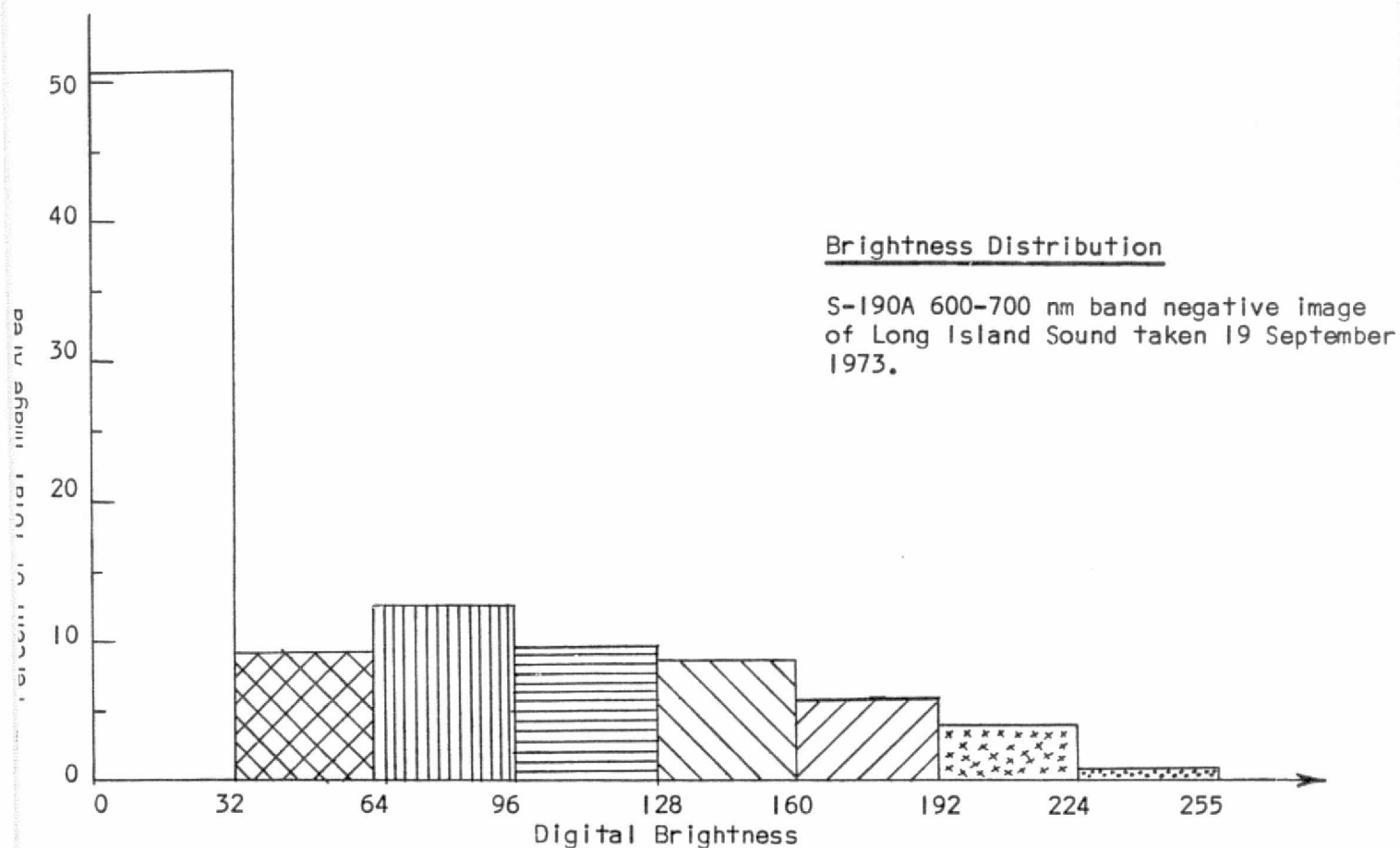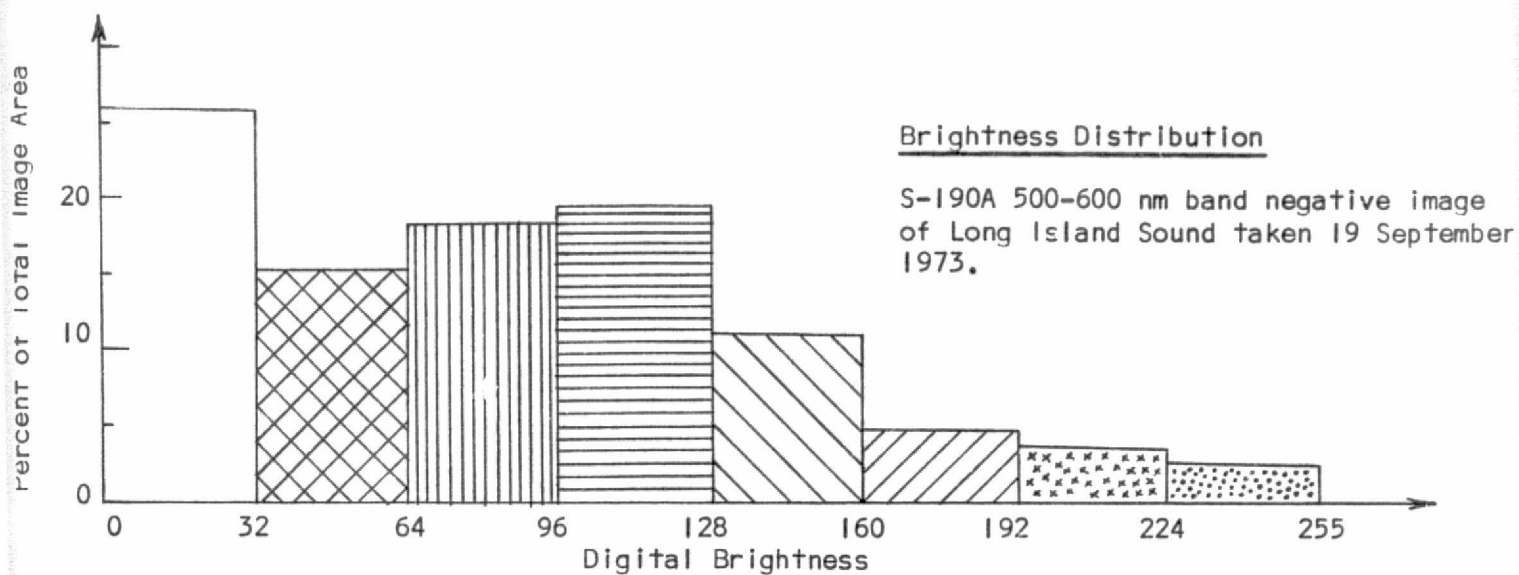
Figure 66. Histogram of digital brightness percent area classification of Skylab-3 S-190A multispectral photography of Long Island Sound acquired 19 September 1973.
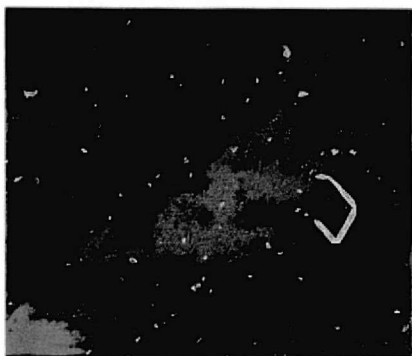
500-600 nm Band
Multispectral Photograph
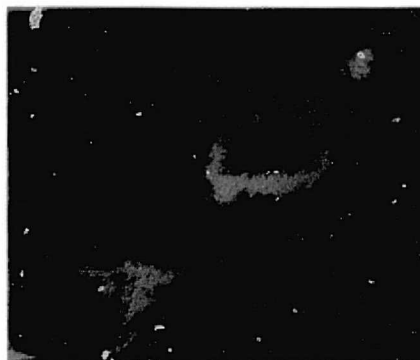
600-700 nm Band
Multispectral Photograph
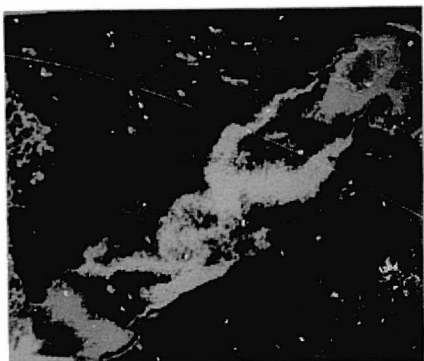
Average of 500-600 nm Band
plus 600-700 nm Band
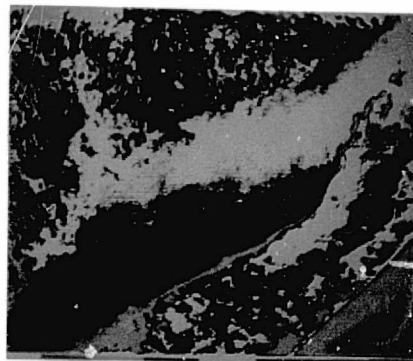
Average of 500-600 nm Band
minus 600-700 nm Band

Figure 67. System 800 color-coded output of digitally processed S-190A imagery of Long Island Sound taken by Skylab-3 on 19 September 1973 (Frame No. 240).
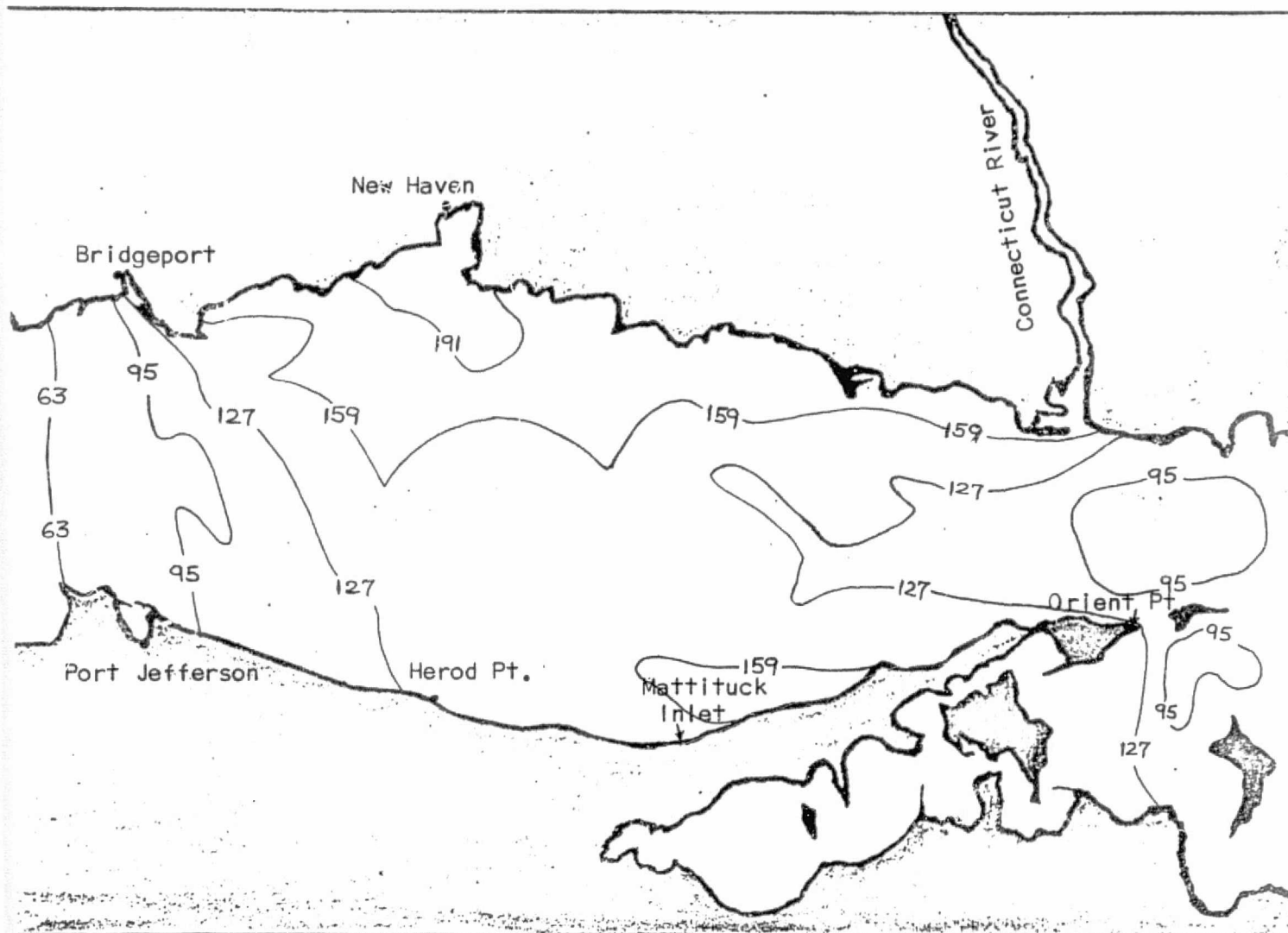
Figure 68. S-190A 500-600 nm multispectral photo relative digital image brightness contour chart of Long Island Sound (Frame No. 240).
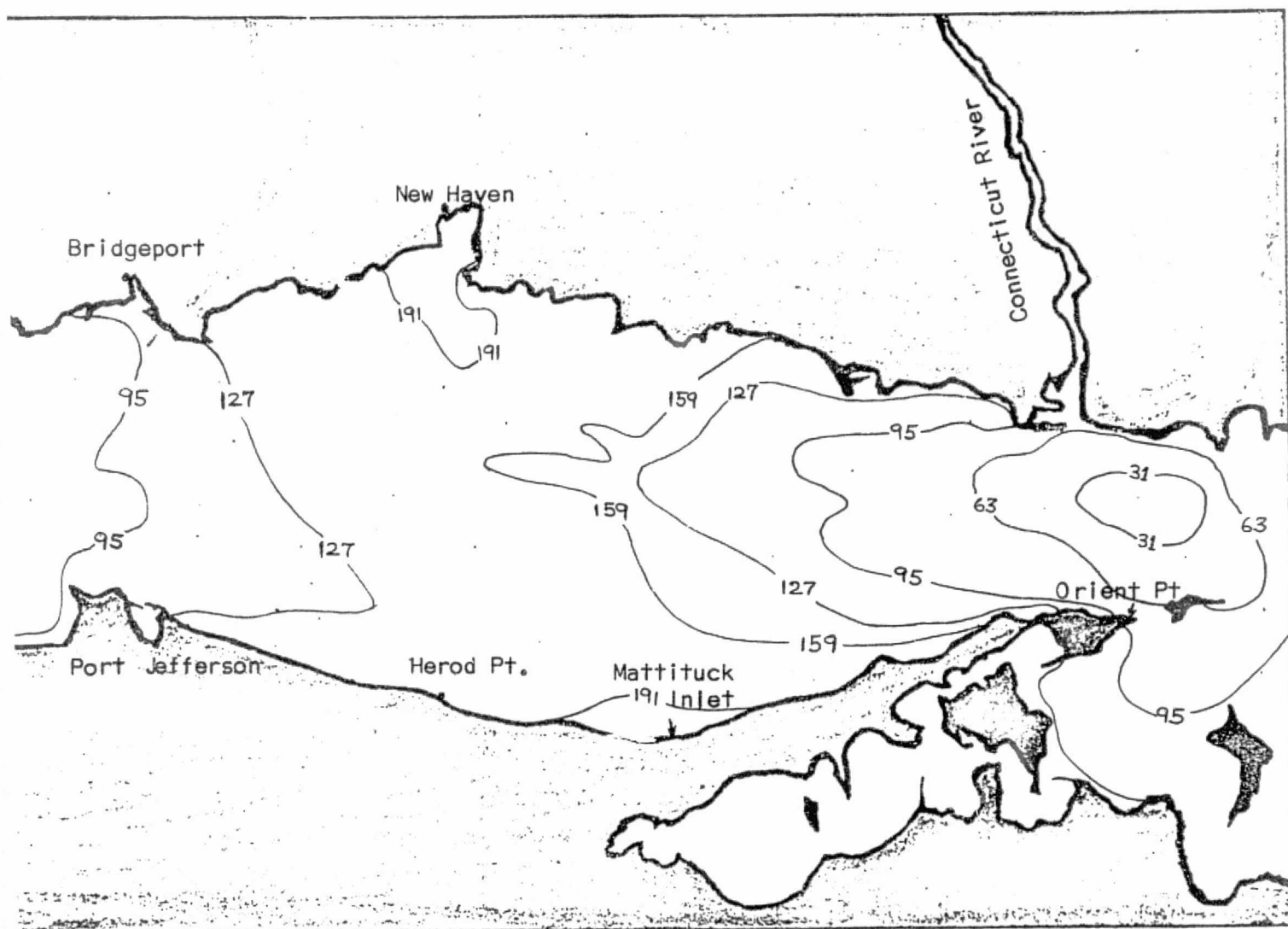
Figure 69. 600-700 nm band relative digital image brightness chart of
Long Island Sound made from S-190A multispectral photo (Frame No. 240).
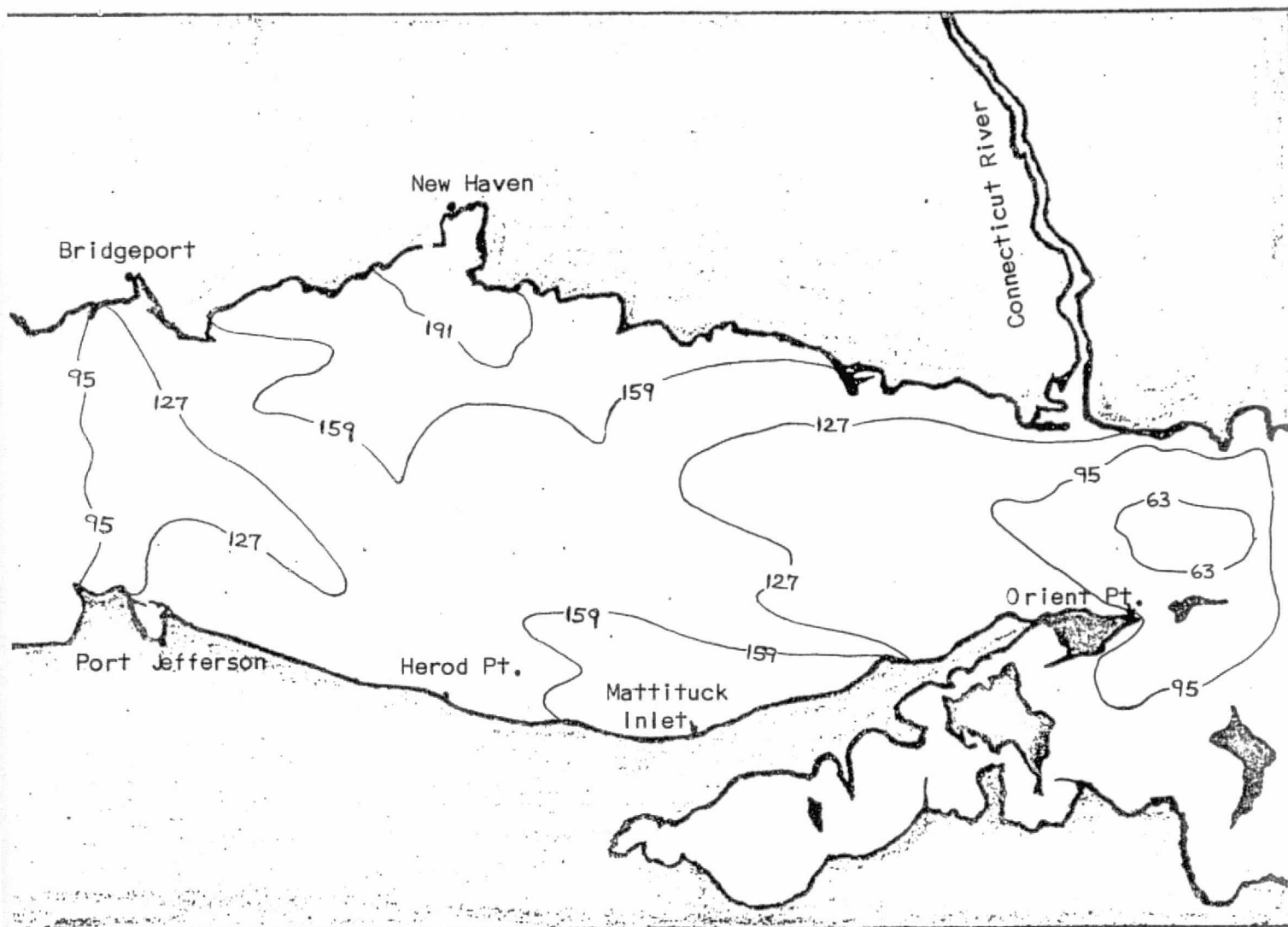
Figure 70. 500-600 nm plus 600-700 nm band average digital brightness contour map of S-190A multispectral photography of Long Island Sound (Frame No. 240).
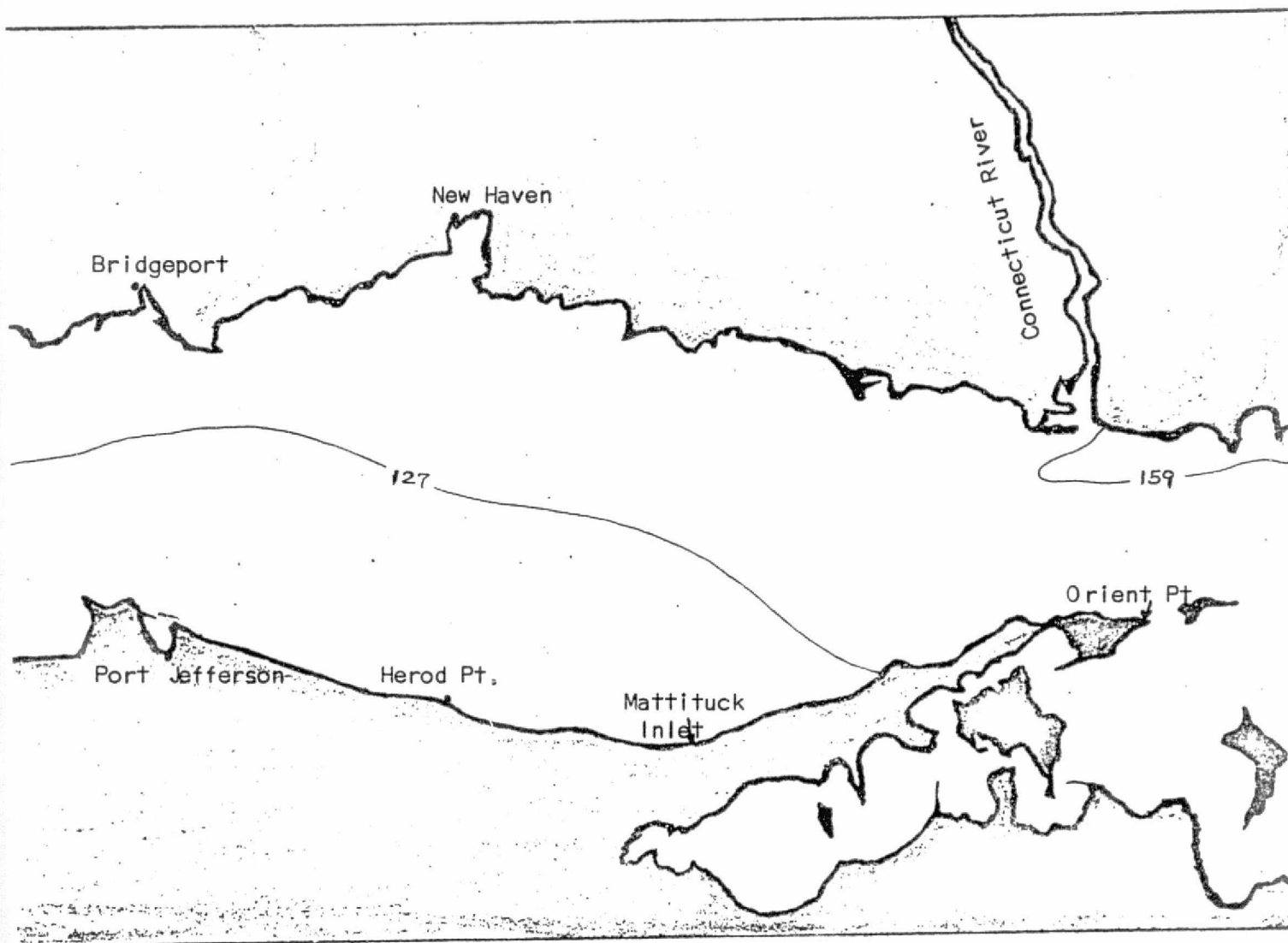
Figure 71. 500–600 nm minus 600–700 nm band average digital brightness contour map of S-190A multispectral photography of Long Island Sound (Frame No. 240).

-- A homogeneous, clear water mass is entering Long
   Island Sound between Plum Island and Fisher's Island
   (at the race).

-- Figure 71 indicates that two sub-surface discontinuities
   exist - one east of the Connecticut River estuary
   along the Connecticut River, the other laterally separates
   the northern half of Long Island Sound from the southern
   half.

Martha's Vineyard and Nantucket Waters

Black-and-white S-190A multispectral negatives (Frame No. 131),
acquired on 12 September 1973 by Skylab 3 covering Nantucket Sound
adjacent to Martha's Vineyard and Nantucket, was linearly digitized
in registration to maximize water detail. The histogram of the distri-
bution of digital brightness is tabularized on the following page.

Figure 72 is a chart of the waters surrounding Nantucket and
Martha's Vineyard, upon which has been annotated approximate water depths
in the area.

Black-and-white reproductions of the linearly digitized negatives
in both the 500-600 nm and 600-700 nm bands are shown in Figures 73 and
75 . Water detail in the 500-600 nm negative is separated into five
brightness classes and in the 600-700 nm negative, the separation of
water details is separated into six classes of brightness. Each class
contains five brightness bits (32 brightness units).

Digitized Gray Levels	Color Code	S-190A Band	
		500-600 nm	600-700 nm
0-32	Black	5.06	13.10
33-64	Red	3.28	2.50
65-96	Green	5.70	4.24
97-128	Yellow	9.78	12.40
129-160	Blue	11.74	30.72
161-192	Magenta	21.46	30.68
193-224	Cyan	32.40	4.08
225-255	White	10.46	2.18
	Totals	99.88	100.90

Table 25. Digital brightness percent area classification of Skylab-3 S-190A black-and-white multispectral photographs (Frame No. 131) of Martha's Vineyard and Nantucket waters acquired on 12 September 1973.

The resultant color-coded outputs of both these bands, as well as the average of the sum and difference of both bands, is shown in Figure 77. In order to facilitate analysis, these color-coded outputs of the input S-190A negatives have been transformed into positive brightness and compiled into four charts (Figures 78 through 81).

The following interpretive analysis is performed using these four compiled brightness charts:

-- Nantucket Sound at this time (1311 EDT on 12 September 1973) contained a homogeneous and relatively clear body of water extending from Vineyard Sound in the west to passage between Monmoy and Nantucket Islands in the east. Usable extinction coefficient is estimated to be .25.

-- A considerable amount of turbidity (and associated suspended particles) exists in Nantucket Sound, along the south shore of Cape Cod and along the north shore of both
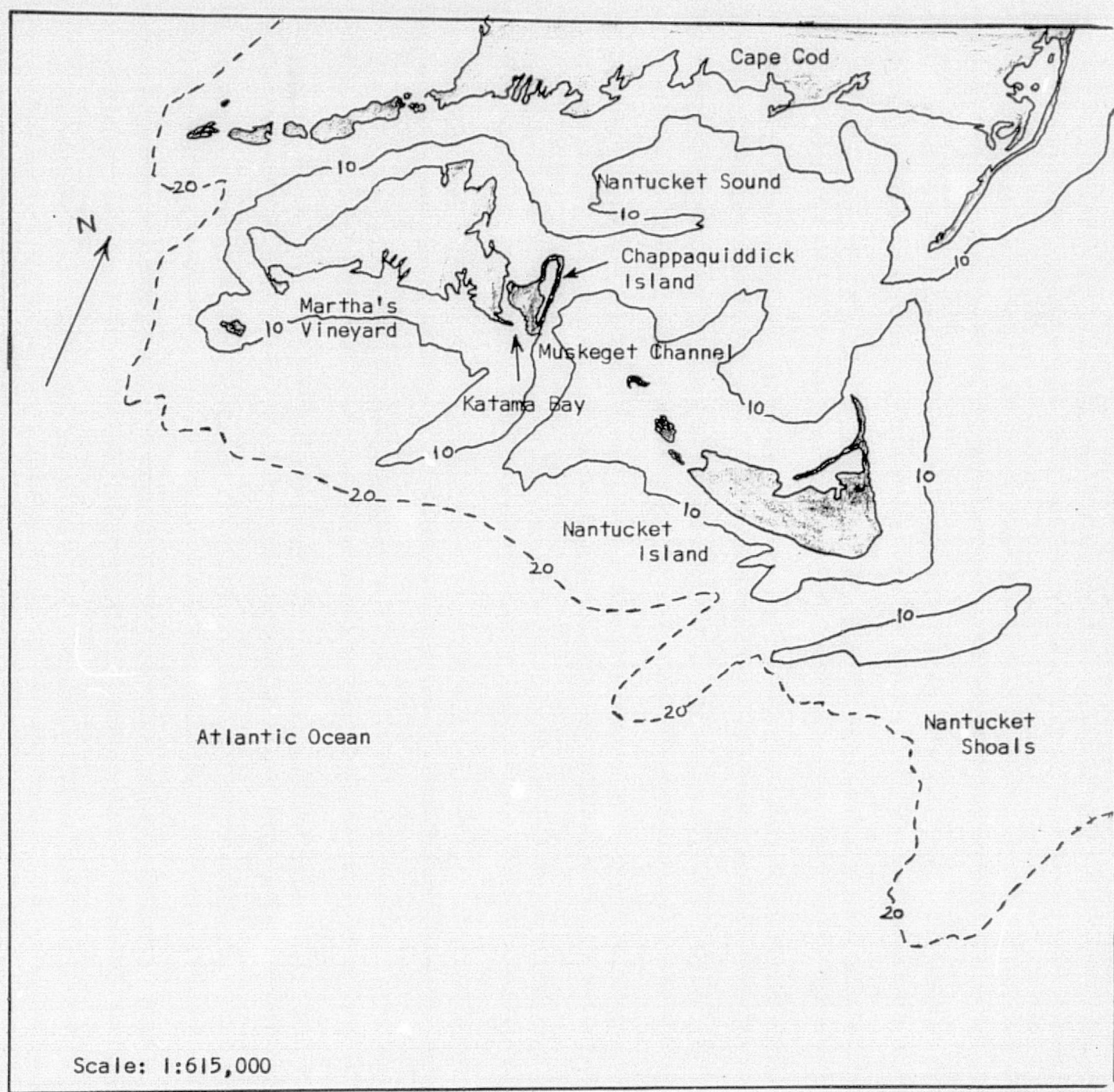
Figure 72. Chart of Nantucket Sound and adjacent waters.

Scale: 1:615,000
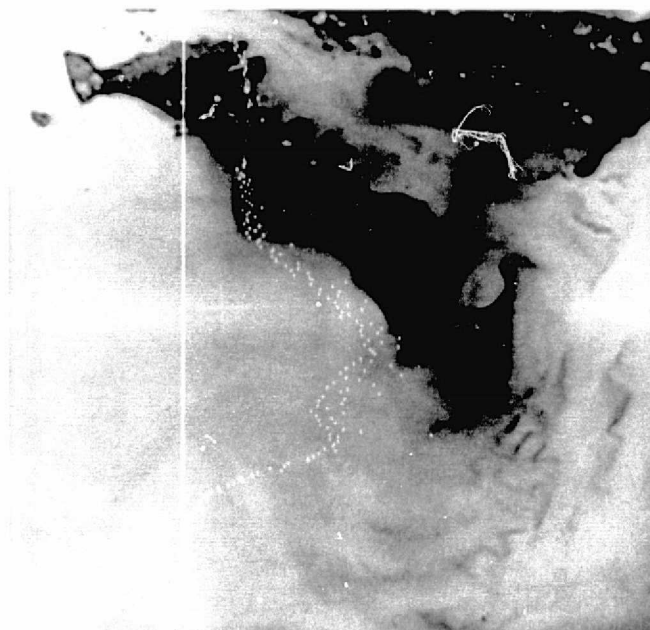
Figure 73. Digitized S-190A 500-600 nm band multispectral negative of Nantucket and Martha's Vineyard's waters with frequency distribution of brightness (0 at top and 255 at bottom of vertical line).
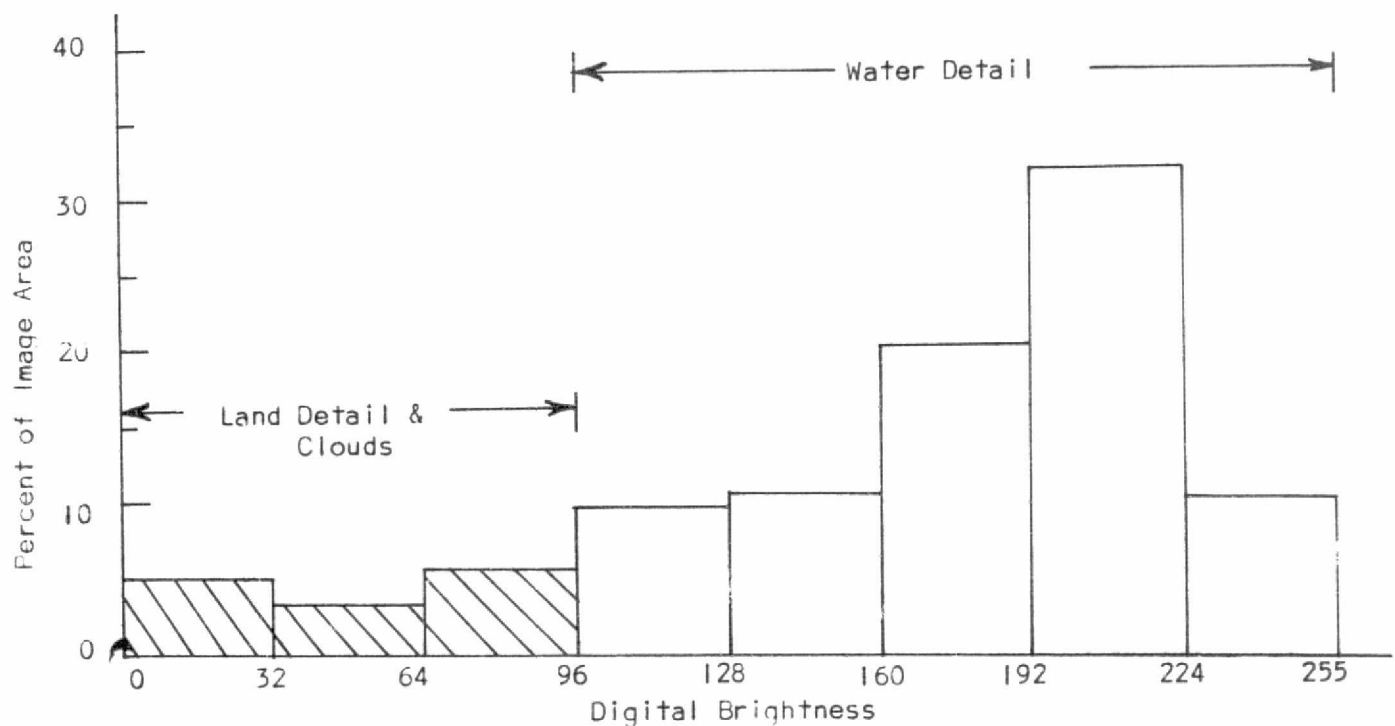
Figure 74. Histogram of digital brightness percent area classifications of Skylab 3 S-190A 500-600 nm multispectral negative of Nantucket and Martha's Vineyard waters taken on 12 September 1973 at 1311 EDT (Frame No. 131).
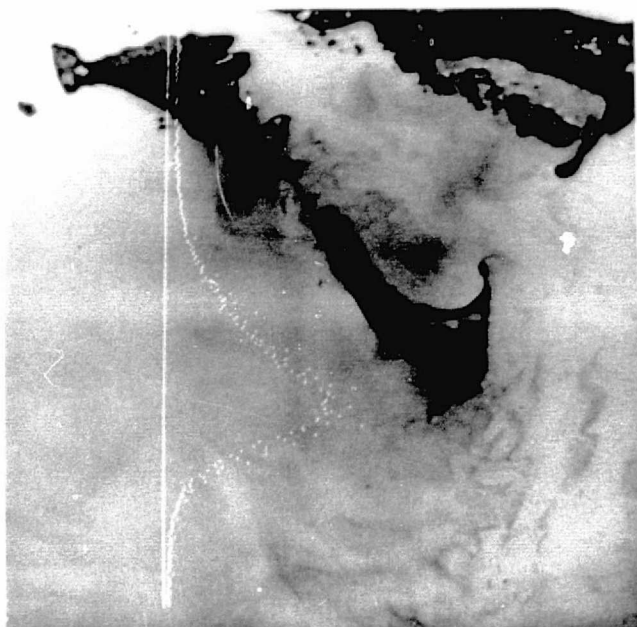
Figure 75. Digitized S-190A 600-700 nm band multispectral negative of
Nantucket and Martha's Vineyard waters. Frequency distribution of bright-
ness is shown with 0 at top and 255 at bottom of vertical line.
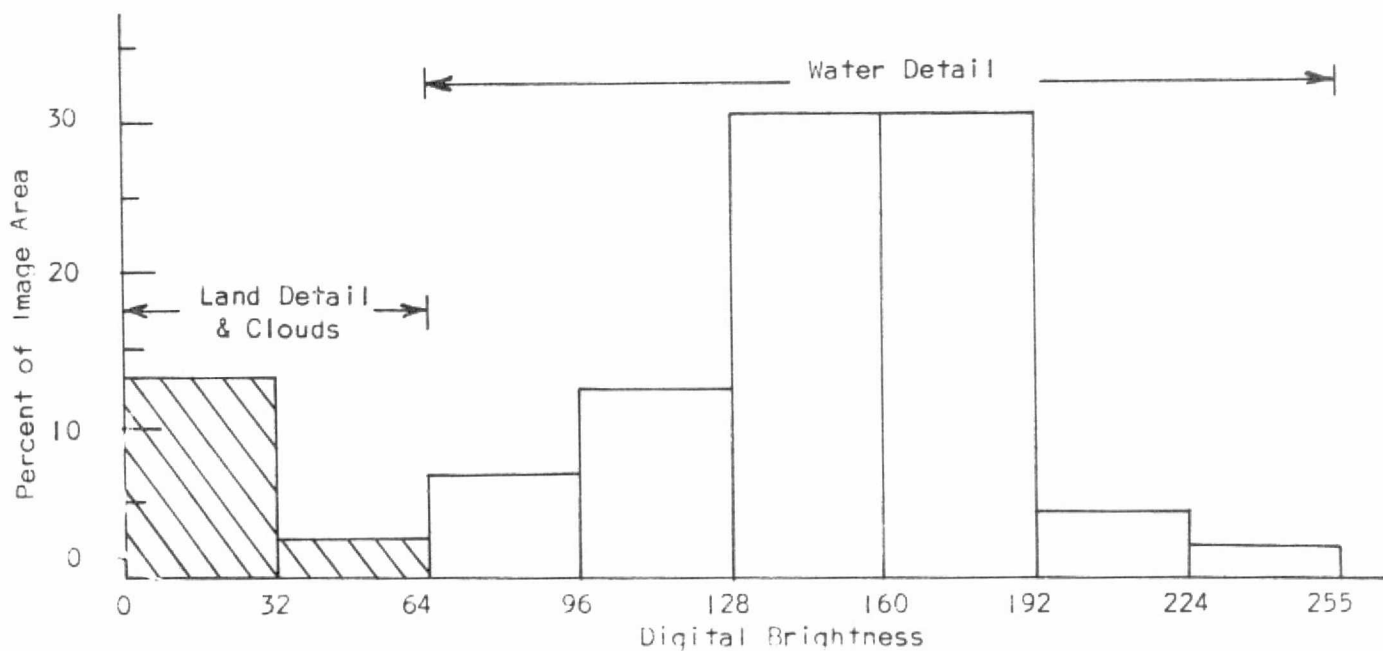
Figure 76. Histogram of digital brightness percent area classification of
Skylab 3 S-190A 600-700 nm multispectral negative of Nantucket and Martha's
Vineyard taken on 12 September 1973 at 1311 EDT (Frame No. 131).

500-600 nm Band
Multispectral Photograph

600-700 nm Band
Multispectral Photograph

Average of 500-600 nm plus
600-700 nm bands shown above.

Average of 500-600 nm minus
600-700 nm bands shown above.

Figure 77. Color-coded "System 800" output showing digitally processed
S-190A black-and-white multispectral photographs of Nantucket and Martha's
Vineyard waters taken by Skylab-3 on 12 September 1973 (Frame No. 131).

Nantucket and Martha's Vineyard. This turbid
water appears homogeneous since a comparison of
the brightness contours for both the 500-600 nm
and 600-700 nm band charts show that they have
approximately the same spatial locations. The
water depth in these areas is apparently 30 feet
and little bottom effect is believed evident.

-- A large turbid plume of water extends south out of
Katama Bay between Martha's Vineyard and Chappaquiddick
Island (there is also some effect of cloud shadows in
this area). Lack of uniform mixing with depth of this
plume in Muskeget Channel is evident by a comparison
of Figures 73 and 80.

-- Sub-surface discontinuities in brightness are indicated
off-shore of Nantucket Island in Nantucket shoals. This
is believed to be caused by phytoplankton.
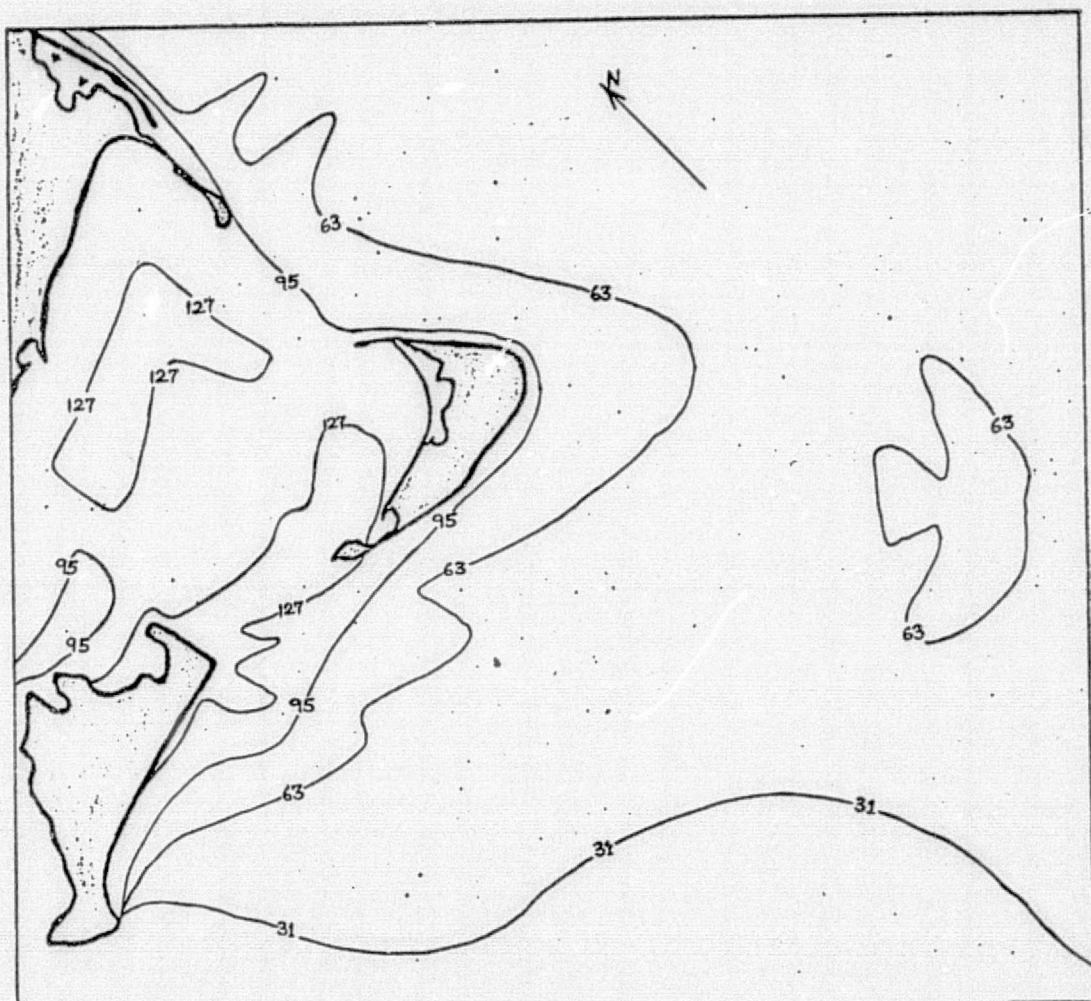
Figure 78. Digital brightness map of the S-190A 500-600 nm multispectral image (Frame No. 131) of Nantucket and Martha's Vineyard waters.
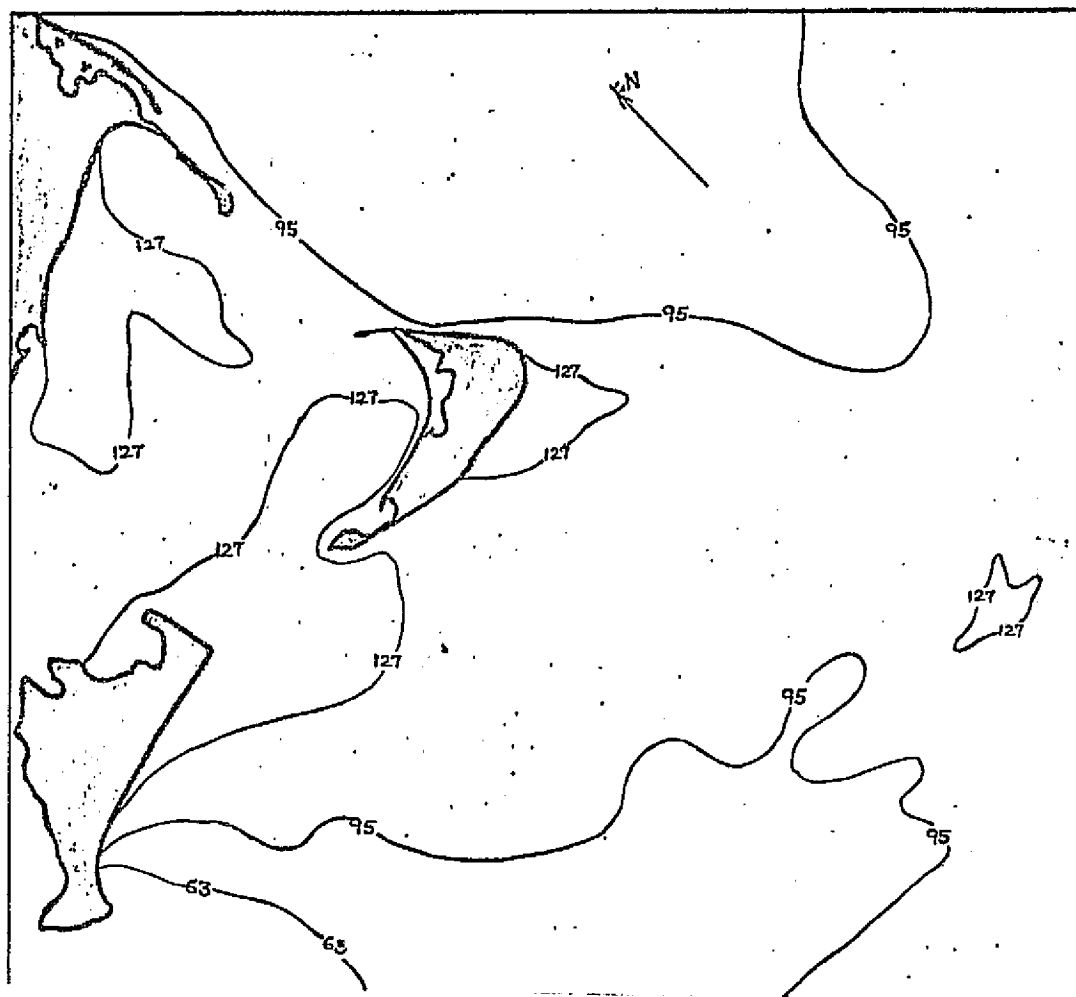
Figure 79. Digital brightness map of 600-700 nm band showing the over-
riding of less dense turbid water between Martha's Vineyard and Nantucket.
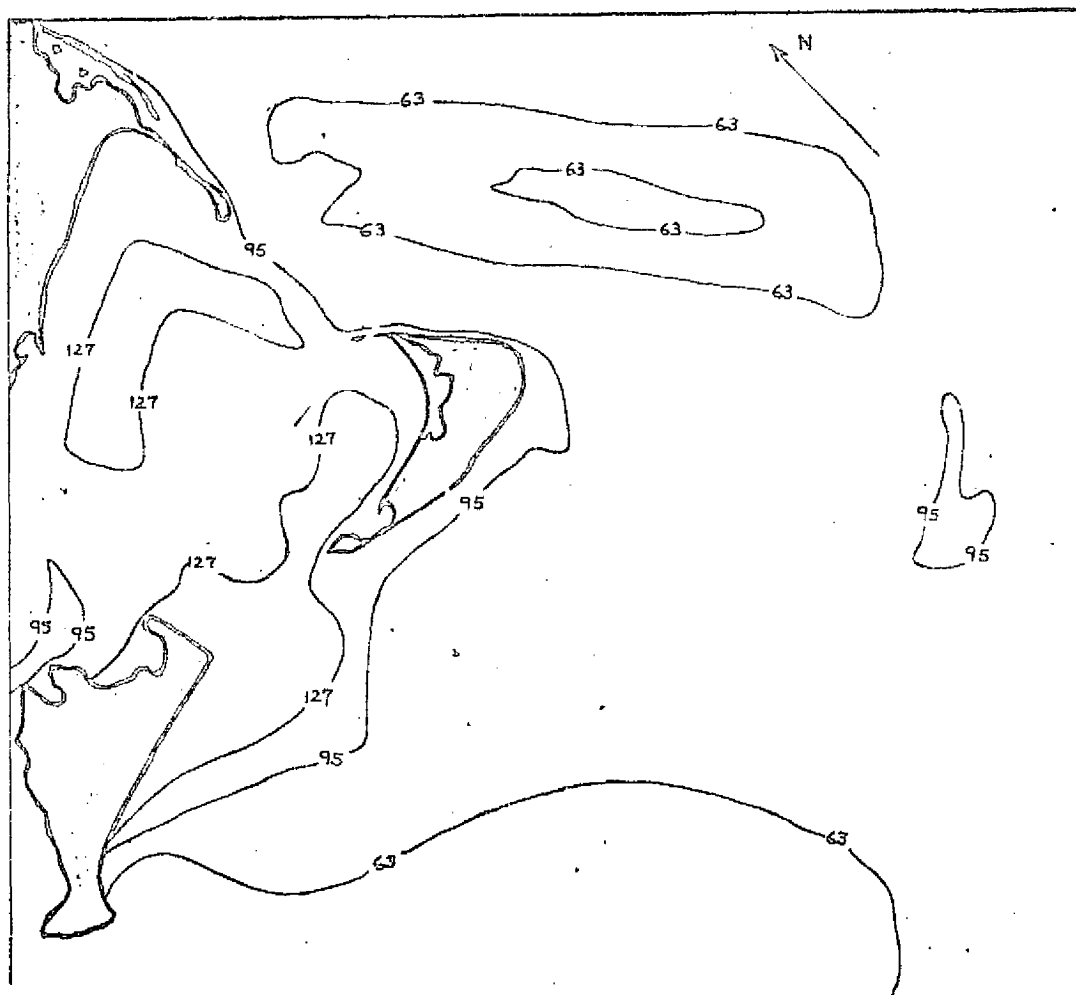
Figure 80. An average of 500-600 nm and 600-700 nm bands compiled into
a digital brightness map of Frame No. 131. This shows the relative
extinction coefficient of the water and is a good measure of total particles
above 5 microns in size.
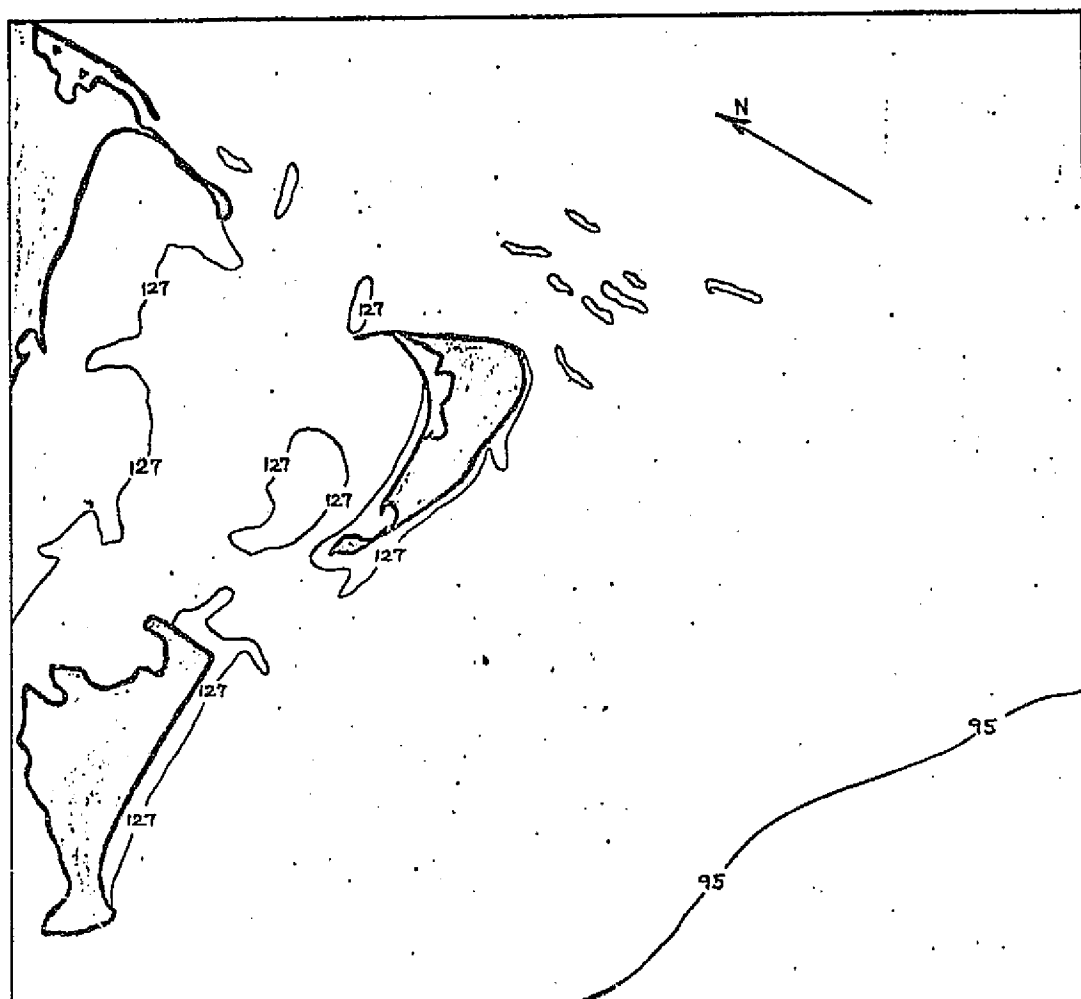
Figure 84. The difference between the 500-600 nm band and the 600-700 nm band S-190A multispectral image brightness. This presentation indicates sub-surface suspended materials and, in particular, phytoplankton.

Section 9

Comparative Photographic Analysis

of S-192 Multispectral Scanner Data

and S-190A Multispectral Photography

An analysis was performed of S-192 thirteen-channel multispectral scanner data acquired over the Martha's Vineyard-Nantucket area during Skylab-3 pass on 12 September 1973. The scanner data for each band was reproduced onto five-inch black-and-white film. The results are shown in Figures 82 and 83.

A casual glance at these images clearly shows that a great deal of noise is evident in the imagery. In order to perform an interpretation which could be compared with the S-190A data, image brightness charts were compiled. These ten charts appear in Figures 84 through 93

The following is a comparison of the effectiveness of each band in depicting whatever characteristics which were determined to be present by interpretation of S-190A digital brightness charts produced by the System 800.

Turbid water in the shallow parts of northern Nantucket Sound is detected in the six bands between 410 and 760 nm, as well as the 980-1080 nm band.

The extent of suspended solids emanating from Katama Bay, between Martha's Vineyard and Chappaquiddick Island, is best detected in the 520-560 and 560-610 nm bands.

Surficial phytoplankton activity south of Nantucket Island is detected in the 620-670 nm band, 680-760 nm band, 780-880 nm band, and

-148-
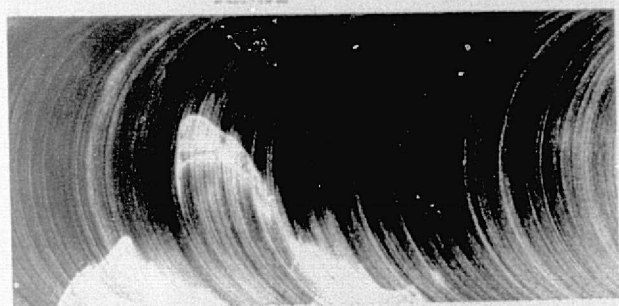
410 NM – 460 NM
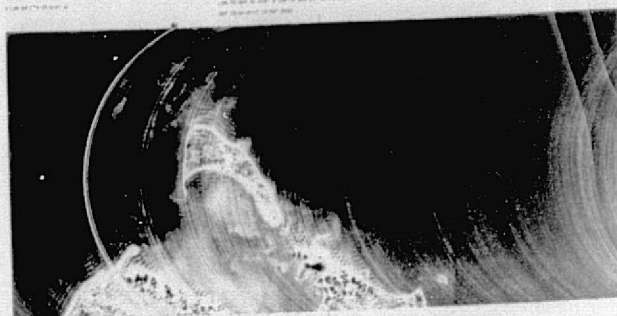
460 NM – 510 NM
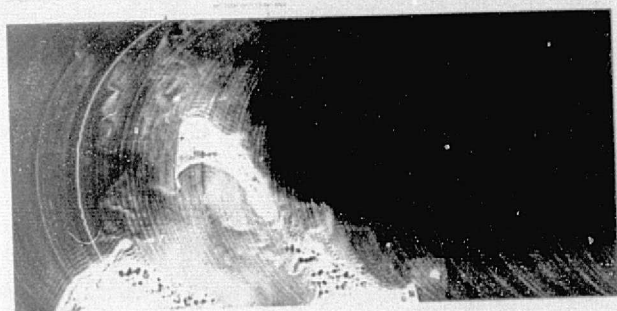
520 NM – 560 NM
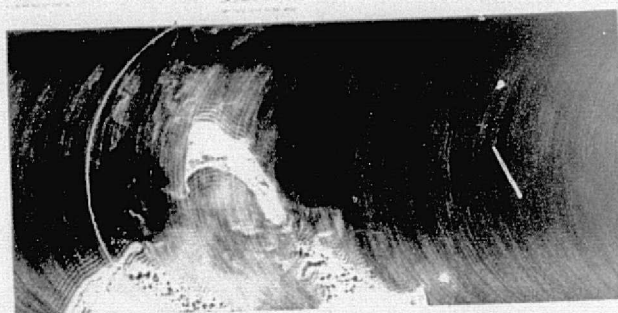
560 NM – 610 NM
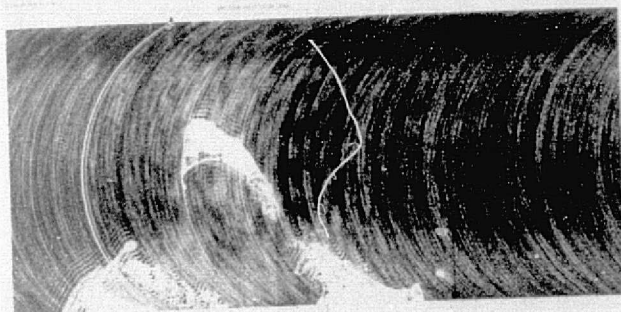
620 NM – 670 NM
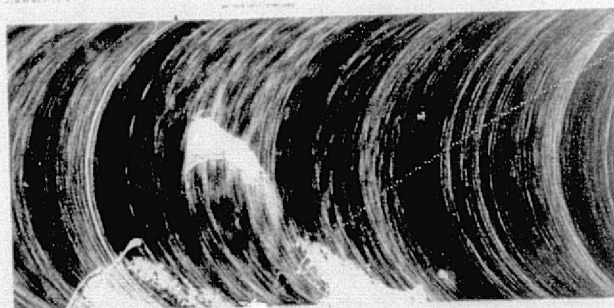
680 NM – 760 NM
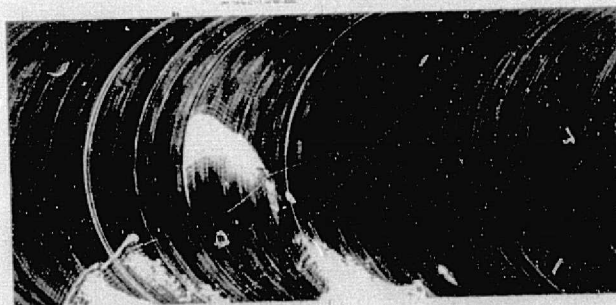
780 NM – 880 NM

Figure 82. Black-and-white reproduction of S-192 scanner data of the Martha's Vineyard-Nantucket area.
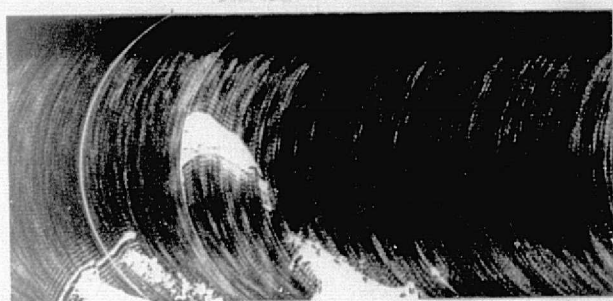
980NM - 1080NM

1090 NM - 1190NM

1200NM - 1300NM

1550NM - 1750 NM

2100NM - 2350NM
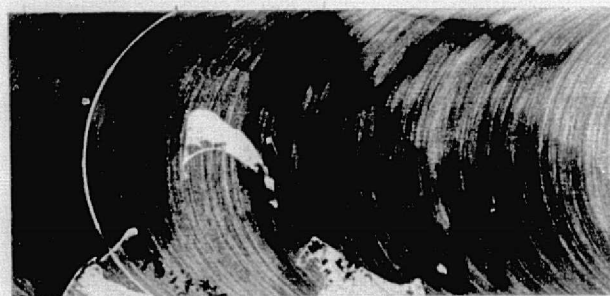
10-12 MICRONS-THERMAL

Figure 83. Black-and-white reproduction of S-192 scanner data of the Martha's Vineyard-Nantucket area.
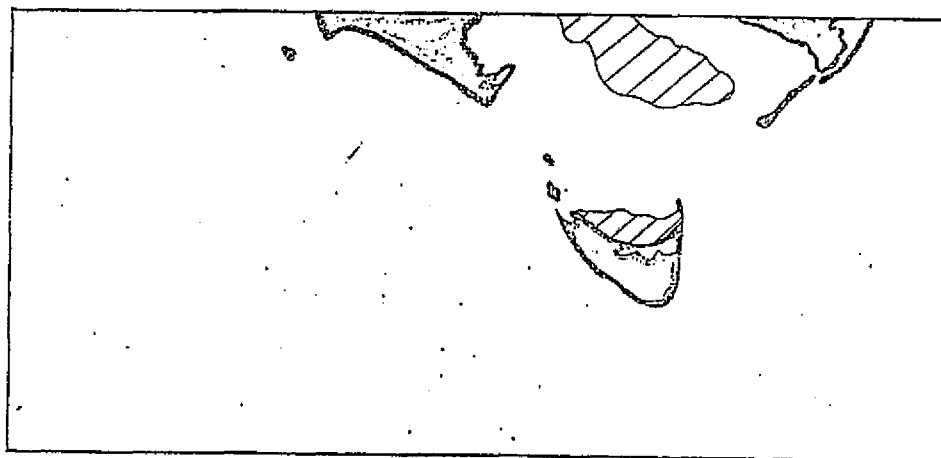
Figure 84. S-192 Image brightness chart of multispectral scanner 410-460 nm band acquired 12 Sept. 1973 at 1311 EDT of Nantucket and Martha's Vineyard.

Figure 85. S-192 Image brightness chart of multispectral scanner 460-510 nm band acquired 12 Sept. 1973 at 1311 EDT of Nantucket and Martha's Vineyard.
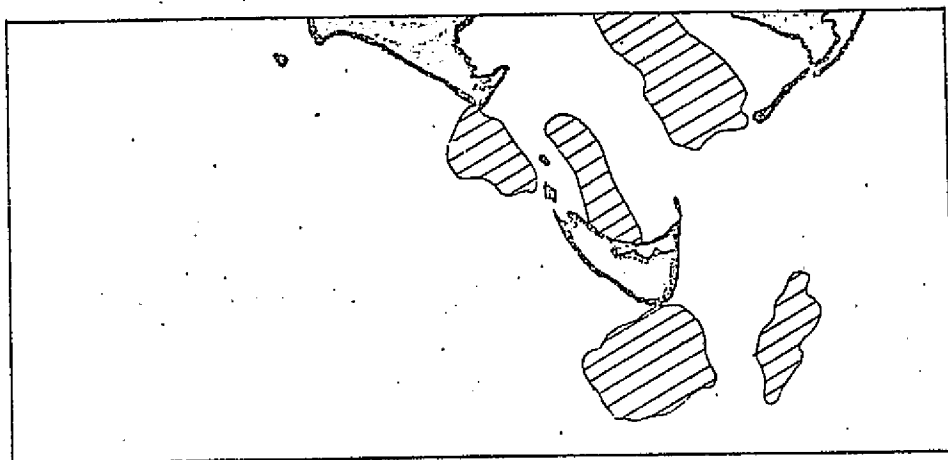
Figure 86. S-192 image brightness chart of multispectral scanner 520-560 nm band acquired 12 Sept. 1973 at 1311 EDT of Nantucket and Martha's Vineyard.

Figure 87. S-192 image brightness chart of multispectral scanner 560-610 nm band acquired 12 Sept. 1973 at 1311 EDT of Nantucket and Martha's Vineyard.
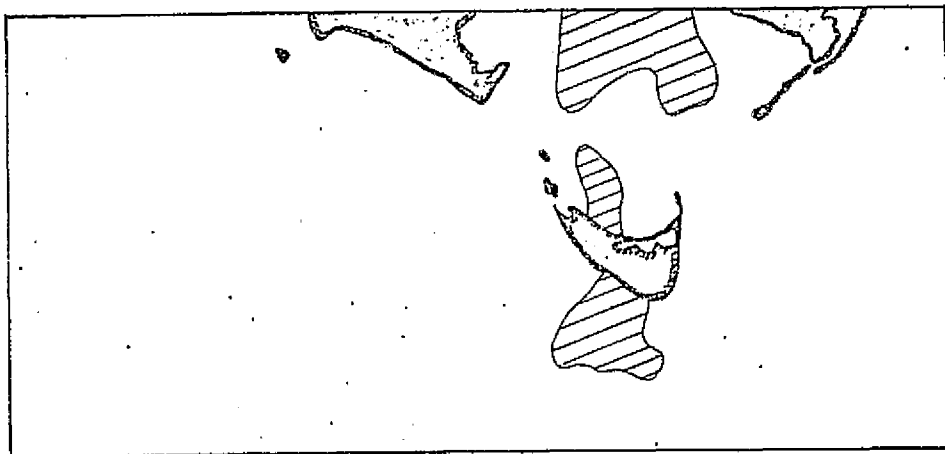
Figure 88. S-192 image brightness chart of multispectral scanner 620-670 nm band acquired 12 Sept. 1973 at 1311 EDT of Nantucket and Martha's Vineyard.
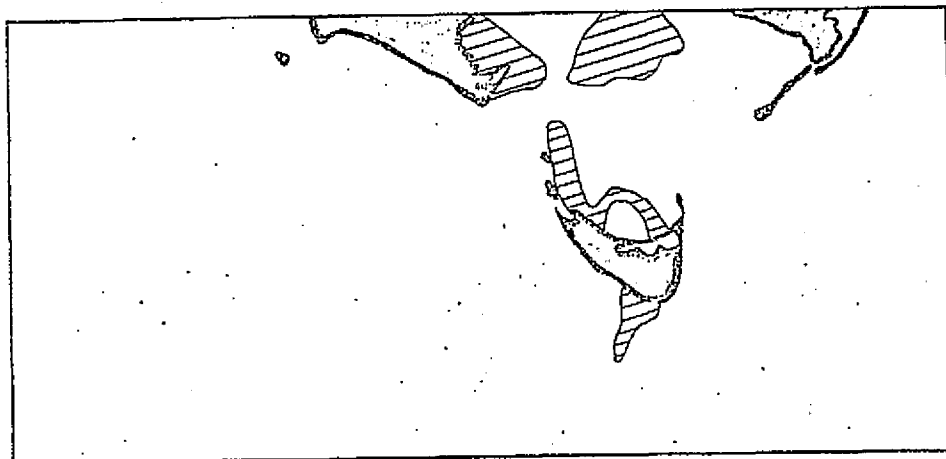
Figure 89. S-192 image brightness chart of multispectral scanner 680-760 nm band acquired 12 Sept. 1973 at 1311 EDT of Nantucket and Martha's Vineyard.
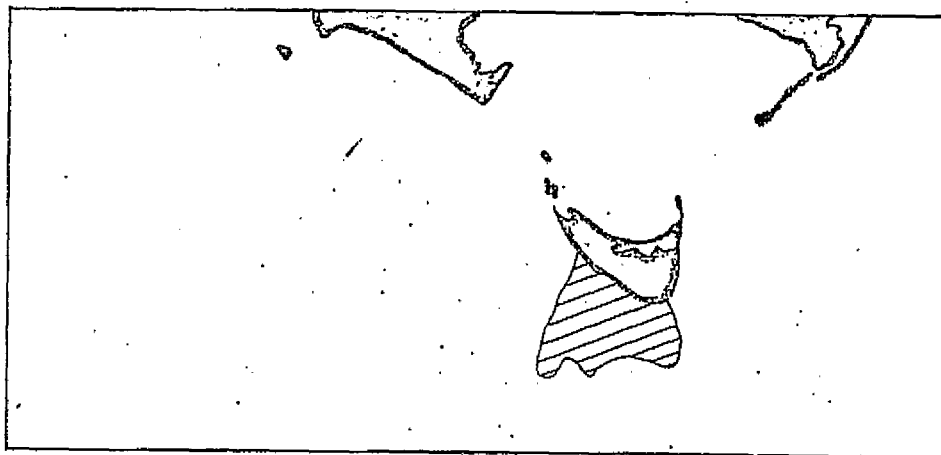
Figure 90. S-192 image brightness chart of multispectral scanner 780-880 nm band acquired 12 Sept. 1973 at 1311 EDT of Nantucket and Martha's Vineyard.
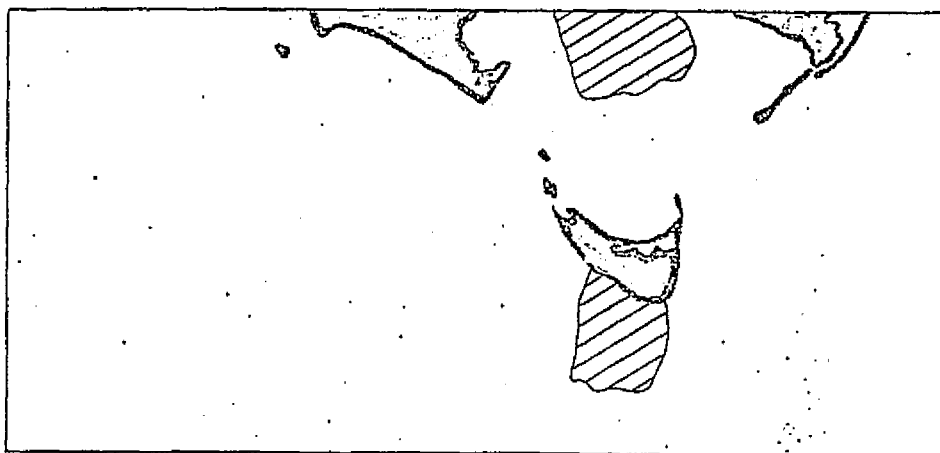
Figure 91. S-192 Image brightness chart of multispectral scanner 980-1080 nm band acquired 12 Sept. 1973 at 1311 EDT of Nantucket and Martha's Vineyard.
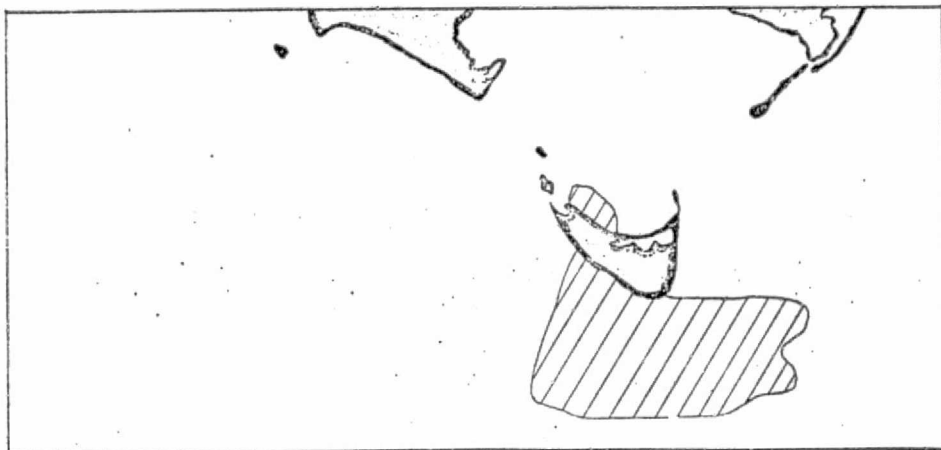
Figure 92. S-192 image brightness chart of multispectral scanner 1550-
1750 nm band acquired 12 Sept. 1973 at 1311 EDT of Nantucket and Martha's
Vineyard.
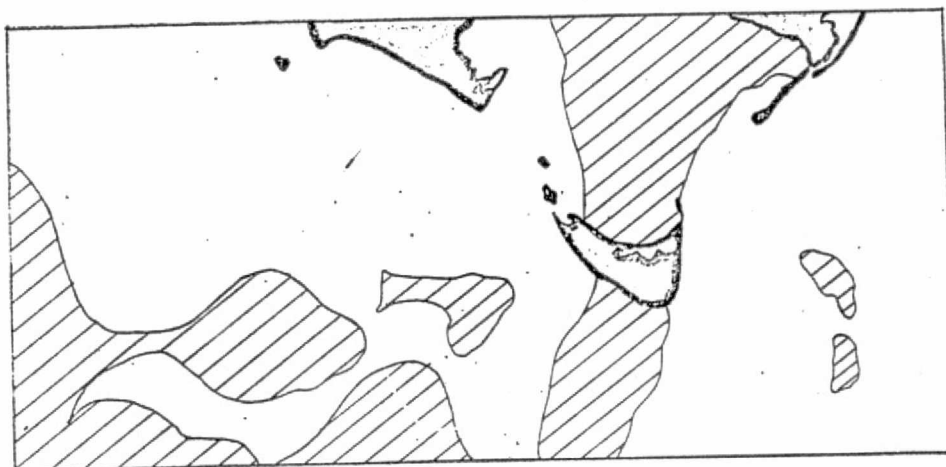
Figure 93. S-192 image brightness chart of multispectral scanner thermal
band acquired 12 Sept. 1973 at 1311 EDT of Nantucket and Martha's Vineyard.

980-1080 nm band.

Image characteristics which were unsuspected from a. analysis of the S-190A data appear in the 1550-1750 nm and the 10-12μ bands. From Figure 92, significant patterns of phytoplankton activity are present in the Atlantic Ocean, southwest of Martha's Vineyard. The thermal band shows also a lack of homogeneity in the surface water temperature of this area.

S-190A Multispectral Photography

An interpretation of S-190A multispectral photography, acquired the same time as the S-192 scanner data, was performed using an additive color viewer. Figure 94 is a color composite photo copied from the viewer screen.

Photo interpretation of this imagery from the viewer screen showed:

-- Turbid water in Nantucket Sound could be differentiated from clear water, as could the effluent emanating from Katama Bay.

-- Surface phytoplankton in the Nantucket shoals could be readily detected and plotted.

-- The water features appearing in the S-192 1550-1750 nm and 10-12 μbands did not appear in the S-190A multi-spectral photography.

-- The same water area contained greater detail near the sub-solar point (in the lower left of the S-190A images) in adjacent frames when the same area was imaged at other locations in the image.

Figure 94, S-190A additive color composite of northern Block Island Sound showing Martha's Vineyard and Nantucket Island, taken on 12 Sept. 1973 at 1310 EDT. 500-600 nm band is imaged as blue, 600-700 nm band as green, and 800-900 nm band as red.

Section 10

Conclusions

A two-part Interpretation Techniques Development Study was conducted which focused on the analyses of S-190A multispectral imagery.

Part A: Quantitative Analysis of S-190A Photographic Characteristics and S-191 Spectrometer Data

A program of obtaining spectral reflectance measurements in situ in the Willcox Playa, Arizona, shows that the surface of the playa has relatively uniform percent spectral reflectance from 400 to 1100 nm. This uniformity exists throughout the center of the playa. The reflectance spectra is shown in Figure 95 below.
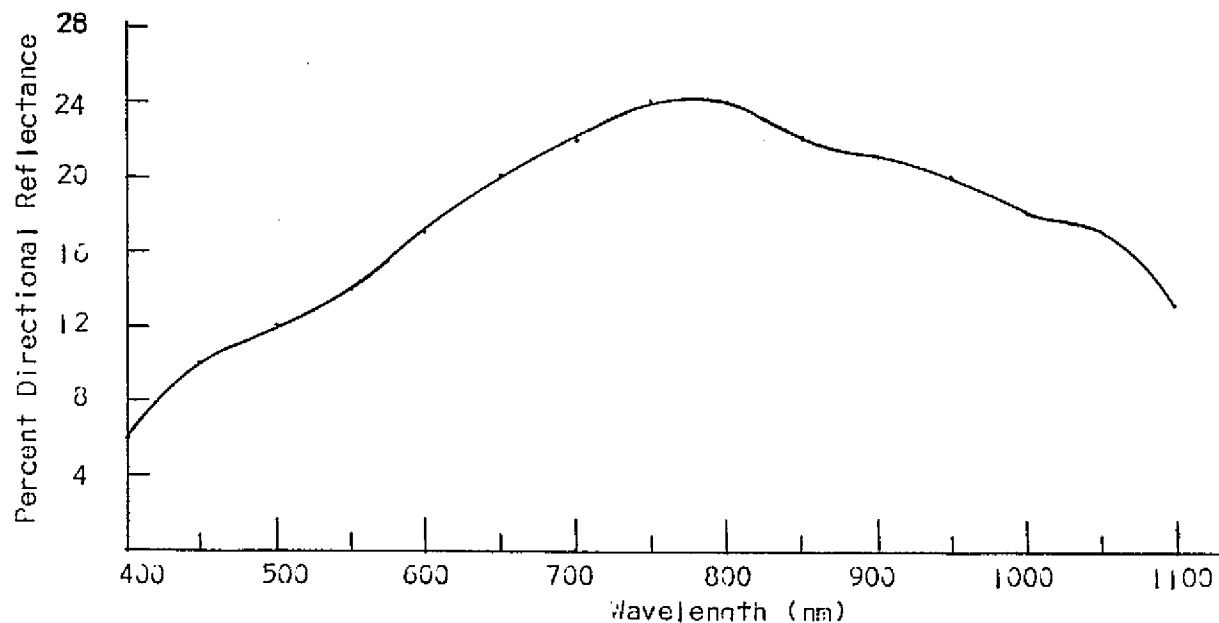
Figure 95 . Average in situ spectral reflectance of the central portion of Willcox Playa.

Analysis of the S-191 spectrometer data, with simultaneously acquired spectral irradiance measurements and corresponding radiance calculations, using average percent reflectance data (Figure 95), resulted in the "factors of correspondence" shown in Figure 96 below. This curve transforms S-191 data into irradiance data for any ground object which, in turn, can be converted into reflectance spectra if the incident radiance is known.
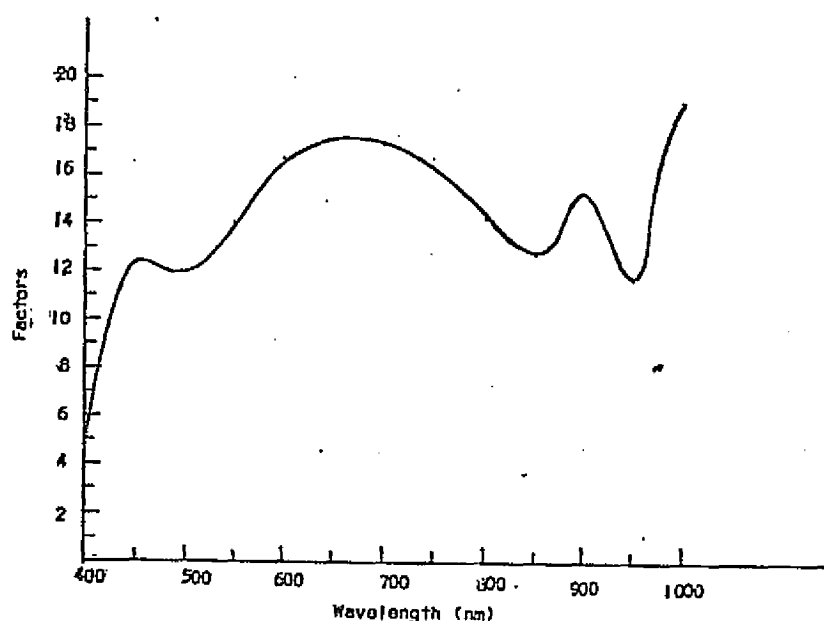
Figure 96. Factors of correspondence between S-191 spectrometer data and the spectral reflectance of desert terrain.

The relationship between S-191 data and terrain irradiance shown in Figure 96 above depends on atmospheric conditions which exist at the time the S-191 data is acquired. The factors of correspondence which were derived are associated with atmospheric optical depth as shown in Figure 97 on the following page.
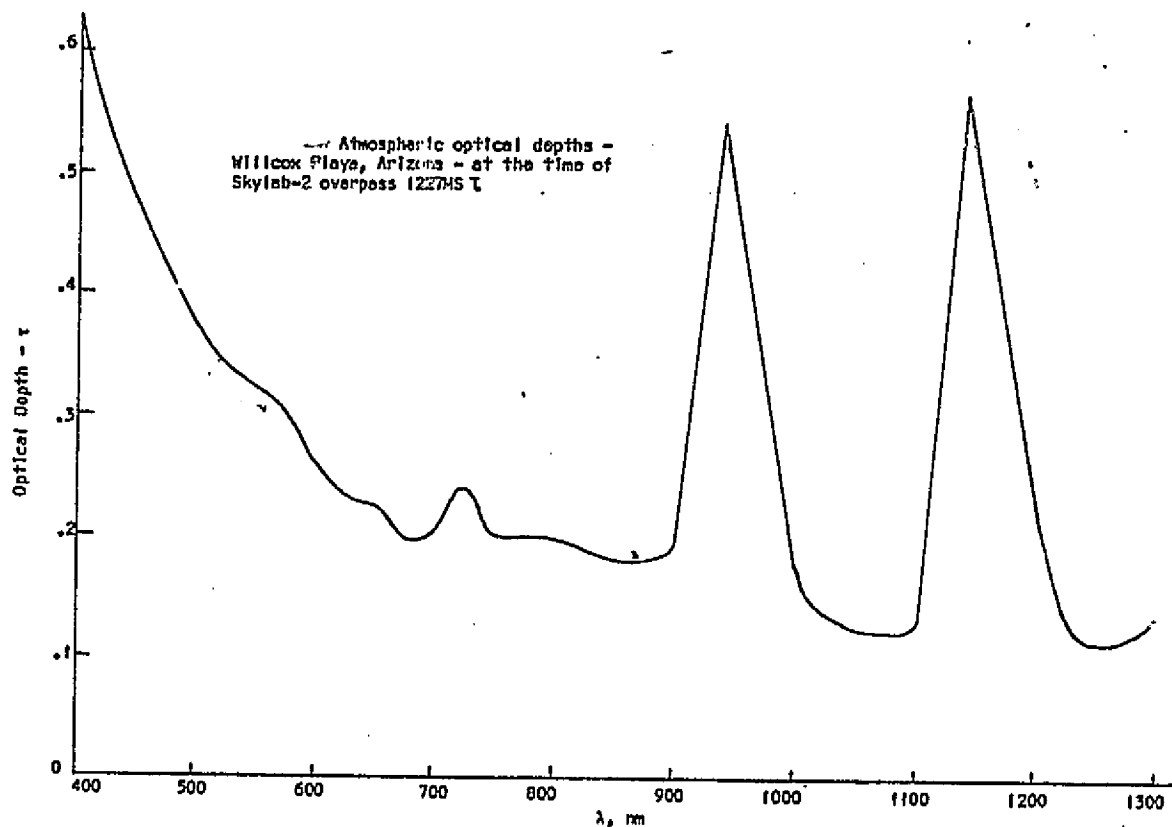
Figure 97. Atmospheric optical depth associated with the factors of correspondence in Figure 96.

Digital measurements of S-190A black-and-white multispectral nega-tive image densities of desert terrain, using the System 800, showed that densities in the four bands were not uniform. Analysis of 294,912 eight-bit pixels showed that the 600-700 nm images were most dense ($\bar{x}$=65.8), followed by 700-800 nm ($\bar{x}$=132.9), 500-600 nm ($\bar{x}$=153.1), and 800-900 nm bands ($\bar{x}$=183.4) in descending value of density. The standard deviation of image density was within the range s=35.1 to s=50.0 for all four bands.

Measurements of S-190A image densities of uniformly reflecting Willcox Playa within and out of shadow, along with bright cloud tops, showed extreme variability of the average image densities between the four bands. Assuming a uniformly reflecting surface of Willcox Playa (which is supported by in situ spectral reflectance measurements) the difference in reflectance of the playa in shadow and in sunlight, due to atmospheric scattering (for identical film processing), showed the greatest screen brightness range in

-160-

the 600-700 nm band and the least in the 800-900 nm band.

A detailed analysis of all 294,912 eight-bit pixels of the north end of the playa digitized from S-190A black-and-white imagery showed significant differences existed in the average image density of an assumed uniformly reflecting surface. As was ascertained for desert terrain previously, the 600-700 nm band had the greatest density. However, for the playa itself, the 500-600 nm band replaced the 700-800 nm band as being second most dense; otherwide, the data were unchanged.

Underflight AMPS black-and-white multispectral imagery of the same area of Willcox Playa also indicated significant non-uniformities on the playa and that the 600-700 nm band density was significantly greater than in both the 800-600 nm and 700-800 nm bands.

Procedures were perfected whereby positives could be made from each Skylab S-190A negative to a different (yet precisely established) characteristic curve. The resulting additive color composites showed significantly improved detail in land features. Figure 98, on the following page, shows a comparison of the negative-positive density relationships between "conventionally" processed and "contrast-stretched" S-190A negatives and positives.

Comparative analysis using an additive color viewer showed that significantly more geological information could be extracted from contrast-stretched multispectral images compared to those conventionally processed. A significant number of unmapped geologic units in the Sulfur Springs Valley in southeastern Arizona were compiled from contrast-stretched imagery.
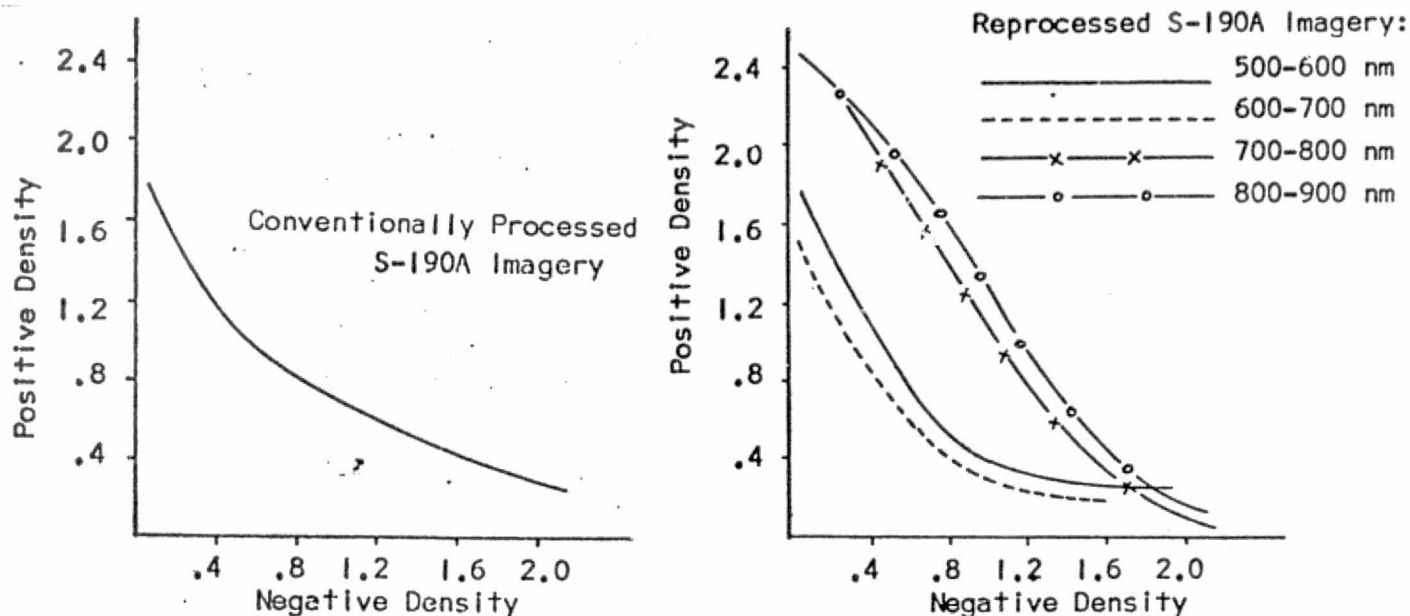
Figure 98. Negative-positive density relationships of "conventionally" processed and "contrast-stretched" S-190A black-and-white multispectral photographs.

Part B: The Feasibility of Utilizing Skylab Remote Sensor Data to Monitor and Manage the Coastal Environment

"Baseline" physical, chemical, and biological oceanographic data were collected in Block Island Sound (New York) and in New York Bight prior to Skylab 3. These data collected on twenty-four cruises showed that:

-- Vertical temperature gradients are governed by vertical mixing and diffusion between a surface layer of harbor or sound water and a bottom layer of coastal water.

-- Maximum temperatures occur in August and minimum in Feburary.

-- Salinity regime is regulated by stream discharge into Long Island Sound and by the Hudson River for New York

Bight with a one-month lag between maximum stream discharge and salinity minimum in both Long Island Sound and Block Island Sound, as well as New York Bight.

-- A two-layered system exists in the central part of Block Island Sound with a surface layer composed of less saline Long Island Sound water and a bottom layer of saline coastal water.

-- The average extinction coefficient in Block Island Sound is 0.335 and in New York Bight 0.663.

-- Blue band extinction coefficient is 0.400 for Block Island Sound and 1.048 for New York Bight.

-- Red band extinction coefficient is 0.554 for Block Island Sound and 0.876 for New York Bight.

-- The maximum wavelength of radiation transmission increases with increasing turbidity.

-- Average extinction coefficients are correlated with total particle count for particles over 5μ in size.

-- In Block Island Sound, the supply of nitrogen is limited and nutrients are quickly utilized by phytoplankton.

-- In Block Island Sound, chlorophyll a concentrations ranged between .85 and 9.4 mg/m^3.

-- There exists a high correlation between phytoplankton and suspended particles (greater than 10.7μ in size) in Block Island Sound indicating that phytoplankton contributes largely to the suspended material there.

-- A low correlation exists between phytoplankton and
   suspended particles (greater than 10.7μ in size) in
   New York Bight, probably due to the disposal of sewage
   sludge.
-- The largest phytoplankton opopulation occurs in the
   Peconic Bay-Gardners Bay region of Block Island Sound.
-- Sparse phytoplankton population exists in central and
   southern Long Island Sound and in central Block Island
   Sound.

Oceanographic data was collected simultaneously with Skylab-3
overpass at the Shagwong Reef area of Block Island Sound on 12 September
1973. This data showed that a plume exists which is caused by seasonal
biological phenomena composed principally of organic material, but not due
to bottom scouring action. The difference in extinction coefficients
between water types at Shagwong Reef (measured at the instant S-190A
imagery was acquired) was -0.07 per meter (-0.33 versus -0.26). At the
surface, the suspended solid difference was 0.60 mg/l (2.79 versus 2.19),
total particle difference 21 x 10^6 per liter (206 vs. 185 x 10^6), and total
cell count differen 4.7 x 10^3 per liter (15.2 versus 10.5 x 10^3).

S-190A multispectral positives which are "conventionally" prepared -
that is, are exposed and processed so that a linear relationship with minus
unity slope,exists between the negative and the positive results in greatly
reduced contrast detail in the water. A procedure whereby each black-and-
white S-190A multispectral negative is exposed and printed, emphasizing subtle
low brightness detail in the water, was developed. This "contrast-stretch"

procedure, which is useful for three of the four multispectral photographic

bands, results in the following density ranges:

500 - 600 nm Band	.33 to 1.92
600 - 700 nm Band	.14 to 1.19
700 - 800 nm Band	.45 to .91

Using these "contrast-stretch" techniques, two water masses having

an extinction coefficient difference of 0.07 (i.e., -0.26 vs. -0.33 per

meter) were readily detected. These water masses which were differentiated

had differences in suspended solids of 0.6 milligrams per liter (2.19 mg/l

vs. 2.79 mg/l) and differences in total particle count of 21×10^6 particles

per liter(185 vs. $206 \times 10^6/l$).

Non-homogeneous vertical stratification of Block Island Sound waters

could be detected by the sharpness of image density boundaries in contrast-

stretched S-190A black-and-white images. Differences in suspended solids

of one .illigram per liter at depths between seven and ten meters were the

only significant indicators sampled simultaneously with the imagery which

showed lack of homogeneity with depth. These differences could not be

detected on S-190A color nor on S-190A color-infrared photography.

Visual photo interpretation of S-190B color imagery showed that,

contrary to existing tidal current charts, two large counter-clockwise

gyres exist in Long Island Sound. Areas of upwelling at Mattituck Inlet

could also readily be detected in the imagery. These circulation patterns

are hypothesized to be due to strong prevailing winds occurring offshore.

Additive color analyses of S-190A multispectral black-and-white imagery

readily showed sewage sludge dump areas in New York Bight. These areas

have suspended solids in the order of 20 milligrams per liter.

Digitization of S-190A multispectral negatives in registration, along with subsequent single and multiple image classification of image brightness, assisted in establishing a vertical model of the mixing of water masses in Block Island Sound showing that:

-- Complex sub-surface mixing patterns could be detected

   by comparison of 500-600 nm and 600-700 nm single

   band brightness contours combined with the brightness

   contours of the average of these two bands.

-- Homogeneous water flows were shown by similarity in

   the digital brightness contours of different S-190A

   spectral bands.

-- The spatial distribution water mass existing off the

   Connecticut shore in Block Island Sound could be

   detected.

Water turbidity, coupled with circular gyres, was plotted in Long Island Sound using digital processing techniques on the S-190A multispectral photography. Extinction coefficients were assigned to different water masses and vertical mixing characteristics identical to those derived from photo-interpretation of the imagery were established. The existence of sub-surface water discontinuity east of the Connecticut River estuary was detected.

Similar digital analysis of S-190A multispectral images was performed on Nantucket Sound. Clear and turbid water masses were differentiated and values of extinction coefficient assigned. Areas of heavy phytoplankton concentration were established based upon the relative brightness contours in the single and multiple image brightness maps.

Comparative analysis of S-192 multispectral scanner imagery with S-190A multispectral photography was performed in the Nantucket coastal area. Significant noise was apparent in the S-192 photographic data products which hampered analysis. In general, the only two S-192 bands which showed water detail which was not apparent in the S-190A multi-spectral imagery were the 1550-1750 nm and 10-12µ bands.

Section 11

References

The following references were cited in this report:

Austin, N.M. and P. Stoops (1973): "A Synoptic Study of the Surface Waters of Block Island Sound and Surrounding Waters, Part II", New York Ocean Science Lab. Technical Report 0024.

Nuzzi, R. (1973): "A Synoptic Study of the Surface Waters of Block Island Sound and Surrounding Waters, Part I", New York Ocean Science Lab. Technical Report 0017.

Hollman, R. (1970): "The Physical Oceanography of New York Bight", WATER POLLUTION, A.A. Johnson (editor), Gordon and Breach, New York, pp. 3-12.

Williams, R. (1967): "The Physical Oceanography of Block Island Sound", U.S. Navy Underwater Sound Laboratory, New London, Connecticut, USL Technical Memo 2213-33-67.

APPENDIX A

PHYSICAL OCEANOGRAPHY

by

Rudolph Hollman
Research Scientist in Physical Oceanography
New York Ocean Science Laboratory
Montauk, New York

Stephen K. Gill
Technician in Physical Oceanography
New York Ocean Science Laboratory
Montauk, New York

INTRODUCTION

This section concerns itself with the physical properties of the water, in particular, its temperature, salinity, density, optical characteristics, and tidal currents.

The distribution of the physical properties of the waters of Block Island Sound has been reviewed by Williams (1964) and is the most comprehensive to date.

In the New York Bight area, the physical properties of the waters and their seasonal and diurnal variations have been reviewed by Hollman (1971).

METHODS

Temperature, salinity, and calculated density values were obtained at multidepths for most stations sampled in Block Island Sound. Only surface salinity samples were taken on the New York Bight cruises.

When stations were sampled more than once per cruise, averages of temperature, salinity, and density (δ_t) were calculated at standard depths of 0, 10, 20, 30, 35, and 40 meters. Flood and ebb averages of these parameters were also calculated over each cruise. Horizontal profiles (contours of t° C, S‰, and δ_t in depth versus distance) were made for each crossing of a transect.

The downwelling irradiance of the visible spectrum was measured at each station in Block Island Sound using an upward-facing irradiance meter (submarine photometer), comprising a photocell and cosine collector equipped with glass filters.

The extinction coefficient, $\bar{k}$, for these light values is defined by the equation:

$$I(z) = I(z=0) \exp - \bar{k}z \qquad (1)$$

where $I(z=0)$ is the total visible light energy in a particular wavelength band that is

incident upon the naviface, I(z) is the remaining light energy at the depth z(m), and $\bar{k}$ is the total "extinction" coefficient for the particular wavelength band in units of m^{-1}.

On most cruises, irradiance measurements were taken as near to noon as possible at each station. Linear regression analyses were performed and correlation coefficients calculated for data sets using total particle counts and average extinction coefficients for each of the Block Island Sound and New York Bight stations.

Regression analysis and correlations were also calculated between monthly freshwater discharge into Long Island Sound and the monthly surface and bottom salinity values at the Block Island Sound stations. Dilution factors, D, defined by:

$$D = (\Delta S/\bar{S}) \times 100\% \qquad (2)$$

where ΔS is the annual range and $\bar{S}$ the mean salinity at a station, were also calculated.

RESULTS

Block Island Sound: Distribution of Temperature, Salinity, and Density

Fundamental to an understanding of the temperature and salinity fields is a picture of their annual variations, both in space and time. In other words, an instantaneous picture of the temperature or salinity field can be placed in a better perspective with a foreknowledge of the annual variations that can be expected. Such annual variations of temperature and salinity for the 12 stations in Block Island Sound are tabulated in Table II-1 through II-3 in the appendix to this section.

As readily seen in the tables, the warmest month in all cases is August, with temperatures of approximately 19° C, and the coldest month is February, with temperatures of approximately 2° C. These results agree with previous results obtained in Block Island Sound. These data are graphically displayed as a function of time in Figure II-1 through II-3 in the

same transect order as found in the tables. The lower portion of each figure shows the variation of both surface and bottom (where applicable) temperatures in °C over the year. The upper portion shows the variation of both surface and bottom (where applicable) salinity in parts per thousand (°/₀₀) over the same time period, together with the mean monthly values for the Total Stream Discharge (SD) into Long Island Sound in cubic feet per second (cfs) as provided by the U.S. Department of the Interior, Geological Survey, Water Resources Division in Hartford, Connecticut.

The temperature profiles show that the average surface waters are warmer than the bottom waters during the warm months and cooler than the bottom waters (inversion) during the coldest months of January and February. This is again typical of the temperature regime in Block Island Sound.

An examination of the salinity profiles shows that the bottom waters are consistently more saline than the surface waters. This is typical of estuaries. The figures also show that a good inverse correlation exists between the surface salinity and the total stream discharge at approximately a 1-month lag. The stream discharge is an important factor in the annual distribution of salinity in Block Island Sound.

Monthly values of the averaged surface temperatures, salinities, and corresponding densities (σ_t) for each station in Block Island Sound are plotted as a function of distance (station location) and shown in Figure II-4. The solid curves are the average surface salinity distributions across the transects for the various dates, the dashed line is the accompanying surface temperatures, and the broken dashed line the corresponding densities.

In general, the lowest salinities are found at Station H1 of the H transect and HB1 of the HB transect, both by Montauk Point (Figure I-1). On the H transect, the most saline waters are found by the Rhode Island shore at Station H4. The highest salinities on the HB transect are located at Station H5 by Block Island. There is no apparent preference for either high or low saline waters on either end or the center of the BR transect. High-low salinity values appear to alternate between the southern end (BR1), the middle (BR2), and the northern end (BR3).

There does not appear to be any significant temperature difference across the transects.

That is to say that, on the average, over a tidal cycle, the surface waters are nearly iso-thermal on each transect with little difference from one station to another. The in-ference to be drawn is that the average surface temperatures over a tidal cycle are a rel-atively poor indicator of water masses, whereas the corresponding salinity averages do show the existence of different water types.

The average surface density distribution over a tidal cycle is largely governed by the salinity distribution, since the temperatures are, for practical intents, isothermal.

Three water masses can be inferred from these figures, particularly along the H and HB transects: significantly fresher and lighter (less dense) waters along the Long Island shore at Montauk that originates in the Peconic Bay System, a water mass in the middle of these two transects that is largely Long Island Sound water, and a water mass to the north offshore of Rhode Island that is significantly more saline and denser that has its origin in Rhode Island Sound to the east. This water mass also occupies most of the BR transect between Block Island and Point Judith, Rhode Island (Figure I-1).

The monthly variations in temperature and salinity from one figure to another are images of the distributions shown in Figure II-1 to " 3. As indicated above, the average surface density, as represented by σ_t, is dependent upon the salinity field. However, the annual variation in density is largely dependent upon the annual temperature variation. The ver-tical density structure is most stable in summer, with warmer and therefore lighter water overlying cooler and denser waters. In winter, however, the density structure is nearly uniform from surface to bottom, and in some brief instances cooler and denser water may be found to overlie warmer and slightly lighter waters. This is an unstable situation that generally leads to convective overturning, producing a well mixed and homogeneous water mass.

Horizontal isopleths of average values taken over half-tidal cycles (flood/ebb) for representa-tive summer and winter cruises along each transect are shown in Figure II-5 through II-7 as a function of depth and distance (station position). The apparent absence of any signif-icant difference in the distribution of temperature, salinity and particularly σ_t between flood and ebb conditions either in summer or winter, along the H transect (Figure II-5),

the HB transect (Figure II-6), or the BR transect (Figure II-7), is most surprising. A change of 180° in the flow of these waters between tidal currents was expected to produce at least a measurable change in the slopes of the 150 isopycnal surfaces, from an upward slope from north to south during a flood tidal cycle to a downward slope during an ebb cycle. The slope for all three variables is persistently downward when going from north to south (from right to left in each figure) regardless of the stage of the tidal cycle or the time of the year.

The most striking changes occur in the temperature distributions between the summer months and the winter months. Vertical gradients are approximately 5°C for the entire water column during the summer and less than 1°C during the winter months.

It is apparent from these figures that the tidal flow alters the values of the various variables such as temperature and salinity through advective processes, but does not appreciably alter the slopes of the isotherms or the isohalines. This implies that the horizontal gradients of temperature and salinity are virtually unaffected by changes in the direction of the tidal flow.

Optical Properties

Values for the extinction coefficients defined by Equation 1 over a wavelength band comprising the visible spectrum (white light) are tabulated in Table II-4 in the appendix to this section for each station in Block Island Sound. The magnitude of the coefficients is related to the amount of suspended particles and dissolved materials in the water column and is, in effect, a measure of the turbidity of the water. As can readily be seen in the table, particularly from the averages from each station, the highest extinction values, and consequently the waters with the greatest turbidity, are those stations by Montauk Point (H1 and HB1), by Block Island (HB5 and BR1), and by Rhode Island (H4 and BR3). These areas with high extinction coefficients coincide with areas of high turbidity, particularly around Montauk Point and Point Judith, Rhode Island, as determined from visual inspections of ERTS-1 imagery. The clearest waters are generally found near the center of each transect (Station H2, H3, HB3, HB4, and BR2).

The depth to which 1% of the visible radiation energy incident at the naviface penetrates can be determined from Equation 1, using the average station values for $\bar{k}$ from Table II-4. This depth represents the compensation depth below which energy produced by photosynthesis is counterbalanced by that energy that is used up by respiration. Major photosynthetic activity, therefore, takes place above this level. For the H transect, these levels occur at 12.1m, 15.4m, 18.4m, and 17.7m for Station H1 through H4 respectively; for the HB transect, the levels are 12.8m, 14.4m, 14.8m, 15.9m, and 12.4m for Station HB1 through HB5; for the BR transect, the depths for the compensation level are 12.4m, 13.2m, and 10.0m for Station BR1 through BR3 respectively. The shallowest depth (10.0m) occurs at Station BR3 at Point Judith, Rhode Island, generally also the most turbid area in the ERTS imagery for Block Island Sound

Extinction coefficients in the blue, green, and red spectral bands for the Block Island Sound stations are tabulated in Table II-5 of the appendix. The blue band has a maximum transmission of 87% between approximately 300 nm and 550 nm; the green band transmits a maximum of 65% between 460 nm and 660 nm, and the red band transmits a maximum of 85% between 500 nm and 720 nm. As the averages for each station show, the maximum extinction is found in the red band, as would be expected, the minimum in the green, and a secondary maximum in the blue. These conditions are typical for mean coastal waters (see for example, Sverdrup, Johnson and Fleming, 1942, Fig. 20, pg. 8_). Here again, the higher extinction values in all wavelengths are found at the stations closest to land, as was the case for the extinction coefficients for the visible spectrum.

Compensation depths using average spectral extinction coefficients from Table II-5 were calculated and tabulated in Table II-6 (appendix). The shallowest depth (6.8m) is in the red band for Station HB1 off Montauk Point. The greatest depth of 18.4m in the green band occurs at Station H3 and BR1.

In general, the clearest waters are found along the H transect. The average transmittance per meter along this transect is 74.3%/m for the visible spectrum band, and 72.8%/m for the blue, 77.1%/m for the green, and 62.7%/m for the red band. The most turbid water over the visible spectrum band in along the BR transect, with an average transmittance of 67.5%/m. In comparison, the average transmittance for the HB transect in visible bands

was 71.9%/m. Over the blue and green spectral band, the most turbid waters were along the HB transect, where the average transmittance values were 63.8%/m and 72.2%/m respectively. The lowest transmittance values in the red band were from the BR transect, with an average value of 54.7%/m.

Interpolated Parameters

Surface values of temperature, salinity, chlorophyll *a*, total particle count, and extinction coefficients were interpolated to coincide with the time of the satellite overpasses on 8 October 1972 and on 19 March, 24 April, and 17 June, 1973. The phases of the tidal cycle at the time of the overpass were used to find the corresponding interpolated times from data obtained from cruises closest in time to the overpass. This is possible since the data acquired on each transect generally covers a tidal excursion during each season of the year. We have, therefore, the variation of any parameter in space and time over a tidal cycle for each period of the year.

The results of such interpolations, or estimations, are tabulated in Table II-7 of the appendix. In the case of the extinction coefficients, $\bar{k}$, the ratio of particle counts to extinction coefficients for the preceding cruises was employed to calculate the values found in the table.

New York Bight: Distribution of Temperature and Salinity

Surface values of temperatures and salinity for the nine stations within the apex of the New York Bight (Figure 1-2) are tabulated in Table II-8 in the appendix. As can be seen in the table, the most saline waters are found at the easternmost stations, i.e., B1 and B9. In winter, these two stations are also the warmest, and in summer (May) the coolest. The least saline waters are found to the west (B3), representing the combined waters of the Hudson and Raritan rivers that have mixed with the harbor waters and are exiting along the Sandy Hook side of the harbor entrance.

Optical Properties

Extinction coefficients (Equation 1) for the stations in the New York Bight are tabulated in Table II-9 in the appendix together with the compensation depth calculated from the individual station averages. The clearest (least turbid) waters are found the furthest offshore at Station B6. The value at B6 (0.47) is still almost a factor of 2 greater than the corresponding values at Station H3 (0.25) in Block Island Sound and is, in fact comparable to the most turbid station, BR3, that had an average value of 0.46 (Table II-4). The most turbid waters are those off of Sandy Hook (B3).

The compensation depths for the stations in the Bight range from approximately 4m to 9m as compared to an approximate range of from 10m to 18m in Block Island Sound, almost a factor of 2 less.

The average spectral extinction coefficients for the stations in the Bight are tabulated in Table II-10 (appendix), with station averages for each color band and associated compensation depths. The band of maximum extinction is now in the blue band and the secondary maximum in the red, indicating more turbid waters. The band of least extinction is still in the green. A shift in the wavelength of maximum penetration from the blue-green band to the orange-red band is expected with an increase in turbidity (see, for example, Sverdrup et al 1941, pg. 84). The compensation depths for these average spectral values are approximately half of the corresponding values from Block Island Sound.

Summary

These results are summarized in Figure II-8 through II-10. Each figure shows the isopleths for surface temperature, salinity, -kr and total particle counts for 20 December 1972 and 25 January and 31 May 1973 respectively.

DISCUSSION

The annual temperature regime within Block Island Sound and the New York Bight is largely governed by solar radiation and correlates with the mean month temperatures in the atmosphere, lagged 1 month. For example, maximum air temperatures occur in July, minimum temperatures in January. For these waters, the maximum temperatures occur in August, the minimum in February. Vertical temperature gradients are largely governed by vertical mixing and diffusion between a surface layer composed of largely Harbor and Sound water and a bottom layer of coastal water.

The annual salinity regime is mainly regulated by the stream discharge entering Long Island Sound and New York Harbor. The two major sources of this stream discharge are the Connecticut River for the Sound and the Hudson River for the Harbor. There is also approximately a 1-month lag between maximum stream discharge and the corresponding salinity minimums (Figure II-1 through II-3).

Linear correlations at a 1-month lag and dilution factors, D, as defined by Equation 2, were calculated for Block Island Sound and are tabulated in Table II-11 in the appendix. The highest correlations occur at the center stations of the H and HB transects and the weakest correlation occurs at Station BR3 (55%). Weak correlations at depth (30m) imply a two-layered system, with a surface layer that is composed of less saline Long Island Sound waters and a bottom layer of saline coastal waters. Vertical mixing and diffusion is relatively weak in Block Island Sound, as indicated by these high correlations and dilution factors.

Average tidal flood and ebb currents for Block Island Sound are shown in Figure II-11. With velocities of greater than 1 knot along most transects, one would expect a shift in the slopes of the isopycnals with a change in the direction of the tidal flow (Figure II-5 to II-7). The only exceptions are the uppermost isopycnals between Station HB2 and HB3 (Figure II-6), where a slight change in slope can be noticed between the flood and ebb cycles. In general, the fact that the isopycnals slope upward from left to right implies a net flow of water in the ebb direction.

The average extinction coefficient for Block Island Sound in the visible spectral band was 0.335, as compared to a mean value for the New York Bight of 0.663, almost a factor of 2 greater. The mean value for the blue band is 0.400 in Block Island Sound and 1.048 in the New York Bight; for the red band, the value is 0.554 and 0.876 in the Sound and the Bight respectively. The disparity in these two wavelength bands dramatizes the shift of the peak of maximum transmissivity from shorter to higher wavelengths with increasing turbidity.

The average extinction coefficients for each transect in Block Island Sound were correlated with total particle counts as determined with a Coulter Counter (to be discussed in Section IV) and for particle counts greater than 5μ in equivalent diameter. The results are tabulated in Table II-12 in the appendix. Highest correlations occur with particles greater than 5μ but less than 10μ in size. Similar results obtain for the Bight stations, as can be seen in Table II-13 (appendix). These results reflect nonselective attenuation, particularly absorption, since the lower limit of the total particle count is approximately 0.7μ in equivalent size (see Section IV), so that selective or Raleigh scattering is not included in these calculations. The correlations would be significantly improved if the resolving power of the Coulter Counter could be increased; however, this is an engineering design problem that hopefully will be resolved in the future.

REFERENCES

Hollman, Rudolph. 1970. The physical oceanography of the New York Bight. In *Water Pollution*, A.A. Johnson, ed. Gordon and Breach, New York. pp 3-12.

Sverdrup, H.U., M.W. Johnson, and R.H. Fleming. 1942. *The Oceans: Their Physics, Chemistry, and General Biology*. Prentice Hall, Englewood Cliffs, N.J. 1061 pp.

Williams, Robert G. 1967. The Physical Oceanography of Block Island Sound, a review report. New London, Conn., U.S. Navy Underwater Sound Laboratory. 15 pp. (USL Technical Memorandum No. 2213-33-67).

TABLE II-1

Average monthly values of temperature and salinity in the H transect
of Block Island Sound (1972-1973)

Station	Variate	Depth	August	October	November	December	February	March	April	June
H1	$\overline{T}°C$	Z=0	19.3	17.3	11.8	8.4	1.9	3.9	6.6	14.5
		Z=30m	·	·	·	·	·	·	·	·
	$\overline{S}‰$	Z=0	30.27	30.85	31.05	30.27	29.65	31.29	29.00	28.96
		Z=30m	·	·	·	·	·	·	·	·
H2	$\overline{T}°C$	Z=0	18.8	17.7	11.9	8.7	2.4	3.8	6.9	13.9
		Z=30m	16.9	17.7	12.0	9.2	-	3.8	5.8	11.0
	$\overline{S}‰$	Z=0	30.24	31.10	31.20	30.17	29.67	29.43	28.67	28.69
		Z=30m	30.90	31.12	31.36	30.89	-	29.80	31.20	31.20
H3	$\overline{T}°C$	Z=0	20.1	17.5	12.2	8.7	2.8	3.5	7.0	14.2
		Z=30m	15.7	17.5	12.4	10.1	-	3.5	5.5	10.5
	$\overline{S}‰$	Z=0	30.67	31.39	31.21	30.80	30.25	30.88	29.59	29.94
		Z=30m	31.46	31.59	31.74	31.58	-	31.12	31.60	31.00
H4	$\overline{T}°C$	Z=0	19.7	17.4	11.4	8.8	2.8	3.7	7.3	13.7
		Z=30m	15.9	17.4	11.6	9.0	-	3.6	5.3	11.5
	$\overline{S}‰$	Z=0	30.52	31.71	31.39	31.01	30.93	31.09	29.42	29.92
		Z=30m	31.70	31.81	31.93	31.36	-	31.28	31.95	31.30

TABLE II-2

Average monthly values of temperature and salinity in the HB transect
of Block Island Sound (1972-1973)

Station	Variate	Depth	August	November	December	February	March	April	June
HB1	$\bar{T}°C$	Z=0	18.0	12.3	8.5	2.8	3.7	7.8	14.7
		Z=30m	-	-	-	-	-	-	-
	$\bar{S}‰$	Z=0	30.65	31.49	30.18	30.15	29.41	29.52	29.31
		Z=0	-	-	-	-	-	-	-
HB2	$\bar{T}°C$	Z=0	17.7	12.4	8.8	3.2	3.9	7.7	14.3
		Z=30m	-	-	-	-	-	-	-
	$\bar{S}‰$	Z=0	30.80	31.65	30.32	30.49	29.71	29.68	29.74
		Z=30m	-	-	-	-	-	-	-
HB3	$\bar{T}°C$	Z=0	18.0	12.5	9.0	3.2	3.6	7.9	14.6
		Z=30m	13.1	12.4	9.5	4.6	-	5.7	11.2
	$\bar{S}‰$	Z=0	30.80	32.05	31.09	30.70	29.84	29.33	29.69
		Z=30m	32.27	32.12	32.11	32.11	-	32.23	31.46
HB4	$\bar{T}°C$	Z=0	18.4	12.5	9.1	3.5	3.8	8.1	14.5
		Z=30m	-	-	-	-	-	-	-
	$\bar{S}‰$	Z=0	31.14	32.11	31.56	31.20	30.25	29.78	30.42
		Z=30m	-	-	-	-	-	-	-
HB5	$\bar{T}°C$	Z=0	18.1	12.3	9.2	3.8	3.6	8.5	13.9
		Z=30m	-	-	-	-	-	-	-
	$\bar{S}‰$	Z=0	31.35	32.12	31.81	31.58	30.51	29.95	30.77
		Z=30m	-	-	-	-	-	-	-

TABLE II-3

Average monthly values of temperature and salinity in the BR transect

of Block Island Sound (1972-1973)

Station	Variate	Depth	September	November	December	March	April	June
BR1	$\overline{T}°C$	Z=0	18.8	10.7	8.6	3.5	7.4	14.0
		Z=30m	18.5	10.8	8.6	3.6	5.1	10.5
	$\overline{S}\%_{oo}$	Z=0	31.41	31.91	31.55	31.14	30.68	30.13
		Z=30m	31.62	31.93	31.65	31.46	31.48	31.50
BR2	$\overline{T}°C$	Z=0	19.1	10.6	8.2	3.5	7.9	14.0
		Z=30m	17.4	11.3	8.6	3.4	5.1	9.3
	$\overline{S}\%_{oo}$	Z=0	31.58	31.50	31.38	31.34	31.12	30.58
		Z=30m	31.79	31.91	31.56	31.70	32.24	31.83
BR3	$\overline{T}°C$	Z=0	19.2	9.8	6.1	3.4	7.8	14.2
		Z=30m	-	-	-	-	-	-
	$\overline{S}\%_{oo}$	Z=0	31.56	31.23	30.30	31.40	30.61	30.64
		Z=30m	-	-	-	-	-	-

TABLE II-4

Average extinction coefficients ($\bar{k}$) in Block Island Sound

a) H Transect

Date	Cruise	Station			
		H1	H2	H3	H4
20 Mar 1973	K7310	0.42*	0.35	0.29	0.24
24 Apr 1973	K7318	0.35*	0.25	0.21	0.27
Averages		0.38	0.30	0.25	0.26

*Extrapolated

b) HB Transect

Date	Cruise	Station				
		HB1	HB2	HB3	HB4	HB5
29 Aug 1972	K7218	0.39	0.29	0.31	0.29	0.34
24 Apr 1973	K7318	0.36	0.30	0.23	0.19	0.44
25 Apr 1973	K7310	0.35	0.31	0.37	0.36	0.27
19 Jun 1973	K7336	0.33	0.39	0.3.	0.31	0.44
Averages		0.36	0.32	0.31	0.29	0.37

c) BR Transect

Date	Cruise	Station		
		BR1	BR2	BR3
5 Sep 1972	K7219	0.35	0.37	0.50
16 Nov 1972	K7232	0.40	0.42	0.52
19 Mar 1973	K7310	0.32	0.42	0.59
20 Mar 1973	K7311	0.54	0.38	0.46
24 Apr 1973	K7318	0.32	0.23	0.31
18 Jun 1973	K7335	0.31	0.28	0.37
Averages		0.37	0.35	0.46

TABLE II-5

Average spectral extinction coefficients (-k [λ]) in Block Island Sound

a) H Transect

Cruise & Date	Color Band	Station			
		H1	H2	H3	H4
K7318 24 Apr 1973	Blue	-	0.35	0.27	0.33
	Green	-	0.27	0.25	0.26
	Red	-	0.42	0.45	0.53

b) HB Transect

Cruise & Date	Color Band	Station				
		HB1	HB2	HB3	HB4	HB5
K7319 25 Apr 1973	Blue	0.56	0.42	0.38	0.46	0.39
	Green	0.41	0.33	0.31	0.34	0.28
	Red	0.73	0.58	0.63	0.60	0.52
K7336 19 Jun 1973	Blue	0.60	0.46	0.34	0.31	0.57
	Green	0.29	0.27	0.30	0.23	0.42
	Red	0.64	0.51	0.48	0.48	0.59
Averages	Blue	0.58	0.44	0.36	0.39	0.48
	Green	0.35	0.30	0.31	0.32	0.35
	Red	0.68	0.54	0.56	0.54	0.56

c) BR Transect

Cruise & Date	Color Band	Station		
		BR1	BR2	BR3
K7232 16 Nov 1972	Blue	0.48	0.49	0.47
	Green	0.36	0.38	0.38
	Red	0.68	0.61	0.80
K7318 24 Apr 1973	Blue	0.35	0.39	0.31
	Green	0.19	0.16	0.25
	Red	0.38	0.67	0.51
K7335 18 Jun 1973	Blue	0.39	0.38	0.33
	Green	0.19	0.25	0.26
	Red	0.55	0.60	0.62
Averages	Blue	0.41	0.42	0.37
	Green	0.25	0.26	0.30
	Red	0.54	0.63	0.64

TABLE II-6

Compensation depths (depths at which 1% of the incident energy is found) in meters

a) H Transect

Wavelength Band	Station			
	H1	H2	H3	H4
Blue	-	13.2	17.0	14.0
Green	-	17.0	18.4	17.7
Red	-	11.0	10.2	8.7

b) HB Transect

Wavelength Band	Station				
	HB1	HB2	HB3	HB4	HB5
Blue	7.9	10.5	12.8	11.8	9.6
Green	13.2	15.4	14.8	14.4	13.2
Red	6.8	8.5	8.2	8.5	8.2

c) BR Transect

Wavelength Band	Station		
	BR1	BR2	BR3
Blue	11.2	11.0	12.4
Green	18.4	17.7	15.4
Red	8.5	7.3	7.2

TABLE II-7

Interpolated values for temperature, salinity, density, chlorophyll a, particle count,
and extinction coefficient to coincide with ERTS-I overflights

a) 8 October 1972   Overflight: 1101 EDST

Interpolated Variate	Station			
	H1	H2	H3	H4
Temperature (°C)	16.9	17.6	17.4	17.4
Salinity (‰)	31.60	31.18	31.20	31.65
Density (σ_t)	22.94	22.48	22.53	22.89
Chlorophyll a (mg/m^3)	2.85	1.46	2.28	3.00
Particle Count (1/L)	-	-	-	-
$-\bar{k}$ (1/m)	-	-	-	-

b) 19 March 1973   Overflight: 1002 EST

Interpolated Variate	Station		
	BR1	BR2	BR3
Temperature (°C)	3.5	3.6	3.3
Salinity (‰)	30.96	31.31	31.37
Density (σ_t)	24.65	24.92	24.99
Chlorophyll a (mg/m^3)	1.00	2.20	2.79
Particle Count (1/L)	140x10^6	155x10^6	270x10^6
$-\bar{k}$ (1/m)	0.22	0.38	0.49

c) 24 April 1973   Overflight: 1002 EST

Interpolated Variate	Station				
	HB1	HB2	HB3	HB4	HB5
Temperature (°C)	7.8	7.8	8.2	8.2	8.2
Salinity (‰)	28.90	29.95	29.42	29.36	30.05
Density (σ_t)	22.55	22.82	22.90	22.85	23.40
Chlorophyll a (mg/m^3)	0.75	1.14	0.75	0.51	1.10
Particle Count (1/L)	177x10^6	219x10^6	164x10^6	163x10^6	163x10^6
$-\bar{k}$ (1/m)	0.40	0.44	0.23	0.22	0.53

TABLE II-7 (Continued)

c) continued

Interpolated Variate	Station		
	BR1	BR2	BR3
Temperature (°C)	7.4	7.9	7.7
Salinity (‰)	30.55	31.15	30.75
Density (σ_t)	23.90	24.29	24.01
Chlorophyll a (mg/m^3)	2.30	0.80	0.84
Particle Count (1/L)	175x10^6	111x10^6	240x10^6
$-\bar{k}$ (1/m)	0.39	0.22	0.34

d) 17 June 1973   Overflight: 1102 EST

Interpolated Variate	Station				
	HB1	HB2	HB3	HB4	HB5
Temperature (°C)	14.4	14.2	15.0	14.4	13.6
Salinity (‰)	28.92	29.71	29.95	30.82	31.00
Density (σ_t)	21.46	22.09	22.11	22.90	23.20
Chlorophyll a (mg/m^3)	3.11	4.08	3.58	2.15	2.60
Particle Count (1/L)	175x10^6	240x10^6	285x10^6	200x10^6	175x10^6
$-\bar{k}$ (1/m)	0.34	0.71	0.34	0.37	0.44

Interpolated Variate	Station		
	BR1	BR2	BR3
Temperature (°C)	14.0	13.9	14.0
Salinity (‰)	30.32	30.20	30.20
Density (σ_t)	22.60	22.53	22.52
Chlorophyll a (mg/m^3)	2.26	2.05	1.98
Particle Count (1/L)	197x10^6	238x10^6	250x10^6
$-\bar{k}$ (1/m)	0.24	0.30	0.43

(1/L = per liter)

TABLE II-8

Surface temperatures (°C) and salinities (‰) for Station 1 through 9 in the New York Bight

Date & Cruise	Variate	Station								
		B1	B2	B3	B4	B5	B6	B7	B8	B9
20 Dec 1972	Temperature	8.0	5.1	3.6	5.0	5.9	5.6	5.5	6.1	6.8
K7239	Salinity	31.74	23.41	18.11	23.75	27.50	26.84	27.32	29.18	31.25
25 Jan 1973	Temperature	7.0	5.3	4.3	4.9	5.4	5.8	5.6	6.3	7.0
K7302	Salinity	32.62	27.59	23.58	27.01	30.10	31.67	30.90	32.23	32.92
31 May 1973	Temperature	13.7	15.8	15.9	15.8	16.2	15.5	16.5	16.0	16.0
K7327	Salinity	29.23	23.05	19.64	23.43	24.10	23.44	23.91	25.58	29.03

TABLE II-9

Average extinction coefficients $(-\overline{k})$ in the New York Bight

Date & Cruise	Station								
	B1	B2	B3	B4	B5	B6	B7	B8	B9
20 Dec 1972 K7239	1.30	0.96	1.20	0.63	0.53	0.51	0.43	0.51	0.77
25 Jan 1973 K7302	0.92	0.71	0.98	0.85	0.69	0.48	0.63	0.59	0.75
31 May 1973 K7327	0.14	0.67	0.93	0.44	0.30	0.43	0.50	0.54	0.52
Average	0.787	0.780	1.037	0.640	0.506	0.473	0.520	0.547	0.680
Compensation Depth (m)	5.85	5.90	4.44	7.200	9.101	9.74	8.86	8.42	6.77

TABLE II-10

Average spectral extinction coefficients ($-\bar{k}[\lambda]$) in the New York Bight

Date & Cruise	Color Band	Station								
		B1	B2	B3	B4	B5	B6	B7	B8	B9
25 Jan 1973 K7302	Blue	1.33	0.98	1.41	1.10	0.96	0.82	0.76	0.79	0.85
	Green	0.79	0.62	1.04	0.70	0.65	0.56	0.55	0.51	0.64
	Red	1.35	1.00	1.17	1.10	0.99	0.86	0.88	1.01	1.18
31 May 1973 K7327	Blue	0.38	1.20	1.78	1.21	0.77	1.17	1.29	1.21	0.86
	Green	0.17	0.78	1.33	0.36	0.28	0.72	0.66	0.60	0.54
	Red	0.34	0.91	0.57	0.74	0.46	0.92	0.66	0.88	0.75
Average	Blue	0.855	1.090	1.595	1.155	0.865	0.995	1.025	1.000	0.855
	Green	0.480	0.700	1.185	0.530	0.465	0.640	0.605	0.555	0.590
	Red	0.845	0.955	0.870	0.920	0.725	0.890	0.770	0.945	0.965
Compensation Depth (m)	Blue	5.4	4.2	2.9	4.0	5.3	4.6	4.5	4.6	5.4
	Green	9.6	6.6	3.9	8.7	9.9	7.2	7.6	8.3	7.8
	Red	5.4	4.8	5.3	5.0	6.4	5.2	6.0	4.9	4.8

TABLE II-11

Correlations between salinity and stream discharge into Long Island Sound

between August 1972 and July 1973 at a 1-month lag,

together with dilution factors, D(%)

Station	Depth	Correlation Coefficient	Dilution Factor D(%)
H1	Z=0m	-0.94	7.7
H2	Z=0m	-0.95	8.5
	Z=30m	-0.29	5.1
H3	Z=0m	-0.84	5.9
	Z=30m	-0.44	3.0
H4	Z=0m	-0.79	7.5
	Z=30m	-0.38	2.1
HB1	Z=0	-0.94	7.2
HB2	Z=0	-0.96	6.5
HB3	Z=0	-0.95	8.9
	Z=30m	-0.22	2.5
HB4	Z=0m	-0.91	7.5
HB5	Z=0m	-0.85	6.9
BR1	Z=0m	-0.73	5.7
	Z=30m	-0.80	1.4
BR2	Z=0m	-0.64	3.2
	Z=30m	-0.26	2.1
BR3	Z=0m	-0.55	4.1

TABLE II-12

Linear correlation coefficients between average extinction coefficients
(visible band) and suspended particles in Block Island Sound

Transect	$-\overline{k}$ vs Total Particles	$-\overline{k}$ vs Particles >5μ
H	0.73	0.73
HB	0.58	0.79
BR	0.71	0.67

TABLE II-13

Linear correlation coefficients between average extinction coefficients
(visible band) and suspended particles in the New York Bight

| Cruise | Correlation | |
	$-\overline{k}$ vs Total Particles	$-\overline{k}$ vs Particles >5μ
K7329	0.63	0.92
K7302	0.61	0.72
K7327	0.88	0.90
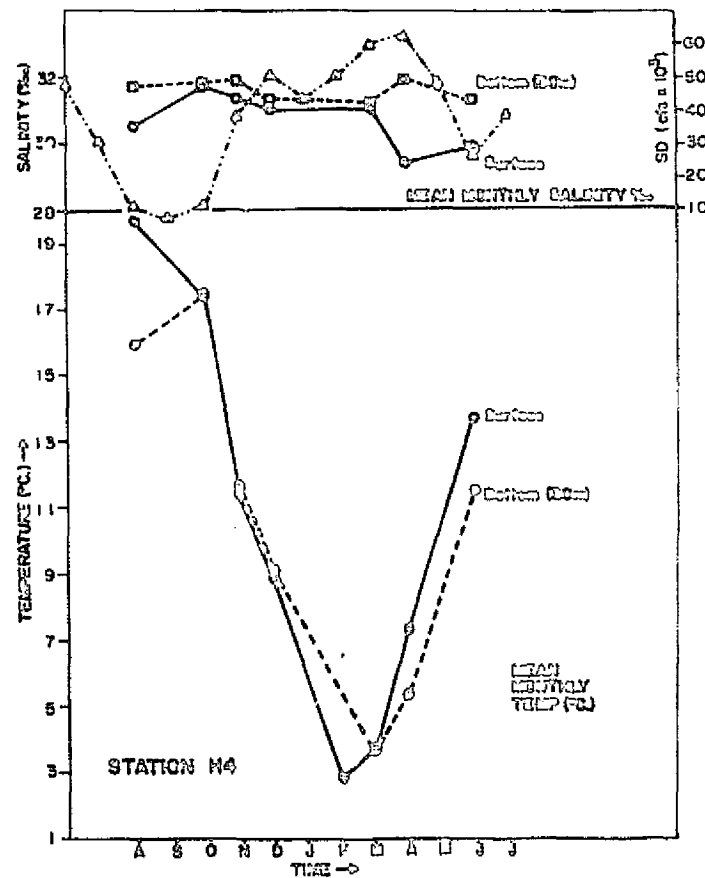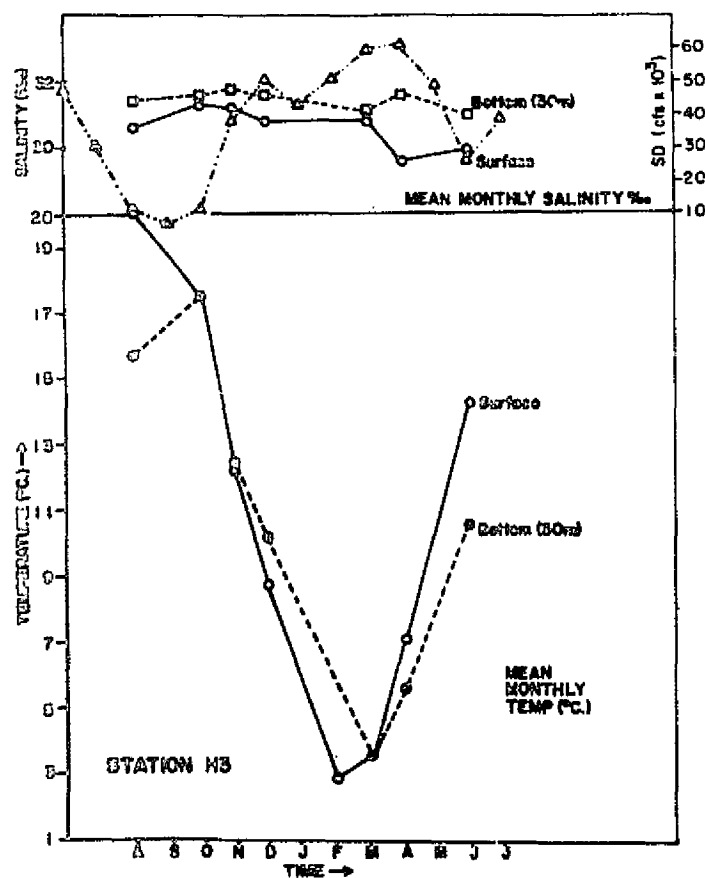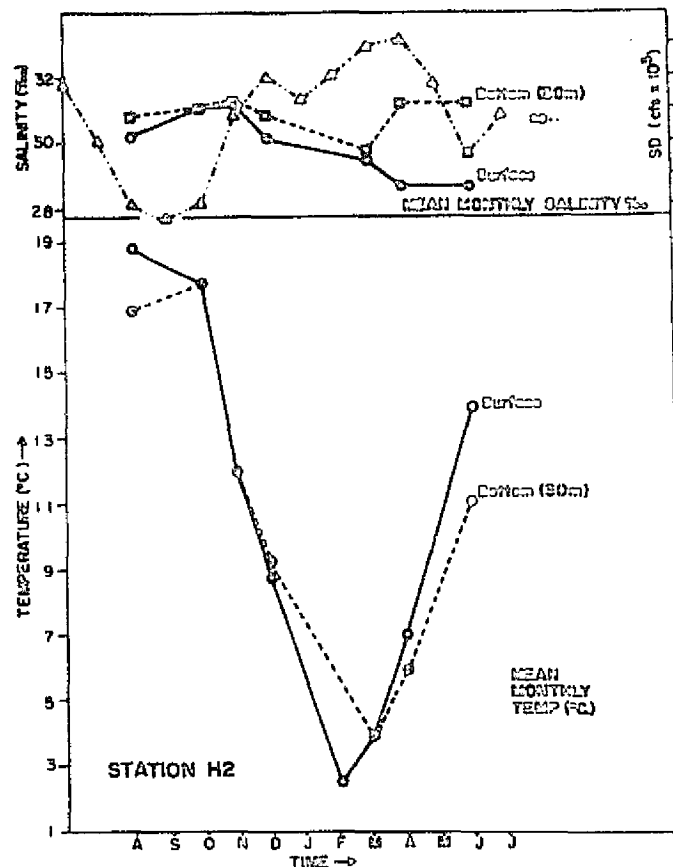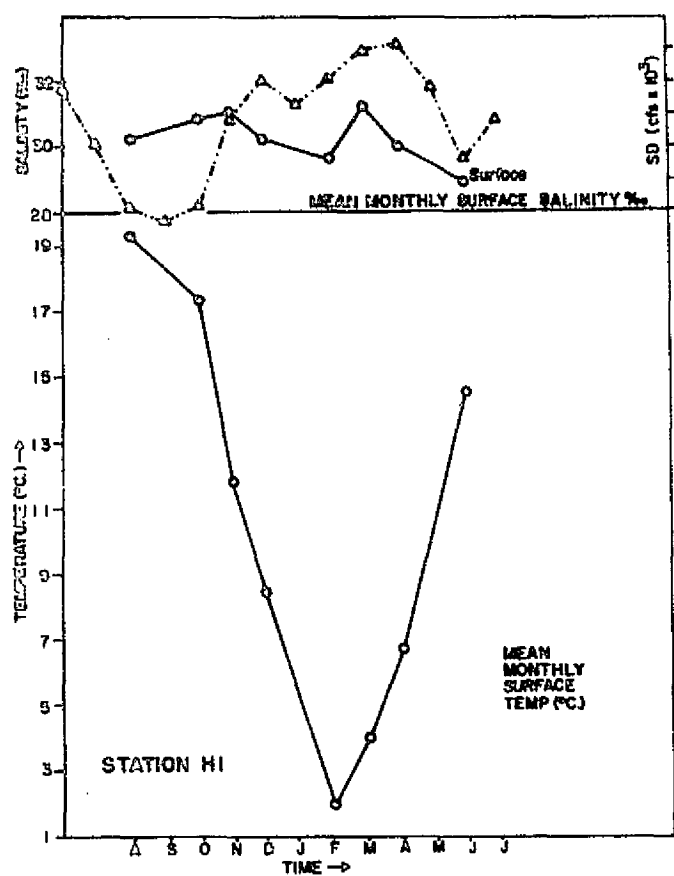
FIGURE II-1

Annual variation of mean monthly temperature, salinity, and stream discharge (SD) into Long Island
Sound for the 4 stations in the H transect
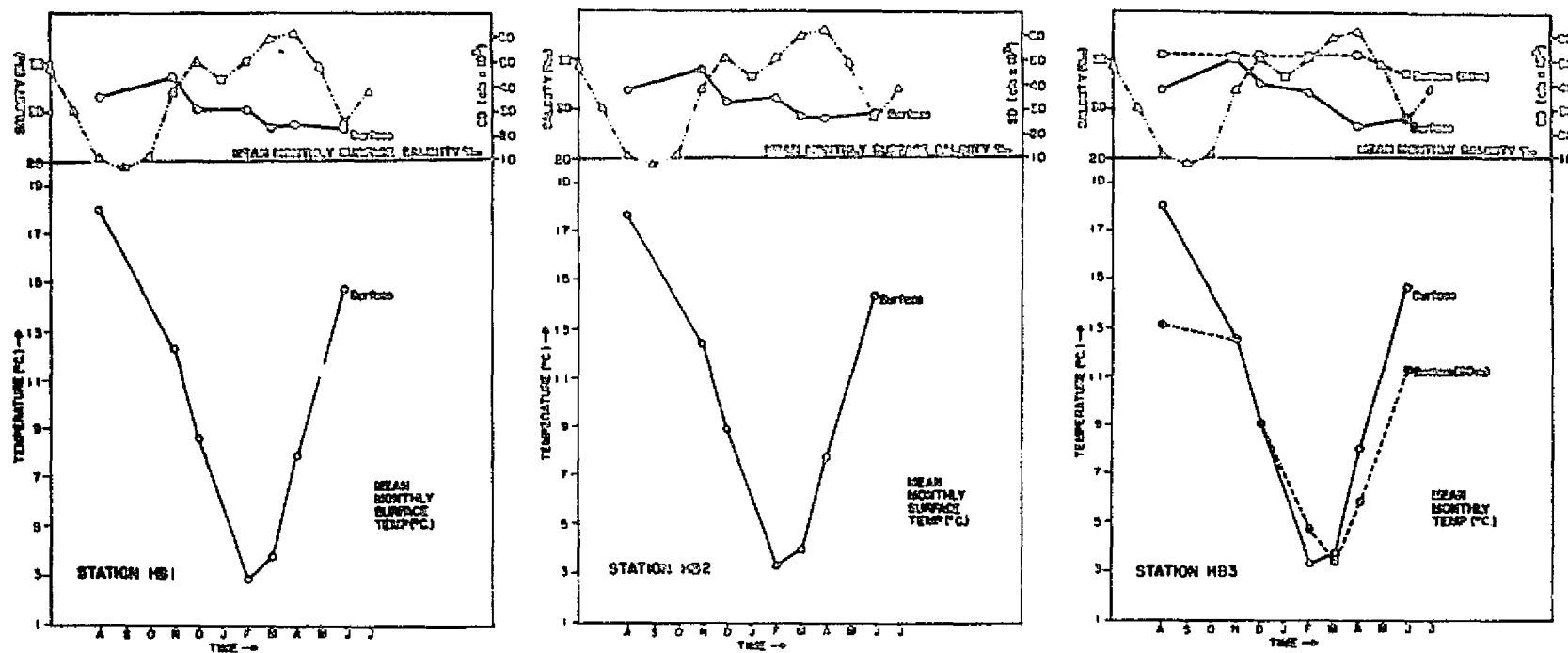
FIGURE II-2

Annual variation of mean monthly temperature, salinity, and stream discharge (SD) into Long Island Sound for the 5 stations in the HB transect
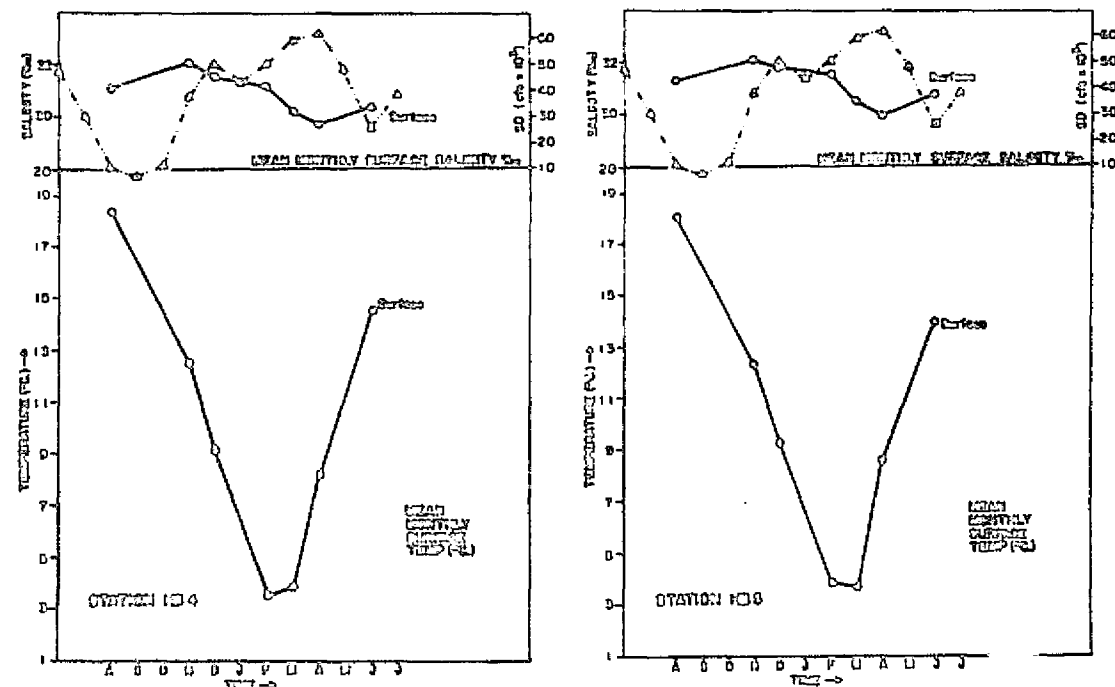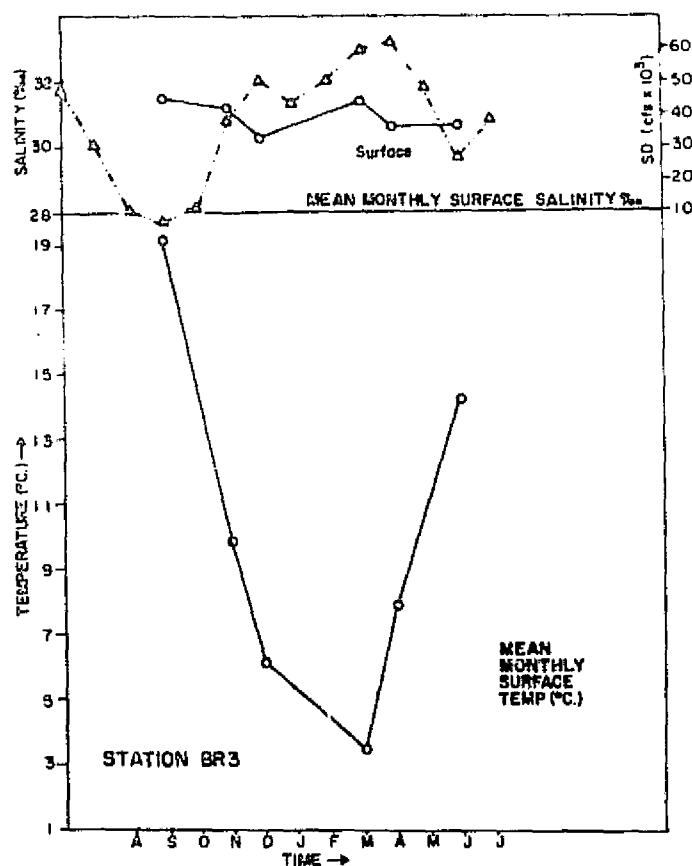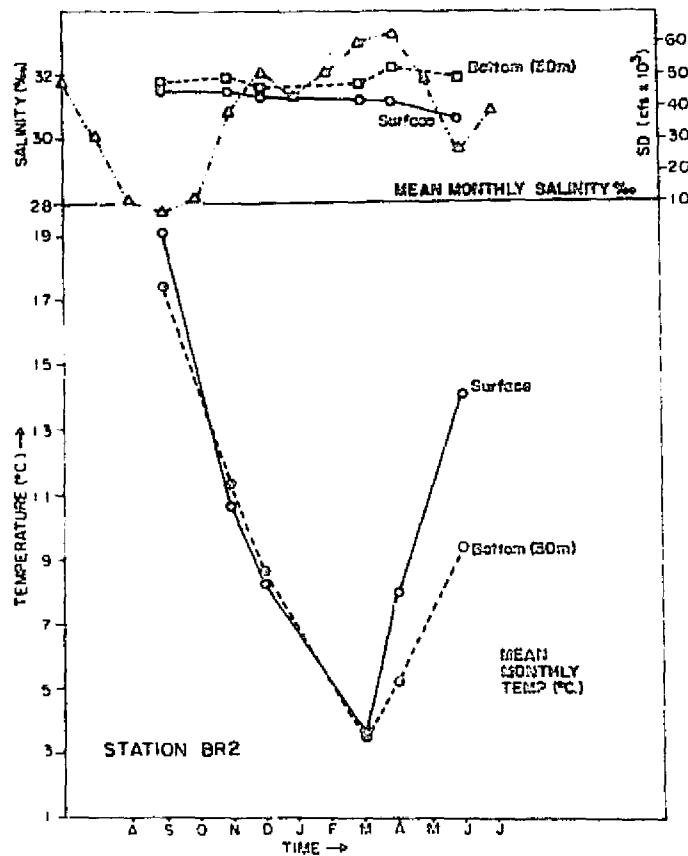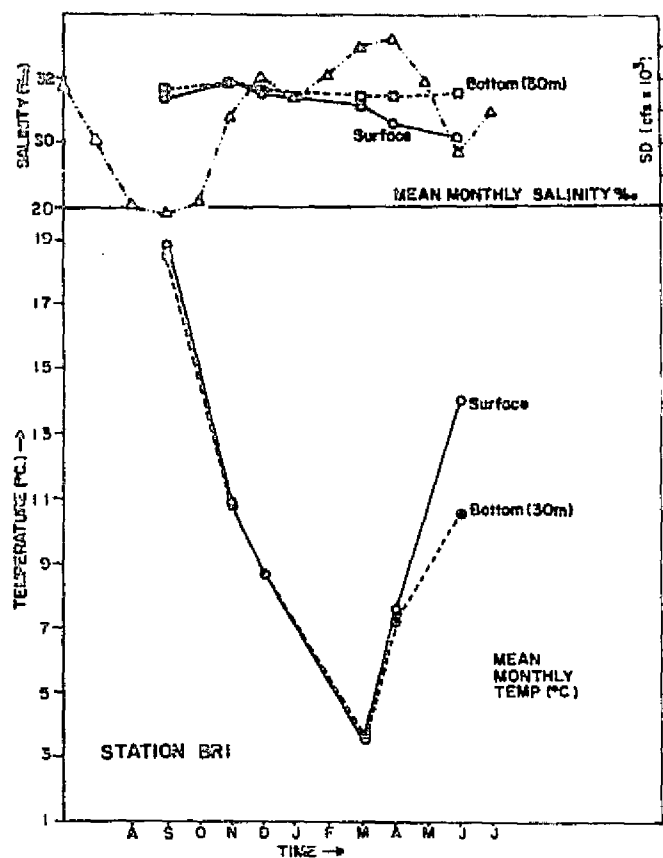
FIGURE II-3

Annual variation of mean monthly temperature, salinity, and stream discharge (SD) into Long Island Sound for the 3 stations on the BR transect
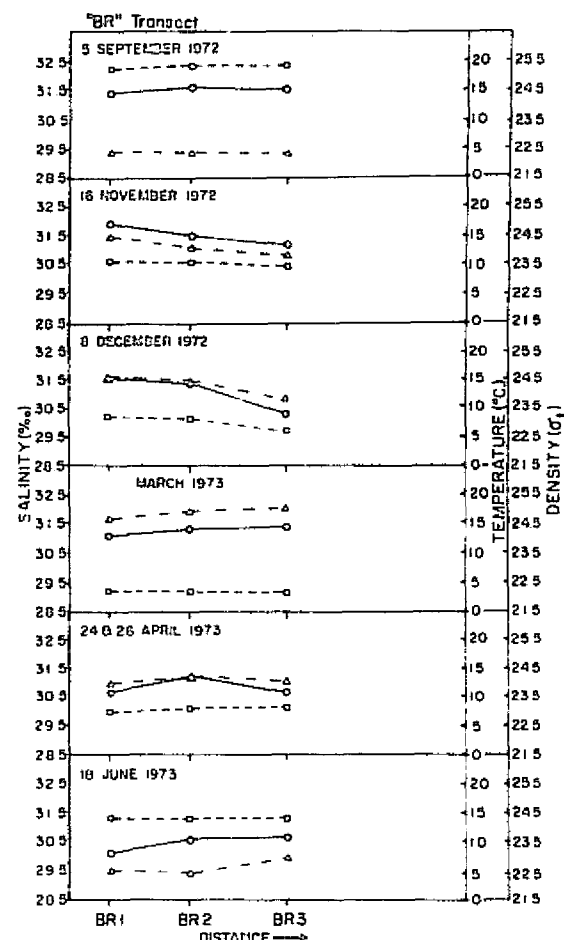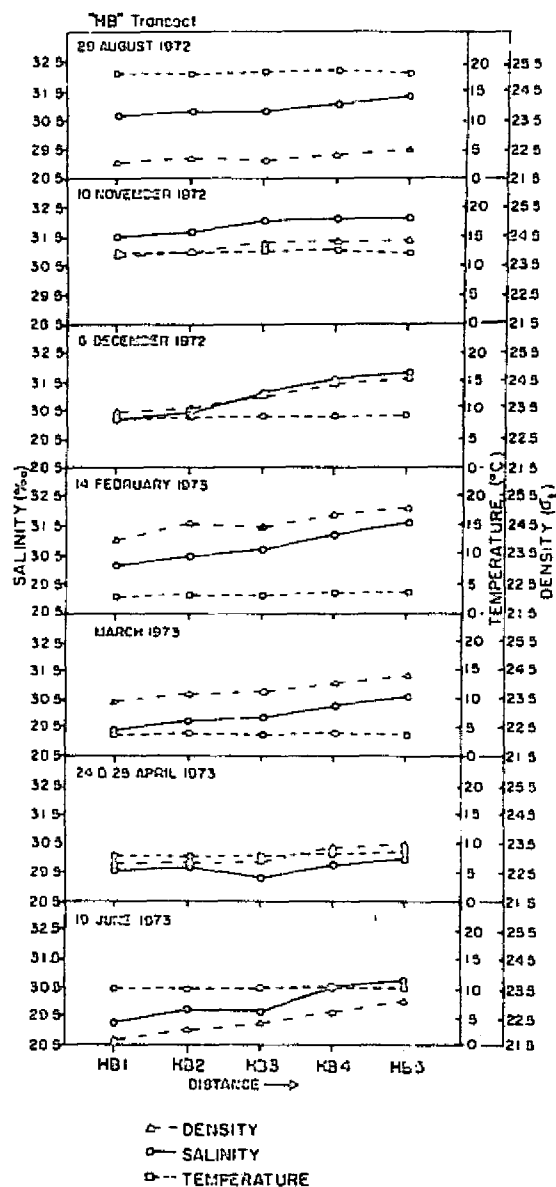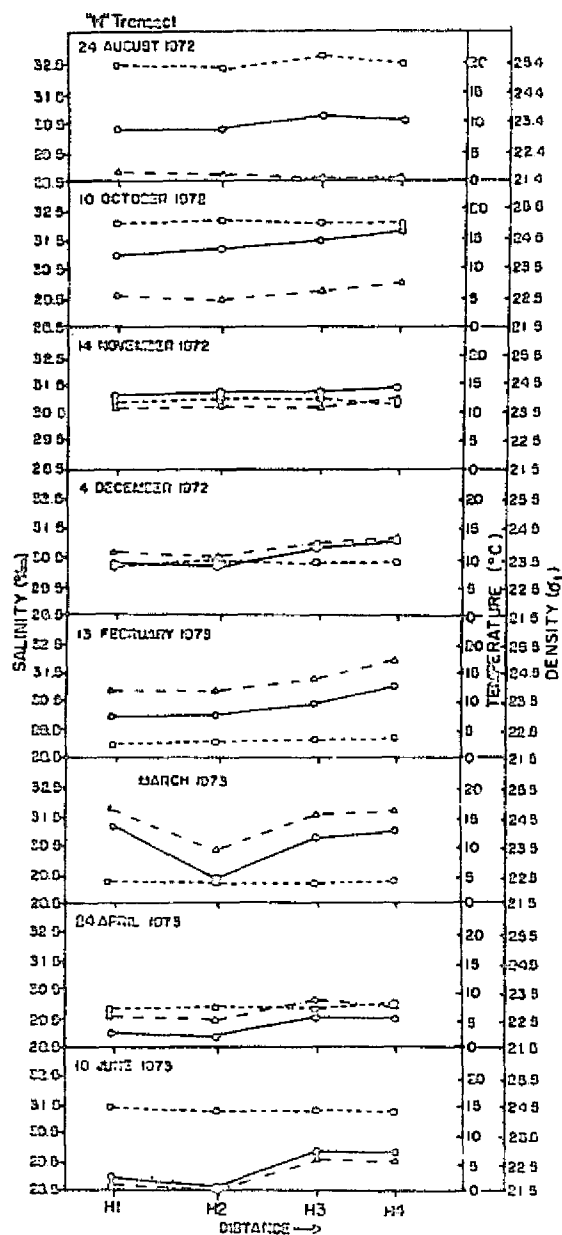
FIGURE II-4

Monthly values of the average surface temperatures,
salinities, and σ_t across each transect in Block Island Sound
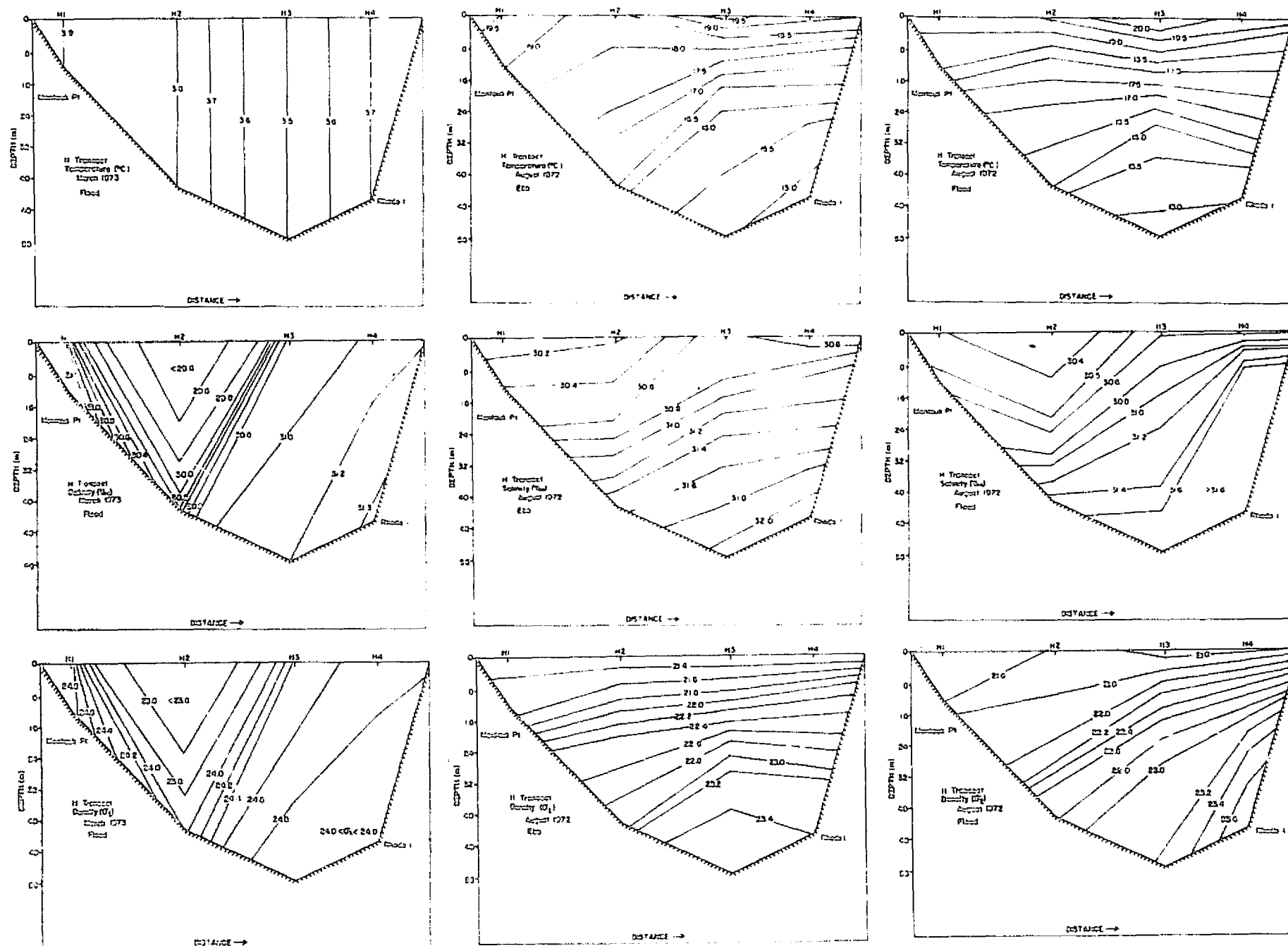
FIGURE II.5

...ral isopleths of temperature, salinity, and σ_t during the flood tidal flow on 20 March 1973 (winter conditions) and average values for ebb and flood tidal flow on 2...
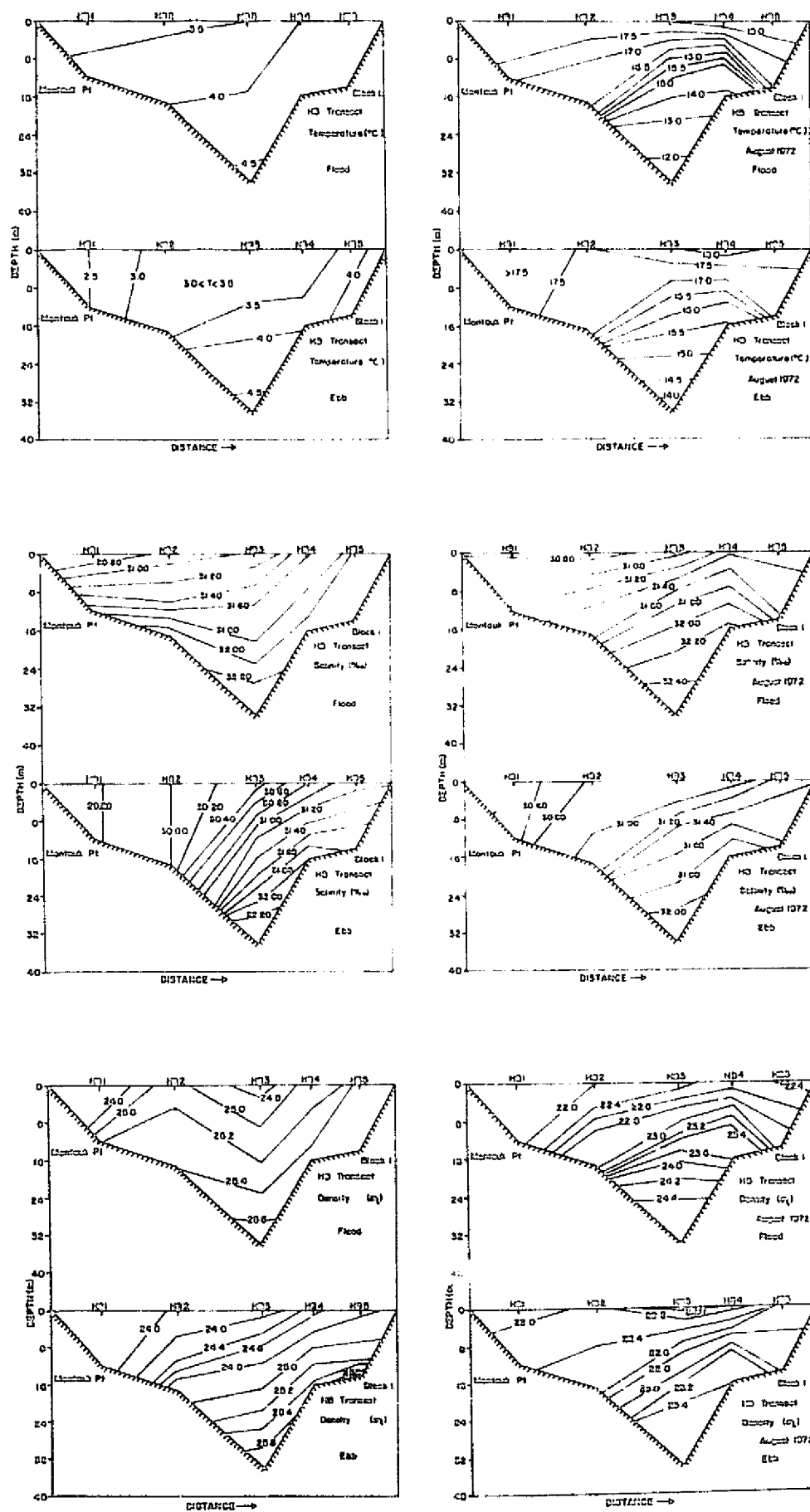
FIGURE II-6

Lateral isopleths of average temperature, salinity, and σ_t for ebb and flood tidal flows on 14 February 1973 (winter conditions) and 29 August 1972 (summer conditions)

FIGURE II-7

Lateral isopleths of average temperature, salinity, and σ_t for ebb and flood tidal flows on 21 March 1973 (winter conditions) and 5 September 1972 (summer conditions)
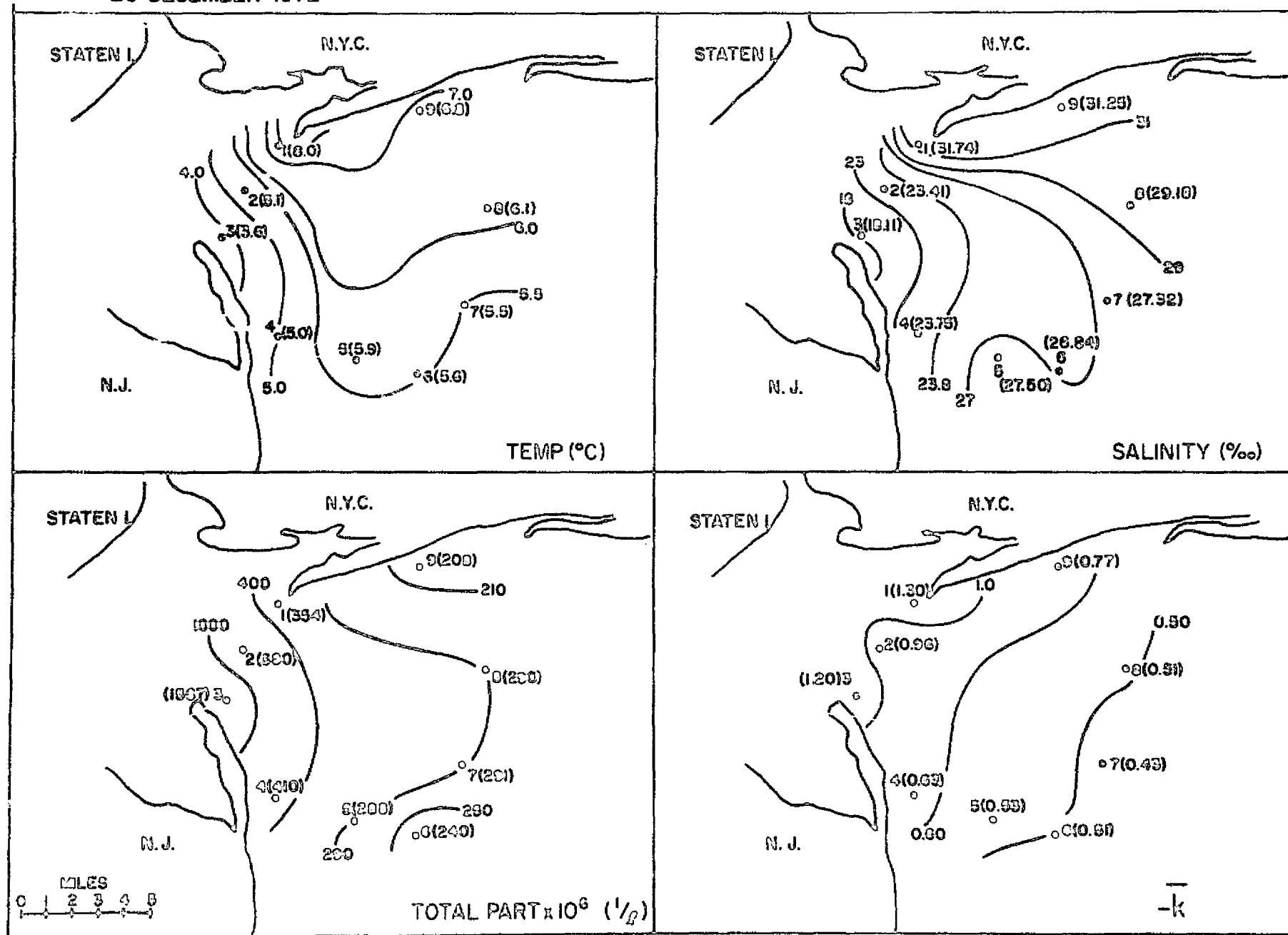
FIGURE II-8

The spatial distribution of surface temperatures, salinities, and total particulate matter and mean "extinction coefficients" for the 9 stations in the apex of the New York Bight on 20 December 1972
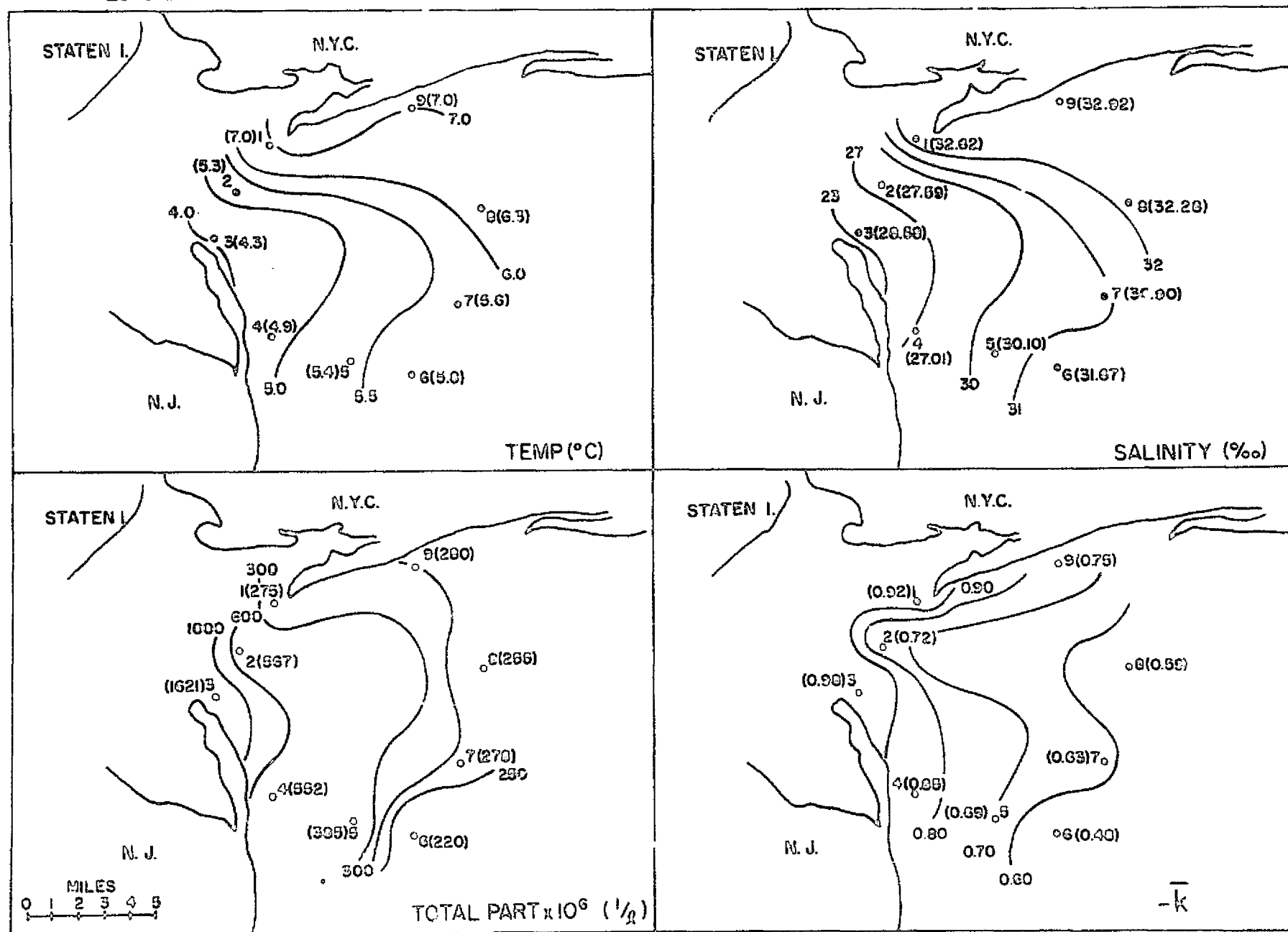
FIGURE II-9

The spatial distribution of surface temperatures, salinities, and total particulate matter and mean "extinction coefficients" for the 9 stations in the apex of the New York Bight on 25 January 1973
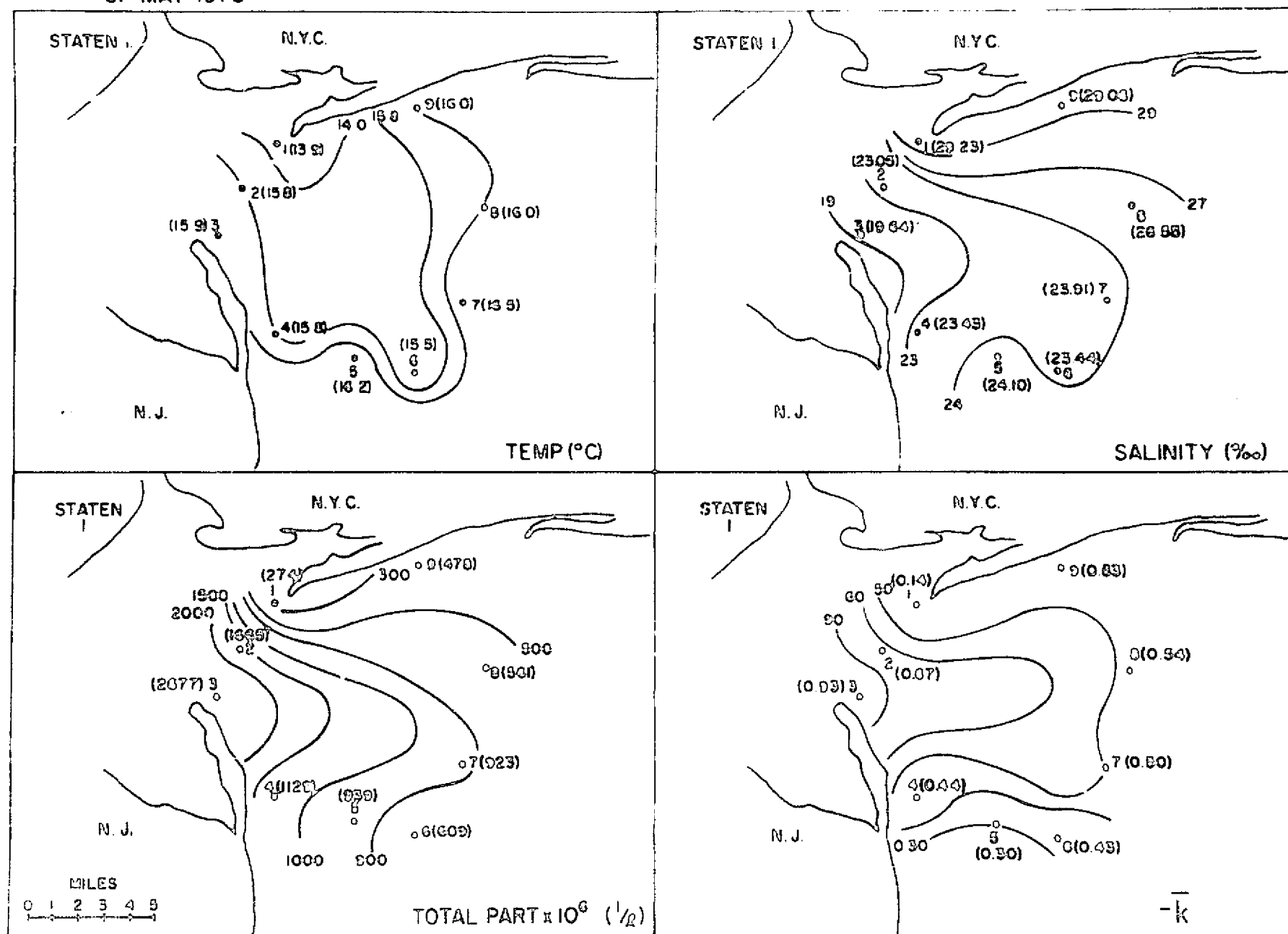
FIGURE II-10

The spatial distribution of surface temperatures, salinities, and total particulate matter and mean "extinction coefficients" for the 9 stations in the apex of the New York Bight on 31 May 1973
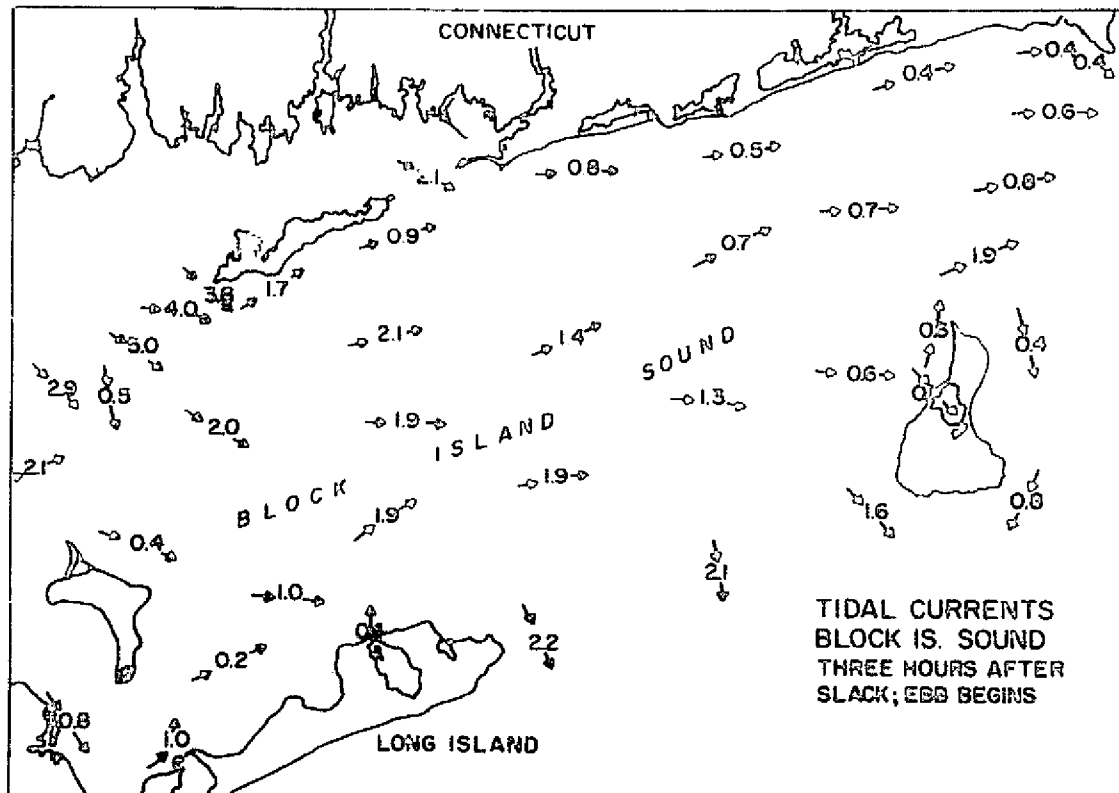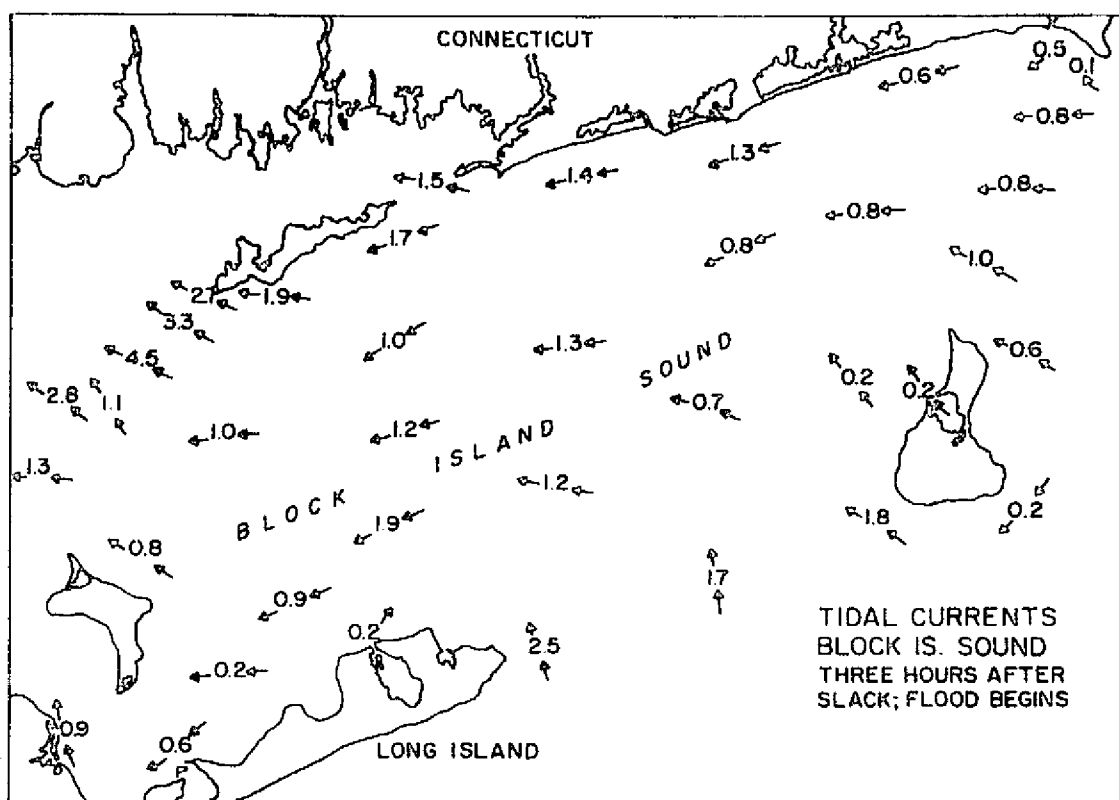
FIGURE II-11

The average flood and ebb tidal currents for Block Island Sound (taken from Tidal Current Charts, Block Island Sound and Eastern Long Island Sound, National Ocean Survey, NOAA, U.S. Dept. of Commerce, 1971)

APPENDIX B

Final Report of a SKYLAB experiment

conducted at Shagwong Reef, Montauk, N.Y.

by

R. Hollman
J.E. Alexander
&
R. Nuzzi

Presented to Long Island University

Under Prime Contract with the National

Aeronautics and Space Administration, NAS9-13308

January, 1975

New York Ocean Science Laboratory

Montauk, N.Y. 11954

TABLE OF CONTENTS

<div align="right">

<u>Page</u>

</div>

i

ACKNOWLEDGEMENTS

LIST OF FIGURES

LIST OF TABLES

Introduction

Satellite imagery has provided the oceanographer with a valuable aid in overcoming certain sampling problems in complex estuarine and coastal environments. Imagery provides a synoptic picture of features that, in many cases, would be missed by usual sampling techniques. Also, historical sampling procedures have produced data that are sometimes labeled as questionable simply because they do not fit a presumed pattern. Obvious visible phenomena such as river plumes and effluents can be seen as persistent features in ERTS-1 imagery, yet these are nearly invisible to an observer at sea level; as important, albeit not as obvious in most cases, are areas where the waters appear to have color characteristics that are different from surrounding waters. These areas generally cannot be noticed by an observer in a boat. Such "discolored" water masses may have no relationship to harbor effluents or river plumes, but are distinct water types that probably have unique origins, or causes (Castiglione, 1973).

Past experience with ERTS-1 imagery and ground truth data (for example, Hollman and Gill, 1974; Alexander and White, 1974 and Nuzzi and Perzan, 1974) from the area around Montauk Point, Long Island, New York, indicates that a very distinct and fairly persistent plume of water may be associated with Shagwong Reef some three miles northwest of Montauk Point (Figure 1). This plume is not an advected phenomenon, that is, it does not appear to be transported to the area by currents nor is it tidal since it appears in imagery taken during both flood and ebb stages of the tide. Therefore, the plume seems to be a phenomenon that is being generated in the area itself.

The fact that there are periods when the plume is not in evidence in the imagery, for example periods in late winter and early fall, leads to speculation that the plume is caused by seasonal biological phenomena. That is to say, that the plume is believed to be largely composed of organic material rather than inorganic detritus brought to the surface by the scouring action of tidal currents across the reef itself. There is no significant seasonal difference in tidal flow in this area that would account for such seasonality.

The aim of the New York Ocean Science Laboratory SKYLAB experiment was to check this hypothesis in more detail. The data obtained were used in providing ground truth for the interpretation of SKYLAB photographs taken of the area at the same time as the study.

Table 1

a) Dates and time periods of experiments

b) Station locations and depths

a)

Date	Time
9 August 1973	0830 to 1430
12 September 1973	1100 to 1600

b)

	Station Positions		Chart Depth
	North	West	
S1	41°06.2'	71°55.3'	16.5
S2	41°06.2'	71°54.9'	8

Methods

Two experiments were conducted. The first was on August 9, 1973 during a
scheduled SKYLAB overflight that was subsequently cancelled; the second
experiment was conducted September 12, 1973 during the rescheduled SKYLAB
overflight.

Each experiment involved two stations that were sampled over an ebb tidal
cycle when the flow is strongest and therefore a more pronounced plume
expected. Station S1 was located just to the west of the Shoal
(Figure 1) and Station S2 was located on the shoal approximately 550m to
the east. The respective dates and time intervals are tabulated in Table 1a,
and station locations and chart depths are to be found in Table 1b.

Station S1 was sampled at three (3) depths in the water column and
Station S2 at two (2). A current meter (General Oceanics Model 2010) was
installed at Station S2 for each sampling date.

Water samples were collected hourly for analysis of salinity, reactive,
total, dissolved, and particulate phosphorous, pigments, suspended solids,
total particles, and phytoplankton. Temperature was measured *in situ* with
a bathythermograph (checked by a mercurial thermometer at the surface) at
Station S1. At Station S2, temperatures were obtained with a Beckman Model
RS5 portable meter.

The salinity of the samples was determined with an induction salinometer
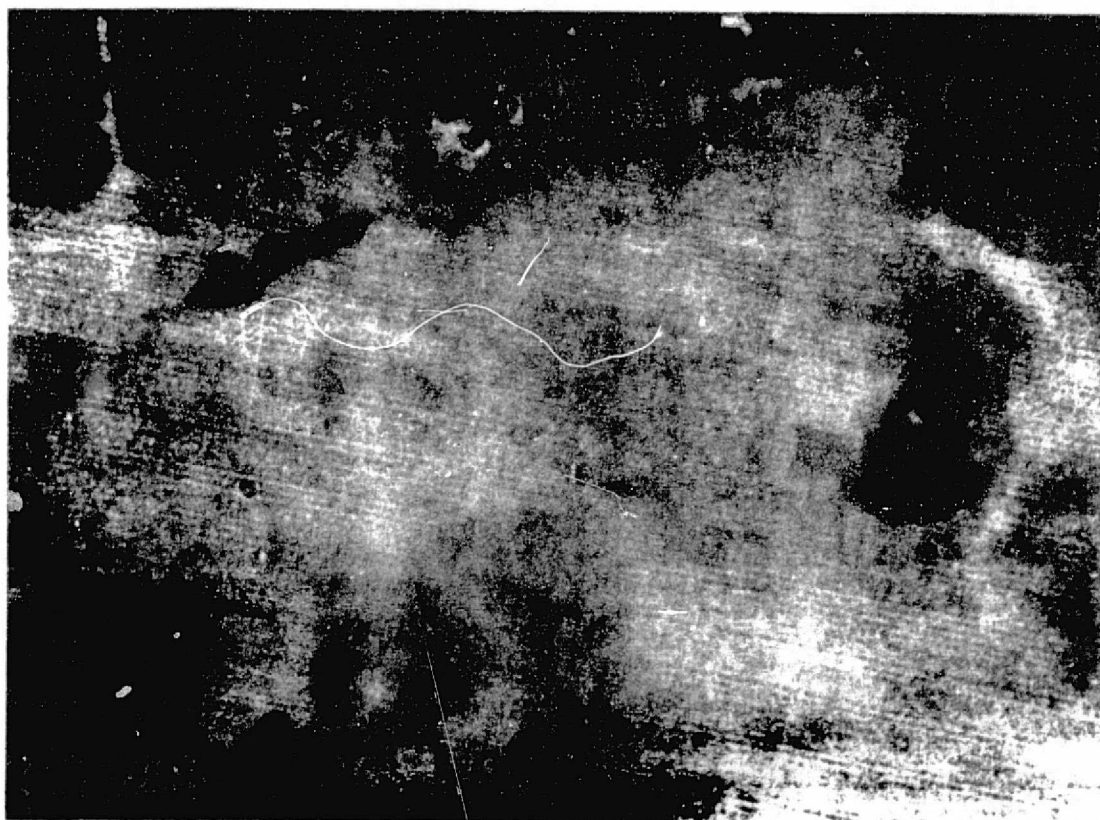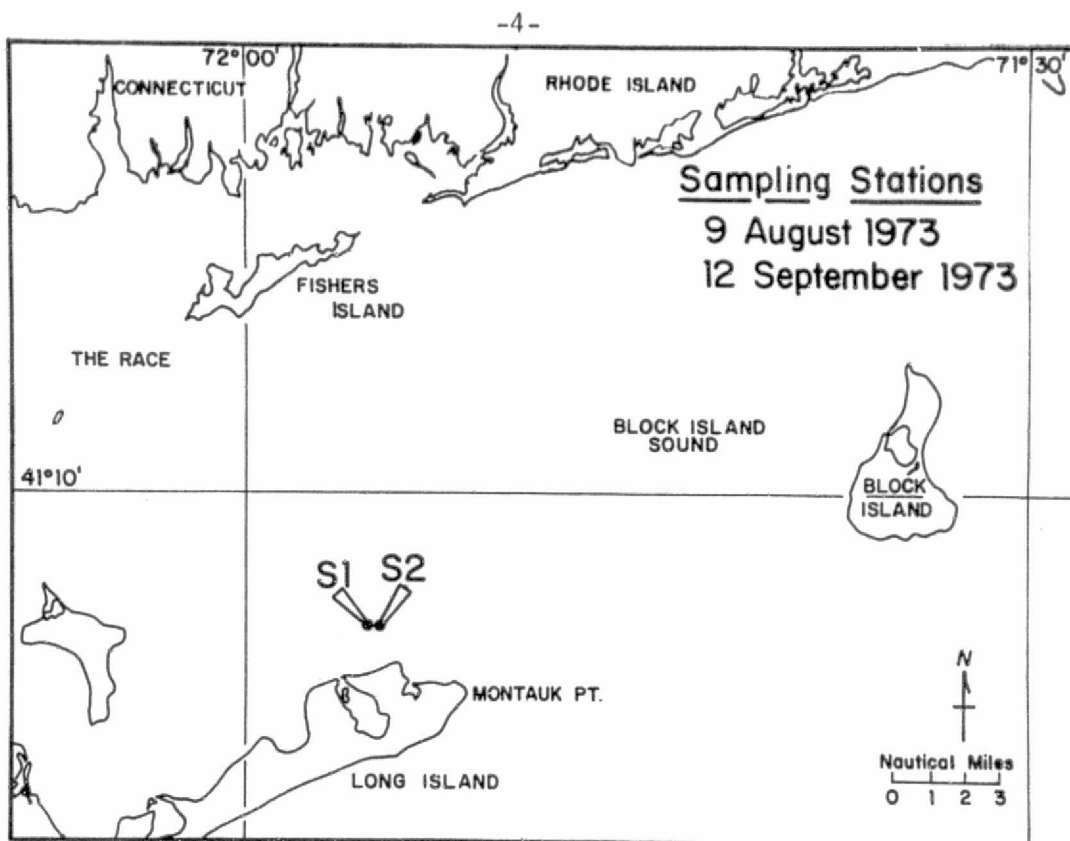
FIGURE 1. Map of Block Island Sound and ERTS-1 Image

(Beckman RS-7B). The various forms of phosphorous and the pigments were determined according to the methods described in Strickland and Parsons (1968) while suspended solids were determined according to the American Public Health Association (1971) methods.

The phytoplankton in one liter of sea water, collected in a 5ℓ Niskin bottle, were concentrated with a continuous plankton centrifuge and the cells within an aliquot of the concentrate were counted microscopically. An unconcentrated 50 mℓ sample of water was returned to the laboratory and a particle analysis performed with a Coulter Counter, Model B. The samples for particle analysis were refrigerated until the analysis was performed which never exceeded 2 hours after collection. Detailed methods for both phytoplankton and particle analysis were given by Nuzzi and Perzan (1974).

The attenuation of incident daylight as a function of depth within the water column (downwelling irradiance) was measured close to local noon at each station using an upward facing irradiance meter comprising a photocell and cosine collector. The "extinction coefficient", k, for these light values is defined by the equation:

$$I(z) = I(z=0) \exp(-k\, z)$$

where $I(z=0)$ is the total visible light energy incident upon the naviface and $I(z)$ is the remaining light energy at the depth z (in meters).

Results

Temperatures, salinities and densities (σ_t) for the August sampling period are tabulated in Tables 2 and 3 for the September sampling period. As can readily be determined from the tables, variations in time as well as space are small. The maximum variations occur at the surface during the August experiment and are 0.7°C and 0.18°/oo at Station S1, and 0.8°C and 0.66°/oo at S2.

The percent of incident light transmitted through the water column and the average extinction coefficient are tabulated in Table 4 for both experiments. The difference in water clarity (high transmittance) is most apparent between Station S1 and S2 during August, particularly at the 1% level of transmittance. During September, however, the differences are less pronounced and reversed with Station S2 being less turbid (clearer).

The current meter results are shown in Figure 2 where the velocity vector has been averaged over a 15 minute interval and reduced to its north/south (v) and east/west (u) components. These components are taken such that u is positive for easterly flows and v is positive for northerly flows. Speeds were slightly higher (approximately 10 cm/sec) in September than in August. Average speeds, and directions for the sampling period, are tabulated in Table 5. The average speed was also higher in September (10.7 cm/sec) as are the u and v components, however, the directions are nearly the same. These differences relate to the phases of the moon: on August 9th, the moon was in apogee, furthest south of the Equator and midway between spring and neap; on September 12th, the moon was full (spring tides prevailed) and the moon was on the Equator, so that in comparison, the tidal currents should be greater.
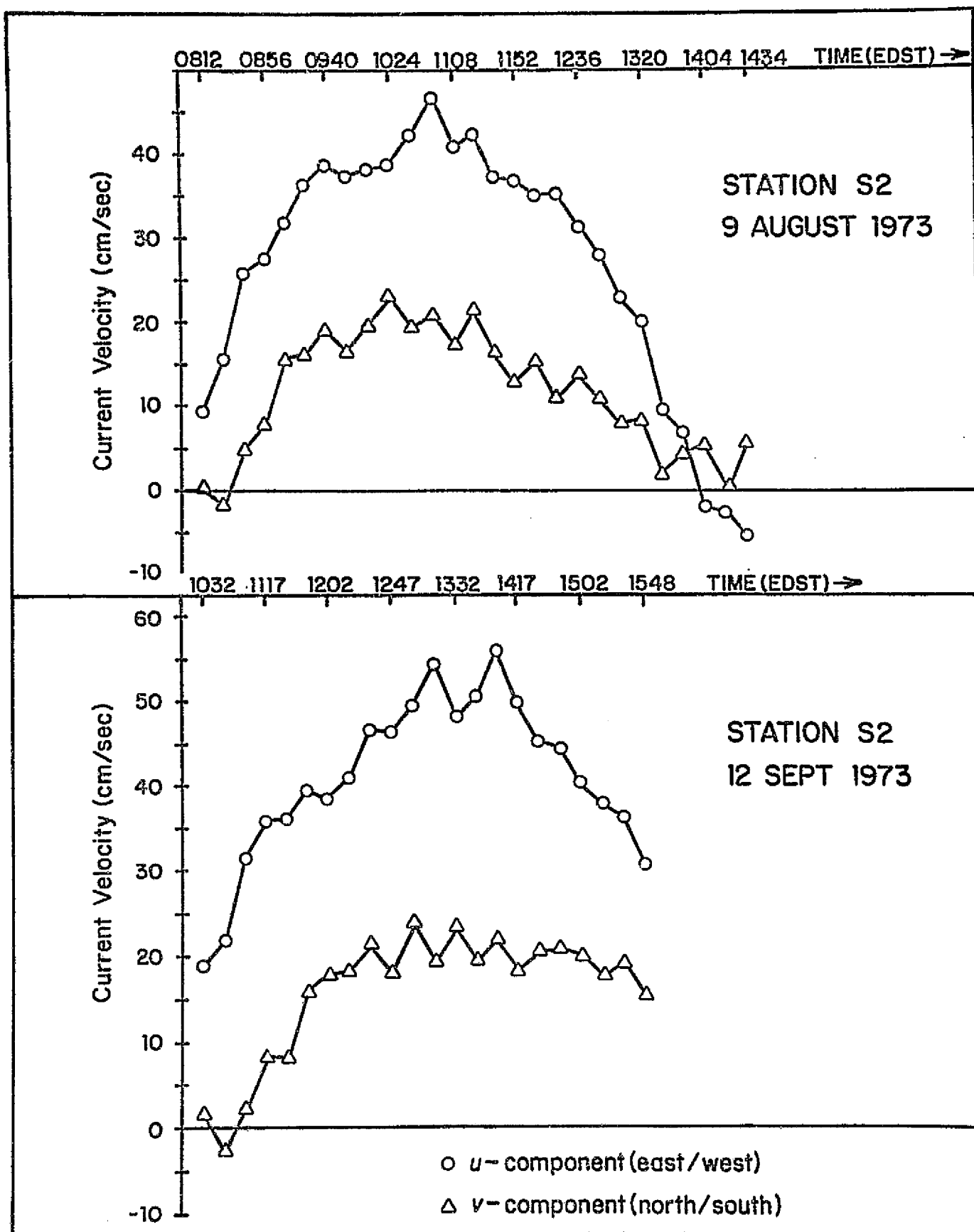
FIGURE 2. Current Meter Data

Table 2. Temperatures, salinities, and σ_t for the August 9th, 1973 experiment

		Station S1					Station S2		
Time	Depth(m)	T°C	S°/oo	σ_t	Time	Depth(m)	T°C	S°/oo	σ_t
0829	0	20.2	29.05	20.21	0830	0	20.1	29.11	20.28
	8	20.1	29.04	20.23		8	19.5	29.16	20.47
	16	20.0	29.04*	20.23					
0930	0	20.6	29.00	20.07	0926	0	20.2	28.94	20.13
	8	20.5	29.08	20.11		8	20.0	29.09	20.29
	16	20.3	29.20*	20.35					
1030	0	20.5	28.87	19.99	1022	0	19.8	28.45	19.87
	8	20.1	28.95	20.16		8	19.6	29.03	20.35
	16	19.7	28.95*	20.30					
1130	0	20.5	28.88	20.01	1125	0	19.9	28.56	19.92
	8	20.1	29.01	20.20		8	19.4	29.03	20.40
	16	19.7	29.20*	20.45					
1230	0	20.7	28.88	20.00	1226	0	20.1	28.86	20.09
	8	20.1	29.03	20.24		8	19.3	28.98	20.38
	16	19.4	29.24*	20.60					
1330	0	20.2	28.96	20.14	1327	0	20.6	28.92	20.01
	8	19.7	29.11	20.29		8	19.3	29.10	20.48
	16	19.3	29.50*	20.40					
1430	0	20.0	29.01	20.22	1420	0	20.3	28.88	20.06
	8	19.7	29.04	20.30		8	19.6	29.00	20.33
	16	19.3	29.16*	20.50					

*Extrapolated

Table 3. Temperatures, salinities, and σ_t for the September 12, 1973 experiment

		Station S1					Station S2		
Time	Depth(m)	T°C	S°/₀₀	σ_t	Time	Depth(m)	T°C	S°/₀₀	σ_t
1100	0	20.0	29.80	20.83	1106	0	19.8	29.83	20.90
	5	19.8	29.84	20.90		7	19.9	30.08	21.07
	10	19.5	30.01*	21.05					
1202	0	20.1	29.79	20.80	1207	0	19.8	29.83	20.90
	5	19.8	29.80	20.85		7	19.8	29.87	20.94
	10	19.6	29.87*	20.95					
1300	0	20.1	29.79	20.80	1255	0	19.8	29.83	20.90
	5	19.9	29.80	20.85		7	19.8	29.86	20.93
	10	19.8	29.84*	20.90					
1400	0	20.0	29.82	20.85	1400	0	19.8	29.85	20.94
	5	19.8	29.86	20.89		7	19.8	29.88	20.94
	10	19.7	29.92*	20.99					
1500	0	20.2	29.83	20.80	1445	0	19.8	29.87	20.92
	5	20.0	29.86	20.85		7	19.8	29.88	20.94
	10	19.8	29.94*	20.99					
1600	0	20.2	29.81	20.79	1555	0	19.8	29.85	20.92
	5	20.0	29.84	20.82		7	19.8	29.88	20.94
	10	19.9	29.87*	20.90					

*Extrapolated

Table 4. The depth in meters of the percent of incident light trans-
mitted through the water column and the average "extinction"
coefficient, k, for (a) 9 August experiment, and (b) 12
September experiment.

(a)   9 August 1973 (10/10 High Cloud Cover)

Percent	Station S1 1200 hrs.	Station S2 1125 hrs.
75%	0.3m	0.4m
50%	0.8m	0.8m
25%	2.3m	1.7m
10%	4.8m	2.7m
1%	10.4m	5.3m
$\bar{k}$	0.57 per meter	0.84 per meter

(b)   12 September 1973 (2/10 Cloud Cover)

Percent	Station S1 1215 hrs.	Station S2 1255 hrs.
75%	0.6m	1.3m
50%	2.0m	2.6m
25%	4.6m	5.0m
10%	8.3m	-*-
1%	-*-	-*-
$\bar{k}$	0.33 per meter	0.26 per meter

*Below the bottom

Table 5.   Average current meter results

Averages	9 August 1973	12 September 1973
Speed	33.1 cm/sec	43.8 cm/sec
Direction	67°True	69°True
u-component	30.6 cm/sec	41.0 cm/sec
v- component	12.6 cm/sec	15.6 cm/sec

Suspended solids, chlorophyll a, and reactive, dissolved organic and particulate phosphorous concentrations are tabulated in Tables 6 and 7 for the August and September sampling periods respectively.

No significant differences were found when the data collected at S-2 were compared to that at S-1. This would indicate that the source of the satellite observed materials is not due to scouring at S-1 as might be suspected. The lack of statistical difference between the two stations is explainable by accepting that Station S-1 was also located within the boundaries of the observed materials.

In both of these experiments the bottom samples at Station S-2 were collected in close proximity to the current meter. Although the short duration of each experiment prohibited extensive statistical testing, preliminary tests do indicate that lag correlations were more meaningful than direct correlations between suspended solids, particulate phosphorous, chlorophyll a and velocity.

Table 6. Variations in Suspended Solids, Phosphorous and Chlorophyll a, 9 August, 1973.

		Station S-1							Station S-2				
Time	Depth (m)	Suspended Solids (mg/ℓ)	R-PO$_4$ (μg-at/ℓ)	T-PO$_4$ (μg-at/ℓ)	P-PO$_4$ (μg-at/ℓ)	Chl a (μg/ℓ)	Time	Depth (m)	Suspended Solids (mg/ℓ)	R-PO$_4$ (μg-at/ℓ)	T-PO$_4$ (μg-at/ℓ)	P-PO$_4$ (μg-at/ℓ)	Chl a (μg/ℓ)
0829	0	2.15		1.69	2.13	1.83	0830	0	2.55		1.15	1.24	1.14
	8	2.05		1.20	1.83	1.61		8	-		-	-	-
	16	2.50		1.20	1.63	2.18							
0930	0	2.55		0.98	0.62	2.17	0926	0	2.11		2.40	2.08	1.53
	8	2.25		0.93	1.80	3.02		8	2.05		1.15	1.31	1.88
	16	2.43		1.15	1.63	2.61							
1030	0	2.45		1.04	1.07	3.81	1022	0	2.69		1.04	2.38	1.99
	8	1.10		0.93	2.08	3.26		8	6.40		2.38	2.98	4.86
	16	2.40	N	1.04	1.61	2.97				N			
1130	0	2.55	E	1.26	1.42	2.13	1125	0	5.17	E	1.04	1.49	2.52
	8	2.80	K	0.98	1.47	3.23		8	2.95	K	0.87	1.64	3.27
	16	2.75	A	0.98	2.04	3.68				A			
1230	0	2.50	T	0.98	1.61	2.79	1226	0	2.45	T	1.26	2.12	0.98
	8	2.55		0.71	2.17	4.12		8	1.47		1.15	1.76	3.01
	16	3.07		1.26	1.82	1.99							
1330	0	2.90		0.93	1.69	3.25	1327	0	4.45		1.47	2.01	1.35
	8	2.35	T	1.53	1.86	3.89		8	2.08	T	1.25	1.97	2.35
	16	3.23	O	1.09	1.64	3.24				O			
1430	0	1.80	N	2.56	-	2.15	1420	0	1.45	N	1.25	2.09	3.02
	8	1.67		1.26	-	3.64		8	1.59		1.15	1.41	3.07
	16	1.95		1.15	1.72	3.77							

(R-PO$_4$ columns: "NOT TAKEN")

Table 7. Variations in Suspended Solids, Phosphorous and Chlorophyll a, 12 Sept., 1973

	Station S-1							Station S-2					
Time	Depth (m)	Suspended Solids (mg/ℓ)	R-PO_4 (μg-at/ℓ)	T-PO_4 (μg-at/ℓ)	P-PO_4 (μg-at/ℓ)	Chl a (μg/ℓ)	Time	Depth (m)	Suspended Solids (mg/ℓ)	R-PO_4 (μg-at/ℓ)	T-PO_4 (μg-at/ℓ)	P-PO_4 (μg-at/ℓ)	Chl a (μg/ℓ)
1100	0	3.20	1.04	1.26	1.06	1.69	1106	0	6.06	1.09	1.81	0.87	3.21
	5	2.34	1.04	1.43	1.27	1.99		7	1.86	1.24	1.87	0.86	1.54
	10	2.21	1.08	1.59	0.89	1.58							
1202	0	2.54	1.01	1.21	1.15	2.35	1207	0	13.64	1.04	1.54	1.51	1.05
	5	2.58	0.99	1.37	1.64	0.75		7	1.92	1.05	1.43	1.27	1.76
	10	1.27	1.03	1.37	1.30	0.95							
1300	0	1.85	1.02	1.76	1.78	2.65	1255	0	3.12	1.06	1.37	1.45	2.52
	5	1.58	1.03	2.31	1.78	2.97		7	2.77	1.09	1.37	1.45	2.43
	10	3.78	1.00	1.32	1.63	2.46							
1400	0	3.91	1.06	1.32	1.45	2.74	1400	0	1.70	1.01	1.26	1.65	2.63
	5	2.70	1.04	1.43	1.54	2.79		7	2.37	1.02	1.32	1.56	1.58
	10	2.93	1.07	1.48	1.40	2.41							
1500	0	2.08	0.98	1.32	1.13	0.66	1445	0	4.85	0.97	1.15	1.18	1.90
	5	7.74	0.96	1.32	1.44	2.60		7	6.43	1.06	1.70	1.34	2.40
	10	2.25	0.99	2.47	1.30	2.50							
1600	0	3.85	0.94	1.43	1.02	2.15	1555	0	1.56	0.94	1.59	1.50	2.35
	5	2.13	0.94	1.26	1.40	2.36		7	1.29	0.97	1.26	1.43	2.34
	10	1.64	1.00	1.98	1.42	2.25							

Table 8 . Distribution of particles and phytoplankton, 9 August 1973

Time (EDST)	S1 – Surface			S1 – Bottom			S2 – Surface			S2 – Bottom		
	Total Particles per liter x 10^6	Particles >10.67μ per liter x 10^3	Cells per liter x 10^3	Total Particles per liter x 10^6	Particles >10.67μ per liter x 10^3	Cells per liter x 10^3	Total Particles per liter x 106	Particles >10.67μ x 10^3	Cells per liter x 10^3	Total Particles per liter x 10^6	Particles >10.67μ per liter x 10^3	Cells per liter x 10^3
0830	163	668	186			309	185	559	76			486
0930	168	972	223			227	133	856	410			170
1030	217	1128	313	145	812	222	131	870	654	336	1390	180
1130			256			583		680	390		905	119
1230		756	275			270			289		778	376
1330			271			428			274			329
1430		703	518			313		803	420		429	360
Av. of all sampling periods	183	845	293	145	812	336	150	754	359	336	876	289

-14-

Table 9 . Distribution of particles and Phytoplankton, 12 September 1973

Time (EDST)	S1 - Surface			S1 - (3.5-4m)			S1 - (7-8m)			S2 - Surface			S2 - (8m)		
	Total Particles per liter x 10^6	Particles >10.67µ per liter x 10^3	Cells per liter x 10^3	Total Particles per liter x 10^6	Particles >10.67µ per liter x 10^3	Cells per liter x 10^3	Total Particles per liter x 10^6	Particles >10.67µ per liter x 10^3	Cells per liter x 10^3	Total Particles per liter x 10^6	Particles >10.67µ per liter x 10^3	Cells per liter x 10^3	Total Particles per liter x 10^6	Particles >10.67µ per liter x 10^3	Cells per liter x 10^3
1100	215	238	14.2	249	193	7.6	218	189	7.6	140	208	8.6	176	236	3.8
1200			6.7			3.8			14.3			8.6			4.8
1300	185	202	10.5	190	247	14.3	207	148	6.7	206	275	5.7	203	263	15.2
1400			5.7			8.6			9.5			9.5			4.8
1500	158	175	12.4	194	149	12.4	299	148	20.9	204	183	4.8	201	181	9.5
1600			4.8			13.3			9.5			4.8			5.7
Average of all sampling periods	186	205	9.1	211	196	10.0	241	162	11.4	183	222	7.0	193	227	7.3

Table 10. Particle and Phytoplankton Concentrations - Averages of
all samples for each date.

	9 August 1973	12 September 1973
Total particles per liter	185×10^6	203×10^6
Particles >10.67μ per liter	821×10^3	202×10^3
Cells per liter	319×10^3	9×10^3

The results of the phytoplankton and particles analysis from the samplings of
9 August and 12 September are presented in Tables 8 and 9. The Coulter Counter
results for 9 August are not complete due to equipment malfunction. The
average particle and phytoplankton concentration for each date is given
in Table 10.
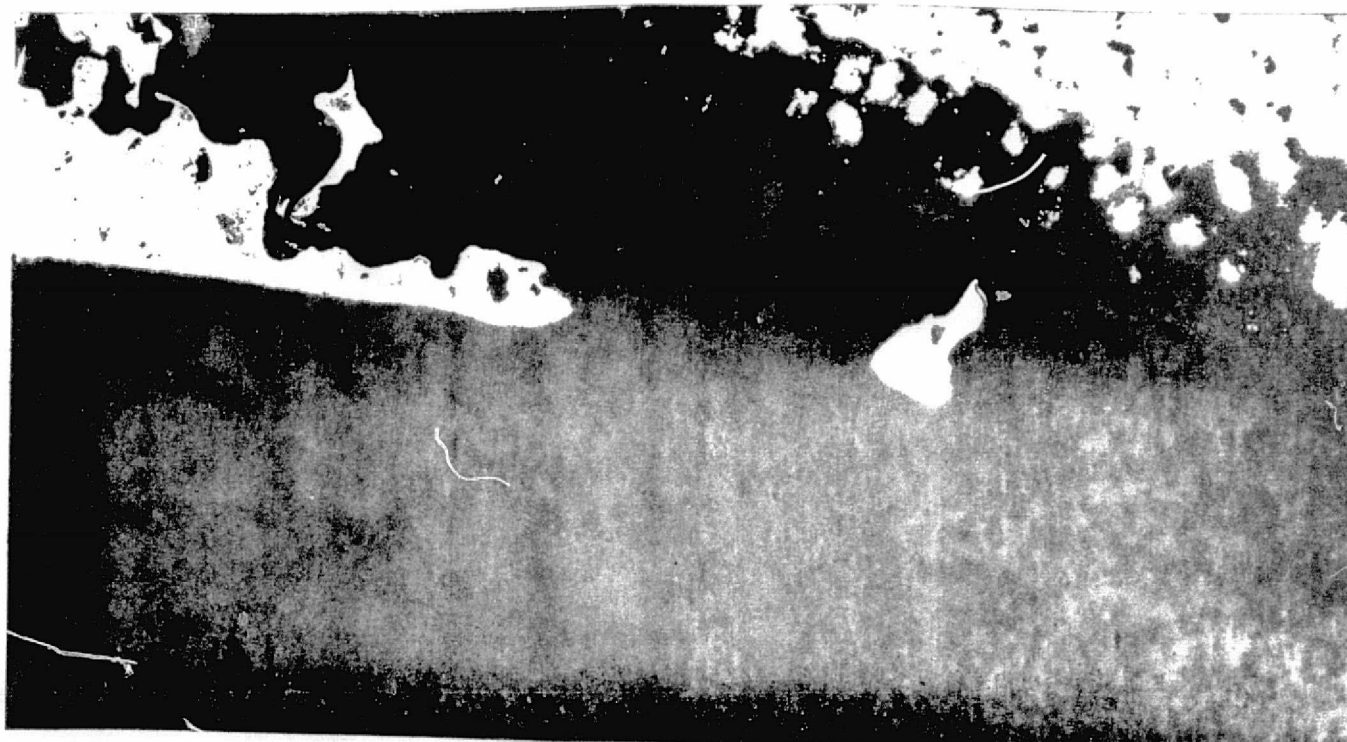
Figure 3. Copy of SKYLAB image from band 4, on 12 Sept.

Discussion

If the plume generally observed in the area of Shagwong Reef (Fig. 1)
was in fact due to scour from tidal currents, then it should have been
a lot more pronounced in the SKYLAB photos. Tidal currents were greater
(by approximately 25%) during the September study in comparison to the
flow during the August study. However, as can be seen in Figure 3, a
very poorly defined plume appears in the area, and its position relative
to the Shagwong test site is questionable. That is to say that the test
site (Stations S1 and S2) may be just west of this weakly turbid water.
More pronounced plumes or turbid water masses can be seen to the west of
the Shagwong test area thus indicating that the particular photos were
capable of detecting such phenomena. In comparison, the ERTS-1 imagery
shown in Figure 1 (taken on October 5, 1972) was taken at near slack
tide (ebb begins), yet there is a very pronounced and strongly turbid
plume. Similar plumes were also outstanding in the March and May imagery
during 1973, coinciding with high total phytoplankton counts for that
period (Nuzzi, unpublished data).

The stations at the Shagwong Test Site were so positioned, based on examina-
tions of ERTS-1 imagery, that S1 would be outside the plume area and S2
within it. Under the conditions of both experiments, S2 was also downstream
during the ebb tidal cycles.

The depth of penetration of incident daylight was a factor of 2 greater at the upstream station, S1, than at Station S2 on the shoal during the August experiment. The mean extinction coefficient was also greater at Station S2 by approximately 32%; during the September study, the extinction coefficient at the upstream station was higher by approximately 20% and the depth of penetration was virtually the same at both stations. It is not unreasonable to expect therefore, that a plume was in the test area during August, but was very weak, if not absent, in September. It could very well be that the weak plume in Figure 3 is just east of Station S2 and therefore was not detected in the sampling, hence the fact that the depth of light penetration was nearly the same at S1 and S2.

There are no apparent correlations between any of the variables tested (phytoplankton, total particles, particles $>10.67\mu$) on either sampling date, due probably to the fact that the variations with each sampling period on each date were quite small, as were the variations between each station.

Preliminary observation of the satellite imagery for 12 September likewise indicated very little difference in image density between the two stations.

The variation between sampling dates, however, is quite marked (Table 10). Whereas there is little difference in total particles per liter (185×10^6 for 9 August vs. 203×10^6 for 12 September), there is a better than four-

fold difference in particles $>10.67\mu$ equivalent diameter per liter and a difference of better than one order of magnitude in cells per liter between the samples collected on 9 August and 12 September. As no imagery was made on 9 August it is impossible to compare the two dates in relation to ground-truth data.

Observation of the satellite imagery (ERTS and SKYLAB) to date indicates that the greatest density differences in the Block Island Sound area occur in March and October. This seasonal variation in relative density corresponds well to the expected periods of phytoplankton blooms in the region. Since there is no corresponding ground truth data available for these periods, one can only speculate that the phytoplankton are one of the major causes of the differences in density shown by the remote imagery.

Summary

The existence of a visible plume at certain times of the year can clearly be established through ERTS-1 imagery. It is located in the general area of Shagwong Reef off Montauk Point, New York, irrespective of the set of tide. Unfortunately, the plume was very weak and apparently east of S2 at the time of the SKYLAB overflight on September 12th as determined from imagery and data compiled from the water column.

It is suspected from the coincidence of the visibility of the plume in ERTS-1 imagery with times of high phytoplankton counts, that the plume

is largely composed of organic suspensoids. It is hypothesized then, that this area is a generating or incubating area of high plankton populations. This may be due to the interaction of nutrients, light, and physical parameters, primarily temperature, that become well mixed due to turbulent action in the water column as the tidal waters flow over the reef.

The SKYLAB experiment has provided the foundation for what may be a most important discovery of estuarine ecological systems that will be more thoroughly investigated in future research activities.

REFERENCES

Alexander, J.E. and T.T. White, 1974. Chemical Oceanography. In: An
Interdisciplinary Study of the Estuarine and Coastal Oceanography
of Block Island Sound and Adjacent New York Coastal Waters: Ground
Truth. R. Hollman, Coordinator. New York Ocean Science Laboratory
Technical Report No. 0027.

American Public Health Association, 1971. Standard Methods for the
Examination of Water and Wastewater, 13th ed.

Castiglione, L.J., 1973. A multivariant study of the distribution of
phytoplankton communities in relation to water color. Ph.D.
Dissertation presented to the Faculty of the Graduate School
of Arts and Sciences, New York University, October, 1973.

Hollman, R. and S.K. Gill, 1974. Physical Oceanography. In: An Inter-
disciplinary Study of the Estuarine and Coastal Oceanography of
Block Island Sound and Adjacent New York Coastal Waters: Ground
Truth. R. Hollman, Coordinator. New York Ocean Science Laboratory
Tehcnical Report No. 0027.

Nuzzi, R. and U.P. Perzan, 1974. Phytoplankton and Suspended Particles.
In: An Interdisciplinary Study of the Estuarine and Coastal Oceano-
graphy of Block Island Sound and Adjacent New York Coastal Waters:
Ground Truth. R. Hollman, Coordinator, New York Ocean Science Labora-
tory Technical Report No. 0027.

Strickland, J.D.H. and T.R. Parsons, 1968. A practical handbook of sea-
water analysis. Fish. Res. Bd. Can., Bull. 167.

APPENDIX C

"System 800"

Computer Printouts

Willcox, Arizona

COUNT= 000956 AT 106 GRAY.

$RUN AREA

COLOR:	0	1	2	3	4	5	6	7
GRAY:	000	000	044	095	138	191	255	255
PERCENT:	01.10	00.90	02.78	10.34	18.48	45.12	23.24	00.00

$RUN HISTOR

SCAN
 COUNT= 000096 AT 034 GRAY.
 COUNT= 000158 AT 031 GRAY.
 COUNT= 000078 AT 032 GRAY.
0> COUNT= 000978 AT 032 GRAY.
 COUNT= 000346 AT 059 GRAY.
 COUNT= 000512 AT 063 GRAY.
 COUNT= 000315 AT 064 GRAY.
1> COUNT= 000315 AT 064 GRAY.
 COUNT= 000977 AT 084 GRAY.
 COUNT= 001042 AT 094 GRAY.
 COUNT= 001172 AT 095 GRAY.
 COUNT= 000949 AT 097 GRAY.
 COUNT= 000976 AT 096 GRAY.
2> COUNT= 000976 AT 096 GRAY.
 COUNT= 001201 AT 120 GRAY.
 COUNT= 001417 AT 125 GRAY.
 COUNT= 001613 AT 127 GRAY.
 COUNT= 002044 AT 128 GRAY.
3> COUNT= 002044 AT 128 GRAY.
 COUNT= 002337 AT 145 GRAY.
 COUNT= 003222 AT 152 GRAY.
 COUNT= 002747 AT 154 GRAY.
 COUNT= 003348 AT 160 GRAY.
4> COUNT= 003348 AT 160 GRAY.
 COUNT= 002249 AT 179 GRAY.
 COUNT= 002286 AT 187 GRAY.
 COUNT= 002286 AT 187 GRAY.
 COUNT= 002252 AT 189 GRAY.
 COUNT= 002069 AT 191 GRAY.
 COUNT= 002471 AT 192 GRAY.
5> COUNT= 002471 AT 192 GRAY.
 COUNT= 001266 AT 212 GRAY.
 COUNT= 000781 AT 222 GRAY.
 COUNT= 000667 AT 225 GRAY.
 COUNT= 000666 AT 223 GRAY.
 COUNT= 000667 AT 225 GRAY.
 COUNT= 000930 AT 224 GRAY.
6> COUNT= 000930 AT 224 GRAY.
 COUNT= 007605 AT 255 GRAY.
7> COUNT= 007605 AT 255 GRAY.

$RUN AREA

COLOR:	0	1	2	3	4	5	6	7
GRAY:	032	064	096	128	160	192	224	255
PERCENT:	02.30	02.40	09.10	12.02	26.44	26.28	15.20	06.20

$RUN DISPLY
#P0

$RUN MARKER

```
$RUN HISTOR

SCAN

$
```

```
 RUN AREA

COLOR:       0        1        2        3        4        5        6        7
GRAY:      032      064      096      128      160      192      224      255
PERCENT  21.46    32.20    29.78    09.64    03.02    01.34    00.78    01.66

$RUN DISPLY
#P1
```

```
$RUN DIGIT

$RUN NEGATE

#P4

$RUN ADDER


 P0,P4

$RUN DISPLY

$RUN MARKER

$RUN DIGIT


 P2

$RUN HISTOR


SCAN

$RUN AREA


COLOR:       0        1        2        3        4        5        6        7
GRAY:      032      064      096      128      160      192      224      255
PERCENT: 01.58    01.66    07.66    30.14    39.54    16.98    01.74    00.62

$RUN DISPLY
#P2
```

$RUN MARKER

G.5 168-64

ORBN DIGIT

$RUN HISTOR
SCAN

$RUN AREA

COLOR:	0	1	2	3	4	5	6	7
GRAY:	032	064	096	128	160	192	224	255
PERCENT:	00.96	00.42	01.48	04.72	18.28	28.14	29.50	16.40

$RUN AREA

COLOR:	0	1	2	3	4	5	6	7
GRAY:	032	064	096	128	160	192	224	255
PERCENT:	00.96	00.42	01.48	04.72	18.28	28.14	29.50	16.40

#RBN DISPLY

$

#RBN DISPLY

$RUN DIGIT
#F4

$RUN NEGATE

```
COUNT= 001461 AT 175 GRAY.
COUNT= 000524 AT 184 GRAY.
COUNT= 001438 AT 176 GRAY.
COUNT= 002906 AT 166 GRAY.
COUNT= 003067 AT 165 GRAY.
COUNT= 002906 AT 166 GRAY.
COUNT= 002906 AT 166 GRAY.
COUNT= 002906 AT 166 GRAY.
COUNT= 002552 AT 167 GRAY.
COUNT= 003067 AT 165 GRAY.
COUNT= 003238 AT 163 GRAY.
COUNT= 003066 AT 144 GRAY.
COUNT= 001627 AT 100 GRAY.
COUNT= 001627 AT 100 GRAY.
COUNT= 000285 AT 077 GRAY.
COUNT= 000036 AT 049 GRAY.
COUNT= 000022 AT 030 GRAY.
COUNT= 000000 AT 255 GRAY.
COUNT= 003004 AT 000 GRAY.
Z=144 AT (315,014)
Z=192 AT (239,262)
```

```
Z=189 AT (244,244)
Z=196 AT (249,250)
Z=189 AT (237,262)
Z=192 AT (331,250)
Z=192 AT (332,238)
Z=175 AT (377,260)
Z=178 AT (383,274)
Z=190 AT (403,364)
Z=182 AT (370,366)
Z=193 AT (248,248)
```

```
Z=100 AT (235,250)
Z=093 AT (230,254)
Z=096 AT (230,248)
Z=092 AT (318,222)
Z=109 AT (322,240)
Z=093 AT (368,262)
Z=083 AT (366,270)
Z=092 AT (374,274)
Z=094 AT (230,260)
Z=092 AT (234,252)
```

COLOR: 0   1   2   3   4   5   6   7
GRAY: 032   064   096   128   160   192   224   255
PERCENT: 01.32   00.46   05.46   40.78   33.58,   16.18   02.08   00.02

$

RUN MARKER
****
$RUN DISPLY
#P0

GR0N DISPLY

$RUN MARKER

$RUN DIGIT
#P1

$RUN HISTOR
SCAN

Z=180 AT (236,260)
Z=175 AT (246,248)
Z=175 AT (241,242)
Z=176 AT (329,234)
Z=168 AT (326,246)
Z=164 AT (366,360)
Z=180 AT (400,360)
Z=157 AT (234,260)
Z=158 AT (245,248)
Z=158 AT (240,240)

Z=043 AT (228,262)
Z=052 AT (234,252)
Z=078 AT (240,252)
Z=074 AT (238,248)
Z=077 AT (236,244)
Z=060 AT (321,248)
Z=055 AT (317,240)
Z=057 AT (321,234)
Z=056 AT (320,226)
Z=054 AT (371,270)

```
Z=083 AT (258,256)
Z=073 AT (258,264)
Z=081 AT (338,244)
Z=069 AT (341,234)
Z=066 AT (340,224)
Z=064 AT (385,248)
Z=057 AT (390,258)
Z=055 AT (394,270)
```

$RUN AREA

COLOR:	0	1	2	3	4	5	6	7
GRAY:	032	064	096	128	160	192	224	255
PERCENT:	05.00	29.90	31.84	23.80	06.08	01.76	01.38	00.14

$RUN DISPLY
            #

DOS/BATCH V9-20C
DATE: 20-SEP-74

DIALOG08?00

₤

PEBRSBIGBGYIN
$

 LO 200,200
DATE:-20-SEP-74
TIME:-20:02:09
$

 RUN DISPLY
#P1

$RUN DISPLY
#P1

$RUN MARKER
$RUN DIGIT

$RUN HISTOR

SCAN
Z=125 AT (253,242)
```
```

```
Z=123 AT (260,272)
Z=125 AT (342,240)
Z=123 AT (342,250)
Z=131 AT (340,258)
Z=115 AT (377,364)
Z=105 AT (378,374)
Z=116 AT (374,378)
```

Playa Alcacer ... Figure 131
Sub biomain Ron...

```
$RUN MARKER

#RUN DIGIT

$RUN HISTOR
SCAN
```

```
Z=178 AT (247,248)
Z=175 AT (247,254)
Z=176 AT (241,244)
Z=177 AT (236,262)
Z=169 AT (328,236)
Z=184 AT (329,250)
Z=182 AT (367,366)
Z=171 AT (401,366)
Z=170 AT (245,250)
Z=177 AT (238,264)
```

Clou.. Shobo... .. ...p...
Fibrous .... 700-... m...

```
Z=114 AT (233,252)
Z=118 AT (229,258)
Z=110 AT (229,250)
Z=115 AT (236,252)
Z=131 AT (322,240)
Z=128 AT (321,226)
Z=125 AT (317,218)
Z=125 AT (368,268)
Z=122 AT (374,272)
Z=116 AT (235,254)
```

Clou.. TiO. .. Fi.... 1..
70. ... . Ron..

```
Z=135 AT (254,236)
Z=134 AT (256,244)
Z=138 AT (262,250)
Z=143 AT (256,262)
Z=143 AT (261,272)
Z=130 AT (342,228)
Z=142 AT (342,242)
Z=139 AT (341,252)
Z=136 AT (379,360)
Z=137 AT (378,376)
```

Playa Alcacer ... . Figur 131
... .

158-27

$RUN AREA   __ __ __ __   __ __ __ __ __

```
COLOR:      0      1      2      3      4      5      6      7
GRAY:      032    064    096    128    160    192    224    255
PERCENT:  01.16  00.10  01.06  16.68  76.38  04.48  00.04  00.00
```

$

#RBN DISPLY

$RUN MARKER
$RUN DIGIT
#P3

$RUN HISTOR
SCAN

```
Z=189 AT (233,260)
Z=198 AT (245,252)
Z=208 AT (243,246)
Z=212 AT (242,242)
Z=207 AT (327,246)
Z=202 AT (327,236)
Z=200 AT (366,360)
Z=196 AT (402,358)
Z=188 AT (379,268)
Z=181 AT (373,256)
```

```
Z=146 AT (236,250)
Z=145 AT (231,254)
Z=141 AT (232,248)
Z=147 AT (236,250)
Z=139 AT (365,266)
Z=141 AT (373,270)
Z=143 AT (369,254)
Z=149 AT (318,220)
Z=153 AT (237,248)
Z=142 AT (228,256)
```

```
Z=169 AT (258,238)
Z=171 AT (263,246)
Z=170 AT (263,258)
Z=170 AT (255,262)
Z=167 AT (341,232)
Z=167 AT (344,242)
Z=170 AT (341,250)
Z=157 AT (379,362)
Z=167 AT (375,370)
Z=159 AT (378,354)
```

$RUN AREA

COLOR:	0	1	2	3	4	5	6	7
GRAY:	032	064	096	128	160	192	224	255
PERCENT:	01.04	00.12	00.30	01.88	37.34	58.28	00.96	00.00

#RBN DISPLY

#RBN DISPLY

$RUN DISPLY
#P1

$RUN DISPLY
#P2

#RBN DIGIT

#RBNPADDER

#RBN DISPLY

#RBN NEGATE

#RBN DISPLY

#RBNPADDER

$RUN DISPLY
#P3

```
#RUN DISPLY

#RUN DISPLY

#RUN DISPLY


#RUN DIGIT

$EB CMD!
#RUN DISPLY

#RUN DISPLY

#RUN DISPLY

$RUN DISPLY
#P0


$
```

```
ERUN MARKER
*******************
$RUN MARKER

$RUN DIGIT
#P0

$RUN HISTOR



SCAN
Z=079 AT (248,330)
Z=085 AT (258,330)
Z=084 AT (264,326)
Z=082 AT (268,326)
Z=080 AT (273,328)
```

$RUN AREA

500-600 NM BAND - NORTH END OF WILLCOX PLAYA

PERCENT AREA

COLOR:	0	1	2	3	4	5	6	7
GRAY:	032	064	096	128	160	192	224	255
PERCENT:	03.86	09.76	37.84	34.52	13.24	00.70	00.00	00.00

$RUN MARKER

$RUN HISTOR

SCAN

Z=024 AT (213,328)
Z=014 AT (225,326)
Z=024 AT (238,322)
Z=029 AT (246,322)
Z=020 AT (254,322)

} PLAYA ALONG NORTH SIDE
OF RAILROAD TRACKS
600-700 mm BAND

$RUN AREA

600-700 mm BAND - NORTH END OF WILLCOX PLAYA

PERCENT AREA

COLOR:	0	1	2	3	4	5	6	7
GRAY:	032	064	096	128	160	192	224	255
PERCENT:	52.50	25.60	18.46	02.36	00.66	00.34	00.00	00.00

$RUN MARKER
$RUN HISTOR

SCAN
Z=097 AT (225,330)
Z=101 AT (239,332)
Z=104 AT (259,326)
Z=096 AT (274,328)
Z=106 AT (287,324)

} PLAYA ALONG NORTH SIDE OF RAILROAD
TRACKS , 700-800 mm BAND

700-800 mm BAND - NORTH END OF WILLCOX PLAYA

PERCENT AREA

COLOR:	0	1	2	3	4	5	6	7
GRAY:	032	064	096	128	160	192	224	255
PERCENT:	02.02	01.80	27.08	66.52	02.46	00.04	00.00	00.00

$RUN MARKER

$RUN HISTOR

SCAN

Z=131 AT (226,326)
Z=128 AT (247,326)
Z=140 AT (264,324)   PLAYA AL A NORTH SIDE OF RAILROAD.
Z=133 AT (279,324)   THROUGH 800-900 mm BAND
Z=131 AT (286,324)

$RUN AREA

800-900 mm. BAND - NORTH END OF WILLCOX PLAYA

PERCENT AREA

COLOR:	0	1	2	3	4	5	6	7
GRAY:	032	064	096	128	160	192	224	255
PERCENT:	01.24	00.64	02.94	40.72	53.70	00.70	00.00	00.00

$ END

SPECTRAL ANALYSIS OF AIRCRAFT (A/C)
S-190 MULTI SPECTRAL PHOTO AFTER
IMAGE

A/C POSITIVE MULTISPECTRAL PHOTOS
OF WILLCOX PLAYA (NORTH END)

RUN HISTOR

SCAN

$RUN AREA

A/C IMAGE #47 - PERCENT AREA

```
COLOR:      0      1      2      3      4      5      6      7
GRAY:      032    064    096    128    160    192    224    255
PERCENT: 01.26  00.48  02.36  28.60  65.46  01.76  00.00  00.00
```

$RUN DIGIT
#P0

$RUN DISPLY
#P0

$

RUN HISTOR
SCAN

$RUN AREA

A/C IMAGE #48 - PERCENT AREA

```
GRAY:       032     064     096     128     160     192     224     255
PERCENT: 01.34   00.78   04.44   58.80   34.32   00.26   00.00   00.00
$
```

7-11

RUN HISTOR

SCAN

$RUN AREA

A/C IMAGE #37 - PERCENT AREA

```
COLOR:      0       1       2       3       4       5       6       7
GRAY:       032     064     096     128     160     192     224     255
PERCENT: 01.28   00.58   02.52   78.12   17.42   00.00   00.00   00.00
$
```

RUN HISTOR
SCAN

$RUN AREA

A/C IMAGE #49 - PERCENT AREA

```
COLOR:      0       1       2       3       4       5       6       7
GRAY:       032     064     096     128     160     192     224     255
PERCENT: 01.12   00.02   00.40   02.00   46.02   50.34   00.00   00.00
$
```

END

APPENDIX D

"System 800"

Computer Printouts

Northeastern U.S. Coastal Waters

①

┌─────────────────────────┐
│ 800 SYSTEM COMPUTER   │
│   PRINTOUT   │
└─────────────────────────┘

#RUN ADDER

BLOCK ISLAND SOUND
NEW YORK

P2, P3

──────────────────────────────────────

ORBN DISPLY

SKYLAB 3   NEGATIVE IMAGES OF
BLOCK ISLAND SOUND & SURROUNDING
WATERS; 21 SEPTEMBER 1973
Frame No. 227

ORBN DIGIT

ORBN DISPLY

$RUN DISPLY
#P2

Image Digitization

ORB0HASTOR05,332)

$RUN HISTOR
SCAN

600-700 NM BAND   FRAME 239   21 SEPT 73
PERCENT AREA

$RUN AREA

COLOR:	0	1	2	3	4	5	6	7
GRAY:	032	064	096	128	160	192	224	255
PERCENT:	44.28	11.44	13.14	11.70	11.68	05.68	01.32	00.68

$RUN MARKER

ORBN DIGIT

$RUN DISPLY
#P2

$RUN HISTOR

500-600 NM BAND   FRAME 239   21 SEPT 73
PERCENT AREA

SCAN

$RUN AREA

COLOR:	0	1	2	3	4	5	6	7
GRAY:	032	064	096	128	160	192	224	255
PERCENT:	20.72	11.18	12.32	22.82	20.50	06.42	03.12	02.82

$RUN DIGIT
#P1

```
$RUN DIGIT
#P0
```

SKYLAB 3   NEGATIVE IMAGES OF

```
$RUN DISPLY
#P0
```

LONG ISLAND SOUND   WATER

```
$RUN MARKER
GRUN DIGIT
```

21 SEPTEMBER 1972   FRAME NO. 240

```
GRUN DISPLY
```

LINEAR DECREATION

```
GRUN DIGIT


$RUN DIGIT
#P3

$RUN NEGATE
#P3

$
```

```
 RUN HISTOR
SCAN
```

600-700 NM BAND   FRAME 240   21 SEPT 72

```
$UN AREA
ILL CMD!
$RUN AREA
```

PERCENT AREA

COLOR:	0	1	2	3	4	5	6	7
GRAY:	032	064	096	128	160	192	224	255
PERCENT:	51.16	09.00	12.48	09.22	08.10	05.92	03.28	00.70

```
$RUN ADDER
#P0, P2

$RUN DISPLY
#P2
```

```
BRUN ADDER


 P0, P3


---- ------
```

ORUN DISPLY

$RUN DISPLY
#PO

$

RUN MARKER

ORUN DIGIT

ORUN DISPLY

ORUN DIGIT

$RI\I\UN DISPLY
#PO

$RUN DISPLY
#P1

$UN \ NU\RUN DISPLY
#PO

$RUN HISTOR   500-600 NM BAND   FRAME 240   21 SEPT '73
SCAN
                              PERCENT AREA
$RUN AREA
COLOR: 0   1   2   3   4   5   6   7
GRAY: 032   064   096   128   160   192   224   255
PERCENT: 26.76   15.52   18.04   19.10   11.40   03.92   02.92   02.24

$
                                                         END
_____

#RUN DIGIT

```
SCAN
  COUNT= 009079 AT 000 GRAY.
  COUNT= 000195 AT 019 GRAY.
  COUNT= 000214 AT 032 GRAY.
0> COUNT= 000214 AT 032 GRAY.
  COUNT= 000239 AT 036 GRAY.
  COUNT= 000306 AT 052 GRAY.
  COUNT= 000363 AT 058 GRAY.
  COUNT= 000350 AT 064 GRAY.
1> COUNT= 000350 AT 064 GRAY.
  COUNT= 000481 AT 075 GRAY.
  COUNT= 000598 AT 090 GRAY.
  COUNT= 000635 AT 095 GRAY.
  COUNT= 000666 AT 098 GRAY.
  COUNT= 000721 AT 096 GRAY.
2> COUNT= 000721 AT 096 GRAY.
  COUNT= 001093 AT 124 GRAY.
  COUNT= 000890 AT 127 GRAY.
  COUNT= 001014 AT 129 GRAY.
  COUNT= 001420 AT 128 GRAY.
3> COUNT= 001420 AT 128 GRAY.
  COUNT= 001049 AT 153 GRAY.
  COUNT= 001091 AT 156 GRAY.
  COUNT= 001409 AT 160 GRAY.
4> COUNT= 001409 AT 160 GRAY.
  COUNT= 002579 AT 189 GRAY.
  COUNT= 003056 AT 193 GRAY.
  COUNT= 004113 AT 192 GRAY.
5> COUNT= 004113 AT 192 GRAY.
  COUNT= 003076 AT 212 GRAY.
  COUNT= 002513 AT 219 GRAY.
  COUNT= 002215 AT 229 GRAY.
  COUNT= 003006 AT 224 GRAY.
6> COUNT= 003006 AT 224 GRAY.
  COUNT= 002604 AT 255 GRAY.
7> COUNT= 002604 AT 255 GRAY.
```

SKYLAB 3 NEGATIVE IMAGES OF
NANTUCKET & MARTHAS VINYARD WA
12 SEPTEMBER 1973   FRAME NO. 13

LINEAR DIGITAL

500-600 NM BAND FRAME 131 12
1973
PERCENT AREA

```
$RUN AREA
COLOR:       0        1        2        3        4        5        6        7
GRAY:       032      064      096      128      160      192      224      255
PERCENT:  05.06    03.28    05.70    09.78    11.74    21.46    32.40    10.46

$
```

```
  RUN MARKER
$RUN DIGIT
#P1


$RUN DISPLY
```

$RUN HISTOR

5CAN

$RUN AREA
COLOR: 0   1   2   3   4   5   6   7
GRAY: 032   064   096   128   160   192   224   255
PERCENT: 13.10   02.50   04.24   12.40   30.72   30.68   04.08   02.18

ORUNPBOVE

600-700 NM BAND   FRAME 131   12 SEPT 1972

PERCENT AREA

END

ORUNPBOVE

ORBN NEGATE

ORBNPBDDER

ORBNPBDDER

APPENDIX E

CHEMICAL OCEANOGRAPHY

by

James E. Alexander
Senior Research Scientist in Chemical Oceanography
New York Ocean Science Laboratory
Montauk, New York

Theodore T. White
Research Assistant in Chemical Oceanography
New York Ocean Science Laboratory
Montauk, New York

III CHEMICAL OCEANOGRAPHY

Contents

INTRODUCTION

In the fall of 1972, a study of the biological, chemical, and physical oceanography of Block Island Sound as a whole was initiated. Prior to this time, observations of these same features in the waters entering the Sound from the west had been made. Particular emphasis had been placed on four stations lying on a transect established between Montauk Point, Long Island, New York, and Watch Hill, Rhode Island.

The aim of this present investigation was to determine the relationship between ERTS-1 imagery and the characteristics of the surface waters in this area. In a previous study (Alexander et al 1973), it was noted that in coastal oceanography the sampling program should be designed around the fact that this zone is highly dynamic, and particular attention must be paid to both tidal and nontidal forces in program design.

METHODS

At each station, the locations of which have been previously described, samples were collected from selected depths with 5-ℓ Niskin bottles. Once on board, samples for the measurement of salinity, oxygen, and phytoplankton analyses were removed. The remainder of the sample was then filtered through Whatman GF/C filters in an all glass filtrations system. The filter pads were then placed in individual vials and frozen for later analysis of chlorophyll and particulate phosphorus. Samples of the filtrate were removed for the measurement of reactive and total soluble phosphorus, nitrite and nitrate nitrogen, and silica.

Salinity was determined with a conductivity system (Beckman RS7-B) and oxygen was determined by the method described by Carpenter (1966). Reactive, total soluble and particulate phosphorus, silica, and chlorophyll were determined according to the methods described by Strickland and Parsons (1968). Nitrite and nitrate nitrogen were determined by the method described by Wood et al (1967).

On 12 May 1973, through the cooperation of the local power squadrons and other private

yachts, a synoptic sampling of the surface waters was conducted. Salinity and suspended solids samples were collected at 0900, 1200, and 1500 hours. The method described by Strickland and Parsons (1968) was used for these analyses.

RESULTS AND DISCUSSION

A. Block Island Sound

The seasonal distribution of oxygen along the H transect is depicted in Figure III-1a-c. No significant differences were apparent between the four stations at the surface. Similar concentrations were found along the HB and BR transect. As anticipated, the observed surface oxygen concentrations, which ranged from approximately 4.5 ml/ℓ in September to 8.5 ml/ℓ in March, were inversely correlated with surface temperatures ($r = -0.863$). On an annual basis, the surface waters of Block Island Sound had a predicted oxygen concentration of $O_2 = -0.18 \, (t°C) + 8.15$. The overall correlation of oxygen with chlorophyll a in these surface waters was not significant ($r = -0.167$).

The observed changes in reactive and soluble organic (total soluble-reactive) phosphorus, nitrite, nitrate, and silicate for the various transects are tabulated in Table III-1, III-2, and III-3.

The nutrients (phosphates, nitrates, and silicates) showed the seasonal variations typical of temperate waters. Indications are that the supply of nitrogen to these waters is limited and that, under the appropriate conditions, the nutrients are utilized by the phytoplankton rather quickly. Although relatively large seasonal changes in concentration were noted, the correlations between these parameters and chlorophyll a were not considered significant.

Particulate phosphorus and chlorophyll a (Figure III-1a, b, c and III-2a, b, c) showed a strong correlation ($r = 0.815$). The equation of the line depicting the relationship was $P-PO_4 = 0.58 \text{ chl. } a + 0.85$. Particulate phosphorus generally ranged between 0.5 and 3.5 μg-at/ℓ. The maximum concentration (6.36 μg/ℓ) was noted at Station H1 in March. Subsurface concentrations (30 m depth) generally paralleled those found at the surface.

In early October, what appeared to be the remnants of an autumn bloom were found at those stations occupied along the H transect. Little evidence of such conditions was found for the other transects. Chlorophyll a concentrations generally remained low (0.5–1.0 mg/m^3) through the remainder of the fall and winter. A spring flowering of relatively short duration was present in March. Peak chlorophyll a concentrations of 9.4 mg/m^3 were present at Station H1. The amount of chlorophyll a present in the surface waters of this transect gradually decreased from the high value noted at Station 7 to 2.1 mg/m^3 at Station 4. No evidence of a spring outburst of similar magnitude was found in the waters of the other transects. The reasons for this may be that the frequency of sampling was such that the bloom was missed along the other transects, or the data reduction techniques affected the graphical presentation. In respect to the latter, the range of chlorophyll a at BR1 was 1.69–3.39; at BR2 a range of 2.01–2.60 mg/m^3, and at BR3 a range of 0.85–3.04 mg/m^3. Along the HB transect, inclement weather prevented our sampling from 14 February until 25 April, and undoubtedly the spring bloom was missed.

This study was designed to determine the relationship between ERTS-1 imagery and the characteristics of surface waters in this area. It was also necessary to determine how representative any of these data were for that day, since in the present ERTS-1 program an image of an area represents the conditions for that moment in time only. Our sampling program was designed to collect data on the effect of both tidal and nontidal forces upon a given parameter and consequently to yield information pertinent to the above. The effect of these upon the distribution of particulate phosphorus and chlorophyll a on 10 October 1972 is shown in Figure III-3. Satellite time was at approximately 1100 hours, and at that time higher concentrations of both particulate phosphorus and the pigmented population were present at Station H1 than at the remaining stations. This station also showed the greatest range of concentration for both of these parameters. Since this range of variation is typical of the variability to be expected for most parameters, it is particularly important that additional information be gathered relevant to the variability of all parameters in both short- and long-term space and time.

With respect to the former, we conducted an experiment on 12 May 1973, with the help of the local power squadrons and private yachts, to collect synoptic samples for the

measurement of suspended material, salinity, and temperature in the surface waters of Block Island Sound and adjacent waters. In this preliminary experiment, logistics prevented the collection of samples for·chlorophyll. The location of each of the sampling vessels is shown in Figure III-4. The sampling times were 0900, 1200, and 1500 hours. It should also be noted that, although care was exercised in the storage of the samples, certain of those collected early in the day remained in the plastic containers for more than 10 hours prior to filtration.

The synoptic distribution of temperature, salinity, and suspended solvents is shown in Figure III-6a, b, c, III-7a, b, c, and III-8a, b, c. For each of the three parameters observed, large ranges in values and concentrations were noted. The effect of the tidal forces upon the distribution of these parameters was apparent.

B. New York Bight

Only three cruises in the New York Bight were completed (December, January, and May), and during each of these any particular site was sampled only once. This places strong limits on the interpretation of the data. The observed data for the TR and NYB transects are shown in Table III-4 and III-5 respectively.

The concentration of nutrients and chlorophyll was generally higher along the New York Harbor transect than along the TR transect. This was especially apparent in the nitrate concentrations. Evidences for seasonal trends were particularly evident in the nitrate and silicate data. Table III-6 lists the average data for all of the parameters for both the TR and NYB transects in December, January, and May.

No significant correlation between the nutrients, particulate phosphate, and chlorophyll a was found for the TR transect at any time. Along the NYB transect, however, strong correlations were found between the concentration of chlorophyll a and soluble organic phosphorus. It was also noted that the correlation was strongest in May. For example, the overall correlation of soluble organic phosphorus with chlorophyll a for the NYB transect was 0.88. In December and January, the correlations were not significant (r = 0.01 and 0.12 respectively), while in May the correlation was 0.95.

SUMMARY

Observations on the spatial and temporal distribution of particulate phosphate, reactive phosphate, and soluble organic phosphate, nitrate nitrogen, silica, and chlorophyll a were conducted in both Block Island Sound and the New York Bight from August 1972 to June 1973. The frequency of sampling was greatest in the former area.

Evidence of the presence of the seasonal cycles expected for these temperate waters was present. The waters of Block Island Sound and those along the southern shore of Long Island were deficient in nitrogen. With the exception of particulate and soluble organic phosphorus, no significant correlations were found between any of the measured parameters and chlorophyll a. In Block Island Sound, correlations of 0.815 were found between particulate phosphorus and chlorophyll a. No correlation was found for these parameters in the New York Bight. In the latter area, a strong correlation (0.88) existed between soluble organic phosphorus and chlorophyll a at the entrance to New York Harbor. Evidence was also presented indicating that the strength of this correlation fluctuates seasonally.

TABLE III-1

Seasonal variations in reactive and soluble organic phosphorus, nitrite and nitrate nitrogen,
and silicate along the "H" transect

Date			10 Oct 1972				14 Nov 1972				4 Dec 1972				13 Feb 1973			
Station Parameter		H1	H2	H3	H4	H1	H2	H3	H4	H1	H2	H3	H4	H1	H2	H3	H4
R-PO$_4$	0m	0.97	1.16	1.14	0.84	1.13	1.06	0.89	0.96	1.28	1.25	1.14	1.17	0.91	N.A.	1 00	0.90
µg-at/ℓ	30m	1.21	-	0.91	0.82	-	N.A.	N.A.	-	-	1.15	0.95	1.03	-	N.A.	N.A.	N.A.
O-PO$_4$	0m	0.38	0.42	0.33	0.49	1.71	0.37	1.34	0.51	0.29	0.23	0.21	0.16	0.75	N.A.	0.21	0.15
µg-at/ℓ	30m	-	0.26	0.60	0.50	-	N.A.	N.A.	N.A.	-	0.20	0.38	0.16	-	N.A.	N.A.	N.A.
NO$_2$	0m	0.48	0.81	0.53	0.13	0.19	0.24	0.11	0.30	0.19	0.33	0.25	0.16	-	N.A.	N.A.	N.A.
µg-at/ℓ	30m	-	0.84	0.42	0.12	-	1.01	0.11	0.11	-	0.21	0.21	0.16	-	N.A.	N.A.	N.A.
NO$_3$	0m	0.88	1.99	1.11	1.44	2.06	7.38	1.29	2.01	1.79	2.88	2.22	2.56	-	N.A.	N.A.	N.A.
µg-at/ℓ	30m	-	1.62	0.91	0.38	-	1.77	0.98	1.15	-	2.39	2.02	3.69	-	N.A.	N.A.	N.A.
Si	0m	4.73	5.46	4.26	1.82	1.61	2.07	3.58	2.73	3.39	5.44	3.45	3.18	10.5	N.A.	11.6	7.3
µg-at/ℓ	30m	-	5.89	4.50	1.66	-	3.20	2.40	3.93	-	3.84	5.28	2.50	-	N.A.	N.A.	N.A.

N.D. = Not Detectable

N.A. = No Data Available

  - = Insufficient Depth

TABLE III-1 (cont'd.)

Date		20 Mar 1973				24 Apr 1973				18 Jun 1973			
Station Parameter		H1	H2	H3	H4	H1	H2	H3	H4	H1	H2	H3	H4
R-PO$_4$	0m	0.68	0.77	0.65	0.62	0.66	1.13	0.76	0.63	0.43	0.60	0.27	0.32
µg-at/ℓ	30m	-	0.77	0.65	0.61	-	0.54	0.47	0.50	-	0.55	0.51	0.55
O-PO$_4$	0m	0.35	0.26	0.33	0.16	0.81	1.09	0.98	N.D.	0.76	0.59	0.71	0.51
µg-at/ℓ	30m	-	0.22	0.28	0.68	-	1.91	7.21	4.19	-	0.28	0.63	0.75
NO$_2$	0m	0.07	0.10	0.11	0.05	0.06	0.04	0.03	0.03	0.02	0.02	0.02	N.A.
µg-at/ℓ	30m	-	0.10	0.07	0.05	-	0.05	0.02	0.01	-	0.06	0.03	N.A.
NO$_3$	0m	1.69	5.05	2.35	2.05	1.47	1.39	1.15	0.90	0.28	0.09	-	0.01
µg-at/ℓ	30m	-	4.75	2.82	1.75	-	1.09	0.70	0.41	-	0.57	0.35	0.40
Si	0m	3.34	7.07	5.58	5.17	7.03	6.86	6.53	5.51	5.6	5.4	3.4	4.0
µg-at/ℓ	30m	-	8.04	7.24	4.67	-	7.91	6.39	5.77	-	7.70	6.55	7.23

TABLE III-2

Seasonal variations in reactive and soluble organic phosphorus, nitrite and nitrate
nitrogen, and silica along the "BR" transect

Date		5 Sep 1972			16 Nov 1972			8 Dec 1972			21 Mar 1973			26 Apr 1973			18 Jun 1973		
Station / Parameter		BR1	BR2	BR3	BR1	BR2	BR3	BR1	BR2	BR3	BR1	BR2	BR3	BR1	BR2	BR3	BR1	BR2	BR3
$R-PO_4$	0m	0.40	0.46	0.70	0.92	1.16	1.43	0.90	0.92	1.03	0.53	0.50	0.37	0.25	0.29	0.30	0.31	0.32	0.47
µg-at/ℓ	30m	0.55	0.62	-	1.04	1.09	-	0.98	0.93	-	0.42	0.50	-	•	0.33	-	0.51	0.52	-
$O-PO_4$	0m	0.33	0.37	0.15	1.13	0.77	0.62	0.38	0.17	0.11	0.72	0.69	0.39	1.16	1.18	2.07	0.59	0.44	0.66
µg-at/ℓ	30m	0.21	0.31	-	0.54	0.45	-	0.11	0.09	-	0.93	0.60	-	-	1.12	-	0.37	0.93	-
NO_2	0m	0.02	0.02	0.06	0.21	0.30	0.35	0.28	0.24	0.40	0.06	0.04	N.A.	N.A.	0.03	0.01	0.01	0.02	0.01
µg-at/ℓ	30m	0.04	0.22	-	0.19	0.24	-	0.32	0.23	-	0.03	0.01	-	-	0.01	-	0.02	0.03	-
NO_3	0m	0.73	0.10	0.31	0.87	1.82	1.97	3.02	2.46	3.57	2.26	1.00	0.10	0.20	N.D.	0.01	0.01	0.02	0.07
µg-at/ℓ	30m	0.25	0.62	-	0.54	0.65	-	0.71	2.61	-	0.98	0.35	-	-	0.12	-	0.39	0.41	-
Si	0m	2.11	0.94	3.17	1.35	2.79	4.83	1.80	2.23	4.89	4.98	3.62	2.20	2.80	0.20	0.30	5.47	3.30	5.34
µg-at/ℓ	30m	2.00	3.42	-	1.35	2.02	-	2.12	2.42	-	3.39	3.23	-	-	3.41	-	5.96	7.40	-

N.D. = Not Detectable

N.A. = No Data Available

  - = Insufficient Depth

TABLE III-3

Seasonal variations in reactive and soluble organic phosphorus, nitrite and nitrate nitrogen, and silica along the "HB" transect

Date	29 Aug 1972					10 Nov 1972					6 Dec 1972				
Station / Parameter	HB1	HB2	HB3	HB4	HB5	HB1	HB2	HB3	HB4	HB5	HB1	HB2	HB3	HB4	HB5
$R\text{-}PO_4$ 0m	0.90	0.85	0.66	0.46	0.37	1.07	1.10	0.85	0.81	0.79	1.59	1.41	1.11	1.05	1.00
µg-at/ℓ 30m	-	-	0.67	-	-	-	-	0.67	-	-	-	-	0.80	-	-
$O\text{-}PO_4$ 0m	1.00	0.87	0.75	1.40	0.26	0.12	0.27	0.13	0.04	0.15	0.27	0.17	0.05	0.20	0.13
µg-at/ℓ 30m	-	-	0.99	-	-	-	-	0.10	-	-	-	-	0.08	-	-
NO_2 0m	0.07	0.06	0.03	0.02	0.03	0.22	0.21	0.12	0.20	0.33	0.31	0.39	0.29	0.30	0.44
µg-at/ℓ 30m	-	-	0.14	-	-	-	-	0.22	-	-	-	-	0.37	-	-
NO_3 0m	0.47	0.57	0.35	0.03	0.38	1.88	1.41	0.77	0.71	0.65	2.39	3.00	2.42	1.79	1.83
µg-at/ℓ 30m	-	-	1.53	-	-	-	-	0.52	-	-	-	-	1.44	-	-
Si 0m	3.50	3.86	2.60	1.75	1.33	2.98	2.18	1.72	2.03	1.50	4.45	5.70	2.38	1.85	1.70
µg-at/ℓ 30m	-	-	4.53	-	-	-	-	1.21	-	-	-	-	0.95	-	-

N.D. = Not Detectable

N.A. = No Data Available

- = Insufficient Depth

TABLE III-3 (cont'd.)

Date		14 Feb 1973					25 Apr 1973					19 Jun 1973				
Station / Parameter		HB1	HB2	HB3	HB4	HB5	HB1	HB2	HB3	HB4	HB5	HB1	HB2	HB3	HB4	HB5
$R-PO_4$	0m	0.99	1.07	1.03	0.91	0.84	0.60	0.49	0.44	0.41	0.35	0.41	0.47	0.32	0.32	0.42
μg-at/ℓ	30m	-	-	0.77	-	-	-	-	0.50	-	-	-	-	-	-	-
$O-PO_4$	0m	0.40	0.23	0.43	0.38	0.47	1.37	3.04	0.62	1.38	0.69	0.67	1.72	0.53	0.57	1.02
μg-at/ℓ	30m	-	-	0.17	-	-	-	-	2.02	-	-	-	-	-	-	-
NO_2	0m	0.09	0.12	0.12	0.15	0.14	0.08	0.05	0.06	0.05	0.05	0.02	0.02	N.A.	0.03	N.D.
μg-at/ℓ	30m	-	-	0.09	-	-	-	-	0.04	-	-	-	-	-	-	-
NO_3	0m	4.90	5.48	4.86	6.16	6.86	1.24	1.14	1.22	0.97	0.57	0.09	0.12	1.06	-	0.03
μg-at/ℓ	30m	-	-	0.02	-	-	-	-	0.88	-	-	-	-	-	-	-
Si	0m	8.77	9.78	10.10	8.14	7.56	7.72	6.74	7.85	7.14	5.16	4.54	5.08	4.36	3.97	3.82
μg-at/ℓ	30m	-	-	6.92	-	-	-	-	6.83	-	-	-	-	-	-	-

TABLE III-4

Observations on the variation of particulate, reactive and soluble organic phosphorus, nitrate nitrogen, silica and chlorophyll a along the TR transect in the New York Bight

Date	20 Dec 1972								24 Jan 1973							
Station / Parameter	1	2	3	4	5	6	7	8	1	2	3	4	5	6	7	8
P–PO$_4$ µg-at/ℓ	1.29	0.86	0.93	0.86	0.85	1.39	1.23	1.33	0.73	1.57	1.44	1.62	1.75	1.59	2.41	2.74
R–PO$_4$ µg-at/ℓ	1.87	1.39	1.19	1.12	1.02	1.95	1.53	1.60	1.16	0.76	0.77	0.76	0.81	0.71	0.80	0.90
O–PO$_4$ µg-at/ℓ	1.85	0.14	1.52	0.24	0.62	1.12	1.07	1.33	0.22	0.29	<0.01	0.13	0.14	0.08	0.15	0.05
NO$_3$ µg-at/ℓ	5.67	2.65	3.44	5.36	2.58	5.02	4.88	4.64	9.49	5.32	4.82	5.07	5.31	5.87	5.95	7.44
Si µg-at/ℓ	-	16.59	22.43	16.78	10.75	6.58	15.02	6.95	12.52	4.37	2.75	3.13	3.90	3.61	3.61	3.42
Chl a mg/m^3	2.32	5.46	1.43	0.78	1.04	1.23	0.98	0.99	0.91	5.32	1.91	1.95	1.30	1.91	2.69	3.07

TABLE III-4 (cont'd.)

Date	30 May 1973							
Station Parameter	1	2	3	4	5	6	7	8
P-PO$_4$ µg-at/ℓ	1.01	0.28	0.17	0.20	0.49	0.29	0.11	0.08
R-PO$_4$ µg-at/ℓ	1.12	0.92	0.72	0.87	0.87	1.37	0.47	0.42
O-PO$_4$ µg-at/ℓ	0.44	0.99	1.58	3.33	1.31	0.41	1.87	3.09
NO$_3$ µg-at/ℓ	1.35	0.02	-	0.17	0.07	0.04	0.05	0.03
Si µg-at/ℓ	1.51	0.51	<0.10	<0.10	<0.10	<0.10	<0.10	<0.10
Chl a mg/m³	1.63	3.01	1.62	2.10	1.30	0.78	1.26	2.72

TABLE III-5

Observations on the variation of particulate, reactive and soluble organic phosphorus,
nitrate nitrogen, silica, and chlorophyll *a* along the NYB transect

Date	20 Dec 1972									24 Jan 1973								
Station Parameter	1	2	3	4	5	6	7	8	9	1	2	3	4	5	6	7	8	9
P–PO$_4$ µg–at/ℓ	0.96	1.85	2.60	1.94	1.50	1.56	1.55	1.24	0.92	3.23	3.55	4.87	3.95	3.83	3.40	3.50	2.63	2.58
R–PO$_4$ µg–at/ℓ	1.22	2.54	3.16	2.60	1.87	1.77	2.17	2.06	3.29	1.00	1.90	2.48	1.84	1.24	0.71	0.96	0.82	0.90
O–PO$_4$ µg–at/ℓ	4.24	2.95	3.20	0.30	0.07	N.D.	N.D.	0.10	0.24	0.05	0.39	0.50	0.77	0.30	0.24	0.25	0.23	0.10
NO$_3$ µg–at/ℓ	4.01	13.24	19.31	14.46	8.98	7.34	11.36	6.10	2.79	6.67	13.36	17.04	10.55	12.76	6.99	9.54	6.38	5.73
Si µg–at/ℓ	2.95	12.04	2.08	2.17	1.69	0.92	5.71	5.91	5.91	5.28	16.50	22.25	12.52	5.93	3.39	6.21	3.80	3.71
Chl *a* mg/m^3	1.63	1.28	1.45	1.96	0.78	0.49	1.40	1.54	0.73	2.26	2.08	2.27	2.97	5.92	7.50	6.71	4.12	1.87

N.D. = Not Detectable

TABLE III-5 (cont'd.)

Date	30 May 1973								
Station Parameter	1	2	3	4	5	6	7	8	9
$P-PO_4$ µg-at/ℓ	0.53	1.00	1.60	0.46	0.98	0.38	0.57	0.29	0.47
$R-PO_4$ µg-at/ℓ	1.42	1.88	2.64	1.12	2.63	1.12	1.62	1.17	1.22
$O-PO_4$ µg-at/ℓ	2.87	7.94	9.44	10.42	5.14	10.88	2.74	10.31	5.22
NO_3 µg-at/ℓ	1.03	12.10	19.14	8.75	10.42	5.57	10.27	1.68	1.25
Si µg-at/ℓ	0.06	1.05	2.95	1.24	0.15	0.51	0.51	0.15	0.60
Chl a mg/m³	4.13	14.80	17.15	19.72	8.89	20.07	6.45	14.94	6.51

TABLE III-6

The average concentration of particulate, reactive and soluble organic phosphate, nitrate nitrogen, silica, and chlorophyll a along the TR and NYB transects for the months of December, January, and May

Date	Dec 1972		Jan 1973		May 1973	
Transect ___ Parameter	TR	NYB	TR	NYB	TR	NYB
P-PO$_4$ µg-at/ℓ	1.09	1.56	1.73	3.50	0.32	1.24
R-PO$_4$ µg-at/ℓ	1.45	2.06	0.83	1.31	0.84	1.64
O-PO$_4$ µg-at/ℓ	0.98	1.25	0.13	0.31	1.62	7.21
NO$_3$ µg-at/ℓ	4.28	9.73	6.15	9.89	0.24	7.80
Si µg-at/ℓ	13.58	4.37	4.66	8.84	0.32	0.80
Chl a mg/m^3	3.15	1.21	2.38	3.96	1.80	12.51
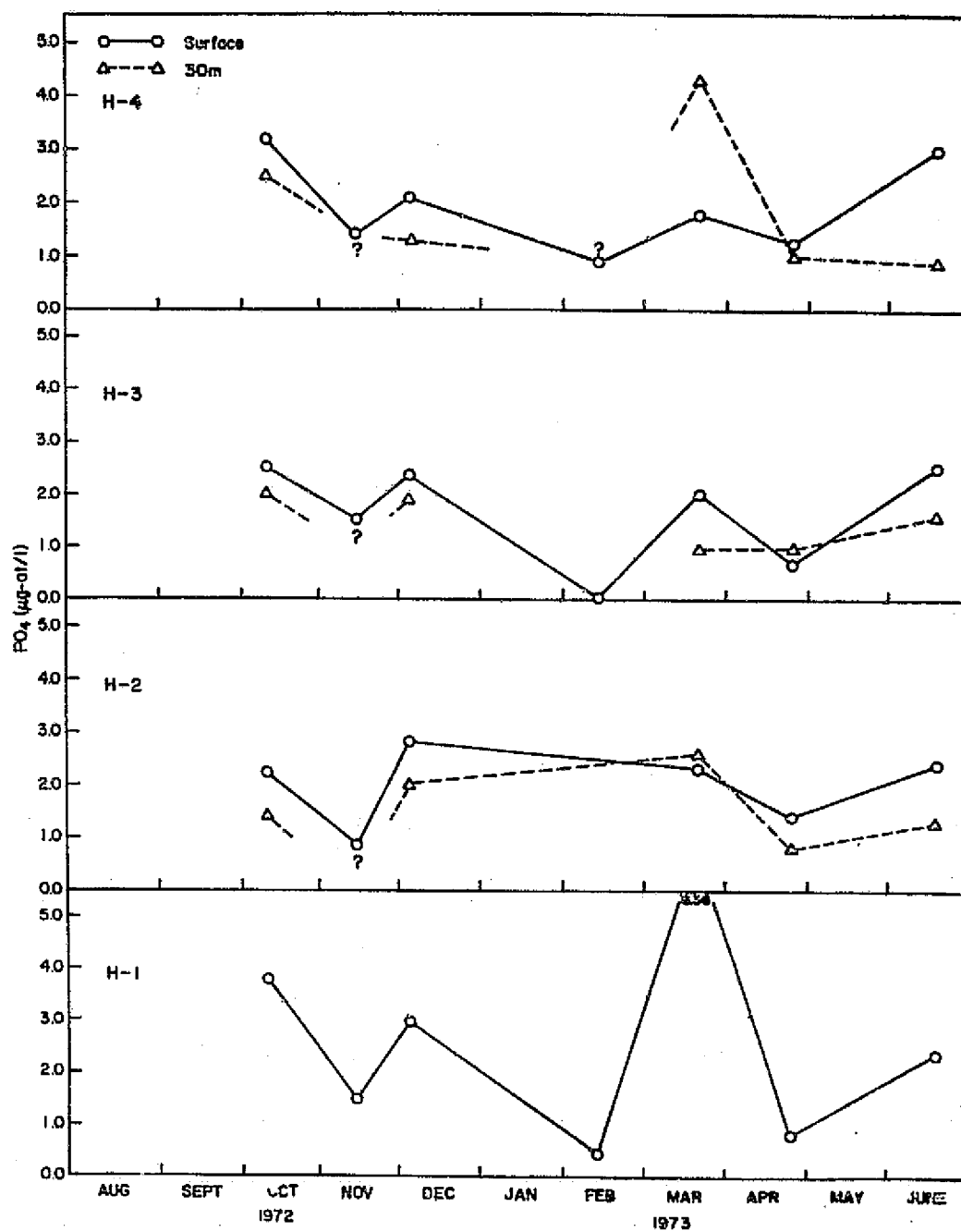
FIGURE III-1a

The seasonal distribution of particulate phosphorus along the H transect
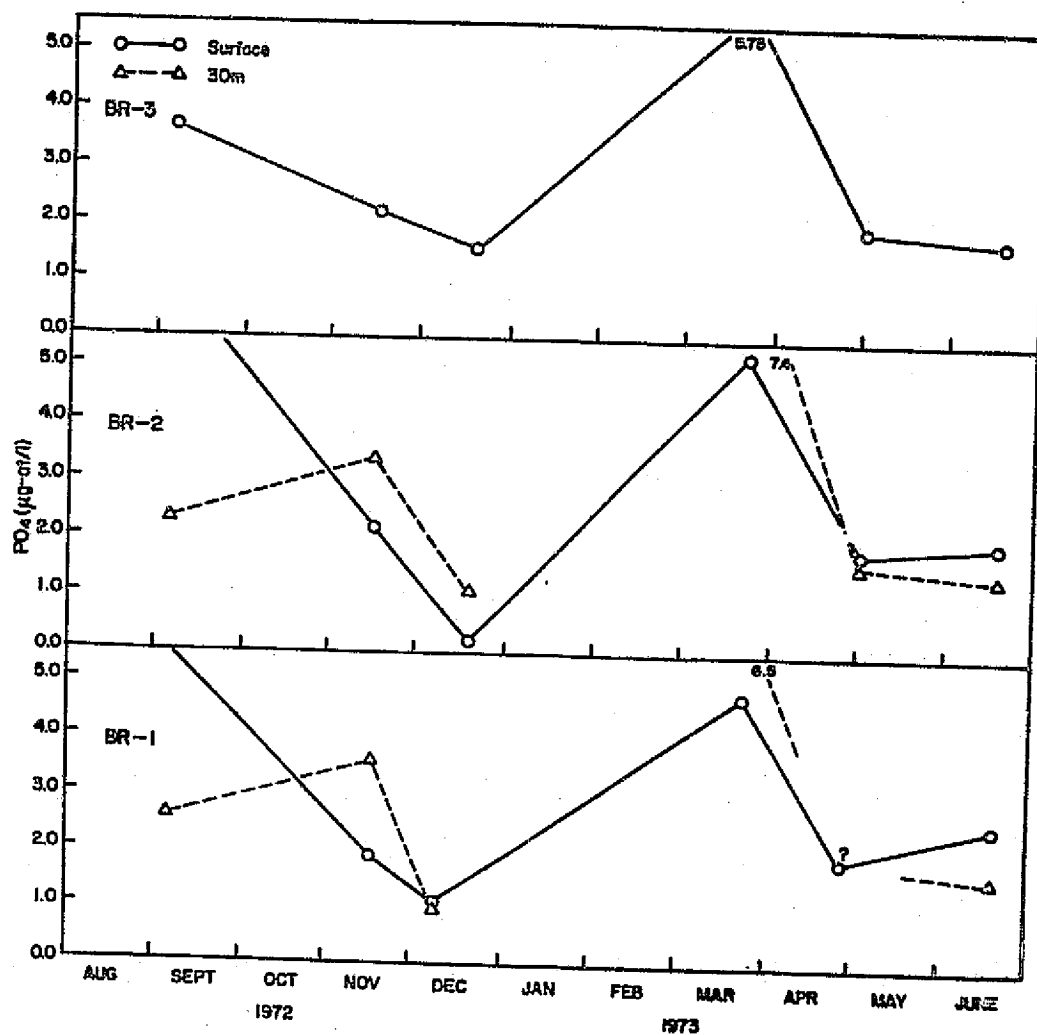
FIGURE III-1b

The seasonal distribution of particulate phosphorus along the BR transect
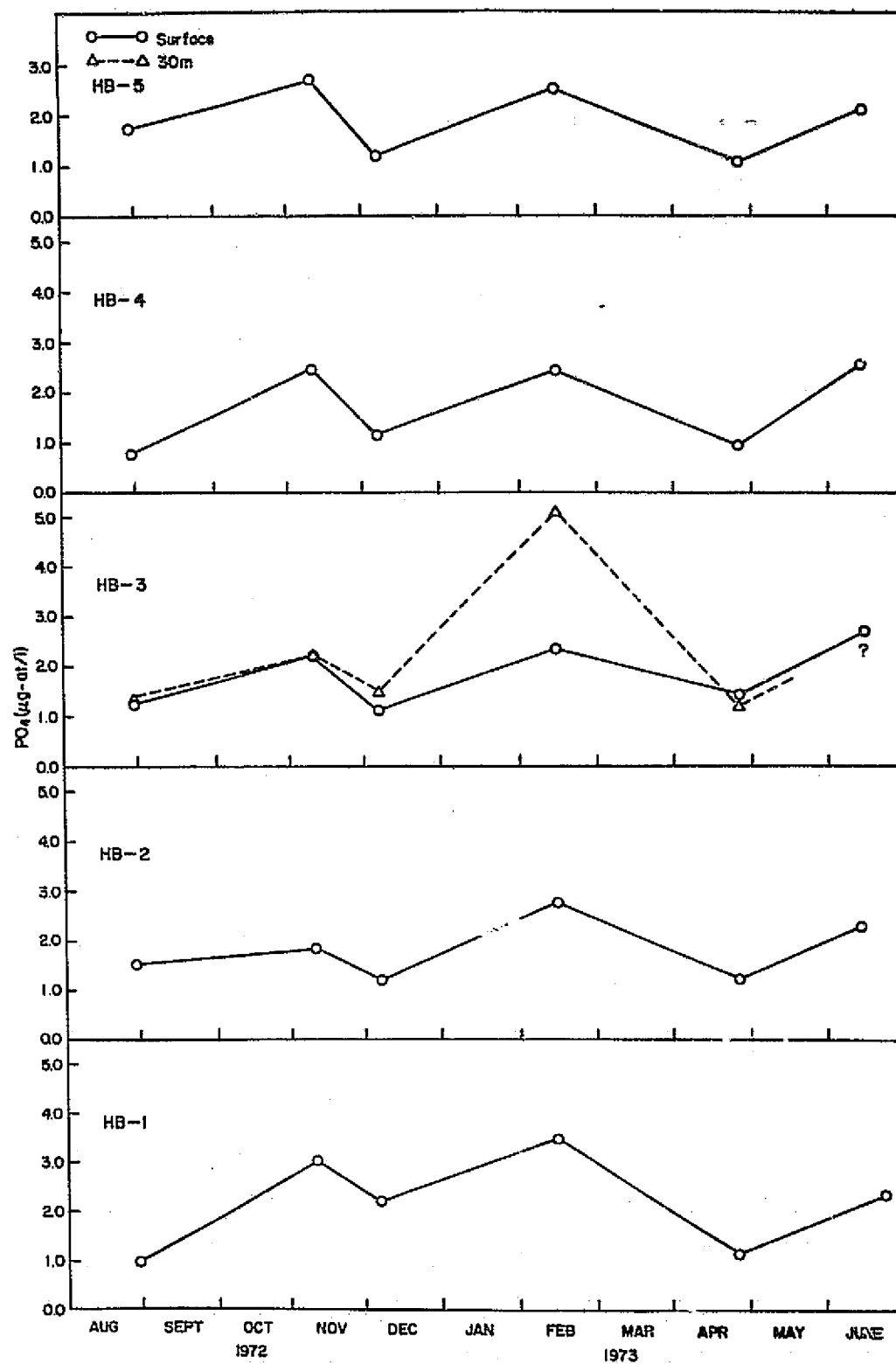
FIGURE III-1c

The seasonal distribution of particulate phosphorus along the HB transect
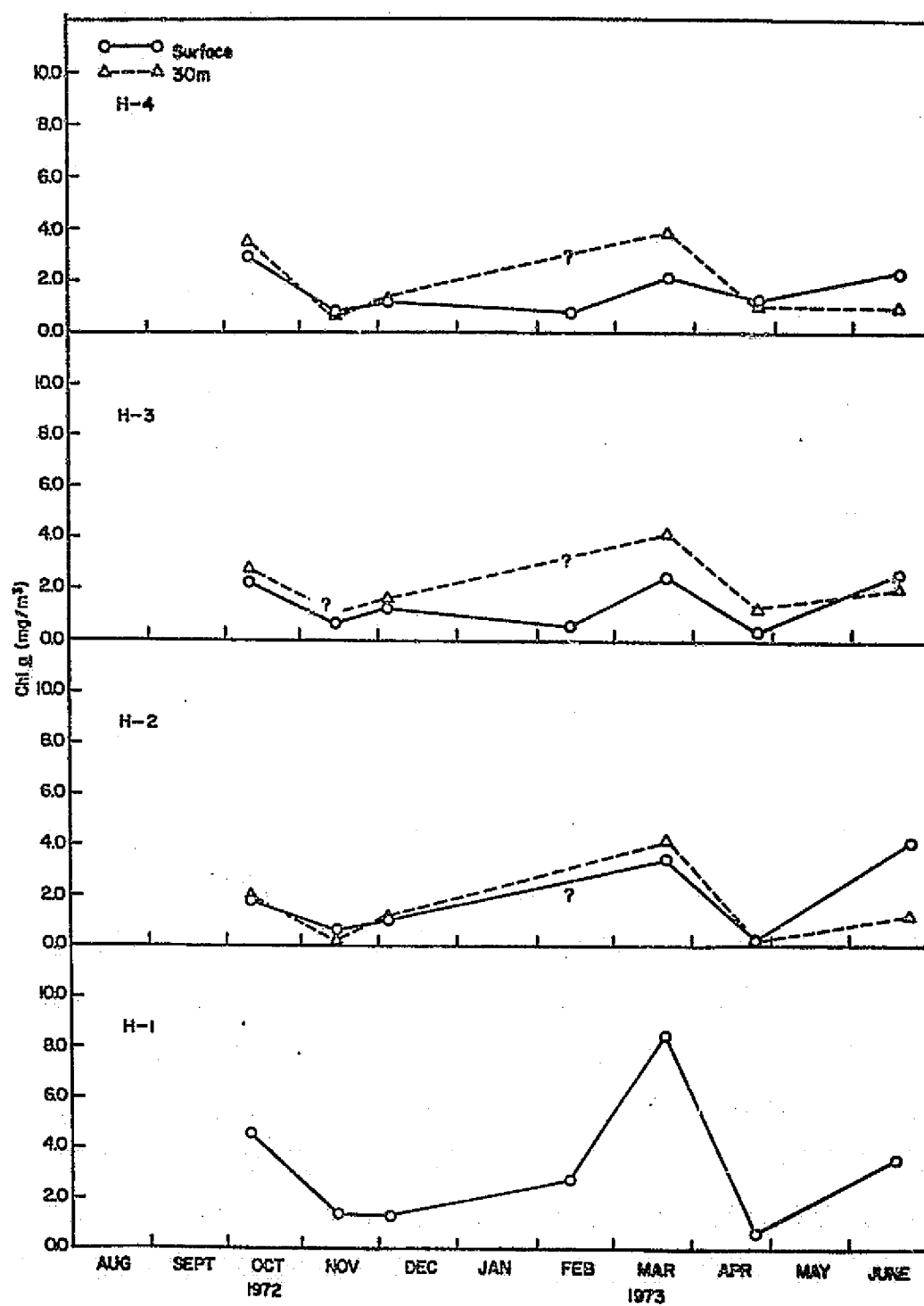
FIGURE III-2a

The seasonal distribution of chlorophyll *a* along the H transect
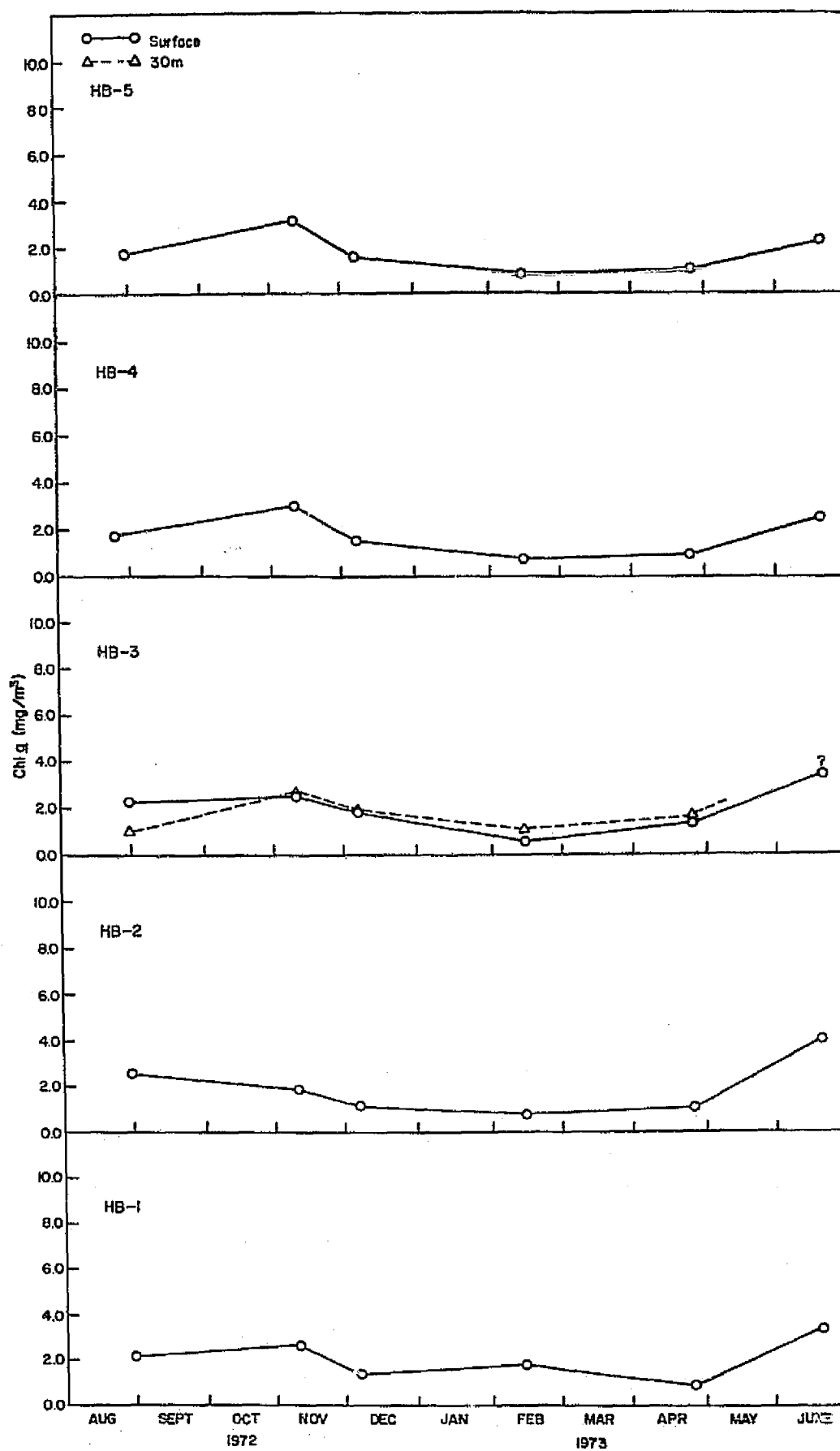
FIGURE III-2b

The seasonal distribution of chlorophyll *a* along the HB transect
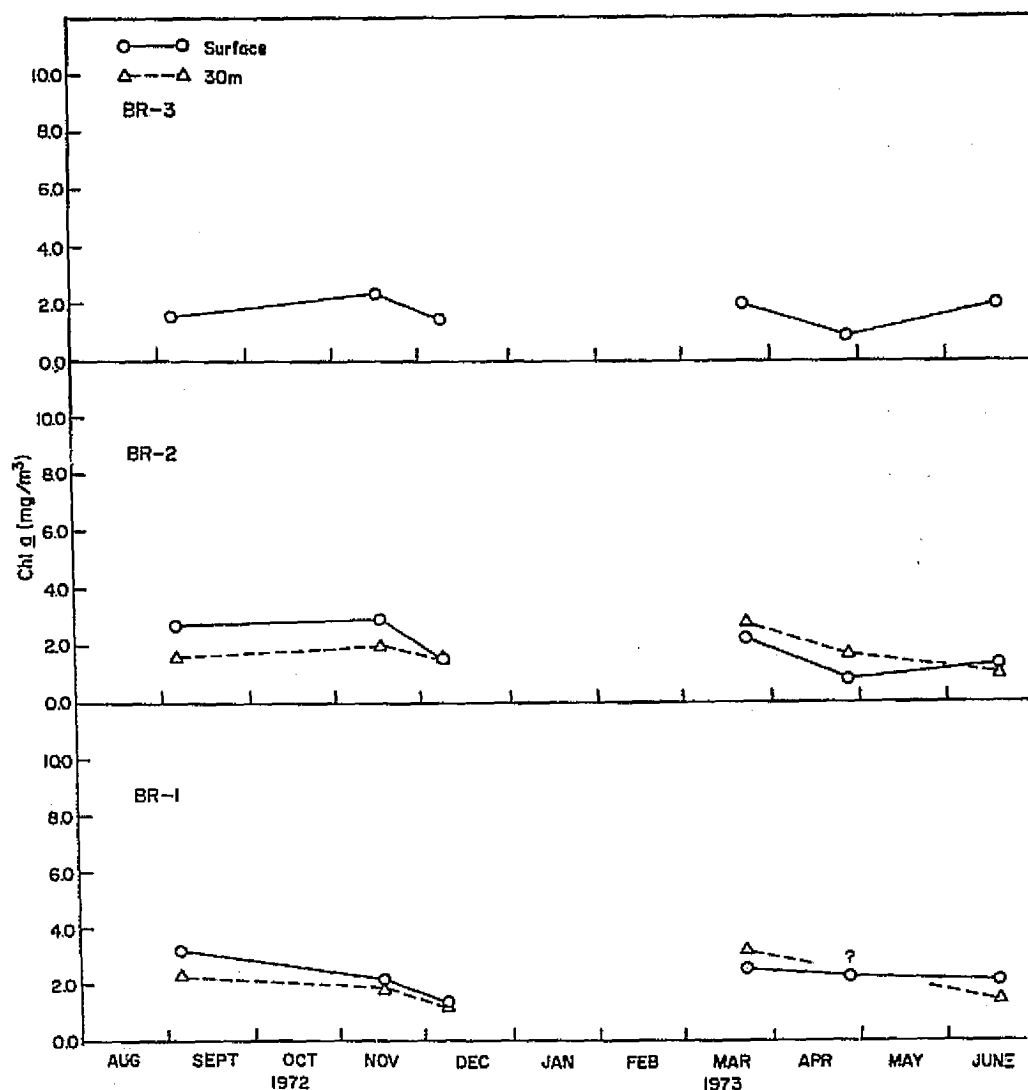
FIGURE III-2c

The seasonal distribution of chlorophyll *a* along the BR transect
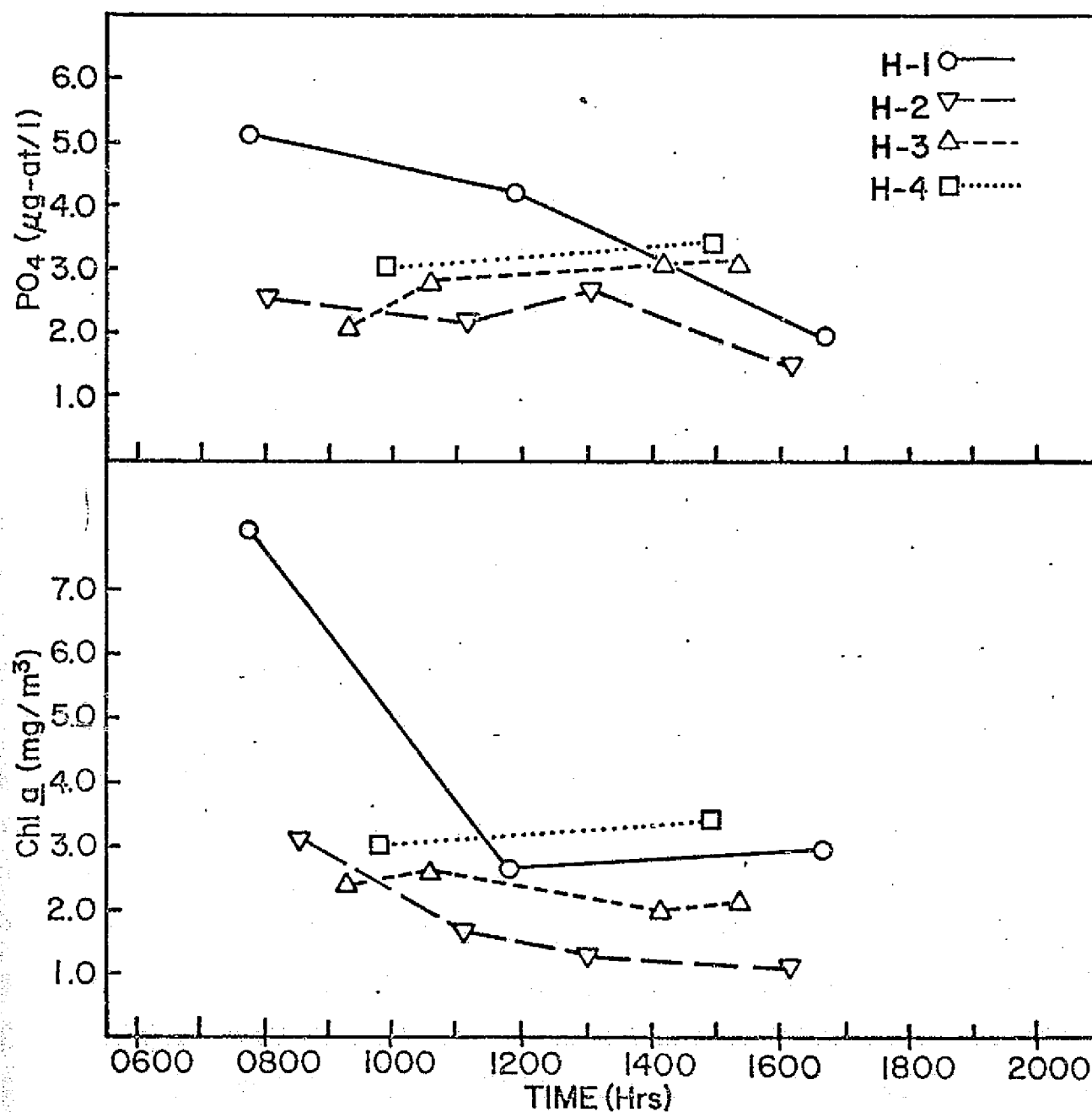
FIGURE III-3

Surface variations in particulate phosphorus and chlorophyll *a*
along the H transect, 10 October 1972
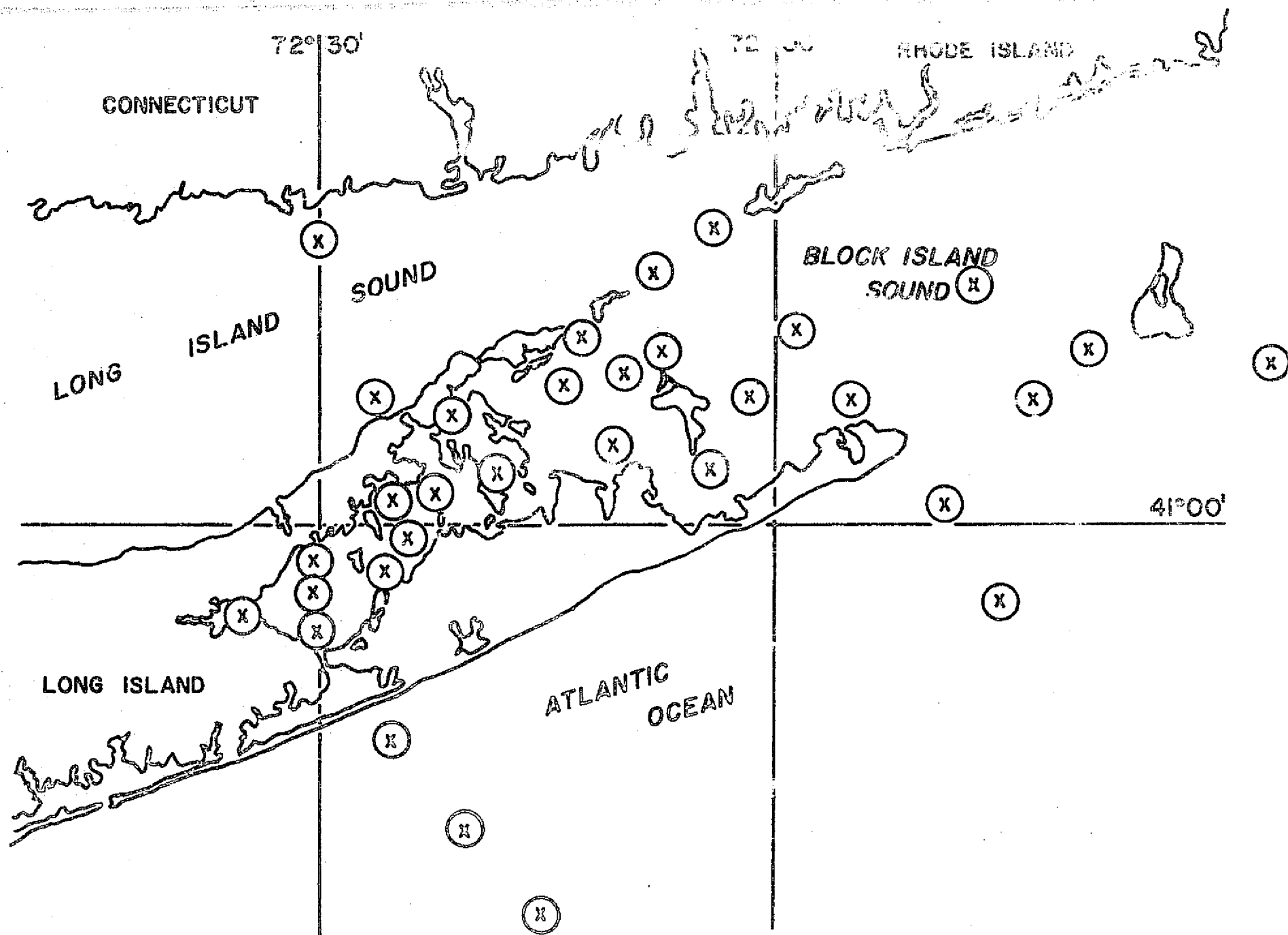
FIGURE III-4

The location of the sampling vessels for the synoptic study conducted on 12 May 1974

FIGURE III-5a

CONNECTICUT

RHODE ISLAND

LONG ISLAND

10.5

10.0

9.7

11

12.5

9.5

9.0

14

14.5

FIGURE III-5b

The distribution of temperature in the surface waters of Block Island Sound and adjacent waters (12 May 1973-1200)

19

RHODE ISLAND

CONNECTICUT

11.5

10.5
11.0

11.3

14 13.5 13.0

10.0

9.5

14

15 14.5

LONG ISLAND

10.7
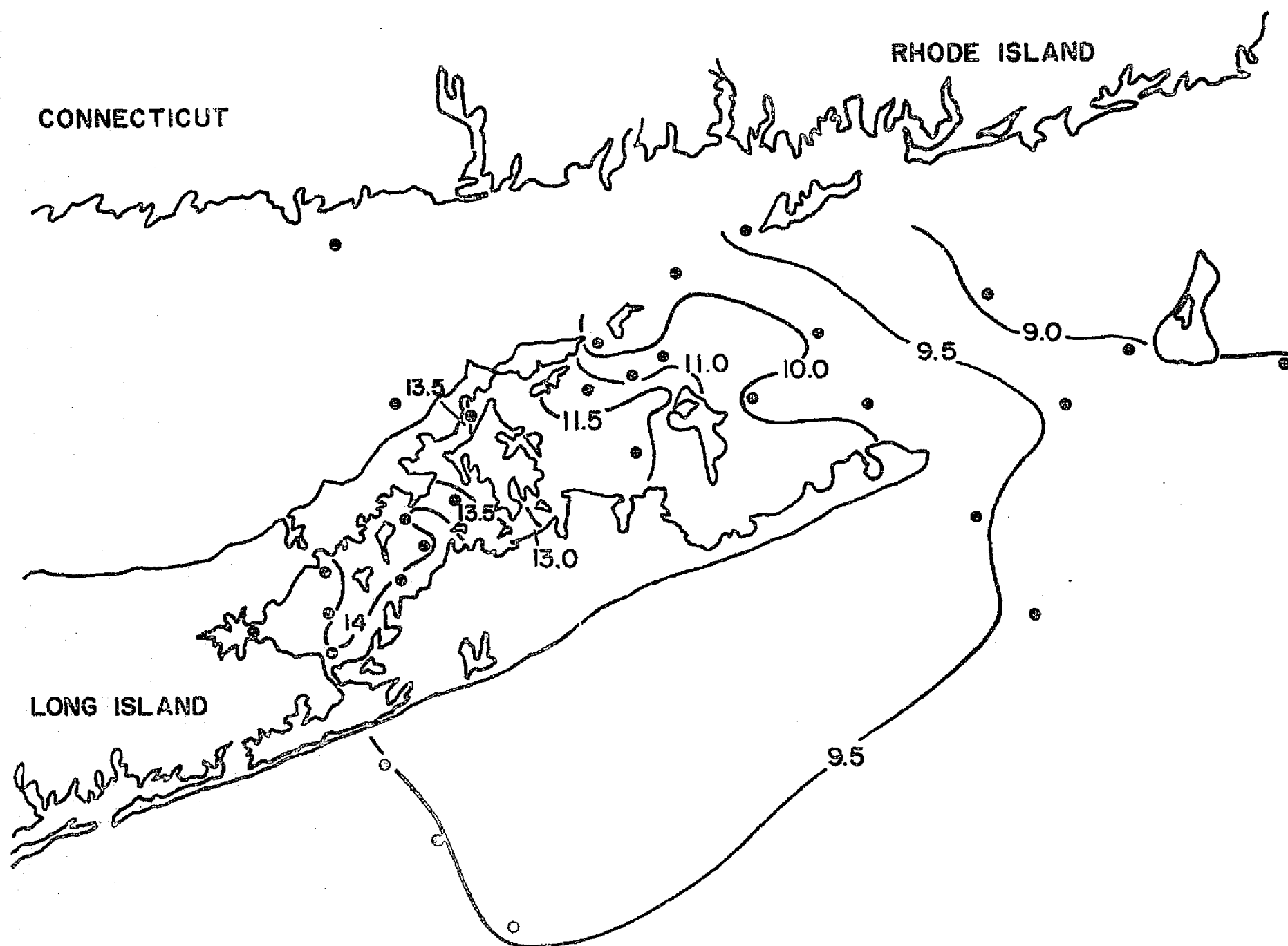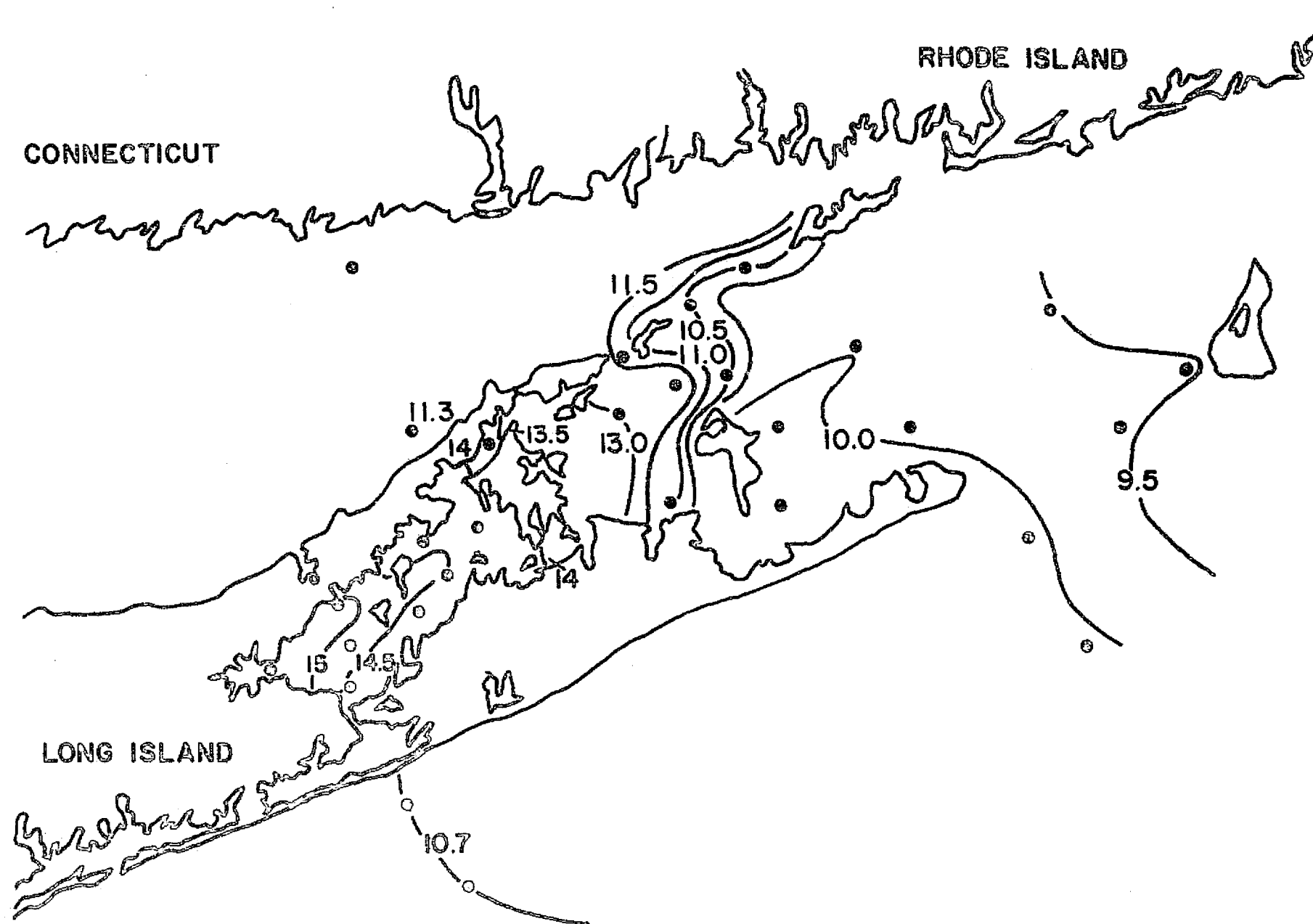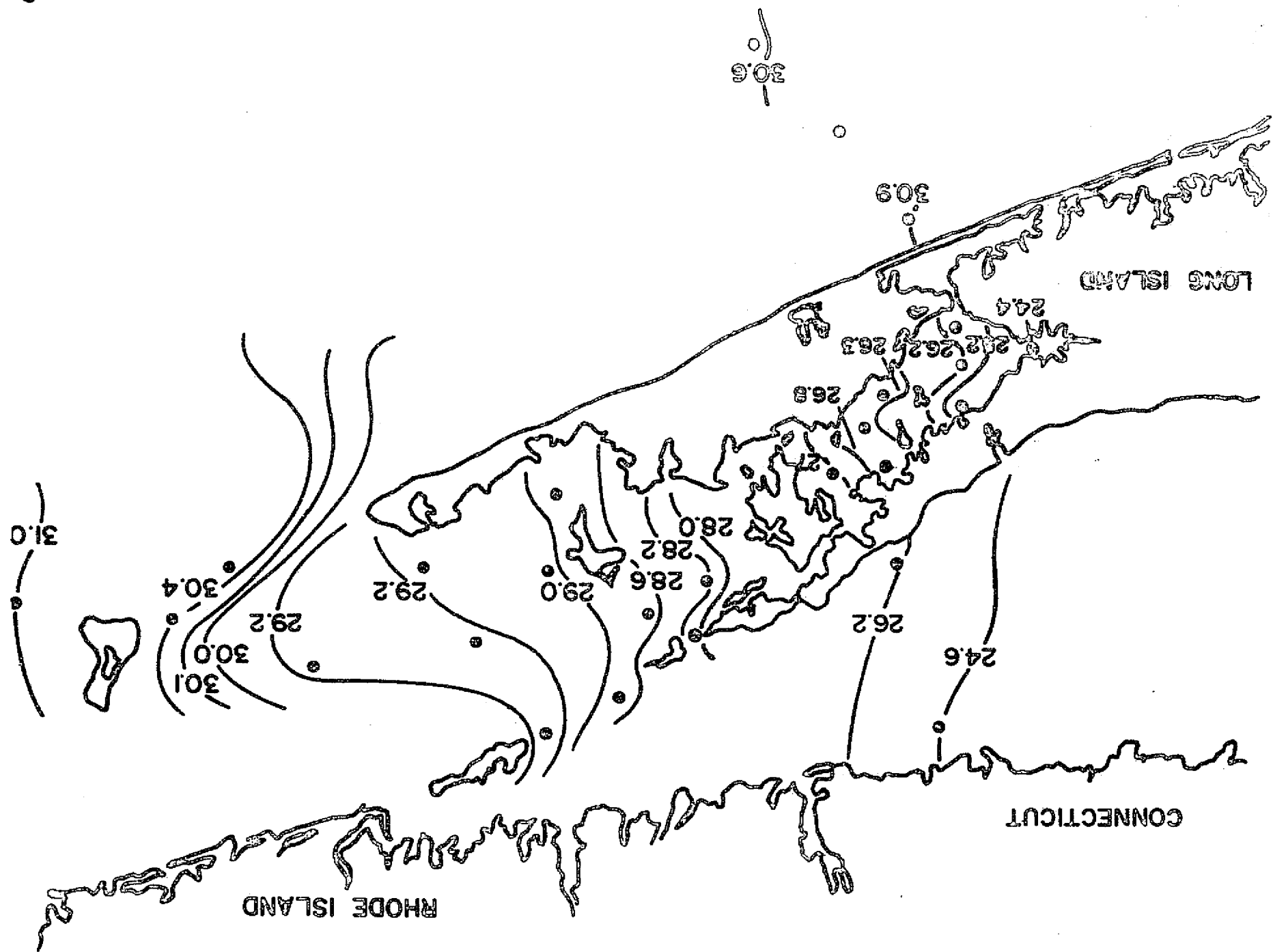
FIGURE III-5c
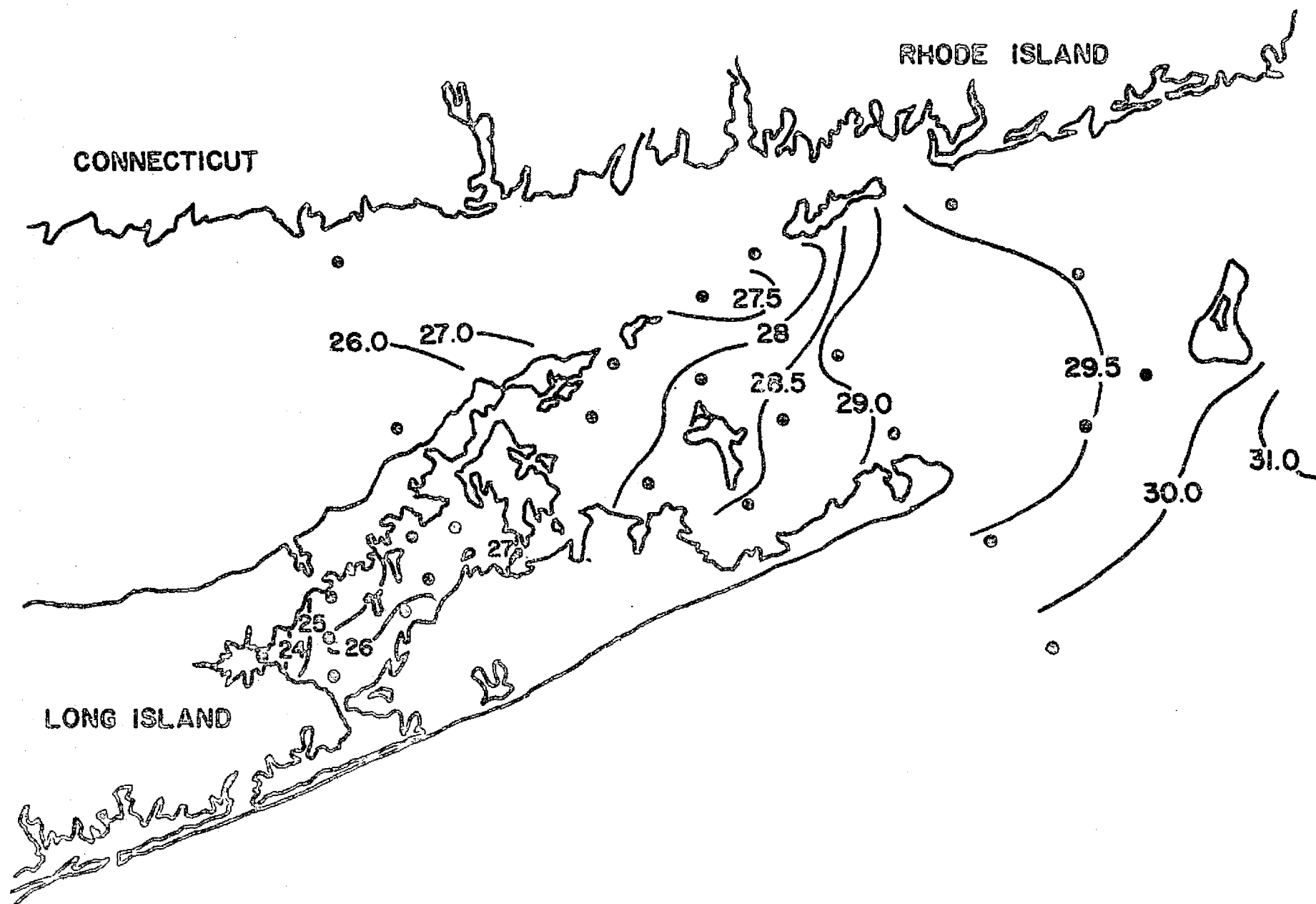
FIGURE III-6b

The distribution of salinity in the surface waters of Block Island Sound and adjacent waters (12 May 1973-1200)

RHODE ISLAND

CONNECTICUT

26.0

27.0

28.0

28.5

29.0

29.5

30.0

28

28

27

24 25

26

LONG ISLAND

30.9

30.9

30.6
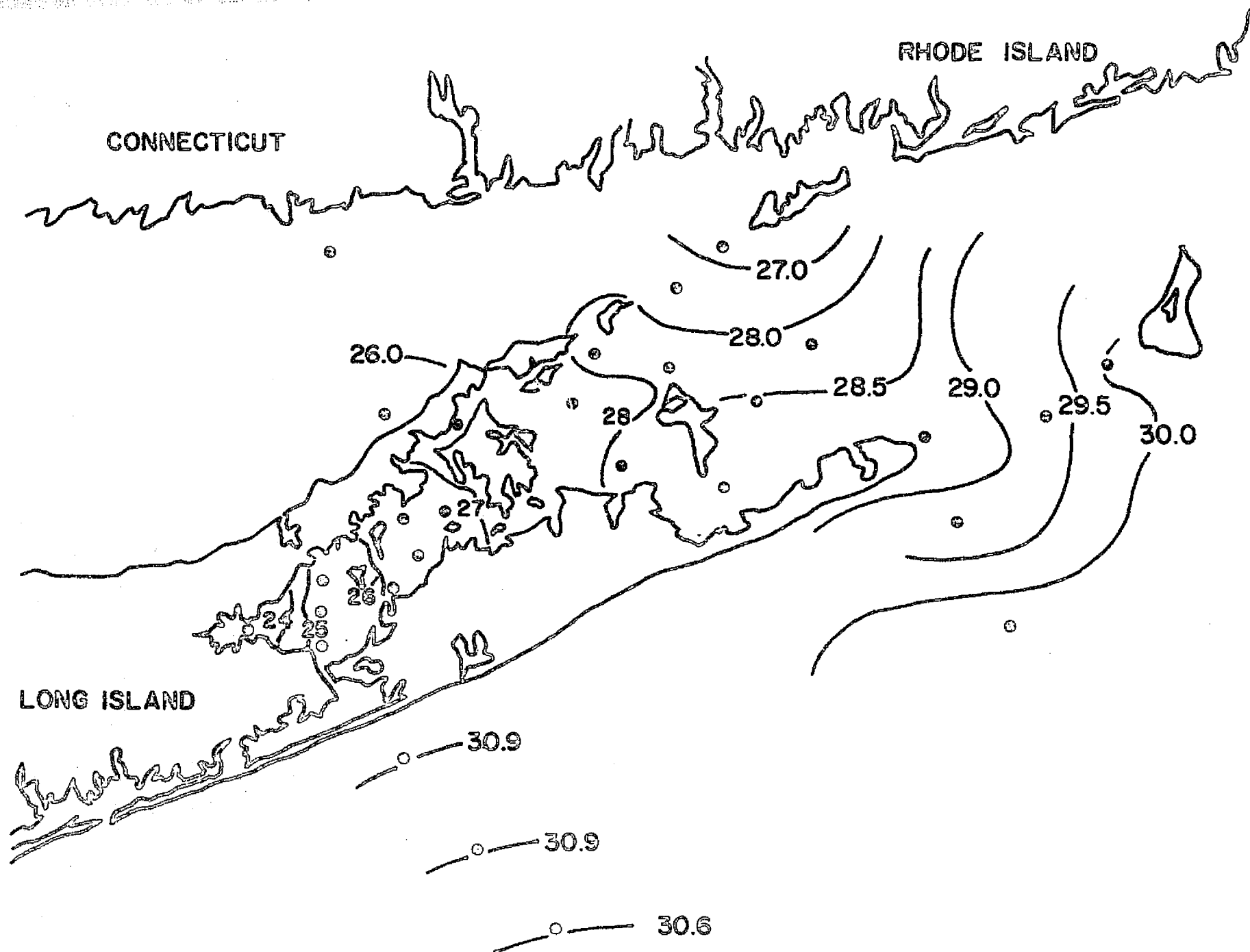
FIGURE III-6c

The distribution of salinity in the surface waters of Block Island Sound in the

RHODE ISLAND

CONNECTICUT

3.4

5.0
4.0
3.0
2.0
1.0

4.7

1.0

6.1
4.0
4.0

2.0

LONG ISLAND
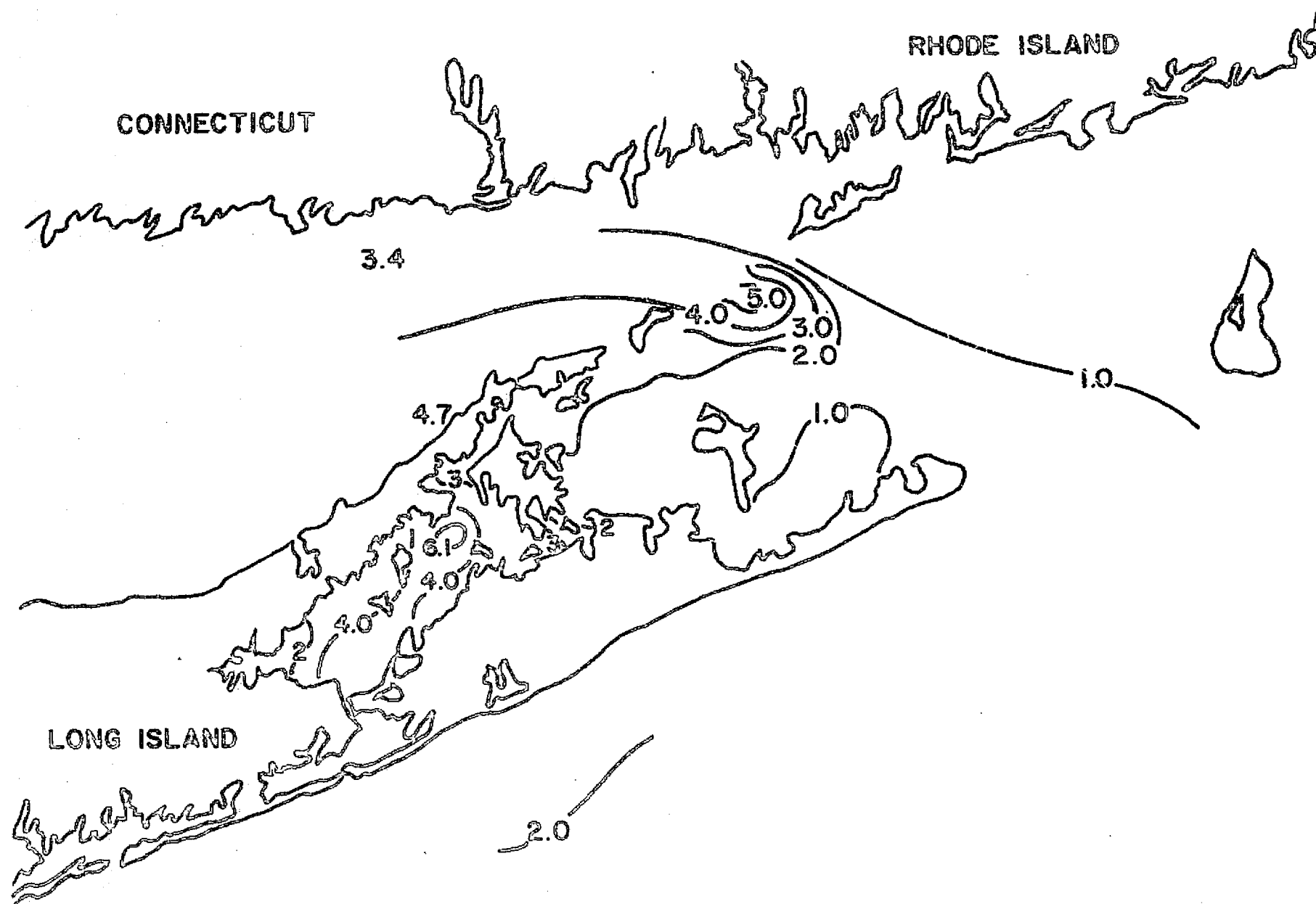
FIGURE III-7a

The distribution of suspended solids (mg/ℓ) in the surface waters of Block Island Sound and adjacent waters (12 May 1973-0900)

CONNECTICUT

10.6

RHODE ISLAND

1.0

2.0

3.0

3.4

.4

4.0

2.0

6.1

3.0

LONG ISLAND
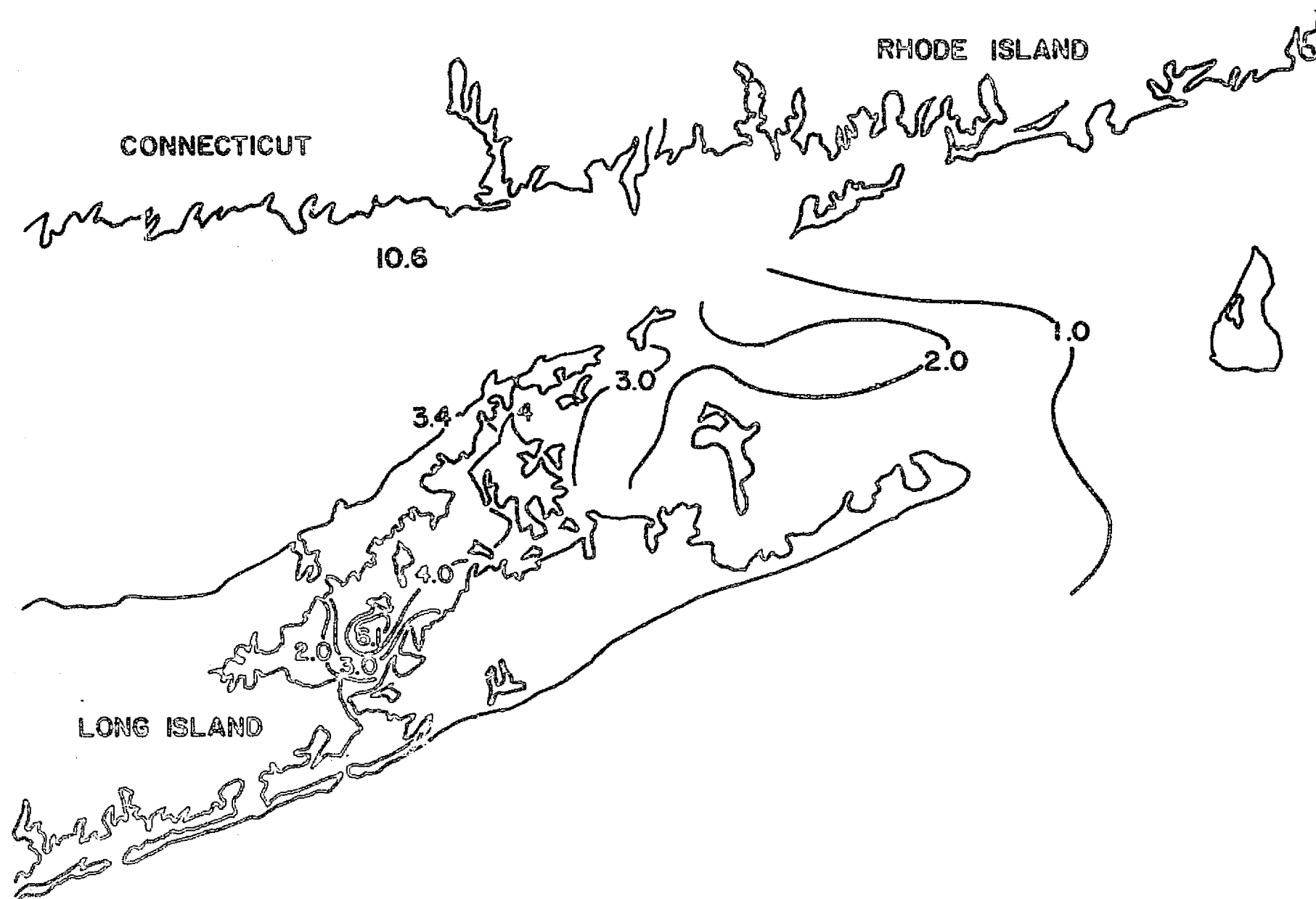
FIGURE III-7b

The distribution of suspended solids (mg/ℓ) in the surface waters of Block Island Sound and adjacent waters (12 May 1973-1200)

RHODE ISLAND

CONNECTICUT

4.0

2.0

3.0

1.0

3.6

3.0

2.0

3.0

3

4

6.7,0

6.7,3

3

4

5

5

LONG ISLAND
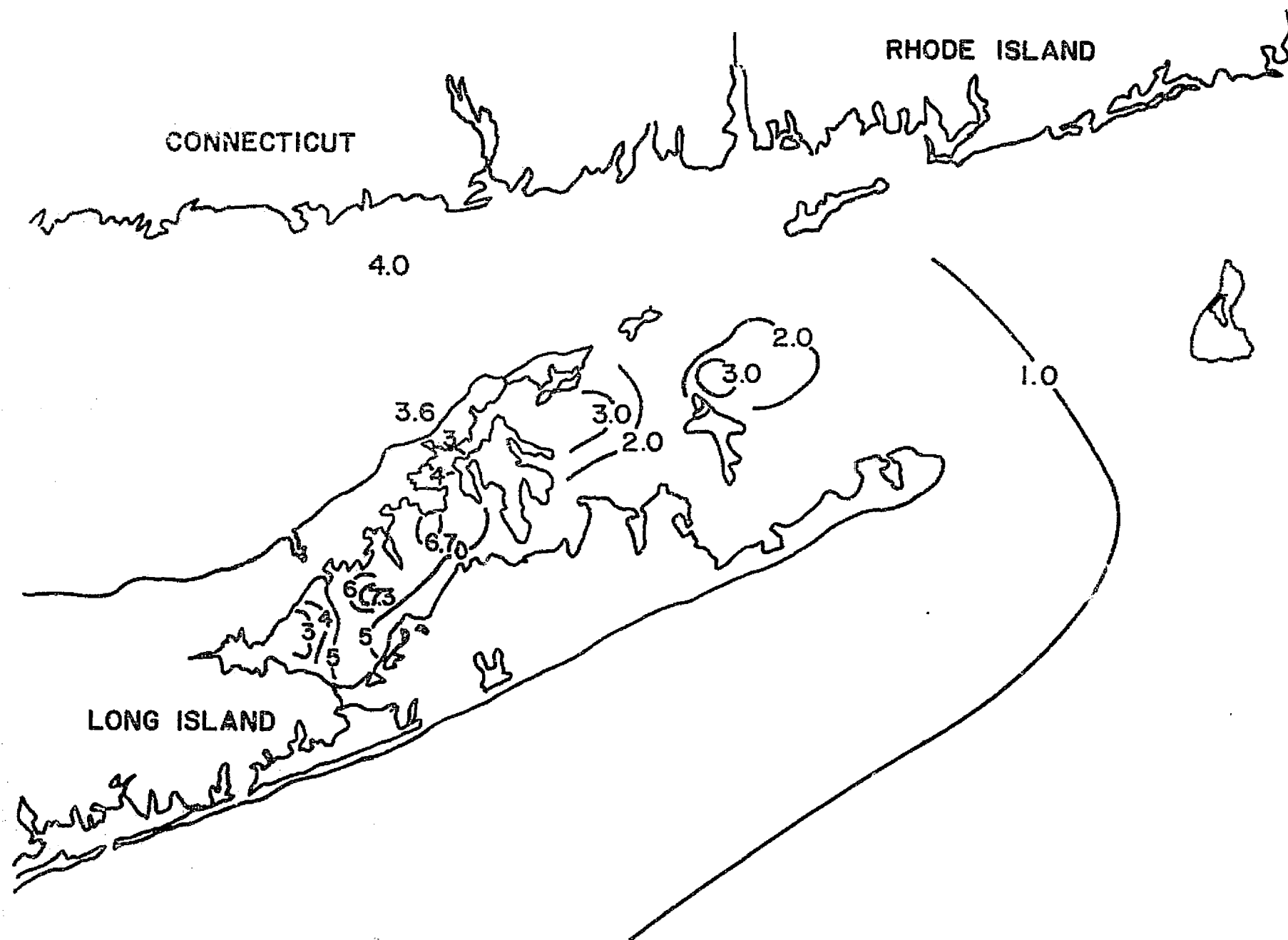
FIGURE III-7c

The distribution of suspended solids (mg/ℓ) in the surface waters of Block Island Sound and adjacent waters (12 May 1973-1500)

APPENDIX F

PHYTOPLANKTON AND SUSPENDED PARTICLES

by

Robert Nuzzi
Associate Research Scientist in Microbiology (Phytoplankton)
New York Ocean Science Laboratory
Montauk, New York

Ugo P. Perzan
Technician in Microbiology (Phytoplankton)
New York Ocean Science Laboratory
Montauk, New York

IV PHYTOPLANKTON AND SUSPENDED PARTICLES

Contents

METHODS

Sample Collection and Treatment

Samples for the analysis of phytoplankton and suspended particles were collected from the surface at each station in 5-ℓ Niskin bottles, concurrently with the chemical samples. One liter of water was removed from the bottle, immediately concentrated in a continuous plankton centrifuge to less than 10 mℓ, and brought to a final volume of 10 mℓ with filtered (0.45μ) seawater and neutral buffered formalin (a final concentration of 3%). This concentrated sample was returned to the laboratory for microscopic analysis of the phytoplankton population.

An additional 50-mℓ aliquot was withdrawn from the Niskin bottle and placed in a 50-mℓ glass vial. This sample was refrigerated until return to the laboratory, when it was immediately analyzed for suspended particles with a Coulter Counter, Model B (Coulter Electronics).

Phytoplankton Analysis

Aliquots of the concentrated sample were placed in a nannoplankton-counting chamber (Palmer and Maloney 1954) and various types of microscopic counts, depending on cell size and number, were performed under 100X and 400X magnification. At least 10 field counts (a wide field being delineated by the microscopic field and a narrow field by a whipple disc placed in one eyepiece) were performed under each magnification, and three survey counts (a scan of the entire counting chamber) were performed under 100X magnification. The average counts were multiplied by the appropriate factors to yield results as cells per liter.

Suspended Particle Analysis

Immediately upon return to the laboratory, the refrigerated 50-mℓ sample was analyzed for suspended particles with a Coulter Counter Model B. Two aperture tubes (30μ and 100μ) were employed so that particles between $0.16\mu^3$ and $635\mu^3$ (equivalent diameter of

0.68µ to 10.67µ) could be counted. Particles between 1 and 10µ equivalent diameter were counted at 1-micron intervals. Particles above 10.67µ equivalent diameter were also counted for most of the samples (Table IV-1).

Calibration of Coulter Counter

The calibration procedure followed was that of Sheldon and Parsons (1967). The 30µ aperture was calibrated with latex particles (1.947µ) and the 100µ aperture with paper mulberry pollen (12-13µ). The matching switch was set at 32-H, which ensured linearity between electrical pulses and particle volume at the aperture current switch setting of 1/2 that was used throughout the study. An amplification setting of 2 was routinely used for sample analysis. The number of particles counted in each sample was always low enough so that coincident passages could be ignored.

Since the samples could not be analyzed immediately after collection, the need for a method of holding the samples without changing the number of particles (or the particle sizes) within it had to be developed. Most chemical fixatives, while insuring the absence of biological replication, pose the problems of precipitation and flocculation. Therefore, refrigeration (4° C) was used to hold the samples until they could be returned to the laboratory for analysis. The percent of variation in counts after 24 hours (Table IV-2) was low enough that this method proved feasible. All samples were analyzed within 24 hours of collection, and generally within 12 hours.

Twenty mℓ disposable sample containers (Accuvettes, Coulter Electronics) were rinsed three times with freshly filtered (0.22µ) distilled water, followed by a triple rinse with freshly filtered (0.22µ) seawater. The same procedure was used to rinse a 24-mm membrane filter holder and 500-mℓ filter flask (Millipore) with a 25µ-mesh screen (Nitex HC nylon monofilament) used as a filter. The final seawater rinse was added to the sample container and background counts for the 30µ-aperture were performed for the various threshold settings listed in Table IV-1. Background counts for the 30µ-aperture were always less than 10% of the sample count. These counts were subtracted from the sample counts to yield results in particles per 0.05mℓ.

A second disposable sample container was rinsed as above, with the final rinse being used for a background count for the 100μ-aperture. These background counts were low enough (< 1% of the sample count) to be considered negligible. The volume of sample counted with the 100μ-aperture at each threshold setting was 0.5mℓ.

RESULTS AND DISCUSSION

Phytoplankton - New York Bight (NYB) and TR Stations

The surface populations resident at the NYB stations varied only slightly in quality in December and January, with *Skeletonema costatum* being dominant in all cases but one (Table IV-3). This was not the case during the May-June sampling, when *S. costatum* was dominant at only five stations.

Although the populations at the NYB stations generally resembled each other qualitatively, there were large quantitative differences. The mean phytoplankton standing crop for the entire period at Station 5, 6, and 7 was 1,059, 1,328, and 1,225 x 10^3 cells per liter respectively, five to six times that at Station 1 and 9, where means of 197 x 10^3 cells per liter were recorded. Station 2, 3, 4, and 8 had intermediate values (Table IV-4).

These differences may be due to the fact that Station 5, 6, and 7 are situated around the sewage-disposal site, an organically rich area. Similar results were found by Nuzzi in 1973.

The most singular feature of the phytoplankton population of the NYB area is its high numbers compared to the TR stations. For the same three sampling periods, the phytoplankton found off the southern shore of Long Island (TR transect) had a mean standing crop of 130 x 10^3 cells per liter, as compared to an overall mean of 799 x 10^3 cells per liter for the NYB stations (Table IV-4).

Quantitatively, the stations of the TR transect show moderate differences, with Station TR7 and TR8 yielding the highest mean counts. These stations are close to the NYB area and may be representative of the abundant growth that was observed there.

Qualitatively, the TR transect demonstrated a diversified phytoplankton composition (Table IV-3). *S. costatum*, the dominant species in the NYB area, showed moderate growth during December and January, but was never observed as the dominant species during the May-June sampling.

The composition of the phytoplankton in the NYB area and the TR transect demonstrates small variation in the number of taxa identified. A total of 85 taxa were identified in December, 66 in January, and 65 in the May-June period, the overwhelming majority being diatoms. Most species encountered, however, were subordinate to 9 diatoms and 4 flagellates, which accounted for 90% of the total phytoplankton. These 13 species were: *S. costatum, Thalassionema nitzschioides, Paralia sulcata, Thalassiosira subtilis, Chaetocerus* sp., *Leptocylindrus danicus, Navicula* sp., *Asterionella japonica, Thalassiosiria nordenskioldii, Gymnodinium* sp., *Ceratium tripos, Ceratium lineatum*, and *Ankistrodesmus falcatus* (a freshwater chlorophyte found only at Station NYB 2, 3, 5, and 7, and apparently originating in the Hudson River).

The pulses of *S. costatum, A. japonica, Gymnodinium* sp., and *C. lineatum* coincided to produce the May-June maxima in the NYB area. Despite this succession, it was almost entirely the variation in numbers of the overall most dominant species, *S. costatum*, that determined the pattern of abundance of the total population. *S. costatum* was present during all sampling periods—December, January, and May-June—and comprised 52%, 82%, and 44% of the total population respectively. The species composition for the waters off the southern shore of Long Island (TR transect) is somewhat different; here an active successional pattern can be seen (Table IV-3 and Figure IV-1).

Phytoplankton - Block Island Sound Stations

A total of 16 cruises were conducted during the period of October 1972 to June 1973. Although the transects were sometimes sampled on different days, they were all sampled during the months of November, December, February, March, April, and June, with the following exceptions: (1) the BR transect was not sampled in February; (2) the H-transect was additionally sampled in October; (3) a special synoptic sampling program, which will be discussed separately, took place in May.

Mean monthly phytoplankton counts for the three transects, HB, H, and BR (Table IV-5) show maxima occurring during the following months: March for the HB transect (645 x 10^3 cells per liter); October, March, and June for the H transect (1,230, 865, 645 x 10^3 cells per liter respectively), and June for the BR transect (497 x 10^3 cells per liter).

The mean phytoplankton standing crop for the entire period in Block Island Sound totaled 451 x 10^3 cells per liter for the H transect, over twice that recorded for the HB and BR transects, where means of 169 and 123 x 10^3 cells per liter respectively were recorded. The stations closest to Montauk Point generally exhibited the largest phytoplankton standing crop. Station HB1 and HB2 constituted 80% to 50% of the mean monthly count for the HB transect except for April and June, when they made up only 24% and 7% of the count respectively. Similarly, Station H1 composed 90% to 46% of the mean monthly count for the H transect except for April and June, when it constituted 18% and 15% respectively.

As in the New York Bight, *S. costatum* is quite abundant in Block Island Sound, where it comprised 60% of the H and HB transect population, excluding the months of April and June.

A total of 85 taxa were recorded during this investigation, the majority being diatoms. Transect H and HB were most similar in species composition, with 85 and 70 taxa identified respectively. A total of 20% of the taxa attained a frequency of >50% in the H transect and 23% of the taxa attained a frequency of >50% in the HB transect. A total of 59 taxa were identified in the BR transect, with 37% of these attaining a frequency of >50%. If only the dominant species (those accounting for 10% or more of any sample) are considered, the significant regional contrasts are: *T. decipiens*, occurring more frequently as a dominant in the BR transect, and *S. costatum* and *T. nitzschioides* in the H and HB transects. One exception was noticeable in the June sampling, when *Cerataulina bergonii* became the dominant species at all three transects.

Particle Counts - New York Bight (NYB) and TR Stations

The particle counts at the NYB and TR stations are given in Table IV-6. As with the

phytoplankton counts, the particle counts were higher in the NYB area. The average for the NYB stations was 667×10^6 particles per liter (total count) and 837×10^3 particles per liter (particles $>10.7\mu$ equivalent diameter), as opposed to 242×10^6 and 422×10^3 particles per liter for the TR stations.

Station NYB3 showed the highest total particle counts (1,567, 1,621, and $2,677 \times 10^6$ particles per liter for December, January, and May respectively) probably due to material being carried into the area by the Hudson River.

The increase in particles at all NYB stations, from December to May, might be due at least in part to increased biotic populations. A comparison of Table IV-5 and IV-6 indicates only a slight increase in both phytoplankton population and particle count during this time period at the TR stations as compared to the NYB stations. The correlation of coefficient (r) for phytoplankton cell counts vs particles $>10.7\mu$ equivalent diameter for 49 paired sets of values for the NYB and TR stations was 0.586, indicating that other factors besides phytoplankton are contributing to the particle counts.

Figure IV-2 compares phytoplankton cell counts with counts of particles $>10.7\mu$ diameter for the TR and NYB stations for all sampling periods.

Particle Counts - Block Island Sound Stations

Table IV-7 gives the results of the particle counts of the Block Island Sound stations. While there is only a slight variation in the total particle counts, the number of particles greater than 10.7μ equivalent diameter varied significantly from station to station. The highest counts of particles $>10.7\mu$ were found at Station H1 and HB1 (stations closest to Montauk Point), these counts corresponding to an increased phytoplankton population (Table IV-4). The counts at the BR stations varied only slightly.

The coefficient of correlation for phytoplankton cell counts and particles $>10.7\mu$ equivalent diameter for 101 sets of paired data in Block Island Sound was 0.858, with the correlation being highest during periods of high phytoplankton populations and lowest during periods when few cells were present. Table IV-8 contrasts the phytoplankton counts

and the counts of particles >10.7μ diameter for each transect in the Block Island Sound area for each sampling date.

Synoptic Sampling Program

On 12 May 1973, the surface waters of 29 stations were sampled synoptically by the New York Ocean Science Laboratory with the aid of the East Hampton and Peconic Bay power squadrons. Each station was sampled at 0900, 1200, and 1500 EDST (the times corresponding to maximum ebb current, slack, and approximately one hour before maximum flood current relative to the Race). Figure IV-3 presents the surface contours of *Thalassionema nitzschioides*, the dominant phytoplankter present during this sampling period.

The largest population occurred in the Peconic Bay-Gardiners Bay region, with a smaller population found in northern Long Island and Block Island Sound waters. These populations were separated by the sparsely populated waters apparently originating in central and southern Long Island Sound, passing through central Block Island Sound, and meeting the waters of the Atlantic Ocean between Montauk Point and Block Island. This type of circulation of the surface waters was shown previously by Nuzzi (1973) and Austin (1973).

SUMMARY

The high correlation between phytoplankton and suspended particles >10.7μ equivalent diameter in Block Island Sound (0.858) indicates that the phytoplankton may contribute largely to the suspended material in this region. In contrast, the lower correlation between these parameters in the New York Bight (0.586) indicates that other factors are adding to the suspended load in this area. Suspended materials are being brought into the area by the Hudson River outflow, as evidenced by the high total particle counts and lowered salinity values (see Section II) at Station NYB3.

The phytoplankton population was highest at the NYB and Block Island Sound stations,

with the TR stations having the lowest number of cells. There are indications that the organic enrichment caused by the disposal of sewage sludge in the New York Bight may play a role in maintaining the relatively high phytoplankton population in this region.

In Block Island Sound, the stations around Montauk Point generally exhibited the largest phytoplankton populations, these populations probably originating in the waters of the Peconic Bay-Gardiners Bay system.

Block Island Sound can be divided into three regions: (1) Northern Block Island Sound, influenced by the coastal waters of Connecticut, Rhode Island, and the Cape Cod region; (2) Southern Block Island Sound, influenced by the waters of the Peconic Bay-Gardiners Bay system; and (3) Central Block Island Sound, influenced by the waters of Long Island to the west and the Atlantic Ocean to the east.

REFERENCES

Austin, H.M. and P.M. Stoops. 1973. A synoptic study of the surface waters of Block Island Sound and surrounding waters, Part II. New York Ocean Science Laboratory Technical Report No. 0024.

Nuzzi, R. 1973. The distribution of phytoplankton in the New York Bight, September and November, 1971. In *The Oceanography of the New York Bight: Physical, Chemical, Biological* Vol. I (ed. R. Nuzzi). New York Ocean Science Laboratory Technical Report No. 0017.

_____. 1973. A synoptic study of the surface waters of Block Island Sound and surrounding waters, Part I. New York Ocean Science Laboratory Technical Report No. 0019.

Palmer, C.M. and T.E. Maloney. 1954. A new counting slide for nannoplankton. American Society of Limnology and Oceanography. Spec. Publ. No. 21.

Sheldon, R.W. and T.R. Parsons. 1967. A Practical Manual on the Use of the Coulter Counter in Marine Science. Coulter Electronics Sales Co., Toronto, Canada.

TABLE IV-1

Aperture tubes and threshold settings used for suspended particle
analysis by Coulter Counter Model B

Aperture	Threshold Settings		Volume (μ^3)	Equivalent Diameter (μ)
	Lower	Upper		
30μ	1	3.3	0.16 – 0.52	0.68 –1
	3.25	26	0.52 – 4.18	1 – 2
	26	88.4	4.18 – 14.14	2 – 3
100μ	2.3	5.3	14.25 – 33.51	3 – 4
	5.3	10.3	33.51 – 65.45	4 – 5
	10.3	17.8	65.45 – 113.03	5 – 6
	17.8	28.3	113.03 – 179.58	6 – 7
	28.3	42.3	179.58 – 267.97	7 – 8
	42.3	60	267.97 – 381.70	8 – 9
	60	82.5	381.70 – 523.63	9 – 10
	82.5	100	523.63 – 635	10 – 10.67
	100	out	>635	>10.67

TABLE IV-2

Variation in counts (Coulter Counter) after refrigeration for various periods of time.
Numbers indicate the percentage difference from the sample
analyzed immediately after collection.

Particle Diameter (μ)	Refrigerated for	
	1 day	3 days
0.68 – 1	+5.4%	+8.5%
1 – 2	–5.9	+20.7
2 – 3	–4.0	+15.9
3 – 4	–3.6	+31.0
4 – 5	–3.1	+19.0
5 – 6	–1.8	+25.8
6 – 7	–1.8	+21.6
7 – 8	+8.9	+15.7
8 – 9	+21.0	+28.4
9 – 10	+13.4	+8.9
10 – 10.67	0	–5.4

TABLE IV-3
Species occurrence and succession. The dominant species for each station and date is in large
type. The subdominant species are in smaller type and are preceeded by an arrow. Codominant
species are indicated by equal type size and are not separated by an arrow.

	TR 1	TR 2	TR 3	TR 4	TR 5	TR 6	TR 7	TR 8
DEC K7235	S.costatum → P.sulcata → T.decipiens	T.nitzschioides → S.costatum → T.decipiens	P.sulcata → T.nitzschioides → T.decipiens	P.sulcata → N.closterium → T.nitzschioides	T.nitzschioides → N.closterium → P.sulcata	P.sulcata → S.costatum → N.closterium	P.sulcata → S.costatum → T.subtilis	S.costatum → T.nitzschioides → P.sulcata
JAN K7302	S.costatum → N.closterium → P.sulcata	T.nitzschioides → T.nitzschioides → N.closterium	S.costatum → T.nitzschioides → N.closterium	N.closterium → T.nitzschioides → S.costatum	T.nitzschioides → N.closterium → P.sulcata	S.costatum → N.closterium → P.sulcata	S.costatum → P.sulcata → T.subtilis	S.costatum → T.nitzschioides → N.closterium
MAY–JUNE K7327	T.nitzschioides → S.costatum → N.closterium	L.danicus → S.costatum → N.closterium	Chaetoceros sp. → L.danicus → N.closterium	Gymnodinium sp → L.danicus → Chaetoceros sp	L.danicus → Gymnodinium sp → Chaetoceros sp	L.danicus → Chaetoceros sp. → Gymnodinium sp.	Chaetoceros sp. → Gymnodinium sp → L.danicus	Gymnodinium sp. → C.tripos → Chaetoceros sp.

	NYB 1	NYB 2	NYB 3	NYB 4	NYB 5	NYB 6	NYB 7	NYB 8	NYB 9
DEC K7235	P.sulcata → T.nitzschioides → T.decipiens	S.costatum → P.sulcata → T.decipiens	S.costatum → T.decipiens → Navicula sp.	S.costatum → T.subtilis → T.decipiens	S.costatum → P.sulcata → T.nitzschioides	S.costatum → T.nitzschioides → P.sulcata	S.costatum → T.subtilis → P.sulcata	S.costatum → T.subtilis → P.sulcata	S.costatum → N.closterium → T.nitzschioides
JAN K7302	S.costatum → T.nitzschioides → T.subtilis	S.costatum → T.subtilis → T.nitzschioides	S.costatum → T.subtilis → T.nordenskioldii	S.costatum → T.subtilis → T.nitzschioides	S.costatum → T.nordenskioldii → T.subtilis	S.costatum → T.nordenskioldii → T.subtilis	S.costatum → T.nordenskioldii → N.closterium	S.costatum → T.nordenskioldii → T.subtilis	S.costatum → N.closterium → T.nitzschioides
MAY–JUNE K7327	A.japonica → C.lineatum → Gymnodinium sp	S.costatum → A.japonica → A.falcatus	S.costatum → A.falcatus → A.japonica	S.costatum → A.japonica → Gymnodinium sp	S.costatum → A.japonica → A.falcatus	Gymnodinium sp → A.japonica → C.lineatum	S.costatum → A.japonica → A.falcatus	C.Lineatum → S.costatum → A.japonica	C.Lineatum → A.japonica → Gymnodinium sp

TABLE IV-4

Phytoplankton cell counts, NYB and TR stations (cells per liter)

Station	19 – 20 Dec 1972	25 – 26 Jan 1973	30 – 31 May 1973	Average, all dates
TR 1	77,802	284,316	124,946	162,354
2	60,815	26,017	323,927	136,919
3	50,885	73,883	247,480	124,082
4	46,419	44,232	216,656	102,435
5	73,669	43,485	38,495	51,883
6	34,617	210,233	27,064	90,638
7	30,217	443,032	88,331	187,193
8	31,417	457,734	79,729	189,626
Av., all stations	50,730	197,866	143,328	130,641
NYB 1	55,134	388,209	149,095	197,479
2	100,602	424,085	1,738,497	754,394
3	67,916	714,584	1,134,779	639,093
4	46,017	811,283	1,997,029	951,443
5	42,571	2,269,373	865,512	1,059,152
6	35,684	3,222,769	726,650	1,328,367
7	24,451	2,587,673	1,063,224	1,225,116
8	38,184	1,347,163	1,138,085	841,144
9	52,350	258,633	279,662	196,881
Av., all stations	51,434	1,335,974	1,010,281	799,229

TABLE IV-5

Phytoplankton cell counts, Block Island Sound stations (cells per liter)

Stations	10 Oct 72	14 Nov 72	4 Dec 72	13 Feb 73	20 Mar 73	24 Apr 73	18 Jun 73	Average, all dates
H1	4,410,497	259,748	80,781	941,923 *	2,185,331	9,862	381,462	1,181,372
H2	225,866	85,518	48,633	59,968 *	873,848	6,611	182,254	211,814
H3	119,951	1,199 *	20,749	38,811 *	264,942	2,962	1,181,625	232,891
H4	164,731	21,533	24,866	16,776 *	136,860	34,658	835,729	176,450
Av., all stations	1,230,261	91,999	43,757	264,369	865,245	13,523	645,267	450,631
Stations	16 Nov 72	8 Dec 72	20 Mar 73	21 Mar 73	24 Apr 73	26 Apr 73	18 Jun 73	Average, all dates
BR1	13,800	43,466	44,565	80,630 *	31,379	79,395	556,942	121,451
BR2	20,199	18,613	45,030	40,229 *	107,178	169,562	859,368	180,025
BR3	21,750	49,750	71,797	58,772 *	60,378	130,160	73,556	66,594
Av., all stations	18,583	37,269	53,797	59,877	66,311	126,372	496,622	122,690
Stations	10 Nov 72	6 Dec 72	14 Feb 73	20 Mar 73	24 Apr 73	25 Apr 73	19 Jun 73	Average, all dates
HB1	152,766	177,349	456,949 *	1,728,919	11,895	9,861 *	61,375	362,730
HB2	79,851	21,033	76,612 *	835,020	27,194	14,813 *	26,544	154,438
HB3	10,149	25,934	35,601 *	222,274	3,164	9,626 *	499,272	115,145
HB4	40,349	16,851	63,414 *	239,312	52,128	13,797 *	164,553	84,343
HB5	32,350	26,332	43,075 *	197,195	69,362	26,151 *	495,891	127,193
Av., all stations	63,093	41,499	135,130	644,544	32,748	14,849	249,527	168,769

* Average of more than one sample.

82

TABLE IV-6

Particle counts TR transect and NYB stations (particles per liter)

Station	19(TR), 20(NYB) Dec Total Particles (x 10^6)	Particles >10.7μ (x 10^3)	25(NYB), 26(TR) Jan Total Particles (x 10^6)	Particles >10.7μ (x 10^3)	30(TR), 31(NYB) May Total Particles (x 10^6)	Particles >10.7μ (x 10^3)	1 June Total Particles (x 10^6)	Particles >10.7μ (x 10^3)	Average	
TR 1	546	1044	143	146	228	374	205	414	281	495
2	132	400	277	292	152	526	208	510	192	432
3	264	532	207	202	204	608	174	488	212	458
4	203	344	213	146	254	-	231	380	225	290
5	211	383	265	136	132	518	153	432	190	367
6	485	470	146	362	80	494	365	742	269	517
7	337	314	219	378	264	386	238	292	265	343
8	390	332	229	464	363	498	219	422	300	429
Av., all stations	321	477	212	265	210	486	224	460	242	422
NYB 1	354	-	275	646	274	578	-	-	301	612
2	681	576	567	484	1666	1628	-	-	971	896
3	1567	464	1621	788	2677	2328	-	-	1433	1193
4	410	282	552	512	1129	1892	-	-	697	895
5	288	212	385	864	939	1180	-	-	537	752
6	240	236	219	858	609	1402	-	-	356	832
7	291	472	278	834	923	1586	-	-	497	964
8	290	410	255	570	561	1690	-	-	369	890
9	208	334	279	522	478	896	-	-	322	584
Av., all stations	481	373	492	675	1028	1464	-	-	667	837

TABLE IV-7

Particle counts (particles per liter) for Block Island Sound stations (Transects H, HB, BR)

Station	10 Nov 1972 Total Particles (x 10^6)	Particles >10μ (x 10^3)	14 Nov 1972 Total Particles (x 10^6)	Particles >10μ (x 10^3)	16 Nov 1972 Total Particles (x 10^6)	Particles >10μ (x 10^3)	4 Dec 1972 Total Particles (x 10^6)	Particles >10μ (x 10^3)	6 Dec 1972 Total Particles (x 10^6)	Particles >10μ (x 10^3)
H 1			1098 *				321 *	.		
2			481 *				320 *	97		
3			278 *				321 *	94		
4			253 **				371 *	133		
Average			527				333	.		
HB 1	281								345 **	274
2	223								246 **	137
3	201								289 **	109
4	214								367 **	107
5	208								204 **	106
Average	225								290	146
BR 1					297 ***					
2					184 ***					
3					185 ***					
Average					222					

* Average of 3 samples taken over 3 crossings of transect.
**   "   " 2   "   "   " 2   "   "   " .
***   "   " 4   "   "   " 4   "   "   " .
+   "   " 5   "   "   " 5   "   "   " .

TABLE IV-7 (cont'd.)

Station	8 Dec 1972		13 Feb 1973		14 Feb 1973		20 Mar 1973		21 Mar 1973	
	Total Particles $(\times 10^6)$	Particles $>10\mu$ $(\times 10^3)$	Total Particles $(\times 10^6)$	Particles $>10\mu$ $(\times 10^3)$	Total Particles $(\times 10^6)$	Particles $>10\mu$ $(\times 10^3)$	Total Particles $(\times 10^6)$	Particles $>10\mu$ $(\times 10^3)$	Total Particles $(\times 10^6)$	Particles $>10\mu$ $(\times 10^3)$
H1			314 *	1005			358	2160		
2			185 ***	556			225	468		
3			226 +	481			232	408		
4			198 *	379			200	268		
Average			231	605			254	826		
HB 1					180 *	690	306	1782		
2					165 *	418	250	462		
3					174 *	349	197	224		
4					162 *	229	213	384		
5					163 *	361	225	354		
Average					168	409	238	641		
BR 1	203 *	185					219	190	181 ***	277
2	287 *	124					568	462	194 ***	237
3	422 **	197					533	428	364 ***	334
Average	304	162					440	360	246 ***	283

TABLE IV-7 (cont'd.)

Station	24 Apr 1973 Total Particles (x 10^6)	Particles >10μ (x 10^3)	25 Apr 1973 Total Particles (x 10^6)	Particles >10μ (x 10^3)	26 Apr 1973 Total Particles (x 10^6)	Particles >10μ (x 10^3)	18 Jun 1973 Total Particles (x 10^6)	Particles >10μ (x 10^3)	19 Jun 1973 Total Particles (x 10^6)	Particles >10μ (x 10^3)	Average Total Particles (x 10^6)	Particles >10μ (x 10^3)
H1	184	227					316	726			432	1030
2	241	246					308	660			293	405
3	144	150					210	1254			235	477
4	197	164					246	375			244	264
Average	191	196					270	753			301	544
HB 1	113	86	172***	185					205***	539	229	593
2	142	202	183***	211					206***	607	202	340
3	167	114	212***	102					254***	593	213	249
4	179	176	165***	128					205***	541	215	261
5	149	194	136***	109					188***	550	182	279
Average	149	154	173	147					211	566	208	344
BR 1	140	140			214	144	251*	920			215	309
2	115	163			113	154	221*	700			240	306
3	220	208			252	188	206*	317			312	279
Average	158	170			193	162	224*	645			255	297

TABLE IV-8

Phytoplankton total cells per liter (x 10^3) vs particles $>10.7\mu$
per liter (x 10^3) for each transect and date in Block Island Sound

Date	Station	Particles $>10.7\mu$ per liter x 10^3	Total cells per liter x 10^3	Correlation for each transect	Correlation for sampling period
12/4/72	H1-2	.	81		
	2-3	124	49	$r = -0.015$	$r = -0.015$
	3-3	102	21		
	4-2	178	25		
	Average	134	44		
12/6/72	HB1-1	196	177		
	2-3	164	21		
	3-3	98	26	$r = 0.775$	$r = 0.775$
	4-3	92	17		
	5-2	116	26		
	Average	133	41		
12/8/72	BR1-3	130	43		
	2-3	90	19	$r = 0.894$	$r = 0.894$
	3-2	200	50		
	Average	140	37		
2/13/73	H1-1	.	277		
	2-1	292	74	$r = -0.624$	
	3-1	272	44		
	4-1	324	12		
	3-2	602	14	$r = 0.401$	$r = 0.929$
	2-2	278	25		
	1-2	564	264	$r = -0.518$	
	2-3	628	81		
	4-2	338	23		
	Average	412	90		
2/14/73	HB1-1	818	218		
	2-1	390	154		
	3-1	176	24	$r = 0.882$	
	4-1	254	34		
	5-1	328	18		
	Average	393	90		

TABLE IV-8 (cont'd.)

Date	Station	Particles >10.7μ per liter x 10³	Total cells per liter x 10³	Correlation for each transect	Correlation for sampling period
2/14/73 (cont'd.)	HB1-2	594	212		
	2-2	428	75		
	3-2	402	65	r = 0.559	r = 0.577
	4-2	306	175		
	5-2	286	37		
	Average	403	113		
	HB1-3	658	772		
	2-3	436	53		
	3-3	470	25	r = 0.674	
	4-3	128	20		
	5-3	440	36		
	Average	432	181		
3/20/73	H1	2160	2185		
	2	468	874	r = 0.961	
	3	408	265		
	4	268	137		
	Average	826	865		
	BR1	190	45		
	2	462	45	r = 0.397	r = 0.939
	3	428	72		
	Average	360	54		
	HB1	1782	1729		
	2	462	835		
	3	224	222	r = 0.945	
	4	384	239		
	5	354	197		
	Average	641	644		
3/21/73	BR1-1	226	89		
	2-1	276	63	r = 0.877	
	3-1	324	140		
	Average	288	97		

TABLE IV-8 (cont'd.)

Date	Station	Particles>10.7μ per liter x 10³	Total cells per liter x 10³	Correlation for each transect	Correlation for sampling period
3/21/73 (cont'd.)	BR1-2	360	123		
	2-2	222	41	r = 0.990	
	3-2	160	23		
	Average	247	62		r = 0.159
	BR1-3	314	51		
	2-3	256	26	r = 0.884	
	3-3	358	50		
	Average	309	42		
	BR1-4	168	60		
	2-4	194	30	r = -0.714	
	3-4	496	22		
	Average	286	37		
4/24/73	H1	227	10		
	2	246	7	r = -0.314	
	3	150	3		
	4	164	35		r = 0.269
	Average	196	14		
	BR1	140	31		
	2	163	107	r = 0.201	
	3	208	60		
	Average	170	66		
4/25/73	HB1-1	198	12		
	2-1	316	27		
	3-1	166	3	r = -0.496	
	4-1	131	52		
	5-1	101	69		
	Average	182	32		
	HB1-2	173	11		
	2-2	206	3	r = 0.519	
	3-2	114	3		
	4-2	138	5		
	5-2	104	37		r = -0.125
	Average	147	12		

TABLE IV-8 (cont'd.)

Date	Station	Particles >10.7μ per liter x 10³	Total cells per liter x 10³	Correlation for each transect	Correlation for sampling period
4/25/73 (cont'd.)	HB1-3	194	6		
	2-3	196	4		
	3-3	124	30	r = -0.917	
	4-3	156	37		
	5-3	108	56		
	Average	155	26		
	HB1-4	178	6		
	2-4	128	10		
	3-4	4	1	r = 0.579	
	4-4	90	9		
	5-4	124	5		
	Average	105	6		
4/26/73	BR1-1	144	79	r = 1.0 *n = 2	r = 1.0 *n = 2
	3-1	188	130		
	Average	166	104		
6/18/73	H1	726	381		
	2	660	182	r = 0.498	
	3	1254	1182		
	4	375	836		
	Average	753	645		r = 0.663
	BR1-1	876	557		
	2-1	894	859	r = 0.933	
	3-1	260	74		
	Average	676	496		
6/19/73	HB1-1	626	61		
	2-1	638	27		
	3-1	788	499	r = 0.509	r = 0.509
	4-1	348	165		
	5-1	692	496		
	Average	618	249		

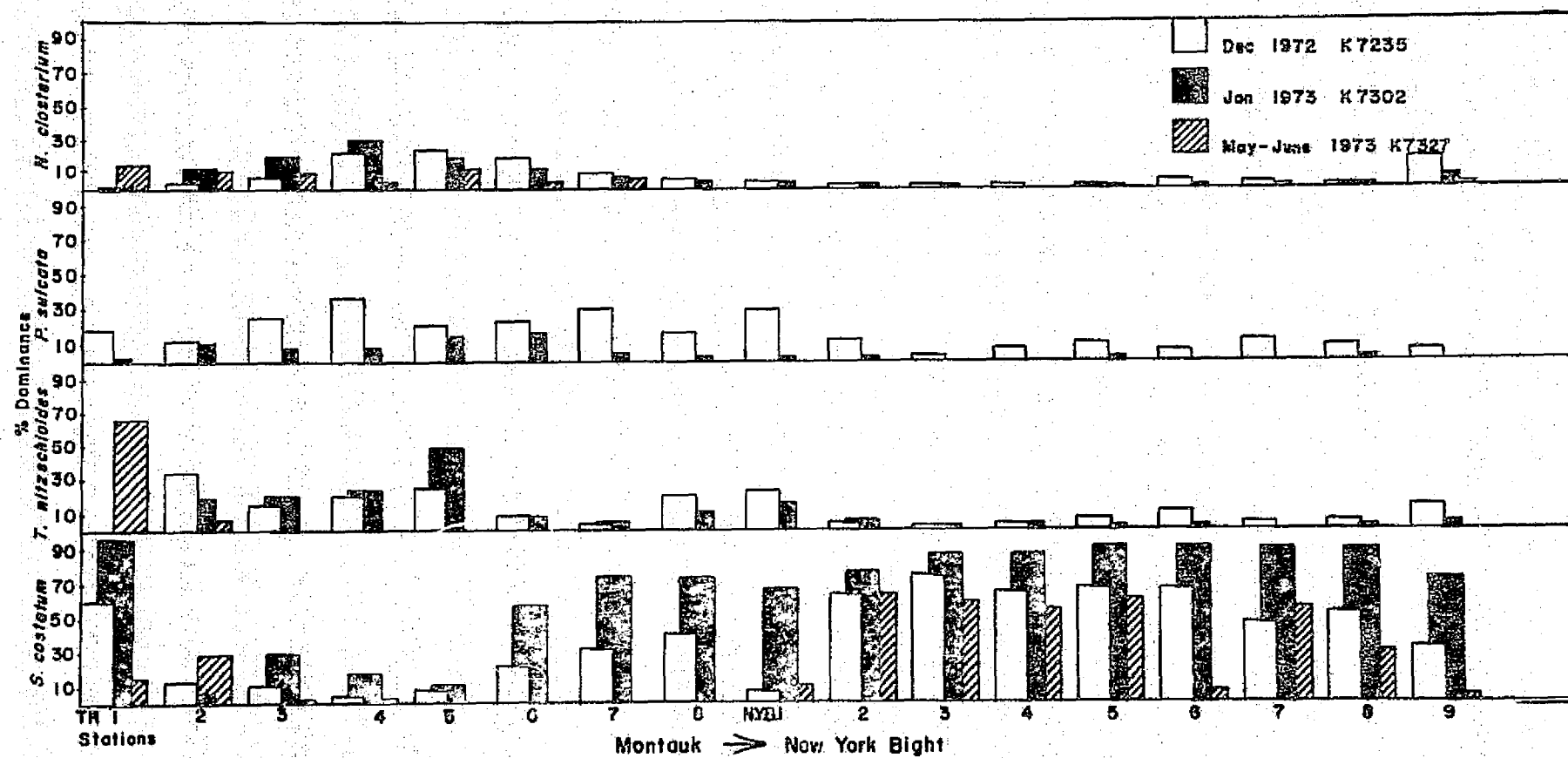Total correlation for all samples and all dates

r = 0.858

FIGURE IV-1

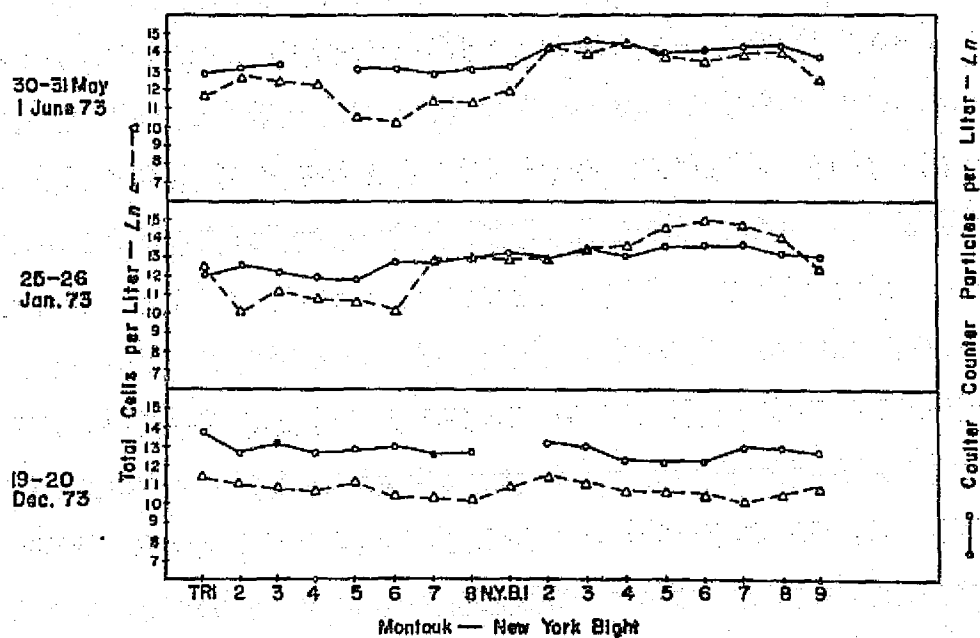Variation of dominant phytoplankton species for each sampling period at the TR and NYB station

FIGURE IV-2

Total phytoplankton cell count and particles
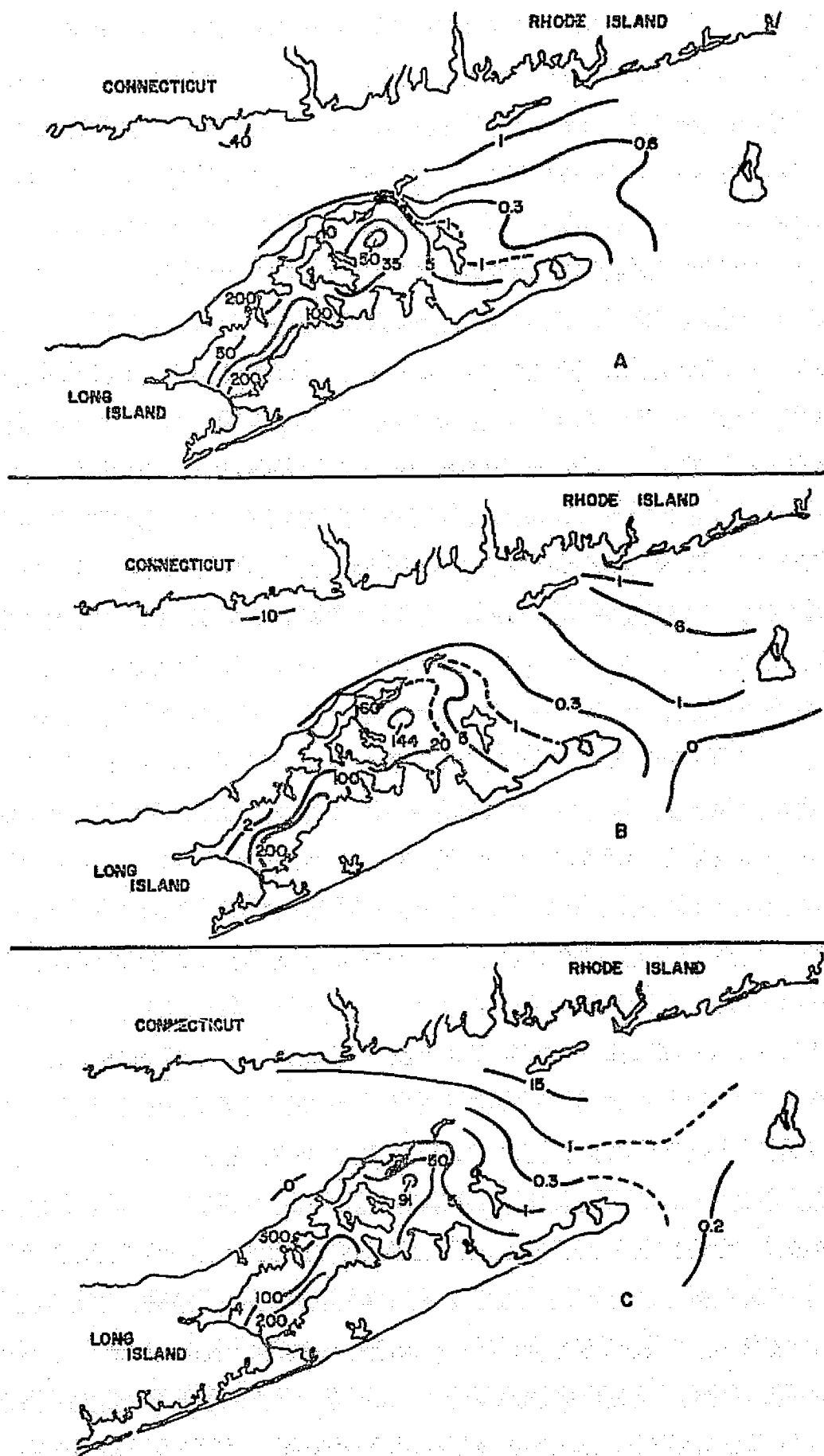>10.7μ for each sampling period at the TR and NYB stations

FIGURE IV-3
Surface contours, *Thalassionema nitzschioides* (cells per liter x 10³)
12 May 1973 (A-0900, B-1200, C-1500)

APPENDIX G

"System 800". Technical Description

SPECIFICATIONS

DISPLAY

TYPE: 19" Shadow Mask Picture Tube, 670x500 color-dot trios.

COLOR DISPLAY: Number of Colors - Selectable 1 thru 32.

Color Assignment - Any one of 32 colors assigned to any picture value. The colors are four shades of Yellow, Cyan, Green, Orange, Magenta, Violet, Red, and Blue. Colors are controlled by graphics data and keyboard to produce black, white, or monochrome.

MONOCHROME DISPLAY: Number of Grey Levels - 32. Monochrome superimposed on color under keyboard and program control.

GRAPHICS DISPLAY: Graphics displayed in black or white. Graphics display under program control.

RESOLUTION: 512x512 raster points stored, 512x489 displayed.

GEOMETRIC DISTORTION: Less than 2% overall.

SIZE: 16x12 (4/3 aspect ratio), 12x12 (1/1 aspect ratio).

REFRESH RATE: Standard 525-line television interlaced 2:1, 60 fields/sec., 30 frames/second.

DISPLAY KEYBOARD: 4x32 pushbuttons for selection of color, black, B/W, and Out.

COLOR PATCH PLUG: 64 pin plug for change in color order. Prewired plugs for normal and reverse order supplied.

CURSOR: Joystick control of cursor position. Activate switch. Maximum interrogation rate 30 times/ second.

MODEL 810 DIGITAL PROCESSOR

CORE STORAGE: 8192 16-bit words.

NUMBER OF REGISTERS: 8

INSTRUCTION SET: Over 400 hardware instructions.

SPEED: Memory Cycle - 1.2 microseconds. Add/Subtract - 5.2 microseconds.

PERIPHERAL EQUIPMENT: Teletypewriter ASR 33, Photoelectric Paper Tape Reader (300 chars/ second), Model 810-1 Magnetic Tape Unit - 9 track, IBM compatible, 800 bpi, 37½ ips, 10½" reels.

SOFTWARE: Diagnostics, Math Functions, Assemblers, BASIC, Debug.

POWER AND PHYSICAL

SYSTEM POWER REQUIREMENTS: 105/125 volts, 60 Hz, 20 amp circuit.

ENVIRONMENT: +15° to +30°C, 10% to 90% Humidity.

SYSTEM CONTROL

The system control accepts a control word from the Processor and supplies a status word to the Processor. When the cursor and joystick option is provided, a two-word X-Y address is also supplied to the Processor indicating the position of the cursor.

Program control of all picture elements simultaneously by a single 16-bit control word produces an all color display, an all grey scale display, graphics only, a complemented (negative) grey scale display, and roll up or roll down of entire picture. The latter command provides a rolling raster for display of continuous strip pictures.

The control word consists of an operation code and a line (Y) address. Only the Buffer to Refresh Store transfers require a line address. Specified bits in the operation code determine whether:

1) elements are displayed as specified by the graphics codes as described above.
2) all elements are displayed as specified by the graphics codes except color elements are displayed in grey scale.
3) all elements are displayed in color (without graphics control).
4) all elements are displayed in grey scale (without graphics control).
5) the graphics black and white elements only are displayed (without picture data).
6) any of the above are displayed with the picture data complemented.

These control functions require only one I/O instruction for operation and immediately switch the display from color, graphics, to grey scale under program control. Thus, the program may present ten types of information display to the operator without reloading the picture store.

In addition to the above operations, the operation code includes roll-up and roll-down. These operations immediately move the displayed picture up or down two horizontal lines. Continuous movement of the picture may be performed by writing new data at the top or bottom of the picture before each roll command. In this way new picture information can continuously replace the old, producing the effect of a continuous roll.

The status word provides the Processor program with updated information on the display status. An interrupt is given to the Processor at the completion of each operation that requires more than one Processor instruction time to complete, such as a buffer-disc transfer.

SOFTWARE

The Model 805 Display is provided with software on punched paper tape for operation with the Model 810 or customer's Processor. Included with the software package are:

1) Diagnostics for the Processor, core memory, and display system
2) Machine language assembler
3) Basic compiler
4) Load and Utility routines
5) Debug Program
6) Math Functions

The Processor is supplied with a software library including display diagnostic routines for checking the operation of the processor and display unit. User programs may be entered originally, edited, and assembled using the teletype keyboard. Programs are stored on paper tape and quickly loaded using the high-speed photoelectric tape reader. Operational activities are controlled through the teletypewriter keyboard and the Processor front-panel switch register.

REFRESH STORE AND BUFFER

The picture and graphics are stored digitally in the Refresh Store. The horizontal lines, each containing 512 picture elements, are circulated, even lines followed by odd lines, so that they may be continuously read in synchronism with the standard interlaced scanning pattern of the color picture display. Successive lines (Y addresses) are read every 1/60 second.

The Refresh Store is addressed by line (Y) address from the control word and, at the proper time, the complete line of 512 picture elements is transferred to/from the Buffer Store. The Buffer Store then transfers to/from the Processor core using a high speed block transfer.

The Buffer Store may be used for transfer of picture or graphics data as specified by the control word sent to the Display Control.

COLOR GENERATION

The 5-bit picture codes and 2-bit graphic codes are read continuously from the Refresh Store. The Color Generator using special digital-to-analog matrix conversion circuits produces red, green, and blue color video signals to drive the three electron guns of the Color Picture Tube. Colors are produced by generating proper proportions of the red, green, and blue primaries on the screen. The color produced for each picture element is controlled by the 2-bit graphic codes as follows:

Binary 00:   One of the 32 standard colors is assigned according to the 5-bit picture code (color picture).

Binary 01:   White is generated regardless of picture code values (white graphics).

Binary 10:   Black is generated regardless of picture code values (black graphics).

Binary 11:   One of 32 shades of grey ranging from black to white are assigned according to the 5-bit picture code (B/W picture).

Thus, the graphic code determines the type of display for each element.

COLOR KEYBOARD

In addition to the software control of the display the colors are also under control of the Color Keyboard. Four interlocking push-keys are provided for each of the 32 colors and control the display of each color as follows:

1)   Normal: Normal Operation, the picture-elements of this value are displayed on the screen as determined by the picture and graphics codes.

2)   Black: Every picture-element of this value is now displayed in black.

3)   B/W: Every picture element of this value is displayed in grey scale.

4)   OUT: Every picture element of this value is displayed in the same mode as next higher order value. For example, the OUT key of value 10 displays value 11 in place of value 10 so that 10 and 11 are now the same color or grey level.

The black and B/W keys perform the same functions as the graphic codes on all elements of the same value or color and are a great help to the operator for recognizing particular colors and features.

The OUT keys eliminate colors so that the complexity of the color display may be reduced quickly without need for the processor to rewrite the picture data.

SYSTEM OPERATION

The block diagram on the opposite page shows the major components of the complete Color Display System. The Model 805 Display is shown to the right of the input-output (I/O) bus of the Model 810 Processor.

The high resolution color picture refreshed at standard television rates is constructed from a rectangular array of 512x512 picture elements. Each picture element is specified by a 5-bit picture code and a 2-bit graphics code. The 32 picture values and the four graphics values are individually controlled from the processor to provide a wide variety of displays.

Two data paths are shown to the 805: one through the upper interface electronics to the Refresh Store for transfer of the picture and graphics codes, and one through the lower interface electronics to the Display Control for transfer of control words, status words, and cursor address.

The digital-to-analog converters in the Color Generator convert, under control of the Color Keyboard, the picture and graphic codes, which are continuously being circulated in the Refresh Store, to red, green, and blue video signals for the Color Picture Tube. According to the four possible values of the graphics code, the 32 possible values produce, for each picture element, either one of 32 colors, or one of 32 grey shades, or black, or white. The picture and graphics codes are separately accessed through the Buffer Store so that they may be modified independently.

DIGITAL PROCESSOR

The Model 810 Digital Processor and Model 810-1 Magnetic Tape Unit are designed to operate with the Model 805 Display as a stand-alone system for the analysis of picture information. The system can perform data editing and formatting, data analysis, and the production of graphics. Data is normally first entered by the 810-1 Magnetic Tape Unit. This data may have originally been digitized from a sensor (such as a thermal, radar, or sonar scanner) or may have been generated by a large-scale digital computer or the Model 810 itself.

The data on the magnetic tape is read, a block at a time, into the processor core storage, and, if not already formatted in a 512x512x5-bit matrix, is converted to 512x5-bit blocks of horizontal rows of picture elements for output to the Display. The data is transferred to the Buffer Store and then to the picture code section of the Refresh Store. The latter transfer takes place by a software-controlled output to the 805 control of a control word which contains the address of the line in the Refresh Store.

The transfer from the Buffer Store is made to one of the 512 horizontal rows of the Refresh Store specified by the control word placed in the Display Control by a programmed transfer.

The graphics codes, 2 bits for each picture element, are transferred to the Display in the same way as the picture data. Areas may thus be shown in grey-scale or color depending on parameters calculated by the processor.
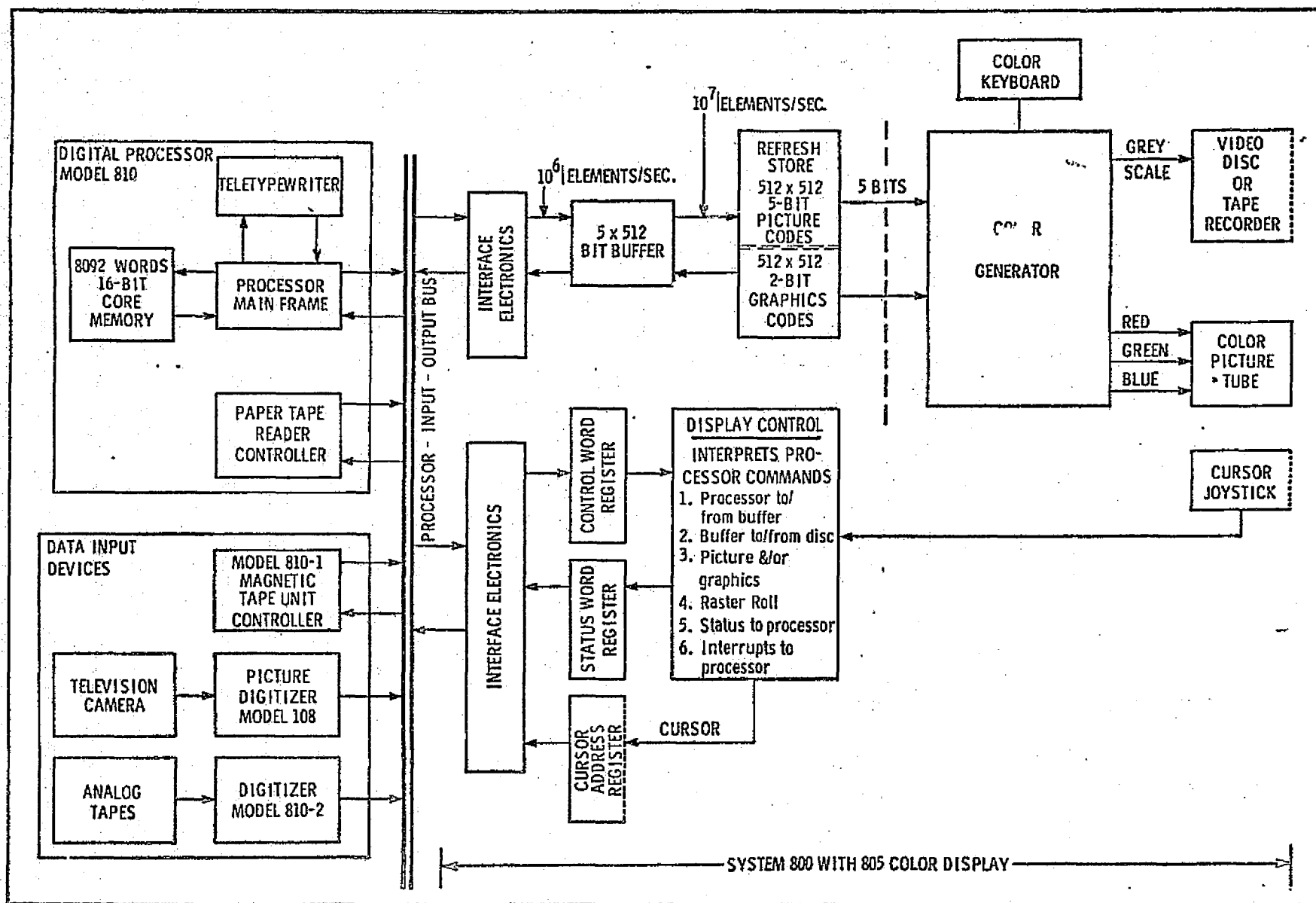
A typical System 800 interactive display system using the Model 805 Color Display combined with the Model 810 Digital Processor is shown on the opposite page.

COLOR DISPLAY

The large screen color picture display is constantly refreshed at 60 fields per second from the refresh store and is constructed from a rectangular array of 512 by 512 picture elements. Each element, under individual program control, may be displayed in 32 colors, in a 32 level grey scale, in black, or in white.

COLOR KEYBOARD

The push-button keyboard in front of the display provides operator control of the picture elements according to their value. Thirty-two columns of keys, one column for each color or grey-scale value, change the display of all picture elements of a particular value from color to grey scale or to black.

In addition, under keyboard control, one or more equal-value sets of elements may be combined to reduce the number of colors or grey shades in the display.

Thus, the Color Keyboard speeds the analysis of displayed data by providing immediate operator control over the number of colors and grey-scale contrast.

DIGITAL PROCESSOR

The Processor and Magnetic Tape Units are supplied to meet the needs of specific applications or the Model 805 may be supplied alone with the proper interface for the customer's processor.

Operator control is provided through the Teletypewriter keyboard and results and programs are listed on the teleprinter. Program entry is rapid and convenient using the high-speed Photoelectric Tape Reader.

REFRESH STORE

The refresh store contains the 262,144 picture elements and continuously transmits them to the display at a peak rate of 10 million per second. At the request of the Processor program, the picture elements are transferred directly to or from core storage in blocks of 512 picture elements (one horizontal line). The transfers take place over the Processor input-output channel in a similar manner as other input-output devices, the magnetic and paper tape readers.

OPERATING SPEED

When operated with the System 800 Digital Processor, the entire 805 Display may be changed in less than eight seconds, new picture data may be added at the top or bottom and the picture moved up or down 60 horizontal lines per second, or the Display may be changed from a positive to a negative, from color to grey scale, or from picture to graphics only, in 1/30 second. The average access time for 512 elements is 1/60 second.